

Heavy Flavours at LEP

CONVENORS: J.H. Kühn¹, P.M. Zerwas²

CONTRIBUTIONS: M. Bosman¹, W. Buchmüller³, J. Chrin⁴, A. Djouadi², B. van Eijk⁴, J.W. Gary⁵, J.-M. Gerard¹, F. Hoogeveen³, G. W.-S. Hou¹, P. Igo-Kemenes⁵, V. Khoze⁶, P. Mättig⁴, A. Masiero⁷, K. Mönig⁸, H.-G. Moser¹, J.L. Pinfold⁹, M. Roos¹⁰, R. Rückl¹¹, L.M. Sehgal¹², R. Settles¹, T. Sjöstrand⁴, S. Überschär⁸, M. Wirbel¹³

¹Max-Planck-Institut für Physik und Astrophysik, München, FRG. ²Inst. Theor. Physik, RWTH Aachen, FRG. ³Inst. Theor. Physik, TU Hannover, FRG. ⁴CERN, Geneva, Switzerland. ⁵Physik. Institut, Univ. Heidelberg, FRG. ⁶Leningrad Nucl. Physics Inst., Gatchina, USSR. ⁷Dipart. di Fisica, Univ. Padova, Italy. ⁸Physik. Institut, Univ. Wuppertal, FRG. ⁹Dep. Physics, Carlton Univ., Ottawa, Canada. ¹⁰TFT Helsinki Univ., Finland. ¹¹Inst. Theor. Physik, Univ. München, FRG. ¹²III. Phys. Inst., RWTH Aachen, FRG. ¹³Inst. Theor. Physik, Univ. Dortmund, FRG.

TABLE OF CONTENTS

1. Introduction	1
2. c, b Quarks	4
2.1. Production of c, b Quarks	4
2.1.1. Z Decays	4
2.1.2. Production Cross Section	9
2.1.3. Forward-Backward Asymmetry	15
2.1.4. Final State Polarization	21
2.1.5. Heavy Quark Monte Carlos	21
2.2. Cross Sections and Charge Asymmetries: Experimental Preview	23
2.2.1. Methods of Tagging Heavy Flavours.	24
2.2.2. Cross Sections	29
2.2.3. Charge Asymmetries	30
2.3. Heavy Quark Fragmentation	34
2.3.1. Fragmentation — mainly nonperturbative	35
2.3.2. Fragmentation — mainly perturbative	40
2.3.3. Experimental Status	41
2.3.4. Heavy Quark Fragmentation in Monte Carlos	42
2.3.5. A Comparison of Heavy Quark Fragmentation in Jetset71 and Herwig32	45
2.4. Particle Flow between Jets	49
2.4.1. Particle Flow in 3-jet Events	51
2.4.2. Correlations of Interjet Particle Flows / String-string Interactions	53
2.4.3. Azimuthal Asymmetry of Quark Jets ...	54
2.4.4. ... and Gluon Jets	55
2.5. Inclusive Production of J/ψ , Υ and B_c	56
2.6. Heavy Flavour Lifetimes	59
2.6.1. Theoretical Summary	59
2.6.2. Experimental Aspects	75
2.7. B Decays	80
2.7.1. Semileptonic Decays	80
2.7.2. Nonleptonic Decays	93
2.7.3. Rare B decays: Standard Model and Beyond	102
2.7.4. Heavy Flavour Decays: EURODEC	111
2.8. $B\bar{B}$ Mixing	133
2.8.1. Theoretical Framework	133
2.8.2. $B\bar{B}$ Mixing Measurements	138
2.9. CP Violation in B Decays	143
3. Top and Toponium	154
3.1. Top in the Continuum	154
3.1.1. Production	154
3.1.2. Top Decay in the Standard Model	156
3.1.3. Top Production through Flavour Changing Neutral Currents	160
3.2. Toponium(Θ)	161
3.2.1. Spectroscopy	161
3.2.2. Main Decay Modes	164
3.2.3. Higgs Decays	170
3.2.4. Toponium in e^+e^- Collisions	174
4. Extending the Standard Model	182
4.1. The Fourth Generation	182
4.2. Leptonic Decays of Neutral D- and B-Mesons	185
4.3. Non-Standard Fermions	192
4.3.1. Constraints: Non-Standard Effects on Standard Fermions	194
4.3.2. Production and Decay Signatures of Non-Standard Fermions	196
4.3.3. Leptoquarks and Diquarks	201

1. Introduction

1. A substantial fraction of all Z decay modes are decays into charm and bottom quarks. The branching ratios are predicted in the Standard Model to be close to

$$BR(Z \rightarrow c\bar{c}) \approx 12\%$$

$$BR(Z \rightarrow b\bar{b}) \approx 15\%$$

so that approximately 2.4×10^6 charmed hadrons and 3×10^6 bottomed hadrons are produced in 10^7 Z decays.

This is a number sufficiently large to carry out precision measurements in the c, b quark sector. Fundamental aspects of the Standard Model can be tested in the heavy quark sector by determining the vector and axial vector electroweak charges from cross sections and asymmetries. The accuracy of $\sin^2 \theta_W$ which can be achieved by measuring the forward-backward asymmetry of b jets, is expected to be at the level of ± 0.001 and better, and thus competes well with the other methods.

QCD inspired fragmentation models developed to describe the hadronization of quarks and gluons in jets, can be scrutinized experimentally. Because heavy quark pair creation in the jet evolution is strongly suppressed, the fragmentation of heavy quarks provides the most powerful tool to tackle this involved problem. The tagging of heavy quark jets will allow us to isolate gluon jets in 3-jet final states so that their properties can be explored thoroughly. Discriminating quark versus gluon jets will also be of great advantage in isolating the 3-gluon coupling — an outstanding problem of QCD — and in exploring many subtle QCD effects, like string-string interactions etc. , that shed new light on hadronization mechanisms.

The properties of c, b hadrons can well be investigated experimentally. The high particle energies make feasible the measurement of individual lifetimes in vertex detectors. The lifetimes of the various weakly decaying B mesons and baryons may differ by as much as 30%, to be compared with an experimental accuracy of 10% in various decay channels. For other aspects of B physics a sample of a few million particles is modest. The mixing in the B_d system can well be demonstrated by analyzing the time evolution of the $B_d^0 - \bar{B}_d^0$ states. The oscillations in the B_s system, however, may be so rapid that, even though nearly complete mixing can easily be established by measuring time-integrated observables, a quantitative measurement of the mixing parameter may be difficult. The prospects for establishing CP violation in the B system are bleak. Adopting the predictions of the Standard Model, an event sample of 10^7 Z 's planned at LEP falls short by one to two orders of magnitude — yet this picture may not be correct, and establishing experimental bounds on CP violating effects is of utmost importance.

2. At the present time it seems highly unlikely that *top quarks* could be observed in the first phase of LEP. e^+e^- colliders are nevertheless the best suited machines to establish firm lower bounds on the top quark mass. In particular, if top would decay dominantly into a charged Higgs particle, it could not have been detected in hadron colliders. Several important questions can exclusively be studied at an e^+e^- collider; among them, the precise determination of the top mass and of its weak coupling, and the exploration of the interquark potential at short distances through toponium spectroscopy. The search for top quarks will therefore be an obvious task also during the early stages of LEP.

3. Even though the Standard Model has been tremendously successful so far, many fundamental problems remain unsolved by this theory. It is therefore imperative to explore possible extensions into which the model can be embedded in a natural way. In the fermionic sector such extensions are provided by introducing further replicas of the first three generations or by expanding the generation multiplets themselves as suggested by grand-unification theories.

The phenomenology of heavy b' quarks belonging to a 4th generation is drastically different from top quarks. Various possibilities could be realized depending on whether b' is heavier or lighter than t . In the (exciting) second case the Fermi decay is strongly suppressed by small mixing angles. As a result, induced flavour-changing neutral current decays could compete or even dominate over the orthodox charged current decays, leading to unusual signatures like γ decays of b' quarks. Because rapid single quark decays are impeded, $(b'\bar{b}')$ bound states sustain a substantial branching ratio for Higgs plus photon decays up to large mass values.

Non-standard fermions are motivated by many extensions of the Standard Model. Among the various scenarios we focus on *mirror fermions* and *exceptional fermions*. They may show up at LEP through direct production or through effects of mixing with the standard fermions. For mirror particles the weak left and right doublet/singlet assignment is reversed with respect to the standard fermions so that they can reveal themselves through "wrong-sign" forward-backward asymmetries. Exceptional E_6 fermions comprise a rich spectrum of novel vectorial charged and neutral [Dirac/Majorana] leptons as well as an isoscalar charge $-1/3$ quark. Spectacular lepton decays would signal the production of these particles.

Physics beyond the Standard Model could also be heralded by the discovery of *flavour-changing neutral current* $\mu\mu$, μe , ... decays of D^0 and B^0 mesons. The analysis of B_s^0 mesons will allow, for the first time, tests involving second and third generation quarks and leptons, with FCNC reactions likely enhanced relative to the low-mass generations. New bounds on masses of leptoquarks, technicolor and Higgs particles can be deduced from the limits on the branching ratios of these rare D and B decays.

Besides complementing and updating earlier papers [1, 2] this report reviews material elaborated in the recent past. A coherent summary of heavy quark physics at LEP on the Z-peak and in the continuum is presented. While the emphasis is put on the Standard Model — precision measurements in the electroweak sector and novel QCD effects — aspects of physics beyond standard orthodoxism are also given due attention*.

Acknowledgements: We benefitted from the collaboration with P. Heiliger and J. Maalampi. Unpublished material from W. Hollik, D. Morris, H. Steger and Z. Was is gratefully acknowledged. We thank R. Guth and B. Kniehl for technical assistance. P.Z. thanks J. Ellis for a stay at CERN where part of this report was prepared.

REFERENCES

- [1] A. Ali et al., CERN Workshop, Physics at LEP, Report CERN 86-02, eds. J. Ellis and R. Peccei.
- [2] P. Igo-Kemenes et al., Proceedings ECFA Workshop on LEP200, Aachen 1986, CERN 87-08, eds. A. Böhm and W. Hoogland.

*A short version of this report is published in the Proceedings of the CERN Workshop on LEP Physics 1989, ed. G. Altarelli.

2. c, b Quarks

2.1. PRODUCTION OF c, b QUARKS*

A large variety of physical problems in the heavy quark sector can experimentally be approached on the basis of 10^6 to 10^7 Z decays. Nearly 40% of all hadronic decays are c and b decay channels. Above all, precision measurements of the electroweak couplings will be feasible, and the determination of $\sin^2 \theta_W$ will be possible at very high accuracy in the forward-backward asymmetry of b -jets. The large fraction of heavy quarks in the final states requires a thorough understanding of their strong interaction properties to allow QCD precision tests of the total hadronic annihilation cross section and in jet distributions. The study of B mesons can shed new light on individual lifetimes and mixing phenomena. However, the investigation of CP violation in the B sector would very likely require a dedicated high statistics effort of at least 10^8 Z decays.

2.1.1. Z DECAYS

For many applications the Born approximation provides an excellent approximation to the partial Z decay width to heavy quarks,

$$\begin{aligned}\Gamma_B(Z \rightarrow Q\bar{Q}) &= \beta \frac{3 - \beta^2}{2} \Gamma_0^V + \beta^3 \Gamma_0^A \\ &= \Gamma_B^V + \Gamma_B^A\end{aligned}\tag{2.1}$$

with

$$\Gamma_0^{V(A)} = \frac{G_\mu m_Z^3}{8\sqrt{2}\pi} v_Q^2 (a_Q^2)$$

The electroweak vector and axial-vector couplings are defined for c and b quarks in the Standard Model as

$$\left. \begin{aligned}v_Q &= 2I_Q^{3L} - 4e_Q \sin^2 \theta_W \\ a_Q &= 2I_Q^{3L}\end{aligned} \right\} \quad 2I_Q^{3L} = \pm 1 \quad \text{for } c, b$$

The mass dependence which enters through the velocity β ,

$$\beta = \sqrt{1 - \mu^2} \quad \mu^2 = 4m_Q^2/s$$

is $\mathcal{O}(\mu^2) = \mathcal{O}(10^{-2})$ in the axial term for b quarks; in the vector term the correction is of order $\mu^4 \sim 10^{-4}$ and thus negligible. Defining the strength of the Z coupling to $Q\bar{Q}$ by Fermi's μ decay constant G_μ and the electroweak mixing angle through $\sin^2 \theta_W = 1 - m_W^2/m_Z^2$ the *bulk* of radiative corrections to the width, i.e. those originating from the running of α_{QED} , are automatically incorporated so long as the top quark mass does not

*J.H. KÜHN, P.M. ZERWAS *in collaboration with* A. DJOUADI

exceed $\mathcal{O}(100 \text{ GeV})$. The remaining ones will be treated below. For $m_Z = 91 \text{ GeV}$ and $\sin^2 \theta_W = 0.23$ the partial decay widths and branching ratios are then

$$\begin{aligned}\Gamma_B(Z \rightarrow c\bar{c}) &\approx 280 \text{ MeV} &\Rightarrow & BR(Z \rightarrow c\bar{c}) \approx 12\% \\ \Gamma_B(Z \rightarrow b\bar{b}) &\approx 360 \text{ MeV} &\Rightarrow & BR(Z \rightarrow b\bar{b}) \approx 15\%\end{aligned}$$

QCD corrections to the width $\Gamma(Z \rightarrow Q\bar{Q} \dots)$ are known for non-zero quark masses up to first order and for zero quark masses up to second order in α_s . They are different for vector and axial-vector couplings not only because masses break chiral invariance but also due to the large mass splitting between bottom and top quarks. Decomposing the width into the vector and the axial-vector part we expand both separately in the strong coupling constant

$$\begin{aligned}\Gamma(Z \rightarrow Q\bar{Q} + \dots) &= \Gamma_B^V \left[1 + c_1 \left(\frac{\alpha_s}{\pi} \right) + c_2 \left(\frac{\alpha_s}{\pi} \right)^2 + c_3 \left(\frac{\alpha_s}{\pi} \right)^3 \right] + \\ &\quad \Gamma_B^A \left[1 + d_1 \left(\frac{\alpha_s}{\pi} \right) + d_2 \left(\frac{\alpha_s}{\pi} \right)^2 + d_3 \left(\frac{\alpha_s}{\pi} \right)^3 \right]\end{aligned}\quad (2.2)$$

The first-order coefficients c_1 and d_1 have been calculated for non-zero quark masses in Ref. 1, 2. The exact expressions, recorded in the Appendix, can well be approximated by [3]

$$\begin{aligned}c_1 &= 1 + 3\mu^2 + \dots \\ d_1 &= 1 + 3\mu^2 \log(4/\mu^2) + \dots\end{aligned}\quad (2.3)$$

The coefficient d_1 exceeds unity by $\approx +0.20$ for b quarks so that the mass correction in 1st order QCD is as important as the entire 2nd order of the Z width – a non-negligible effect if the QCD scale parameter will be extracted from hadronic Z decays.

The 2nd order coefficient c_2 is given in the \overline{MS} scheme for massless quarks by [4]

$$c_2 = 1.985 - 0.115N_F$$

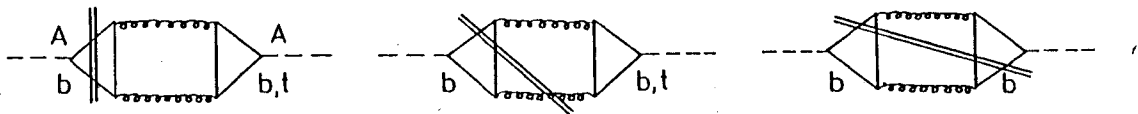


Fig. 2.1: Feynman diagrams pertinent to the $\mathcal{O}(\alpha_s^2)$ corrections calculated in Ref. [5].

However, the coefficient d_2 deviates from c_2 even for massless quarks [5]. This is a consequence of the cut triangular diagrams, exemplified above for b quarks. Whereas vector couplings do not give a contribution because of C invariance, axial couplings do. This is due to the $4b$ final state in the last diagram and the mass difference between the top and the bottom quark in the first two diagrams. The large mass splitting between top and bottom breaks the symmetry in this weak isodoublet so that up and down contributions

do not add up to zero any longer. In the \overline{MS} renormalization scheme one finds for $N_F = 5$ flavours [5]

$$\begin{aligned} c_2 &= 1.41 \\ d_2 &= 1.41 \mp f(m_t) \quad \mp \text{ for } Q = \text{up/down} \end{aligned} \quad (2.4)$$

$f(m_t)$ is well parametrized by

$$f(m_t) = 3 \ln(m_Z/m_t) - 3.083 + 0.346/\left(\frac{m_Z}{2m_t}\right)^2 + 0.211/\left(\frac{m_Z}{2m_t}\right)^4 \quad (2.5)$$

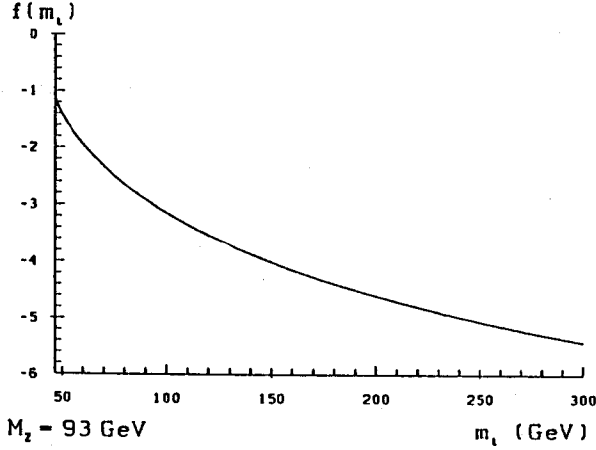


Fig. 2.2: The function $f(m_t)$ which characterizes the singlet part of the second order QCD correction to the Z decay rate.

and is shown in Fig. 2.2. The total Z width is thus affected by the unpaired correction to the b channel. For top quark masses between 50 and 250 GeV the correction $f(m_t)$ varies from ~ -1 to ~ -5 . The exact analytic formula for f is given in Ref. 5.

A recent calculation [6], originally performed for the electromagnetic current, gave a huge value for the third vector coefficient c_3 , rendering the third order as large as the second order in the present energy range,

$$c_3 = 64.861 + c_3(S) \quad (2.6)$$

The flavour singlet contribution $c_3(S)$ is different for the various vector (electromagnetic and NC) and axial vector currents, but is small (≤ 0.5) in any case [7]. The axial coefficient

$$d_3 = 64.861 + d_3(S) \quad (2.7)$$

is expected to be close to c_3 since all flavour-singlet contributions, responsible for the difference between vector and axial-vector terms are very small [7].

For the sake of completeness we repeat the definition of α_s in the \overline{MS} scheme for $N_F = 5$ flavours [8]

$$\frac{\alpha_s(\overline{MS})}{4\pi} = \frac{1/\beta_0}{\log s/\Lambda^2} \left\{ 1 - \frac{\beta_1/\beta_0^2 \log \log s/\Lambda^2}{\log s/\Lambda^2} + \frac{(\beta_1/\beta_0)^2}{\log^2 s/\Lambda^2} \left[\left(\log \log s/\Lambda^2 - \frac{1}{2} \right)^2 + \frac{\beta_2\beta_0}{\beta_1^2} - \frac{5}{4} \right] \right\} \quad (2.8a)$$

with the coefficients of the β function up to three loops

$$\begin{aligned}\beta_0 &= 11 - \frac{2}{3}N_F & \beta_2 &= \frac{1}{2}\left(2857 - \frac{5033}{9}N_F + \frac{325}{27}N_F^2\right) \\ \beta_1 &= 102 - \frac{38}{3}N_F\end{aligned}$$

The QCD scale parameter $\Lambda_{\overline{MS}}^{(5)}$ is related to $\Lambda_{\overline{MS}}^{(4)}$ for $N_F = 4$ flavours [9, 8] by

$$\Lambda_{\overline{MS}}^{(4)} = 1.6\Lambda_{\overline{MS}}^{(5)} \quad (2.8b)$$

which is usually quoted as the general reference value [10].

QED corrections can be copied from the QCD corrections by changing the couplings appropriately,

$$\begin{aligned}\Gamma_B &\rightarrow \Gamma_B[1 + \delta_{QED}] \\ \delta_{QED} &= \frac{3}{4}\frac{\alpha}{\pi}e_Q^2\end{aligned} \quad (2.9)$$

This radiative correction is 0.019% for b and 0.077% for c quarks.

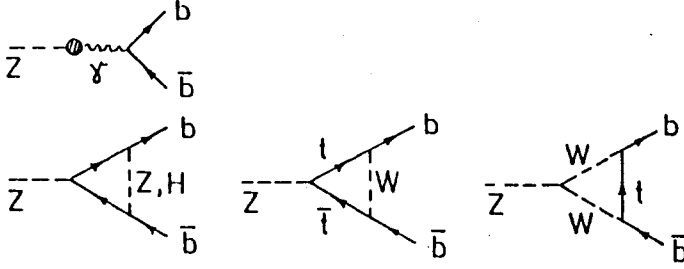


Fig. 2.3: Genuine electroweak corrections for the Z - $b\bar{b}$ vertex.

Finally, the genuine electroweak corrections are built-up by $\gamma - Z$ mixing and vertex corrections (Fig. 2.3). These effects are particularly interesting for b quark final states where the top quark couples in the vertices with full strength. The leading correction in m_t^2/m_W^2 can be incorporated [11] in the Born term expression eq. (1) by slightly shifting the coupling G_μ and the electroweak mixing angle, and by adding a piece to v and a that results from the last two of the vertex diagrams in Fig. 2.3 involving the heavy top quarks, present for $b\bar{b}$ final states only:

$$\begin{aligned}G_\mu &\rightarrow G_\mu(1 + \delta\rho_t) & \delta\rho_t &= \frac{3\sqrt{2}G_\mu m_t^2}{(4\pi)^2} \\ \sin^2 \theta_W &\rightarrow \sin^2 \theta_{eff} = \sin^2 \theta_W + \cos^2 \theta_W \delta\rho_t \\ a_f &\rightarrow a_f + \delta_b \frac{2}{3} \delta\rho_t & v_f &\rightarrow v_f + \delta_b \frac{2}{3} \delta\rho_t\end{aligned} \quad (2.10)$$

$\delta_b = 1$ for b quarks, and 0 otherwise. At this level of accuracy, $\sin^2 \theta_W$ can be deduced from m_Z and G_μ through the implicit relation $[\alpha(m_Z^2) = 1/127.6]$

$$\sin^2 \theta_W = \frac{1}{2} \left[1 - \sqrt{1 - \frac{4\pi\alpha(m_Z^2)}{\sqrt{2}m_Z^2 G_\mu (1 + \cot^2 \theta_W \delta\rho_t)}} \right] \quad (2.11)$$

It turns out (*a posteriori*) that one arrives at a fairly accurate description of the decay rate and FB asymmetry for all quark species as shown in Fig. 2.4 if one adds a term to the effective mixing angle that parametrizes the Higgs mass dependence as $\frac{\alpha}{4\pi}[\ln(m_H/17.3 \text{ GeV} + 1) - 2]$.

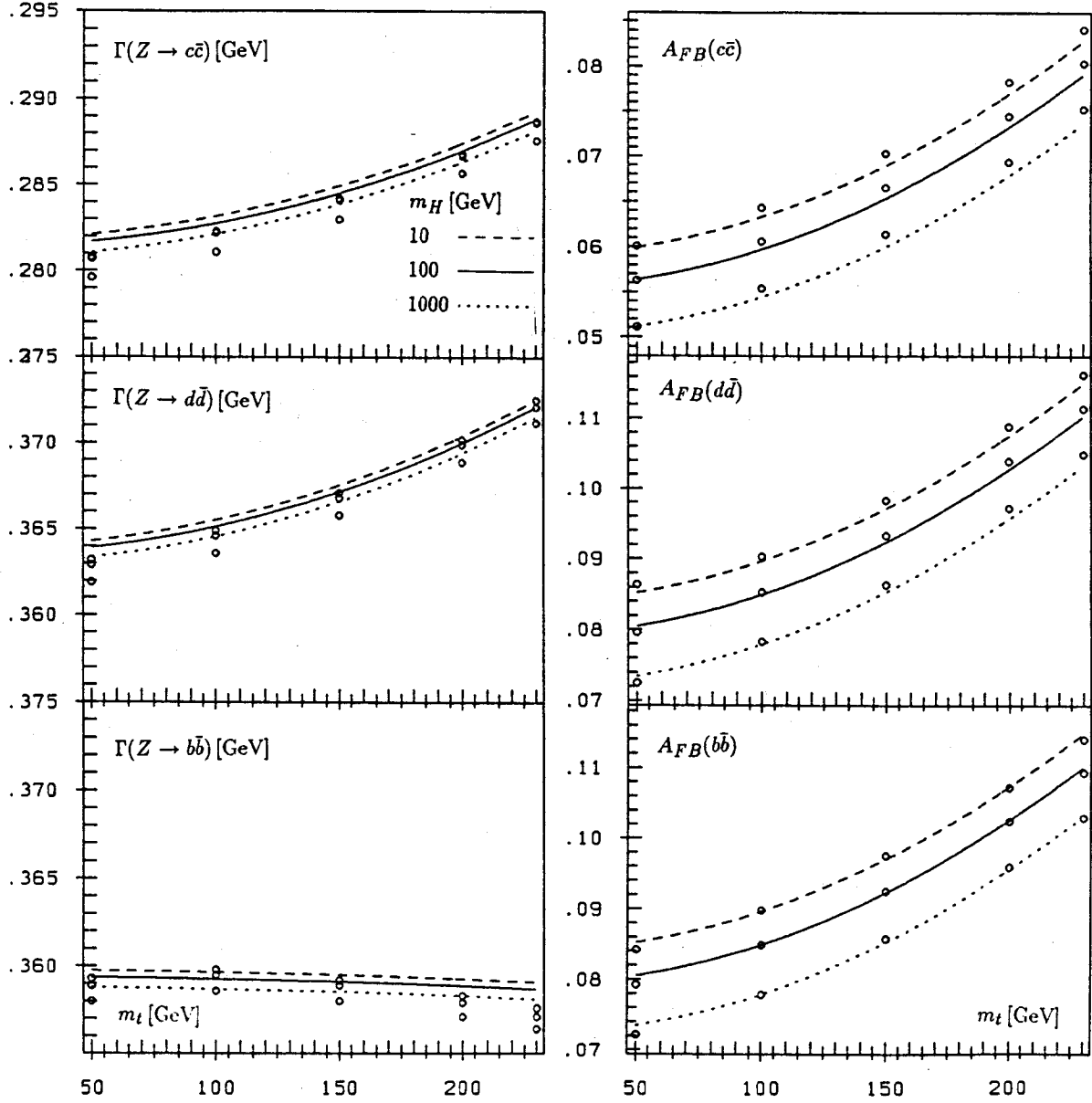


Fig. 2.4: The dependence of the partial Z widths (left) and of the forward-backward asymmetries (right) on the top and Higgs masses. Curves: approximate formulas as described in the text [3]; diamonds: full one loop calculation from [12].

The expressions which include the subleading corrections are lengthy and we must refer to the original literature or the computer programs BATCHZ and SIN2TH for details. The corrections depend strongly on the top mass and to a much lesser extent on the Higgs mass. The partial widths

$$\Gamma_B^{V,A} \rightarrow \Gamma_B^{V,A} [1 + \delta_{elw}^{V,A}]$$

m_Z	m_t	10	100	1000
91	50	0.1162	0.1161	0.1152
91	100	0.1167	0.1165	0.1157
91	150	0.1168	0.1166	0.1158
91	200	0.1168	0.1167	0.1159
91	230	0.1168	0.1167	0.1159
92	50	0.1234	0.1233	0.1224
92	100	0.1239	0.1238	0.1229
92	150	0.1240	0.1239	0.1230
92	200	0.1240	0.1239	0.1231
92	230	0.1239	0.1238	0.1231

m_Z	m_t	10	100	1000
91	50	0.2427	0.2432	0.2428
91	100	0.2428	0.2433	0.2429
91	150	0.2421	0.2426	0.2422
91	200	0.2411	0.2416	0.2412
91	230	0.2403	0.2409	0.2405
92	50	0.2508	0.2514	0.2509
92	100	0.2510	0.2515	0.2510
92	150	0.2503	0.2508	0.2504
92	200	0.2492	0.2498	0.2494
92	230	0.2484	0.2490	0.2486

Tab. 2.1: Vector (left) and axial parts (right) of $\Gamma(Z \rightarrow b\bar{b})$ in GeV for ($m_H = 10, 100, 1000$ GeV). [QED and QCD corrections not included.]

are tabulated in Tab. 2.1 for $m_t = 91$ and 92 GeV, top masses between 50 and 230 GeV and Higgs masses between 10 GeV and 1 TeV [12]. At fixed $m_Z = 92$ GeV the maximal spread of is $\pm 3\%$. Relative to the μ decay width the maximal variation reduces to $\pm 1.2\%$.

Adding up the entire set of strong, QED radiative and genuine electroweak corrections, we finally find

$$\Gamma(Z \rightarrow Q\bar{Q} \dots) = \Gamma^V + \Gamma^A$$

$$\Gamma^V = \Gamma_B^V [1 + \delta_{QCD}^V + \delta_{QED} + \delta_{elw}^V]$$

$$\Gamma^A = \Gamma_B^A [1 + \delta_{QCD}^A + \delta_{QED} + \delta_{elw}^A]$$

with the δ 's denoting all the individual corrections detailed above.

2.1.2. PRODUCTION CROSS SECTION

The steps followed in the discussion of the Z decay widths to heavy quarks, can to a large extent be transferred to the evaluation of the e^+e^- annihilation cross section to heavy quark pairs. Characteristic differences however derive from $Z - \gamma$ interference, from box diagrams in which initial and final state fermions are linked by exchanging two gauge bosons, and – above all – the huge impact of initial state QED radiative corrections on the line-shape.

For many purposes the accuracy of the Born approximation for the cross section [2] is sufficient in the c, b sector [before folded with the large initial state QED corrections],

$$\begin{aligned} \sigma &= \beta \frac{3 - \beta^2}{2} \sigma^{VV} + \beta^3 \sigma^{AA} \\ &= \sigma_B^V + \sigma_B^A \end{aligned} \tag{2.12}$$

with

$$\begin{aligned}\sigma^{VV} &= \frac{4\pi\alpha^2(m_Z^2)e_e^2e_Q^2}{s} + \frac{G_\mu\alpha(m_Z^2)}{\sqrt{2}}e_e e_Q v_e v_Q \frac{m_Z^2(s - m_Z^2)}{(s - m_Z^2)^2 + (\frac{s}{m_Z}\Gamma_Z)^2} \\ &\quad + \frac{G_\mu^2}{32\pi}(v_e^2 + a_e^2)v_Q^2 \frac{m_Z^4 s}{(s - m_Z^2)^2 + (\frac{s}{m_Z}\Gamma_Z)^2} \\ \sigma^{AA} &= \frac{G_\mu^2}{32\pi}(v_e^2 + a_e^2)a_Q^2 \frac{m_Z^4 s}{(s - m_Z^2)^2 + (\frac{s}{m_Z}\Gamma_Z)^2}\end{aligned}$$

Again, the bulk of radiative corrections is incorporated by expressing the cross section in terms of the coupling G_μ and the running QED coupling constant

$$\begin{aligned}\frac{1}{\alpha(m_Z^2)} &= \frac{1}{\alpha} - \frac{1}{3} \sum_f e_f^2 \log \frac{m_Z^2}{m_f^2} \\ &\approx 128\end{aligned}\tag{2.13}$$

[The contribution of the light quarks has actually been obtained through dispersion relations based on the low energy e^+e^- annihilation cross section [13].] The width of the Z has been introduced with a variation $\sim s$ as appropriate for light quarks. If a heavy quark threshold were close to the Z , the dependence on the quark mass had to be included properly, see eq. (1).

QCD radiative corrections, affecting only the final state, are identical with those to the Z width,

$$\begin{aligned}\sigma_B^V &\rightarrow \sigma_B^V \left[1 + c_1 \left(\frac{\alpha_s}{\pi} \right) + c_2 \left(\frac{\alpha_s}{\pi} \right)^2 + c_3 \left(\frac{\alpha_s}{\pi} \right)^3 \right] \\ \sigma_B^A &\rightarrow \sigma_B^A \left[1 + d_1 \left(\frac{\alpha_s}{\pi} \right) + d_2 \left(\frac{\alpha_s}{\pi} \right)^2 + d_3 \left(\frac{\alpha_s}{\pi} \right)^3 \right]\end{aligned}\tag{2.14}$$

c_i, d_i are given in (3) to (4). The $\mathcal{O}(\alpha_s^3)$ corrections to the QED part have been evaluated [6] in the limit $m_q = 0$. They are different, however, for all four pieces in eq. (12) but cannot be discussed here (see e.g. Ref. 7).

Genuine electroweak corrections [12, 14, 15] include, besides the $\gamma - Z$ mixing and the vertex corrections, box diagrams in which initial and final state fermions are linked by two massive gauge bosons (WW and ZZ). The latter are of order $\frac{g_W^2}{4\pi^2}$ and, furthermore, they are not enhanced through the resonance. Close to the Z peak their influence is below $\mathcal{O}(10^{-4})$. The leading terms can be accounted for through eqs. (10-11).

Similarly to μ pair production, QED corrections are of utmost importance. As a consequence of the initial state photon radiation they have a strong influence on the cross section around the Z peak, cancel however largely when ratios of cross sections are taken.

This is demonstrated in Tab. 2.2 where the Born cross sections for $b\bar{b}$ and $\mu^+\mu^-$ at the peak [based on eq. (12) with $M_Z = 92$ GeV, $\Gamma_Z = 2.465$ GeV, $\sin^2 \theta_W = 0.234$, $\sqrt{s_{eff}} \geq 10$ GeV, $\alpha_s/\pi = 0.04$] is compared with the values when corrections from initial

	Born		$\mathcal{O}(\alpha)$		$\mathcal{O}(\alpha^2) + \text{expon.}$	
	$E_{\text{max}}[\text{GeV}]$	$\sigma_{\text{max}}[\text{nb}]$	$E_{\text{max}}[\text{GeV}]$	$\sigma_{\text{max}}[\text{nb}]$	$E_{\text{max}}[\text{GeV}]$	$\sigma_{\text{max}}[\text{nb}]$
$\sigma_{\mu\bar{\mu}}$	90.984	2.0090	91.166	1.4219	91.090	1.4834
$\sigma_{b\bar{b}}$	90.984	8.6882	91.167	6.1211	91.091	6.3880
$\frac{\sigma_{b\bar{b}}}{\sigma_{\mu\bar{\mu}}}$		4.3246		4.3049		4.3063

Tab. 2.2: Peak Cross sections for $\mu^+\mu^-$ and $b\bar{b}$ final states in Born approximation and including QED corrections.

state radiation to $\mathcal{O}(\alpha^1)$ and $\mathcal{O}(\alpha^2) + \text{exponentiation}$ [16] are included. Fig. 2.5 shows the s dependence of the $\mu^+\mu^-$, $b\bar{b}$, $c\bar{c}$ cross sections in the peak region and their ratios.

QED corrections from the interference between initial and final state emission plus the corresponding box amplitudes have been calculated at the parton level. Their effect on the total cross section is finite for vanishing fermion masses and thus not enhanced by large logarithms. The estimate of the correction is thus expected to be as reliable as the calculation for final state radiation. Including the full phase space for photon emission [17, 11] (for the cutoff dependence see Ref. [17]) the contribution to the total cross section from the $Z\gamma$ and $\gamma\gamma$ box amplitudes interfering with the Z and γ amplitude plus the corresponding real emission is given by

$$\begin{aligned}
\sigma^{Z\gamma\otimes Z} &= \frac{G_\mu^2 \alpha}{8\pi \pi} c_f Q_e Q_f v_e a_e v_f a_f \frac{m_Z^4 s}{|s - m_Z^2 + i\Gamma_Z m_Z|^2} \cdot \ln |s/(m_Z^2 - i\Gamma_Z m_Z)| \\
\sigma^{Z\gamma\otimes\gamma} &= \frac{G_\mu}{2\sqrt{2}} \frac{\alpha^2}{\pi} c_f Q_e^2 Q_f^2 a_e a_f \text{Re} \frac{m_Z^2 \ln[s/(m_Z^2 - i\Gamma_Z m_Z)]}{s - m_Z^2 + i\Gamma_Z m_Z} \\
\sigma^{\gamma\gamma\otimes Z} &= \frac{G_\mu}{2\sqrt{2}} \frac{\alpha^2}{\pi} c_f Q_e^2 Q_f^2 a_e a_f \frac{3}{2} \text{Re} \frac{m_Z^2}{s - m_Z^2 + i\Gamma_Z m_Z} \\
\sigma^{\gamma\gamma\otimes\gamma} &= 0
\end{aligned} \tag{2.15}$$

For $|\sqrt{s} - m_Z| \lesssim \Gamma_Z$ these terms are of order $\frac{\alpha}{\pi} \frac{\Gamma_Z}{m_Z}$ or below relative to the Born term. They will be neglected in the following.

In the preceding discussion quarks have been treated in the same way as leptons (modulo perturbative QCD effects). This appears adequate for inclusive quantities like the Z width and the total cross section and to some extent to the forward backward asymmetry. However, if photons are tagged, e.g. in order to apply cuts on the final-state configurations, the picture changes considerably. Adopting the arguments outlined above, we neglect initial-final state interference effects and analyze both domains separately.

– The characteristic features of initial state radiation are the same as in μ -pair production where it has been treated extensively [16], and these points need therefore not be repeated here.

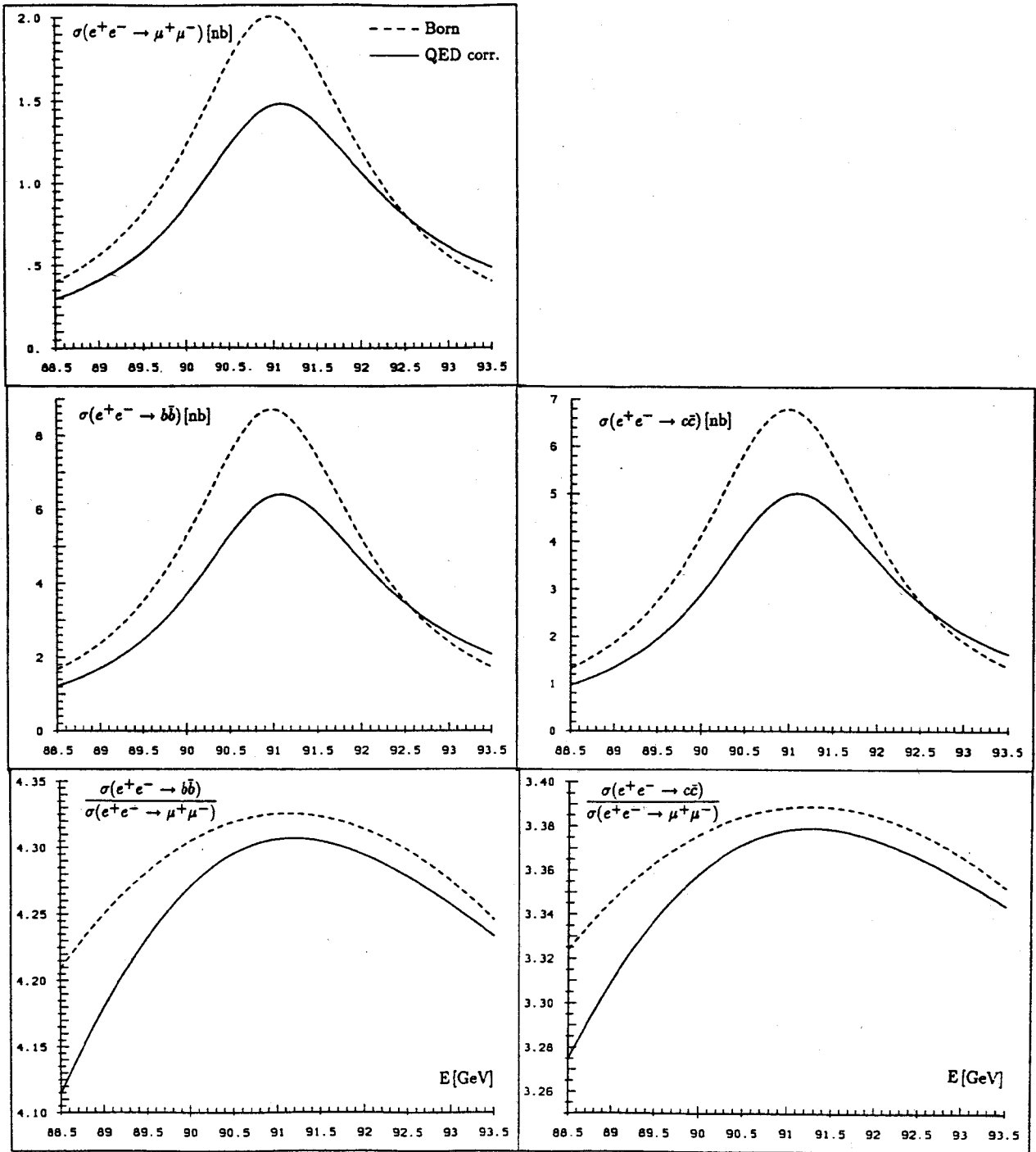


Fig. 2.5: Impact of QED corrections on the $\mu^+\mu^-$, $b\bar{b}$ and $c\bar{c}$ cross sections and on their ratio with parameters as described in the text. Dashed: without, solid: with QED corrections.

– For final state radiation

$$e^+e^- \xrightarrow{Z,\gamma} Q\bar{Q} + \gamma + \dots$$

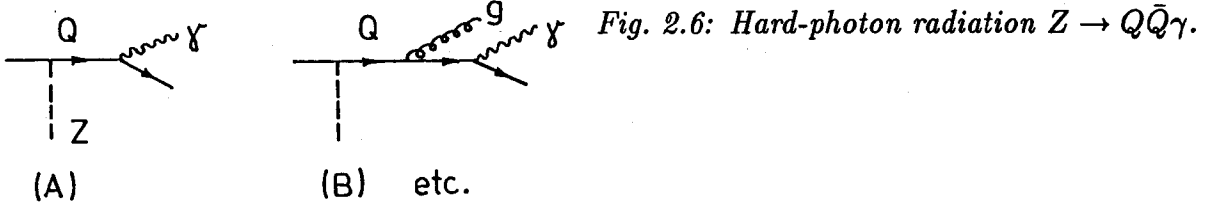
three different areas can be distinguished:

(i) Hard-photon radiation at large angles to the hadron jets is emitted from quarks at

short distances. The general radiation formula

$$\frac{1}{\sigma} \frac{d\sigma}{dx_\gamma dx_Q} = \frac{\alpha e_Q^2}{2\pi} \frac{x_Q^2 + x_{\bar{Q}}^2}{(1-x_Q)(1-x_{\bar{Q}})} \quad (2.16)$$

is adequate for this case [$x_\gamma = 2E_\gamma/\sqrt{s}$ etc.]. QCD radiative corrections are under control so long as the quark jets are defined sufficiently wide [18]. Additional gluon jet activities are either suppressed $\sim \alpha_s$ if they are emitted at times comparable to the γ emission (hard, large angles), or they are emitted at later times, forming a small angle with one of the quark jets, and thus do not affect the γ emission probability anymore.



(ii) *Hard-photon emission at small angles* may best be interpreted as a fragmentation process $Q \rightarrow \gamma + \dots$ where γ is one of the Q jet fragments. The spectrum following from (16), which corresponds to the pattern depicted in (A), is characterized by the typical bremsstrahl behaviour

$$D_Q^\gamma(x_\gamma, s)^{\text{BORN}} = \frac{\alpha e_Q^2}{2\pi} \frac{1 + (1-x_\gamma)^2}{x_\gamma} \log \frac{s}{m_Q^2}$$

However, gluon emission before γ radiation (B) degrades the Q beam energy and softens the γ spectrum. Summing all gluon emission probabilities, e.g. by means of Altarelli-Parisi type techniques, leads to the fragmentation function [19]

$$D_Q^\gamma(x_\gamma, s) = \frac{\alpha e_Q^2}{2\pi} d(x_\gamma) \log \frac{s}{m_Q^2} \quad (2.17)$$

The modified energy distribution is compared with the Weizsäcker-Williams spectrum in Fig. 2.7. [The degrading of the γ energy is most transparent for moments of the spectrum which are altered from $d(N)^{\text{BORN}}$ to $d(N) = d(N)^{\text{BORN}} / (1 + d_N^{NS})$ with d_N^{NS} being the non-singlet anomalous dimension.] Note that this treatment applies only to sufficiently hard γ 's as *gluon* $\rightarrow \gamma$ fragmentation, being a two-step process, has been neglected. A corollary follows from the angular distribution of the photon with respect to the flight direction of the parent quark Q

$$dN_\gamma \sim \frac{\theta^2 d\theta^2}{[\theta^2 + \gamma^{-2}]^2} \quad (2.18)$$

The angular distribution is effectively cut off for heavy currents at

$$\theta_c \lesssim \gamma^{-1} = m_Q/E_Q$$

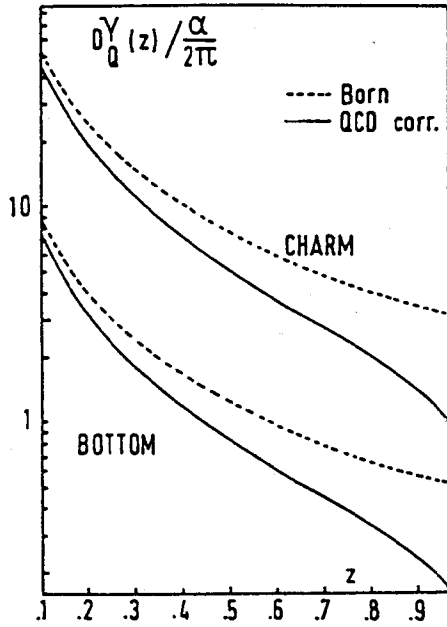


Fig. 2.7: Quark fragmentation into photons.

leaving a cone of aperture θ_c about the Q axis depleted from γ radiation. The photons are concentrated on the surface of the cone — with θ_c as large as 6° for bottom quark jets an interesting phenomenon.

(iii) *Soft-photons* can be radiated from a large variety of sources. All charged hadrons in the final state can emit infrared radiation with a spectrum determined by Low's theorem [20]. Gluon jets can emit soft γ 's. And last but not least soft quark-antiquark pairs before condensing into hadrons during the fragmentation process can emit radiation. From experimental analyses in hadron-hadron [21] and deep-inelastic muon-proton collisions [22] it must be concluded that this area is not well controlled at the present time. We therefore can only catalogue the radiation sources and prepare for experimental clarification by means of the excellent photon detectors at LEP.

Appendix

QCD radiative corrections to the vector and axial-vector part of the Z width [1, 2, 23], in the notation of Ref. 23:

$$c_1 = \frac{4}{3} \frac{1}{\beta(1 - \frac{1}{3}\beta^2)} \left[\left(1 - \frac{1}{3}\beta^2\right) A(\beta) + \frac{\beta}{4} (5 - 3\beta^2) - \frac{1}{24} (33 + 22\beta^2 - 7\beta^4) \log \frac{1-\beta}{1+\beta} \right] \quad (2.19)$$

$$d_1 = \frac{4}{3} \frac{1}{\beta^3} \left[\beta^2 A(\beta) + \frac{3\beta}{16} (\beta^4 + 10\beta^2 - 7) - \frac{1}{32} (21 + 59\beta^2 + 19\beta^4 - 3\beta^6) \log \frac{1-\beta}{1+\beta} \right] \quad (2.20)$$

with

$$A(\beta) = (1 + \beta) \left[\frac{\pi^2}{6} + 2 \log \frac{1+\beta}{2} \log \frac{1+\beta}{1-\beta} + 2Li\left(\frac{1-\beta}{1+\beta}\right) - 2Li\left(\frac{1+\beta}{2}\right) - 4Li(\beta) + Li(\beta^2) \right] + 3\beta \log \frac{1-\beta^2}{4\beta} - \beta \log \beta$$

$$Li(x) = - \int_0^x \frac{dt}{t} \log(1-t)$$

2.1.3. FORWARD-BACKWARD ASYMMETRY

The production cross section for quarks tagged at the angle ϑ

$$e^+e^- \xrightarrow{Z,\gamma} Q(\vartheta) + \dots$$

is a binomial in $\cos \vartheta$ [2]

$$\frac{d\sigma}{d\cos\vartheta} = \frac{3}{8}(1 + \cos^2\vartheta)\sigma_U + \frac{3}{4}\sin^2\vartheta\sigma_L + \frac{3}{4}\cos\vartheta\sigma_F \quad (2.21)$$

U and L denote the contribution of unpolarized and longitudinally polarized gauge bosons along the ϑ axis, and F denotes the difference between right and left polarizations. After separation of higher-order QED effects, a non-zero σ_F ensues from vector-axial vector interference. The total cross section is the sum of U and L ,

$$\sigma = \sigma_U + \sigma_L \quad (2.22)$$

The forward-backward asymmetry for a fixed angle ϑ vs. $\pi - \vartheta$ can be cast into the form

$$A^{FB}(\vartheta) = \frac{2\cos\vartheta}{1 + \alpha_Q \cos^2\vartheta} \beta_Q \quad (2.23)$$

with the parameters

$$\alpha_Q = \frac{\sigma_U - 2\sigma_L}{\sigma_U + 2\sigma_L} \quad \beta_Q = \frac{\sigma_F}{\sigma_U + 2\sigma_L} \quad (2.24)$$

Integrated out, the asymmetry simplifies to

$$A^{FB} = \frac{3}{4} \frac{\sigma_F}{\sigma} \quad (2.25)$$

In Born approximation the cross sections σ_i can be expressed in terms of the cross sections σ^{VV} and σ^{AA} introduced earlier in eqs. (12)

$$\begin{aligned} \sigma_B^U &= \beta\sigma^{VV} + \beta^3\sigma^{AA} \\ \sigma_B^L &= \frac{1}{2}(1 - \beta^2)\beta\sigma^{VV} \\ \sigma_B^F &= \beta^2\sigma^{VA} \end{aligned} \quad (2.26)$$

and

$$\begin{aligned} \sigma^{VA} &= \frac{G_\mu \alpha(m_Z^2)}{\sqrt{2}} e e_Q a_e a_Q \frac{m_Z^2(s - m_Z^2)}{(s - m_Z^2)^2 + (\frac{s}{m_Z} \Gamma_Z)^2} \\ &+ \frac{G_\mu^2}{8\pi} v_e v_Q a_e a_Q \frac{m_Z^4 s}{(s - m_Z^2)^2 + (\frac{s}{m_Z} \Gamma_Z)^2} \end{aligned} \quad (2.27)$$

On top of the Z resonance the asymmetry reduces to the well-known approximate form

$$A_B^{FB} = \frac{3}{4} \frac{2v_e a_e}{v_e^2 + a_e^2} \frac{2v_Q a_Q \beta}{v_Q^2 (3 - \beta^2)/2 + a_Q^2 \beta^2} \quad (2.28)$$

$$\approx \frac{3}{4} \frac{2v_e a_e}{v_e^2 + a_e^2} \frac{2v_Q v_Q}{v_Q^2 + a_Q^2} (1 + \delta)$$

As a consequence of an accidental cancellation among the couplings ($v_b^2 \approx a_b^2/2$) the mass correction $\delta \simeq \mu^2(-v_Q^2 + a_Q^2/2)/(v_Q^2 + a_Q^2)$ is strongly suppressed to $\mathcal{O}(10^{-4})$. Based on the Born approximation the expected asymmetries for c, b quarks on the Z peak ($m_Z = 91 \text{ GeV}$, $\sin^2 \theta_W = 0.234$) are

$$A^{FB}(c) \approx 0.061$$

$$A^{FB}(b) \approx 0.085$$

and the energy dependence is given in Fig. 2.8

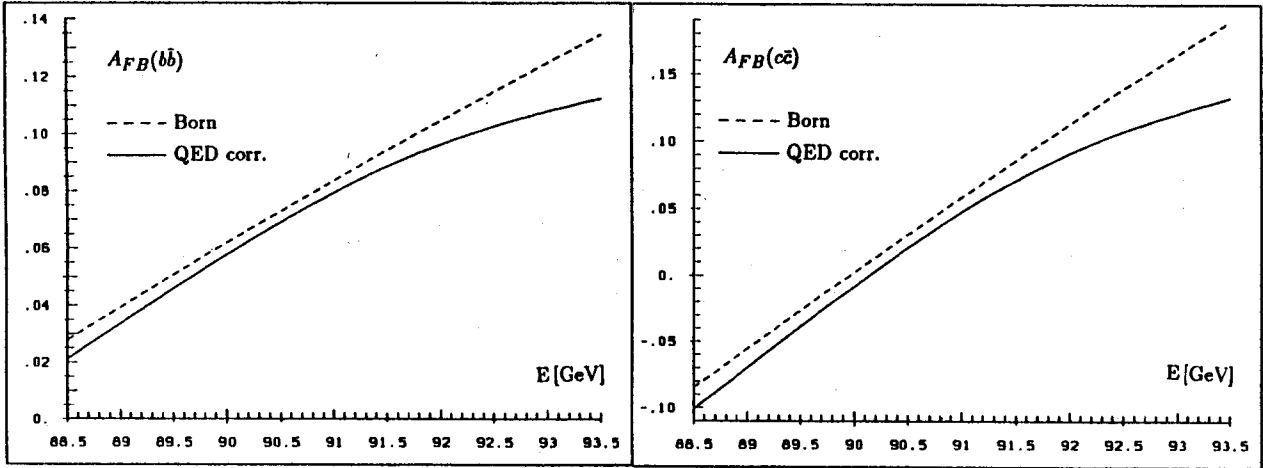
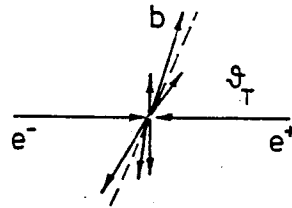
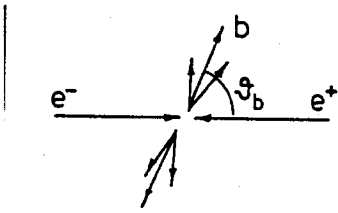


Fig. 2.8: Forward-backward asymmetry for $b\bar{b}$ and $c\bar{c}$ production with the same parameters as Fig. 2.5 [without QCD corrections]. Dashed: without, solid: with QED corrections.

QED and QCD corrections make a proper definition of the scattering angle ϑ mandatory. We shall use two different definitions which are appropriate for heavy quark production:

- (1) b quark direction: $e^+e^- \rightarrow b(\vartheta_b) + \dots$ (2) thrust axis: $e^+e^- \rightarrow j_b(\vartheta_T) + j$



QCD corrections for the semiinclusive definition of the scattering angle are known to 1st order for non-zero quark masses [2]. The rather clumsy expression can well be approximated [3] by an expansion in $\mu = 2m_Q/\sqrt{s}$,

$$\sigma_B^F \rightarrow \sigma_B^F \left[1 + f_1^F \left(\frac{\alpha_s}{\pi} \right) \right] \quad (2.29)$$

$$f_1^F = \frac{2\pi}{3}\mu + \frac{2\mu^2}{3} \left[\frac{9}{2} + \frac{\pi^2}{8} + \frac{1}{8} \left(\log \frac{\mu^2}{4} \right)^2 - \frac{3}{2} \log \frac{\mu^2}{4} - \frac{5}{2} \log 2 \right] \quad (2.30)$$

i.e. the first order correction to σ_F vanishes in the zero-mass limit. We therefore find for the correction to the asymmetry

$$A_B^{FB} \rightarrow A^{FB} = A_B^{FB} \left[1 - \frac{\alpha_s}{\pi} \left(1 - \frac{2\pi}{3}\mu \right) \right] \quad (2.31)$$

with the leading part due to the change of the normalization.

If ϑ_b is not summed over, we also need the corrections for the vector and axial-vector parts of the U and L terms separately. Setting

$$\begin{aligned} \sigma^U &= \left[\beta + \frac{\alpha_s}{\pi} f_1^U(VV) \right] \sigma^{VV} + \left[\beta^3 + \frac{\alpha_s}{\pi} f_1^U(AA) \right] \sigma^{AA} \\ \sigma^L &= \left[\frac{\beta}{2}(1 - \beta^2) + \frac{\alpha_s}{\pi} f_1^L(VV) \right] \sigma^{VV} + \frac{\alpha_s}{\pi} f_1^L(AA) \sigma^{AA} \end{aligned} \quad (2.32)$$

we find

$$\begin{aligned} f_1^U(VV) &= f_1^U(AA) = 1/3 \\ f_1^L(VV) &= f_1^L(AA) = 2/3 \end{aligned} \quad (2.33)$$

in the zero-mass limit. Expansions in μ may be taken from the Appendix.

Reference axis : thrust / b -quark axis				
	y	k_2	k_F	k_A
$m_c = 1.5 \text{ GeV}$	0.02	-11.25	-11.43	-0.18
	0.04	-6.12	-6.41	-0.30
	0.08	-2.36	-2.86	-0.50
$m_b = 4.5 \text{ GeV}$	0.02	-11.60	-11.80	-0.20
	0.04	-6.17	-6.39	-0.23
	0.08	-2.30	-2.68	-0.39

Tab. 2.3: QCD corrections to 2-jet cross sections and forward-backward asymmetries.

For the thrust axis (or the b -quark axis) chosen as the reference axis in 2-jet events, the QCD corrections [24] are tabulated in Tab. 2.3. The two-jet cross section is defined

m_Z	m_t	10	100	1000
91	50	0.0846	0.0796	0.0725
91	100	0.0903	0.0853	0.0783
91	150	0.0983	0.0933	0.0864
91	200	0.1088	0.1039	0.0972
91	230	0.1163	0.1114	0.1049
92	50	0.1243	0.1194	0.1127
92	100	0.1298	0.1250	0.1183
92	150	0.1373	0.1325	0.1260
92	200	0.1473	0.1426	0.1362
92	230	0.1544	0.1497	0.1435

m_Z	m_t	10	100	1000
91	50	0.0842	0.0792	0.0721
91	100	0.0898	0.0849	0.0779
91	150	0.0975	0.0925	0.0858
91	200	0.1072	0.1024	0.0959
91	230	0.1140	0.1039	0.1029
92	50	0.1237	0.1189	0.1121
92	100	0.1291	0.1243	0.1177
92	150	0.1363	0.1316	0.1252
92	200	0.1455	0.1409	0.1347
92	230	0.1519	0.1473	0.1413

m_Z	m_t	10	100	1000
91	50	0.0601	0.0563	0.0511
91	100	0.0643	0.0606	0.0554
91	150	0.0703	0.0665	0.0614
91	200	0.0783	0.0745	0.0694
91	230	0.0841	0.0804	0.0753
92	50	0.0907	0.0869	0.0816
92	100	0.0950	0.0912	0.0860
92	150	0.1010	0.0972	0.0920
92	200	0.1090	0.1052	0.1001
92	230	0.1148	0.1110	0.1059

Tab. 2.4: Forward-backward asymmetry, consecutively, for $d\bar{d}$, $b\bar{b}$ and $c\bar{c}$ ($m_H = 10, 100, 1000$ GeV) [QED and QCD corrections not included].

for all events in which the invariant masses of the jets are less than a fraction \sqrt{y} of the total energy,

$$\begin{aligned}\sigma(2 \text{ jet}) &= \sigma[m^2 \leq ys] \\ &= \sigma_B \left[1 + k_2 \left(\frac{\alpha_s}{\pi} \right) \right]\end{aligned}$$

For small y , k_2 is large and negative — due to cutting out infrared and collinear gluon bremsstrahlung. A nearly identical loss however affects σ_F as well and as a result, the corrections to the asymmetry

$$A^{FB}(2 \text{ jet}) = A_B^{FB} \left[1 + k_A \left(\frac{\alpha_s}{\pi} \right) \right]$$

remain small as intuitively anticipated.

Genuine electroweak corrections to the c, b asymmetries are widely spread over the parameter set underlying Tab. 2.4 [12]. For $m_Z = 92$ GeV the variation amounts to 0.04 between the minimal and maximal values A_b^{FB} . As shown in Fig. 2.5, the effective Born approximation leads to fairly accurate description also for the quark asymmetries.

The impact of QED corrections on A_{FB} for $b\bar{b}$ final states can be treated at the parton level in a way similar to the discussion of A_{FB} for muons. For completeness we shall repeat the points which are most relevant in this context.

Final state radiation is treated in complete analogy to gluon radiation. Defining the scattering angle through the direction of the b quark (as adopted above) the asymmetry is reduced by a factor $(1 + \frac{3}{4}Q_b^2\frac{\alpha}{\pi})^{-1}$ through the increase in the overall normalization, an effect completely negligible.

Analytical results for the influence of the *interference* between γ -emission from the initial and final states can be found in [11, 25]. Although two different definitions of the scattering angle are adopted, the effect is found to be negligible, just as for the total cross section. Around the Z peak the corrections are of relative order $< \frac{\alpha}{\pi}(\Gamma_Z/m_Z)$.

The influence of *initial state radiation* is strongly energy dependent. It is modest below and on top of the Z peak. A full treatment, including the impact on the kinematics and the change of the effective energy can only be performed in a Monte Carlo calculation. Approximate formulae have been developed for the μ -pair asymmetry, which are based on the approximation of collinear radiation and which are accurate to better than 0.3×10^{-2} . They can easily be improved to include also multiple photon emission. Without any cut on the photon energy [25, 26] (see also [27])

$$\langle A_{FB} \rangle = \frac{3}{4} \frac{\int_0^1 dz F(s, z) (\frac{1-z}{1+z})^2 \sigma_F(s, z)}{\int_0^1 dz F(s, z) \sigma(s, z)} \quad (2.34)$$

To $\mathcal{O}(\alpha)$, the distribution $F(s, z)$ is given by the Bonneau-Martin formula, to $\mathcal{O}(\alpha^2)$ – including exponentiation – $F(s, z)$ is given in [16]. The result is compared to the Born prediction in Fig. 2.8. For \sqrt{s} about 200 MeV above m_Z the corrected asymmetry coincides with $A_{FB}^0(m_Z)$ (see also Ref. 28, Table 4.1).

Mixing. Forward-backward asymmetries of quarks are extracted by measuring the asymmetries of mesons and baryons endowed with this particular quark flavour. For b quarks this is not a one-to-one correspondence due to mixing in the neutral B_d^0 and B_s^0 system [29]. Because associated production of $b\bar{b}$ -pairs in the jet development, perturbatively as well as non-perturbatively, can safely be neglected, the hadronic asymmetries are related to the asymmetry of the primarily produced b quarks in the following way.

(i) *b tagging through B_u^- , Λ_b :*

$$A^{FB}(B_u^-, \Lambda_b) = A^{FB}(b) \quad (2.35a)$$

(ii) *b tagging through \bar{B}_d^0 or \bar{B}_s^0 :*

These particles mix with their partners $\bar{B}_d^0 \leftrightarrow B_d^0$ and $\bar{B}_s^0 \leftrightarrow B_s^0$ so that the b flavour is changed at a rate comparable or much more frequent than the decay rate for \bar{B}_d^0 and

\bar{B}_s^0 , respectively. Denoting the time-integrated probability for observing a B_q^0 particle in a beam of originally produced \bar{B}_q^0 particles by χ_q , these parameters have been measured [30, 31] for B_d^0

$$\chi_d = 0.17 \pm 0.05$$

or are bounded strongly in the Standard Model by

$$\chi_s \geq 0.45$$

Mixing reduces the observed asymmetry so that

$$A^{FB}(\bar{B}_q^0) = (1 - 2\chi_q)A^{FB}(b) \quad (2.35b)$$

While the impact of B_d mixing is already quite noticeable $\sim 35\%$, the asymmetry in the B_s system is almost completely washed out.

(iii) *b tagging through ℓ^-* :

Denoting the probability to find a \bar{b} quark in a b beam by $\bar{\chi}$, a weighted mixture of B_d and B_s mixing parameters, this probability is directly measurable in the like-sign dilepton rate,

$$R_{\ell\ell} = \frac{\ell^\pm \ell^\pm}{\text{all } \ell\ell} = 2\bar{\chi}(1 - \bar{\chi})$$

With $\bar{\chi} = 0.12 \pm 0.05$ [32] the ensuing lepton asymmetry

$$\begin{aligned} A^{FB}(\ell^-) &= (1 - 2\bar{\chi})A^{FB}(b) \\ &= \sqrt{1 - 2R_{\ell\ell}}A^{FB}(b) \end{aligned} \quad (2.35c)$$

is reduced to $\sim 75\%$ of the original b quark asymmetry.

Appendix

Mass dependence of the QCD corrections to the polarized cross sections, completing eqs. (33)(from [3]):

$$\begin{aligned} f_1^U(VV) &= \frac{1}{3} + \mu \frac{\pi^2}{6} + \mu^2 \left[\frac{11}{3} + \frac{23}{6} \log \frac{\mu^2}{4} + t \right] \\ f_1^U(AA) &= \frac{1}{3} + \mu \frac{\pi^2}{6} + \mu^2 \left[\frac{5}{3} + \frac{11}{6} \log \frac{\mu^2}{4} + t \right] \\ f_1^L(VV) &= \frac{2}{3} - \mu \frac{\pi^2}{6} - \mu^2 \left[\frac{2}{3} + \frac{23}{6} \log \frac{\mu^2}{4} + t \right] \\ f_1^L(AA) &= \frac{2}{3} - \mu \frac{\pi^2}{6} - \mu^2 \left[\frac{19}{6} + \frac{29}{6} \log \frac{\mu^2}{4} + t \right] \end{aligned}$$

$$t = \frac{\pi^2}{9} + \frac{1}{3} \log 2 + \frac{1}{12} \log \frac{\mu^2}{4}$$

2.1.4. FINAL STATE POLARIZATION

Due to the parity violation of the electroweak interactions, quarks are produced with non-zero polarization in e^+e^- annihilation. For “light” heavy flavours (c, b), only the longitudinal component along the flight direction is sufficiently large [33] to be accessible experimentally, while transverse and perpendicular components are suppressed $\sim m_Q/m_Z$. For $\sqrt{s} = m_Z$ and neglecting non-zero-mass corrections the variation of the longitudinal polarization with the scattering angle ϑ is given by

$$P_L(\vartheta) = -\frac{\lambda_Q(1 + \cos^2 \vartheta) + \lambda_e \cdot 2 \cos \vartheta}{(1 + \cos^2 \vartheta) + \lambda_e \lambda_Q \cos \vartheta} \quad (2.36)$$

where $\lambda_Q = 2v_Q a_Q / (v_Q^2 + a_Q^2)$ etc. Because the Z vector coupling to electrons is small, the variation with ϑ is moderate and, in contrast to the τ polarization, the average value ($\sin^2 \theta_W = 0.23$)

$$P_L = -\lambda_Q = \begin{cases} -0.68 & \text{for charm} \\ -0.94 & \text{for bottom} \end{cases} \quad (2.37)$$

provides an adequate approximation. Thus the longitudinal quark polarizations are almost maximal.

The observable polarization is strongly affected by the hadronization. Assuming 100% longitudinal quark polarization, one expects *vector and pseudoscalar mesons* to be produced with the relative proportion 50:25:0:25 for the different spin configurations $[S, S_z] = [1, 1] : [1, 0] : [1, -1] : [0, 0]$. Similar relations could be derived for baryons. Experimentally little is known about the spin transfer in hard reactions.

A variety of decay modes have been investigated to measure the baryon polarization, in particular for Λ_c . The semileptonic $\Lambda_c \rightarrow \Lambda \ell^+ \nu_\ell$ decay [34] as well as the nonleptonic decays [35] appear to be promising candidates.

Besides the parity-violating polarization itself, spin-spin corrections between quarks and antiquarks have been studied. The formalism is somewhat involved and we refer to the original papers [33, 36] for details.

2.1.5. HEAVY QUARK MONTE CARLOS

Monte Carlo programs which have been developed for muon, tau or light quark pair final states can, to a limited extent, be adopted to describe also heavy flavour production. These programs [see table] which put the emphasis on the highly accurate treatment of QED effects and of electroweak corrections, include (at present) non-zero quark mass effects only on the kinematical level. By a simple modification, however, the correct matrix elements can be included for the Born cross sections.

The influence of mass effects on electroweak corrections is negligible in general for charm and bottom, with the notable exception of vertex corrections from virtual top

	Mass	Spin	QED	ELW	Fragmentation
Mustraal [37]	not incl.	not incl.	α^1	not incl.	not incl.
KoralZ [38]	not incl.	incl.	$ini : \alpha^1 + YFS$ $fin : \alpha^1$ $ini - fin : \alpha^1$	incl. ($q \neq b!$)	not incl.
Tiptop [39] t, b', \dots		incl.	$ini : \alpha^1$	not incl.	"Lund"

Tab. 2.5: Monte Carlo Implementations.

exchange (cf. Fig. 2.3) in $b\bar{b}$ final states.

To simulate the production of hadrons these programs have to be linked to fragmentation programs like the Lund package, Eurojet or Herwig. QCD loop corrections to the forward-backward asymmetry are not reproduced this way. However, because the resulting changes amount to about 0.004 and because they can be accounted for analytically, this is not of immediate concern. Spin effects are not accounted for.

A complementary strategy has been implemented in the program TIPTOP which is specifically designed to describe the production of extremely heavy fermion pairs like top, the members of a fourth family or exotic fermions in horizontal extensions of the Standard Model. Initial state radiation is included and the decay of the heavy (anti-)fermion into three lighter ones through charged current interactions is implemented. The effect of the W propagator is included as well as all spin correlation⁴ which for heavy quarks may survive the hadronization process with a depolarization factor f . f ranging from 0 in the case of a b' with strongly suppressed CC decay, to $\sim 1/2$ for top in the LEP range, and even up to ~ 1 for $m_t \gtrsim 125$ GeV when the weak decay time undercuts the hadronization time.

The program is easily adapted to the production of exotic fermions (see e.g. Ref. 40 for heavy neutrinos) as long as the particle decays into three fermions through a current-current interaction. Neither final state QED radiation nor weak corrections are incorporated – not a severe restriction in view of the exploratory nature of such an investigation. Exotic decay modes like $t \rightarrow H + b$ or flavour changing neutral current decays of b' to $b + g$ or γ are not included in the present versions of the Monte Carlo programs.

2.2. CROSS SECTIONS AND CHARGE ASYMMETRIES: EXPERIMENTAL PREVIEW*

During the coming years several hundred-thousand $c\bar{c}$ and $b\bar{b}$ events will be accumulated at the Z^0 resonance, and high-statistics measurements of the cross section and of the charge asymmetry for individual heavy flavours will become possible. These measurements are part of the LEP experimental programme, one of the goals of which is to test the parameters of the standard model.

In previous sections expressions have been derived which relate the cross section and the asymmetry to the weak vector and axial-vector couplings and to $\sin^2 \theta_W$, and contributions not included in the Born approximation, from QED, higher-order weak effects and from QCD, have also been discussed. This section is devoted to experimental aspects only. The various methods to tag heavy flavours will be reviewed and the main sources of systematic errors enumerated. To a large extent these errors are due to our lack of knowledge of QCD, quark fragmentation and of detailed decay properties in the heavy quark sector; however, in the coming years some of these uncertainties will gradually decrease, and the interpretation of the high-statistics measurements as a test of the standard model will become possible.

Most methods for tagging heavy flavours are familiar from former, lower-energy experiments, and in many respects the LEP environment is similar to that of PEP, PETRA and TRISTAN. It is true that the complexity of hadronic final states will increase with energy (more gluon radiation, a higher track multiplicity); but, on the other hand, the definition of jets will be more pronounced and the separation of the events into a quark and an anti-quark hemisphere will become easier, a clear bonus for asymmetry measurement. A further advantage of the increased c.m.s. energy for heavy flavour physics is the boosted decay-length of c and b quarks. D and B mesons will travel several millimeters before their decay, and the experiments are equipped to recognize secondary vertices. Tagging by means of the decay-length will become a common tool, with an efficiency comparable to other methods employed in the past. In the next section we summarize the various tagging methods which are likely to play a role in LEP experiments. Efficiencies and sample purities will be quoted, but these have to be taken as estimates rather than at their face-value; even more so for the quoted systematic errors which may strongly vary from one experiment to the other and which are, in practice, the outcome of a long and tedious learning process. The tagging methods will then be discussed in the context of the $b\bar{b}$ and $c\bar{c}$ cross-section and asymmetry measurements. The recent observation of $B^0 - \bar{B}^0$ mixing has serious implications for the interpretation of the $b\bar{b}$ asymmetry which will also

*P. IGO-KEMENES *in collaboration with* K. MÖNIG, H.-G. MOSER, J.L PINFOLD, R. SETTLES, S. ÜBERSCHÄR

be briefly discussed.

2.2.1. METHODS OF TAGGING HEAVY FLAVOURS.

High p_t Leptons

In the past, high p_t leptons from semi-leptonic decays have played an outstanding role in the tagging of heavy flavours. The p_t distribution of the lepton (Fig. 2.9) reflects the high mass of the b (and c) quarks and is thereby an excellent separation variable. Electrons are identified by comparing the calorimeter energy to the track-momentum ($E/P \approx 1$) and by the specific ionization (dE/dx) in the tracking-chamber gas, and muons by their traversal of the muon filter (hadron calorimeter) and by a track in the outside muon chambers.

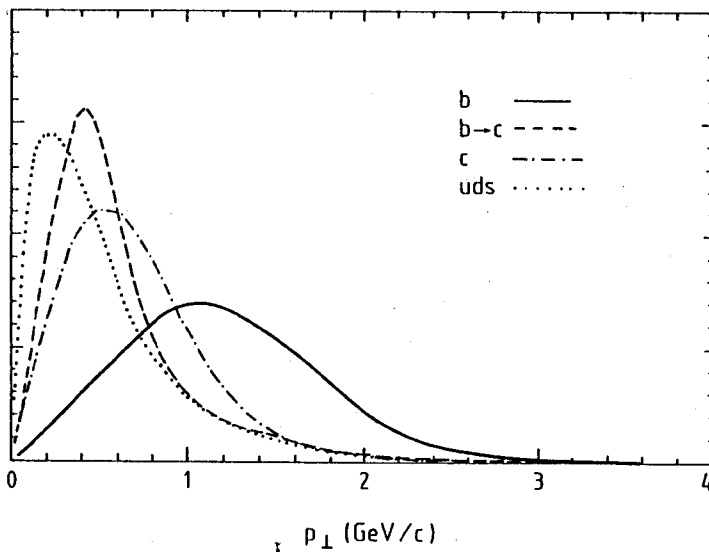


Fig. 2.9: Unnormalized lepton p_t distributions for separated flavours.

Misidentified, fake leptons, from gamma conversions, hadronic "punchthrough", pion and kaon decays, are strongly suppressed by requiring a high momentum ($P > 3$ GeV typically) for the lepton. However, misidentification of leptons remains a source of confusion and cannot be dismissed from being a source of systematic error. The p_t of the lepton is determined with respect to the main event axis (e.g. the thrust axis) which reproduces with good accuracy (5 to 10 degrees) (Fig. 2.10) the direction of the quark anti-quark pair before gluon radiation and defines the polar angle of the event for the asymmetry measurement.

By using the lepton p_t as a selection variable one obtains typical tagging efficiencies for $b\bar{b}$ events of 20% with a sample purity of 75%. The remaining background consists of $c\bar{c}$ (5%) and of light quark pairs (20%). These numbers* are subject to an uncertainty of about 10%, the dominant reasons being the error on the event axis (which influences the

*Throughout this section the numbers quoted without explicit reference are the result of discussions with representatives of the various LEP experiments.

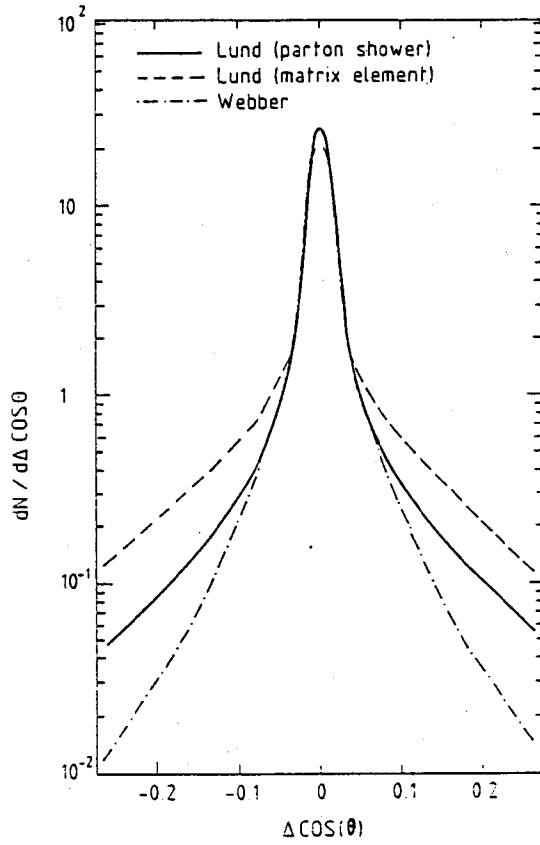


Fig. 2.10: Comparison of the $q\bar{q}$ direction and the thrust axis. The three distributions of $\cos\theta(q\bar{q}) - \cos\theta(\text{thrust})$ correspond to different fragmentation schemes; from Ref. 41.

lepton p_t and thereby the tagging efficiency), lacking knowledge of the b -fragmentation function, and misidentified leptons. The experimental error on the inclusive semi-leptonic branching ratio, $BR(b \rightarrow c l \nu) = (11.8 \pm 0.5)\%$ [42], is not included.

Another variable of discrimination, used in connection with high- p_t leptons, is the transverse mass [42] :

$$M_t = \frac{\sqrt{s} \Sigma(E_i^{\text{out}})}{2E_{\text{vis.}}} \quad (2.38)$$

where E_i^{out} is the transverse energy of particle "i", or the component not contained in the main event plane. The sum goes over all tracks except the high- p_t lepton. By excluding the lepton, the two separation variables, p_t and M_t are fairly uncorrelated. To first order, M_t also measures the mass of the primary quark, and its use in connection with the lepton p_t improves the flavour separation.

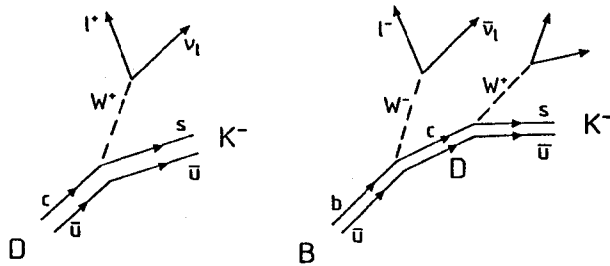


Fig. 2.11: D and B meson decay schemes according to the spectator model.

To obtain a sample enriched in $c\bar{c}$ events requires more involved techniques, as the rate of semi-leptonic c -decays is disfavoured, both by a lower cross-section at the Z^0

and by a smaller semi-leptonic branching ratio [42]: $BR(c \rightarrow sl\nu) = (8.6 \pm 0.9)\%$. The LEP detectors have various means to identify particles; in particular, the identification of charged kaons seems possible over an extended momentum range (see e.g. Ref. 43 for the DELPHI detector). In $c\bar{c}$ events, the high- p_t lepton is often accompanied by a high-momentum kaon of opposite electric charge (Fig. 2.11). (Alternatively, kaons from the $b \rightarrow cl\nu$, $c \rightarrow s$ cascade have the same electric charge as the lepton and lower momenta). Thus, the requirement of a lepton-kaon pair of opposite (same) electric charge in the same hemisphere is a means to tag $c\bar{c}$ ($b\bar{b}$) events. The following results have been obtained [41]:

Flavour	Tag. Efficiency	Purity
$c\bar{c}$	3.6%	65%
$b\bar{b}$	8.7%	90%

Tab. 2.6: Tagging with high- p_t leptons (no detector effects).

Uncertainties have been estimated in part by comparing various fragmentation models; these amount to about 35% for the $c\bar{c}$ tagging efficiency and to 7% for $b\bar{b}$.

Tagging with D-mesons

The presence of D-mesons in the final state is another tag for heavy flavours. For $c\bar{c}$ events, the decay chains $D^{*+} \rightarrow D^0\pi^+$, $D^0 \rightarrow K^-\pi^+$ or $D^0 \rightarrow K^-\pi^+\pi^-\pi^+$ (or their charge-conjugates), have a probability of about 5% to occur [44]. Due to a favourable kinematic effect, these final states can be reconstructed with good efficiency: they appear as a sharp peak (Fig. 2.12) in the D^*-D^0 mass difference, on top of a continuous spectrum of combinatorial background. In practice, D^* s are also produced by $b\bar{b}$ events through the $b \rightarrow c$ cascade, but the two contributions can be separated by using the D^0 -meson momentum-distribution which shows pronounced differences (Fig. 2.13). Typically, a $c\bar{c}$ tagging efficiency of 2% and a sample purity of 65% can be achieved [43]. These numbers are subject to large errors, of about 30%, due to the uncertainty from fragmentation and from the various branching ratios involved in the cascades.

Secondary Vertices

To tag heavy flavours by detecting secondary vertices is a technique which can be applied without restricting the sample to semi-leptonic decays or to another particular final state; it is therefore of high interest for the measurement of cross sections. The B and D mesons produced at LEP energies have typical decay lengths of 2 to 3 millimeters, and tracks originating from secondary vertices are recognized by the high-resolution vertex-detectors,

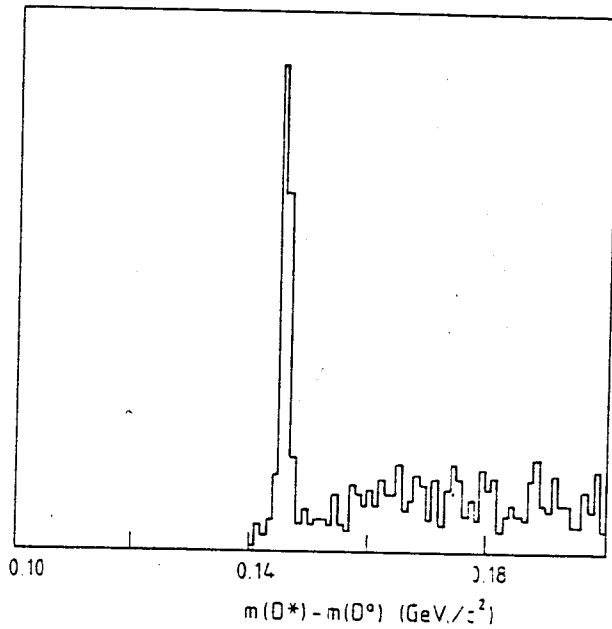


Fig. 2.12: The $D^* - D^0$ mass difference reconstructed in $D^0 \rightarrow K^- \pi^+$ channel; from Ref. 43.

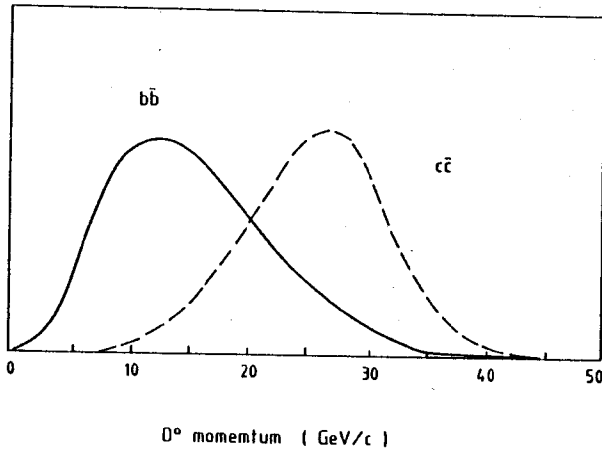


Fig. 2.13: D^0 momentum distributions for $b\bar{b}$ and $c\bar{c}$ events. The mean momenta are 15 GeV and 26 GeV, respectively [45].

which cover about 80% of the geometrical acceptance. Despite the unfavourable, large radius of the beampipe (8 cm in the first phase of LEP) and the effect of multiple scattering, secondary vertices can be measured with a typical space resolution of 250 microns and can thus be resolved from the primary interaction point. In fact, for tagging heavy flavours, it is not necessary to actually reconstruct secondary vertices. Simpler and thus more efficient ways have been considered [45], [46] and lead to sizeable tagging efficiencies. A possible algorithm uses the weighted average (weighted by the measurement error) of the "N" (typically 3) largest impact parameters (Fig. 2.14) to discriminate against light quarks. The method is not efficient to discriminate between $b\bar{b}$ and $c\bar{c}$ events as can be easily understood from the figure. For $(b+c)$, a tagging efficiency of about 25% can be reached, with a residual background of 20% from light quarks [46]. The tagged sample contains 26% of the $b\bar{b}$ and 14% of the $c\bar{c}$ events. The uncertainty on the efficiency is estimated to 20%, and is mainly due to the lack of knowledge of the B-lifetimes: $\tau = (13.1 \pm 1.4)10^{-13}$ sec [44].

More sophisticated methods, combining the information from secondary vertices with

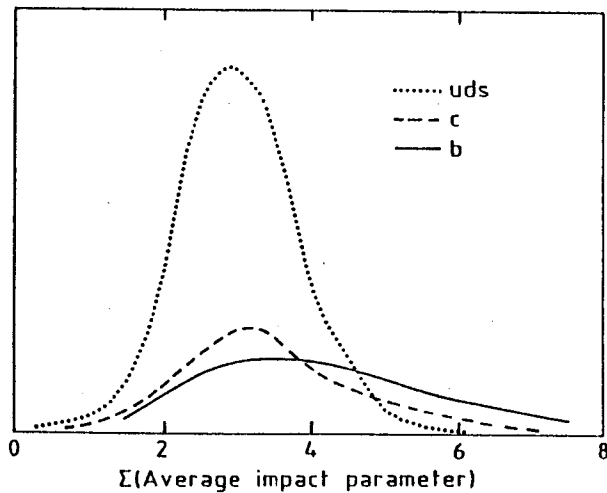


Fig. 2.14: Average of the three largest impact parameters in units of the experimental resolution. Unnormalized distributions; from Ref. 46. A similar distribution can be found in Ref. 45.

several other separation variables, have also been proposed [45]. Monte Carlo studies seem to indicate a good efficiency for tagging $b\bar{b}$ and $c\bar{c}$ events separately; however, the performance of these methods in practice has yet to be proven.

To summarize, large fractions of heavy-flavour events produced at the Z^0 resonance can be isolated, by the use of high- p_t leptons, D^* -decays, or by using the finite decay-length of B and D mesons. The resulting samples are rich in $b\bar{b}$ events and contain some contamination from $c\bar{c}$ and from light quarks. It is more laborious to obtain a $c\bar{c}$ sample of high purity, the $c\bar{c}$ production being disfavoured at the Z^0 resonance. The most promising method is the reconstruction of the $D^* - D^0$ cascade and the selection of c flavour by requiring a high D^0 momentum.

The tagging efficiencies are subject to sizeable uncertainties. Apart from the various instrumental effects (e.g. fake leptons, pion-kaon confusion, track confusion in the vertex detector ...), one has to consider the lack of precise knowledge of many physics ingredients such as: inclusive semi-leptonic branching ratios, B and D meson production rates, lifetimes and decay branching ratios and, in general, details of QCD and the hadronization process. Today, and in the first year of LEP, these uncertainties will limit the precision of cross-section and asymmetry measurements in the heavy flavour sector; however, the situation is bound to improve as large samples of Z^0 decays will be analysed and the fragmentation models tuned to describe more closely the data.

The various tagging methods can be used separately or in conjunction with each other. It is important to note the widely differing nature of their uncertainties.

2.2.2. CROSS SECTIONS

The large uncertainties related to the tagging of heavy flavours affect directly the precision one can hope to achieve for the $b\bar{b}$ and $c\bar{c}$ cross-sections. Other contributions, from the acceptance and from the luminosity measurement are much smaller.

The cross section for a given flavour "f" is obtained from the expression

$$\sigma_{f\bar{f}} = N(1 - \beta)/L\varepsilon, \quad (2.39)$$

where N is the number of events in the selected sample, β the fraction of background events, L the integrated luminosity and ε the combined geometric and selection efficiency. β and ε are obtained from Monte Carlo simulation, including all details of the detector, initial-state bremsstrahlung, QCD effects and fragmentation. Needless to say that the cross section one derives from the measurement is affected by all uncertainties of the Monte Carlo model.

The geometric acceptance of most LEP detectors is close to 4π . Triggering on multi-hadronic events and requiring the events to satisfy some basic criteria (approximate balance in momentum and energy, a loose geometrical restriction on the primary vertex position and a cut against low-multiplicity leptonic events) reduces the acceptance by about 5% and suppresses the background from two-photon interaction, beam-gas, cosmic radiation and τ pairs below the percent level. The systematic errors related to this pre-selection are expected to be less than 1%. The luminosity is obtained from Bhabha events detected either in the forward luminosity monitors or at large angle, by the whole detector. The ultimate precision one hopes to achieve on the luminosity is about 1% ; thus, an overall precision of 2% for the total hadronic cross section is a reasonable assumption; it represents also the minimum uncertainty for the cross section of a particular flavour. (A similar precision has been achieved by the most precise measurements at lower energies [47], [48]). Note that the total hadron to muon branching ratio will be obtained with a higher precision, 1% or better, as it is not affected by the normalization error from the luminosity measurement.

Any of the tagging methods can be used for the $c\bar{c}$ and $b\bar{b}$ cross-section measurement. No distinction between quarks and anti-quarks is required, and the aim is a high tagging efficiency, which can be traded for a better sample purity.

Considering the large uncertainties which affect the various tagging methods, the perspectives for a high-precision measurement of the $b\bar{b}$ and $c\bar{c}$ cross sections at LEP1 look rather dim. It has to be stressed, however, that the limitations are not of instrumental nature but arise mainly from many physics parameters with large experimental errors which are bound to decrease with the advent of high-statistics samples of e^+e^- events. Also, the ultimate precision will have to emerge from the redundancy of the results obtained for

the various tagging methods, which are fairly independent and which have uncertainties of widely different nature. A final precision of 5% for the ($b\bar{b} + c\bar{c}$) cross-section and 6% to 8% for the separated $b\bar{b}$ cross section seem therefore not unrealistic.

2.2.3. CHARGE ASYMMETRIES

The forward-backward charge asymmetry A_{FB}^f , for a given quark flavour "f" is obtained from

$$A_{FB}^f = \frac{(N_F^f - N_B^f)}{(N_F^f + N_B^f)}, \quad (2.40)$$

The forward (F) and backward (B) hemispheres are defined with respect to the direction of the e^- beam. $N_F^f(N_B^f)$ is the number of $f\bar{f}$ events with the quark momentum-vector contained in the forward (backward) hemisphere. To measure the charge asymmetry it is not enough to determine the quark anti-quark direction which is reproduced with good accuracy by the thrust axis (Fig. 2.10); one has also to tell the quark from the anti-quark. This is possible if the selection of the $b\bar{b}$ or $c\bar{c}$ samples is based on semi-leptonic decays or on the reconstruction of the D^* ; in both cases the electric charge of the selected particles apports the necessary information.

Whatever method is choosen, the selected sample is never pure. As the various quark flavours contribute to the overall asymmetry by different amounts (due to their proper electro-weak couplings), the precise knowledge of the sample composition is a prerequisite for the interpretation of the measurement. Uncertainties from fragmentation will affect the sample composition and thereby introduce a systemetic error on the asymmetry. The size of the effect has been estimated in Ref. 41, 43 by comparing the asymmetry obtained for various fragmentation schemes. For $b\bar{b}$, the method based on lepton-kaon pairs has been used while for $c\bar{c}$ the selection by reconstruction of the D^* was used. A typical sample-composition for $b\bar{b}$ is reproduced in Tab. 2.7, taken from [41].

Model	Eff	Bkgd	Background composition								
	%	%	$u\bar{u}$	$d\bar{d}$	$s\bar{s}$	$c\bar{c}$	$\bar{u}u$	$\bar{d}d$	$\bar{s}s$	$\bar{c}c$	$\bar{b}b$
Lund PS	8.7	10.	.1	.2	1.1	.3	.3	.2	.1	5.4	2.3
Lund ME	9.2	9.5	0.	.1	.9	.3	.2	.1	0.	5.5	2.3
Webber	8.0	6.3	.1	.2	.3	.1	.1	.1	.1	3.9	1.5

Tab. 2.7: Example of a simulated $b\bar{b}$ sample.

The attention is drawn to the relatively high contribution from events where the quark and the anti-quark have been confused; this confusion is dangerous, as it contributes to the asymmetry with opposite sign. By comparing the total asymmetry for the different

fragmentation schemes, the uncertainty related to fragmentation is estimated to 0.002 to 0.003. (The standard model predictions for the $b\bar{b}$ and $c\bar{c}$ asymmetries at the Z^0 , are 0.12 and 0.08, respectively.)

Other contributions to the error come from QED and QCD corrections [49], from the interplay of the uncertainty in the beam-energy setting (≈ 20 MeV) and the rapid variation of the asymmetry at the Z^0 resonance and from intrinsic charge-dependent detector effects. The various contributions are summarized in Tab. 2.8, together with the statistical error corresponding to a total luminosity of 200 pb^{-1} (3 years of running at the Z^0 peak).

Source of error	$b\bar{b}$	$c\bar{c}$
Flavour tagging	0.0020	0.0030
Beam setting	0.0004	0.0006
Detector (Delphi)	0.0002	0.0005
QED	0.0002	0.0002
QCD	0.0016	0.0013
Total syst.	0.0026	0.0034
Stat. error	0.0035	0.0070

Tab. 2.8: Estimated error contributions to b and c charge asymmetry.

The conclusion of this study is that the $b\bar{b}$ and $c\bar{c}$ charge asymmetries will be measured at LEP with a precision better than 0.005 and 0.010, respectively. Although this initial study may be questioned as to its completeness and validity for all LEP experiments, the quoted errors constitute a valid estimate for the precision one may hope to achieve at LEP for the heavy flavour asymmetries.

Recent experiments have detected sizeable mixing in the $B^0 - \bar{B}^0$ system, which has serious implications for the interpretation of the $b\bar{b}$ charge asymmetry [50]. The experimental situation is summarized in Ref. 51. The large $B^0 - \bar{B}^0$ transition rate tends to produce charge-symmetric events, thereby diminishing considerably the observed asymmetry:

$$A_{FB}^f = A_{FB}^f(\text{no mixing})[1 - 2\bar{\chi}]. \quad (2.41)$$

Here $\bar{\chi}$ is the combined mixing rate for B_d^0 and B_s^0 mesons. The experimental value, $\bar{\chi} = 0.158 \pm 0.059$ thus implies a reduction of the observed asymmetry by an amount which depends on the tagging procedure choosen and which may be as large as 30% ! In other terms, the precise value of A_{FB}^b one may obtain at LEP cannot be interpreted in terms of the standard model parameters without the accurate knowledge of the mixing rate. However, the LEP experiments hope to measure the χ relevant for the respective

flavour tagging method with an accuracy of 10% which translates into an uncertainty of 0.003 in the asymmetry, not exceeding the expected overall experimental error.

REFERENCES

- [1] J. Schwinger, "Particles, Sources and Fields", Vol.II, (Addison-Wesley, New York, 1973).
- [2] J. Jersak, E. Laermann and P.M. Zerwas, *Phys. Lett.* **98 B** (1981) 363 and *Phys. Rev. D* **25** (1982) 1218.
- [3] A. Djouadi, J.H. Kühn and P.M. Zerwas, MPI-PAE/PTh/48/89.
- [4] M. Dine and J. Sapirstein, *Phys. Rev. Lett.* **43** (1979) 668; K.G. Chetyrkin, A.L. Kataev and F.V. Tachov, *Phys. Lett.* **85 B** (1979) 277; W. Celmaster and R.J. Gonsalves, *Phys. Rev. Lett.* **44** (1980) 560.
- [5] B.A. Kniehl and J.H. Kühn, *Phys. Lett.* **224 B** (1989) 229.
- [6] S.G. Gorishny, A.L. Kataev and S.A. Larin, *Phys. Lett.* **212 B** (1988) 238.
- [7] J.H. Kühn, Proceedings of the Workshop on Radiative Corrections for e^+e^- Collisions, Springer Verlag, 1989, ed. J.H. Kühn; B.A. Kniehl and J.H. Kühn, MPI/PAE/PTh39/89.
- [8] W.J. Marciano, *Phys. Rev. D* **29** (1984) 580.
- [9] W. Bernreuther and W. Wetzel, *Nucl. Phys. B* **197** (1982) 228.
- [10] G. Altarelli, Experimental Tests of Perturbative QCD, CERN-TH.5290/89.
- [11] D.Yu. Bardin et al., Dubna Preprint E2-88-324.
- [12] W.F.L. Hollik, *Z. Phys. C* **43** (1989) 497.
- [13] H. Burkhard et al., in "Polarization at LEP", CERN 88-06.
- [14] F. Jegerlehner, Proc. XI Int. School of Theor. Physics, Szczyrk, Poland, World Scientific (1988).
- [15] B.W. Lynn and R.G. Stuart, *Nucl. Phys. B* **253** (1985) 216.
- [16] F.A. Berends, G.J.H. Burgers and W.L. van Neerven, *Phys. Lett.* **185 B** (1987) 395; *Nucl. Phys. B* **297** (1988) 429; Erratum, *Nucl. Phys. B* **304** (1988) 92.
- [17] J.H. Kühn and R.G. Stuart *Phys. Lett.* **200 B** (1988) 360; S. Jadach, J.H. Kühn, R.G. Stuart and Z. Wąs, *Z. Phys. C* **38** (1988) 609.
- [18] E. Laermann, T.F. Walsh, I. Schmitt and P. Zerwas, *Nucl. Phys. B* **207** (1982) 273.
- [19] K. Koller, T.F. Walsh and P. Zerwas, *Z. Phys. C* **2** (1979) 197.
- [20] F. Low, *Phys. Rev.* **110** (1958) 974.
- [21] L. van Hove, Cold Quark-Gluon Plasma and Multiparticle Production, CERN-TH.5236/88.
- [22] J. Aubert et al. (EMC), *Phys. Lett.* **218 B** (1989) 248.
- [23] L.J. Reinders, H. Rubinstein and S. Yazaki, *Phys. Rep.* **127C** (1985) 1; see also T.H. Chang, K.J.F. Gaemers and W.L. van Neerven, *Nucl. Phys. B* **202** (1982) 407.
- [24] A. Djouadi, *Z. Phys. C* **39** (1988) 561.
- [25] Z. Wąs and S. Jadach, *Phys. Lett.* **219 B** (1989) 103.
- [26] J.E. Campagne and R. Zitoun, *Z. Phys. C* **43** (1989) 469.
- [27] D. Bardin et al., Preprint CERN-TH.5411/89.
- [28] B.A. Kniehl, J.H. Kühn and R.G. Stuart, in Polarization at LEP, Vol. 1, CERN 88-06.
- [29] I. Bigi, *Phys. Lett.* **155 B** (1985) 125.
- [30] H. Albrecht et al. (ARGUS), *Phys. Lett.* **192 B** (1987) 245.
- [31] M. Artuso et al. (CLEO), *Phys. Rev. Lett.* **62** (1989) 2233.
- [32] C. Albajar et al. (UA1), *Phys. Lett.* **186 B** (1987) 247.
- [33] J.H. Kühn, A. Reiter and P.M. Zerwas, *Nucl. Phys. B* **272** (1986) 560.
- [34] G. Köpp, L.M. Sehgal and P. Zerwas, *Nucl. Phys. B* **123** (1977) 77.
- [35] J.D. Bjorken, Spin Dependent Decays of Λ_c , FERMILAB-Pub-88/133.

- [36] R.H. Dalitz, G.R. Goldstein and R. Marshall, *Phys. Lett.* **215 B** (1988) 783 and *Z. Phys. C* **42** (1989) 441.
- [37] F.A. Berends, R. Kleiss and S. Jadach, *Comp. Phys. Commun.* **29** (1983) 185.
- [38] S.Jadach, Z. Was, R.G. Stuart and B.F. Ward, unpublished.
- [39] S. Jadach and J.H. Kühn, MPI-PAE/PTh 64/86.
- [40] P. Igo-Kemenes et al., Proceedings ECFA Workshop on LEP200, Aachen 1986, CERN 87-08.
- [41] H. Staeck, DELPHI, Diploma Thesis, WU D 88-19, Wuppertal University.
- [42] W. Bartel et al., *Z. Phys. C* **33** (1987) 339.
- [43] S. Ueberschaer, DELPHI, Diploma Thesis, WU B 89-4, Wuppertal University.
- [44] Particle Data Group, *Phys. Lett.* **204 B** (1988) 1.
- [45] B. van Eijk, Contribution to the Workshop on Heavy Flavours, Erice, 1988.
- [46] J. Pinfold, OPAL Note, April 1989.
- [47] E. Fernandez et al., *Phys. Rev. D* **31** (1985) 1537.
- [48] W. Bartel et al., *Phys. Lett.* **129 B** (1983) 145.
- [49] J. Drees et al., CERN 88-06, Vol.1, p.317.
- [50] P.J. Dornan, CERN 88-06, Vol.1, p.344.
- [51] K. Eggert and H.G.Moser, CERN-EP/89-42.

2.3. HEAVY QUARK FRAGMENTATION*

The fragmentation of quarks into hadrons can qualitatively be deduced from QCD, yet a rigorous quantitative understanding is still lacking due to its complex nature. The intertwining of perturbative and nonperturbative mechanisms has therefore been formulated in algorithmic models. The gross characteristics of hadron (energy) distributions are adequately described in the independent jet fragmentation model [1, 2, 3]. This model is based on the minimal assumption that quark-gluon configurations in the femto-universe transform into jets, bunches of hadrons with small relative transverse momenta, at large distances. Not relying on unproved theoretical assumptions, the model provided a solid basis for establishing experimentally the existence of gluon jets. Picturing the basic jet structures sufficiently well, the model is too crude though, to account properly for the small particle flow between the jets. Two different approaches have been pursued which refine this picture. Non-perturbative strong forces are the driving forces in the string picture [4], an approximation to the colour flux tube stretched between quarks in QCD. Perturbative gluon bremsstrahlung, on the other hand, is considered to be the main mechanism for building-up jets in parton shower models [5]. Even though a mixture of both elements is responsible for the jet development as a whole, it remains an important physical problem to explore the dynamical driving mechanism of jet formation. Heavy quarks are the simplest system to study the hadronization mechanism because heavy quark-pair production is suppressed in the jet evolution.

Apart from these fundamental QCD problems, predictions of energy spectra of heavy flavour hadrons are of tantamount practical importance for measurements of particle lifetimes and oscillations in vertex detectors

In contrast to light-quark hadronization the fragmentation of heavy quarks is hard [6, 7, 8] because the inertia carried by the heavy quark is retained in the hadron. This can most transparently be deduced by analyzing the hadronization $Q \rightarrow (Q\bar{q}) + q$ in the rest frame of the heavy quark Q [6]. In this frame the left-over light quark q is endowed with only a little bit of energy so that, when boosting the particles back to the e^+e^- cm frame with the γ factor $\gamma = \sqrt{s}/2m_Q$, q develops a light quark jet of energy $E_q \sim \gamma m_q^{eff} \sim \sqrt{s}/2m_Q \times \text{GeV}$. The average scaled energy transferred to the heavy hadron ($Q\bar{q}$) is therefore expected to be

$$\langle z \rangle_{NP} \sim 1 - 1 \text{ GeV}/m_Q \quad (2.42)$$

The ensuing particle distribution is depicted in Fig. 2.15.

The spectra of heavy hadrons are predicted to be hard also in parton shower models because gluon radiation from heavy quark lines is suppressed, leaving more energy to the

*Parts elaborated by J.W. GARY, T. SJÖSTRAND, P.M. ZERWAS

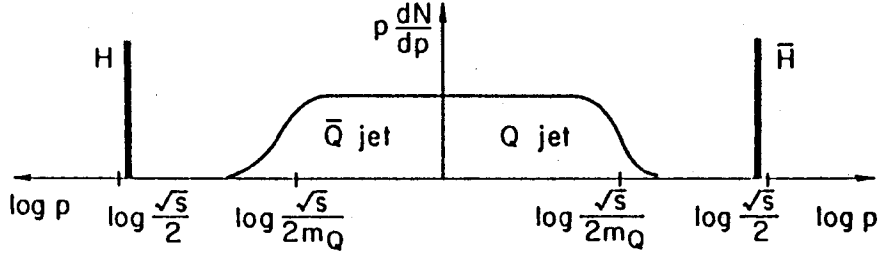


Fig. 2.15: Momentum distribution of hadrons produced in $e^+e^- \rightarrow \bar{Q}Q$, viewed in the e^+e^- center-of-mass frame; from [6].

leading particle than in light quark jets [9]:

$$\langle z \rangle_{PQCD} \sim \left[\frac{\alpha_s(s/4)}{\alpha_s(m_Q^2)} \right]^{\frac{32}{9(11-\frac{2}{3}N_f)}} \quad (2.43)$$

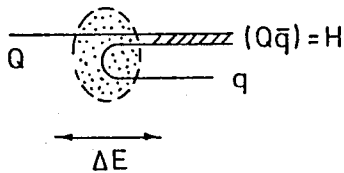
On the Z , the average values of ~ 0.8 and ~ 0.5 for bottom and charm particles, respectively, are numerically close to the estimate (42).

2.3.1. FRAGMENTATION — MAINLY NONPERTURBATIVE

The primordial fragmentation function, which describes the step $Q \rightarrow (Q\bar{q}) + q$, determines the profile of the nonperturbative particle jet. Because heavy-quark pair creation is strongly suppressed in the jet evolution, the primordial function coincides in this case with the nonperturbative fragmentation function itself. Several forms have been proposed for the fragmentation function that are based on different physical pictures.

(a) Peterson form [10]

To derive this form the parton model ideas outlined above are elaborated in the following way. The transition amplitude for a fast moving quark Q to fragment into $(Q\bar{q}) + q$ is proportional to the inverse of the energy transfer ΔE^{-1} . Denoting by z the fraction of energy (\approx momentum) retained in the heavy meson, it follows that



$$\Delta E = \sqrt{m_Q^2 + P^2} - \sqrt{m_H^2 + (zP)^2} - \sqrt{m_q^2 + ((1-z)P)^2}$$

$$\sim 1 - \frac{1}{z} - \frac{\epsilon_Q}{1-z}$$

The parameter ϵ_Q is the squared ratio of the effective light-quark mass to the heavy-quark mass

$$\text{charm : } \epsilon_c \approx \frac{m_q^2}{m_c^2} \sim 0.10$$

$$\text{bottom : } \frac{\epsilon_b}{\epsilon_c} \approx \frac{m_c^2}{m_b^2} \sim \frac{1}{10}$$

Including proper flux/phase space factors and suppressing the distribution by a dynamical factor $(1 - z)$ [familiar from light-quark fragmentation in the parton model], we derive the following form of the heavy-quark fragmentation function

$$d_Q(z) = \frac{N}{z[1 - \frac{1}{z} - \frac{\epsilon_Q}{1-z}]^2} \quad (2.44)$$

(Fig. 2.16). The normalization factor N is given by $4\sqrt{\epsilon_Q}/\pi$ for small ϵ_Q . The average scaled energy of the heavy meson

$$\langle z \rangle = 1 - \sqrt{\epsilon_Q}$$

approaches unity proportional to $1/m_Q$.

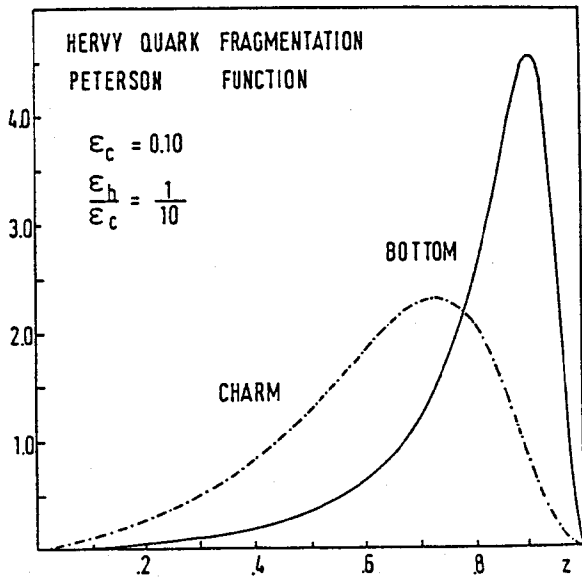


Fig. 2.16: Peterson form of the heavy quark fragmentation function for charm and bottom.

A refined treatment of the wave function in the numerator has been proposed in [11]. At the expense of a fairly complicated form, the function is hardened very close to $z = 1$, with a fall-off proportional to $(1 - z)$. The shape, however, remains qualitatively the same in general, as expected. Other parametrizations were based on Reggeology [12], or they were derived by folding nonperturbative $(Q\bar{q})$ wave functions with perturbatively generated light antiquark distributions [13].

Modeling the nonperturbative part of the jet evolution, these primordial fragmentation functions do not account for hard-gluon bremsstrahlung emitted before the nonperturbative jet develops. However, soft-gluon emission — as a mechanism for building up the jet energy density in QCD parton showers — is effectively accounted for by this form of the fragmentation function.

(b) String forms [14, 15, 16]

In string fragmentation, two different approaches have been studied to solve the problem of heavy flavour fragmentation. They differ in that one model, emphasizing the

momentum-space aspects, assumes the production of on-mass-shell hadrons to be fundamental, whereas the other model is derived from the space-time properties of the string, leading to a cluster picture yet with sharply peaked mass distributions for heavy flavour particles.

In order to illuminate the fragmentation process in the Lund approach [14], it is helpful to start with the production of ordinary particles in the central, "rapidity plateau" region of the string. The kinematics for the production of a particle is illustrated in Fig. 2.17a, using light-cone momentum variables $p^+ = E + p_L$ and $p^- = E - p_L$. The string breaks by $q\bar{q}$ pair production at the two vertices i and $i + 1$; the quark from one pair combines with the antiquark from the other to form a hadron with transverse mass-squared m_\perp^2 . The invariant distances-squared, in momentum space, from the origin to the breakup vertices are called Γ_+ and Γ_- ; the assumption of uniform particle production in rapidity (in the plateau region) implies that the rapidity coordinates of the vertices are irrelevant.

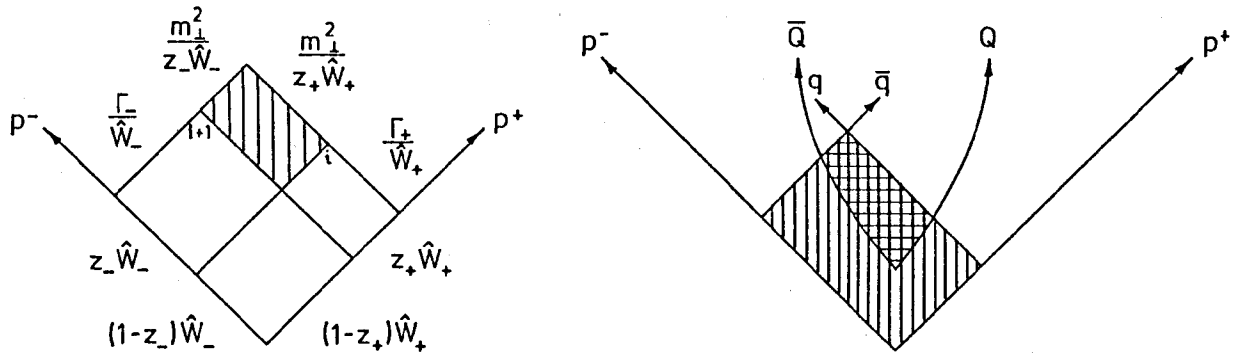


Fig. 2.17: (a) Kinematical variables in momentum space for string breakings. (b) The motion of heavy quarks along hyperbolae in space-time and the breaking of a string, compared with the momentum-space picture.

A description of the fragmentation process is possible, either in terms of a sequence of string breaks moving from the quark end of the string to the antiquark end, or the other way around. In the former description, the hadron takes a fraction z_+ of the remaining light-cone momentum \hat{W}_+ , leaving $(1 - z_+)\hat{W}_+$ for subsequent fragmentation. For the iteration from the antiquark end, replace $+$ by $-$. The two variables z_+ and z_- are related by

$$z_+ z_- \hat{W}_+ \hat{W}_- = m_\perp^2 \quad (2.45)$$

If the hadron mass is assumed fix, it is thus only necessary to specify either z_+ or z_- according to a fragmentation function $f(z_+)$ or $f(z_-)$. For the production in the central region of the string, physical consistency requires that the two possible descriptions give the same result, "left-right symmetry".

A detailed study of Fig. 2.17a reveals that the following left-right symmetric combi-

nations of variables may be formed:

$$(1 - z_+) \hat{W}_+ (1 - z_-) \hat{W}_- = (1 - z_+) \Gamma_+ = (1 - z_-) \Gamma_- \quad (2.46)$$

$$\hat{W}_+ \hat{W}_- = \frac{m_\perp^2}{z_+} + \Gamma_+ = \frac{m_\perp^2}{z_-} + \Gamma_- \quad (2.47)$$

$$m_\perp^2 z_+^2 z_-^2 dz_+ dz_- = \frac{1}{z_+} dz_+ d\Gamma_+ = \frac{1}{z_-} dz_- d\Gamma_- \quad (2.48)$$

The Γ and z dependence may be factored by exponentiating eq. (47). Multiplying the three equations with free parameters a and b for the powers of eq. (46) and eq. (47), respectively, one obtains

$$\begin{aligned} & (1 - z_+)^a \Gamma_+^a \exp\left(-\frac{bm_\perp^2}{z_+}\right) \exp(-b\Gamma_+) \frac{1}{z_+} dz_+ d\Gamma_+ \\ & = (1 - z_-)^a \Gamma_-^a \exp\left(-\frac{bm_\perp^2}{z_-}\right) \exp(-b\Gamma_-) \frac{1}{z_-} dz_- d\Gamma_- \end{aligned} \quad (2.49)$$

The z dependent piece is the "Lund symmetric fragmentation function"

$$f(z) = \frac{1}{z} (1 - z)^a \exp\left(-\frac{bm_\perp^2}{z}\right) \quad (2.50)$$

It is possible to show that $f(z)$ is the most general function that will give the same overall event description, if applied for fragmentation from one end of the jet system or from the other. [A slight generalization is allowed, with different a values for different flavours, but the dependence on endpoint flavours is small, and so can be neglected here.]

The full derivation is perfectly general, and valid also for the production of a central $c\bar{c}$ pair in a string, except that this process is strongly suppressed in string fragmentation. It can also be shown to be valid (up to some numerically small corrections) for the endpoint behaviour of the string, so long as the endpoint quarks are massless. For massive endpoint quarks, one complication does exist: the validity of the derivation is based on the assumption that the space-time and momentum-energy pictures of string evolution are simply related by a constant of proportionality, the string tension κ . However, as illustrated in Fig. 2.17b, massive endpoint quarks move along hyperbolae in space-time, with a production vertex displaced upwards from the origin of the momentum-energy picture. Two choices of the Γ variable have been advocated for a light $q\bar{q}$ pair produced in the intermediate field. Relying on the momentum-energy picture corresponds to the vertically hatched area of Fig. 2.17b, while the space-time picture gives the smaller horizontally hatched area. In the Lund program, the former possibility is used. This preserves the left-right symmetry concept also at the endpoints. The shape of $f(z)$ then does not agree with the Bjorken picture in that, for m_\perp^2 large,

$$\langle z \rangle = 1 - \frac{1 + a}{bm_\perp^2} \approx 1 - \frac{2 \text{ GeV}^2}{m_\perp^2} \quad (2.51)$$

i.e. $f(z)$ is a harder spectrum. Physically, this translates into the picture that heavier hadrons take larger string pieces and are therefore less densely spaced in rapidity.

An alternative picture (Fig. 2.17b), based on the space-time properties of the string, has been elaborated in Ref. 15,16 following the Artru-Mennessier string model [17]. In a physically plausible analogy to point-particle decays, an area decay law is postulated. The probability of a string breaking after an area A has been swept, is taken to be

$$dP_{BREAK} = P_0 e^{-P_0 A} dA \quad (2.52)$$

A is defined as the area [see Fig. 2.17b] bounded by the world lines of the heavy quarks and a light-like line along which the string break occurs randomly. Relating the string break coordinates to the mass and energy of the first daughter string leads to the spectrum [15]

$$f_1 = \frac{P_0}{2\kappa^2 z} \exp \left\{ -\frac{P_0 m_Q^2}{2\kappa^2} \left[\frac{M^2}{m_Q^2} \frac{1}{z} - 1 - \log \left(\frac{M^2}{m_Q^2} \frac{1}{z} \right) \right] \right\} \quad (2.53)$$

in the limit $m_Q^2/s \rightarrow 0$. Elaborating the mechanism for finite energies and accounting for repeated breakings of the daughter strings, the energy spectrum of the final $(Q\bar{q})$ clusters develops a pronounced peak and the cluster masses accumulate strongly at the minimum heavy flavour particle mass [16]. The numerical results [16] are shown in Fig. 2.18 for charm and bottom fragmentation functions in Z decays. A reasonable parametrization is provided by the simple form

$$D_Q(z) \sim \frac{(1-z)^a}{z^{1+bm_Q^2}} \exp \left[-\frac{bm_Q^2}{z} \right] \quad (2.54)$$

with $b = 0.8 \text{ GeV}^{-2}$ and $a \approx 0.5$, the charm/bottom quark masses identified with the masses of the lowest-lying vector meson states.

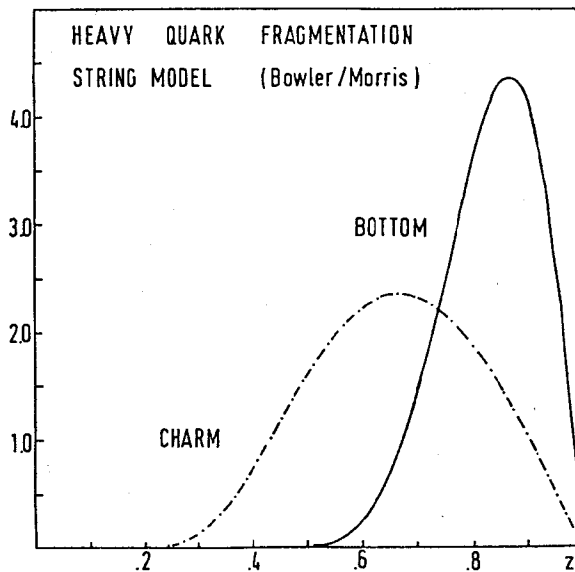


Fig. 2.18: Heavy quark fragmentation in the Bowler - Morris string approach [18].

This form of the string fragmentation function is surprisingly close to the Peterson form as can be seen by comparing Fig. 2.16 and Fig. 2.18. The spectrum is considerably softer than the flavour-independent Lund form as a result of the different z factor in front which shifts the maximum of the distribution to lower z values. The average z value predicted by this space-time motivated string picture

$$\langle z \rangle \approx 1 - \frac{1 \text{ GeV}}{m_Q}$$

coincides with Bjorken's conjecture outlined at the beginning of this section. This is not surprising because in both approaches the hadronic interaction energy between the heavy and light quark is provided by the energy of the string piece or of the flux tube, independently of the nature of the quarks as gluonic field sources. This string picture of heavy quark fragmentation may therefore be considered as an approximation to (nonperturbative) QCD that comes closest to our intuitive expectations.

2.3.2. FRAGMENTATION — MAINLY PERTURBATIVE

For light quarks there is a successful alternative to the hadronization scheme described before, that is based on the perturbative evolution of quark and gluon partons down to very low virtualness. This approach is highly developed both analytically [19] as well as algorithmically [5, 20, 21]. The inherent suppression of gluon bremsstrahlung off heavy quarks renders this sector an interesting testing ground for the underlying ideas.

As alluded to before, the angular distribution of (transversely polarized) gluon radiation off heavy quarks is described by the bremsstrahl spectrum [22] ($\gamma = E_Q/m_Q$)

$$dN_g = \frac{4}{3} \frac{\alpha_s}{\pi} \frac{\Theta^2 d\Theta^2}{[\Theta^2 + \gamma^{-2}]^2} \frac{d\omega}{\omega} \quad (2.55)$$

To ensure that perturbation theory be applicable, the transverse momentum $k_\perp = \Theta\omega$ should exceed some quantity R^{-1} (of the order of a few hundred MeV). On the other hand, the radiation is suppressed for $\Theta \leq \gamma^{-1}$ according to (55), i.e. the emission of primary gluons is restricted to angles

$$\Theta \geq \max \left\{ \gamma^{-1}, \frac{1}{R\omega} \right\}$$

Thus the large energy region and the forward region are depleted from gluon radiation. The first point is in accord with the expectation of hard fragmentation, leading to a lack of energetic light hadrons in the heavy quark jet. The second point predicts that light hadrons accompanying a bottom hadron accumulate on the surface of a cone with (half-)aperture $\Theta_c \sim \gamma^{-1} \sim 6^\circ$; in the transverse momentum plane the heavy hadron is isolated from light hadrons within a radius $k_\perp \geq \gamma^{-1}\omega$. The light hadron distributions

in the interior of the cone are therefore of special interest for investigating manifestations of nonperturbative dynamics.

The perturbative quark – gluon shower evolution cannot provide a satisfactory picture of heavy quark fragmentation without invoking the action of nonperturbative fragmentation mechanisms. This can be demonstrated by analyzing the space-time evolution of parton showers (see, for example, Ref. 23). In purely perturbative fragmentation models quarks and antiquarks would have to be combined to light mesons over distances exceeding the confinement radius of 1 fm substantially. This is corroborated by the observing that in a few percent of all events no gluons are radiated, neither from the heavy quarks nor from the heavy antiquarks so that the b, \bar{b} colour blobs are separated by ~ 20 fm before hadrons are formed. As a result, perturbative jet models must be complemented by strong nonperturbative fragmentation mechanisms to avoid colour separations over many fermis.

2.3.3. EXPERIMENTAL STATUS*

As yet, data collected by e^+e^- experiments is insufficient to distinguish between the analytical forms of the heavy quark fragmentation functions. However, that the charm and bottom quark functions are indeed ‘hard’, is unambiguously established [24,25]. The convention adopted by experiments has hence been to use the Peterson functional form to parameterise the fragmentation process of heavy quarks. From studies of inclusive lepton production employing Monte Carlo modelling techniques, it is determined [26] that the mean fractional energy taken up by the primordial heavy hadron, as reconstructed from the generated Monte Carlo four-vectors, i.e. $z_{rec} = \frac{(E+p_{||})_{hadron}}{(E+p)_{quark}}$, is 0.68 ± 0.04 for charm and 0.835 ± 0.035 for bottom. The corresponding values of ϵ_Q are $\epsilon_c^{rec} = 0.055_{-0.025}^{+0.035}$ and $\epsilon_b^{rec} = 0.0055_{-0.003}^{+0.0045}$. Indeed, the ratio ϵ_c/ϵ_b even returns a value for the square of the bottom to charm mass ratio of the order of 10, in agreement with expectations. An independent analysis of the energy spectrum of D^* s [27] gives a result for charm which is in agreement with the inclusive lepton analysis: $\langle z_{rec} \rangle_{D^*} = 0.704 \pm 0.032$.

It should be noted, however, that these results are based on the use of the Lund matrix elements Monte Carlo and are not therefore directly applicable to the Lund parton shower model. The evolution of gluon bremsstrahlung with increasing centre of mass energy is quite different in the two approaches. Taking this into account, it is estimated that the values of $\langle z_{rec} \rangle_Q$, as reconstructed from the four-vectors of the parton shower, that give best agreement with data are $\langle z_{rec} \rangle_c = 0.77 \pm 0.04$ and $\langle z_{rec} \rangle_b = 0.81 \pm 0.04$. (Note that for b ’s, this is actually a softer fragmentation when compared with the matrix

*J. CHRIN

elements result.) The corresponding ϵ_Q values are $\epsilon_c^{rec} = 0.015_{-0.007}^{+0.015}$, $\epsilon_b^{rec} = 0.008_{-0.004}^{+0.007}$. In optimising the Monte Carlo simulation model to reproduce the above values, steps must be taken to account for the inequality between the value of z allocated by the primordial fragmentation function, z_{pri} , and that value reconstructed from the generated four-vectors, z_{rec} . This difference arises from the approximation in z_{rec} that fragmentation occurs along the primary quark direction, rather than along the colour-flux lines stretched between the partons. The effect is thus of particular significance in events which radiate energetic gluons. At the Z^0 pole, such cases in the Lund parton shower model are many, and values of z_{rec} greater than unity are often observed, leading to $\langle z_{rec} \rangle_c \approx \langle z_{pri} \rangle_c + 0.11$ and $\langle z_{rec} \rangle_b \approx \langle z_{pri} \rangle_b + 0.08$. The required values of ϵ_Q^{pri} , as used by the primordial fragmentation function embedded within the framework of the Lund parton shower Monte Carlo, are thus somewhat softer: $\epsilon_c^{pri} \approx 0.07$ and $\epsilon_b^{pri} \approx 0.03$. Whilst these figures may be regarded as the present optimum values to be used in the Lund parton shower Monte Carlo at 91 GeV, caution must be applied to their physical interpretation in terms of the underlying heavy quark fragmentation function. Clearly, one would hope to arrive at a function that is fundamental to nature, rather than a model-dependent parameter. For this purpose it is more meaningful to restrict analysis of data to 2-jet like events where the dependence on the Monte Carlo modelling of many-parton events, which leads to ambiguities in the interpretation of the underlying fragmentation function, is generally avoided.

The present day situation is thus that both theory and experiment agree that the heavy quark fragmentation function is 'forward peaked', though the detailed shape of the function, and its dependence on the mass of the fragmenting heavy quark, is yet to be scrutinized. LEP experiments, with statistics of 10^7 Z^0 s, which corresponds, for example, to ≈ 15000 reconstructed D^* s, ≈ 250000 (125000) penetrating muons from primary $b(c)$ decay, per detector, will thus be suitably placed to distinguish between theoretical models and to directly determine the primordial fragmentation function of the heavy quarks.

2.3.4. HEAVY QUARK FRAGMENTATION IN MONTE CARLOS

In this section we shortly describe the present status of heavy quark fragmentation in a few representative Monte Carlos that will be used at LEP. A detailed comparative study concludes this section.

(a) LUND – Matrix Elements *

In the matrix element option it is possible to switch between zeroth, first and second order QCD treatment. In the two former cases mass effects are properly included according to

*T. Sjöstrand

perturbative QCD formulae. In the second order case, where no complete formulae are available (for the loop corrections), massless matrix elements are used, but phase space for gluon emission is still constrained by mass effects. The orientation of events in the laboratory frame does not include mass corrections. The orientation of four-jet events is done in an approximate scheme, where effective three-jet variables are calculated by recombining the gg or soft $q\bar{q}$ pair into one gluon. The Lund type fragmentation function is chosen with the parameters $a = 1$ and $b = 0.7 \text{ GeV}^{-2}$ as preferred values.

(b) LUND – Parton Showers * [20]

Production rate and angular orientation are given by the zeroth order two-jet cross section, incorporating the exact mass terms. The subsequent parton shower evolution uses exactly the same algorithm for evolution of light and heavy flavour showers. The only difference is in the cut-off value for stopping the shower evolution. With $Q_0 \sim 1 \text{ GeV}$ representing the minimum mass for a gluon to branch, the corresponding values for quarks are given by

$$m_{min} = \frac{Q_0}{2} + \sqrt{m_q^2 + \frac{Q_0^2}{4}}. \quad (2.56)$$

The increased amount of gluon emission, compared to the matrix element case, means that the nonperturbative fragmentation function is harder. The default values are $a = 0.5$, $b = 0.9 \text{ GeV}^2$, but the TASSO Collaboration has suggested that $a = 0.18$, $b = 0.34 \text{ GeV}^2$ gives a somewhat better agreement. [Remember that a and b are strongly correlated so that simultaneous shifts of the two parameters along curves of fix total multiplicity leaves most distributions almost unchanged.]

(c) Cluster Models: Production of Charmed and Bottomed Hadrons in Herwig32 *

We now wish to discuss the production mechanism for charmed and bottomed hadrons in the Herwig Monte Carlo [5]. There are three distinct stages at which heavy quark-antiquark pairs may be produced in the model: (1) at the electro-weak vertex, (2) in the perturbative shower and (3) in cluster decay.

The modeling of the electro-weak scattering in Herwig is based on the Born level equation for the annihilation of an electron and a positron into a photon or a Z^0 , which subsequently decays into a quark and an antiquark. Thus there are no corrections for initial or final state QED or QCD radiation. Furthermore there is no accounting for finite quark masses or for the energy dependence of the Z^0 width or of the electromagnetic coupling strength. The full formula for the electro-weak scattering in e^+e^- annihilations as implemented by Herwig is presented in the companion book on event generators. With the Herwig default parameter values, about seventeen per cent of all quark pairs created

*J.W. Gary

at the electroweak vertex are $c\bar{c}$ and about twenty-two per cent are $b\bar{b}$, for a center-of-mass energy of 92 GeV, as is to be expected.

A second mechanism for the creation of $c\bar{c}$ and $b\bar{b}$ pairs in Herwig is gluon splitting $g \rightarrow q\bar{q}$ in the perturbative shower. In the Monte Carlo simulation, the decision on whether such a splitting will occur is made by comparing a random number to the value of an integrated probability distribution, namely the probability distribution for a gluon of virtuality t to decay into a quark-antiquark pair

$$\frac{dt}{t} \frac{\alpha_s(t)}{2\pi} \cdot P_{g \rightarrow q\bar{q}}(z) \quad (2.57)$$

integrated over the possible values of t and of the energy splitting variable z . The functions $P_{g \rightarrow q\bar{q}}(z)$ are the Altarelli-Parisi splitting kernels. In the Herwig implementation, variable t in eq. (57) is not the invariant mass of the gluon but an “evolution variable” constructed from the energy of the decaying gluon and from the polar angle between the daughters q and \bar{q} . Again, we refer the reader to the companion book on event generators for a more complete discussion. About 1.7 per cent and 0.3 per cent of Herwig events possess a $c\bar{c}$ or $b\bar{b}$ pair, respectively, which is created in the perturbative shower at a center-of-mass energy of 92 GeV.

The third mechanism for heavy quark production in Herwig is cluster decay. A cluster is a colour-singlet object made of a final-state quark and antiquark. By final-state we mean a parton which exists after termination of the shower and after all gluons have been split into $q\bar{q}$ pairs. Clusters in the Herwig Monte Carlo serve to effect the transition between partons and hadrons. A cluster is characterized by its mass and by the flavours of the quark and antiquark of which it is comprised. Suppose that the flavours of a cluster are q_1 and \bar{q}_2 . In Herwig a cluster usually decays through production of a quark-antiquark pair or a diquark-antidiquark pair in the colour field between q_1 and \bar{q}_2 . Let $q_3\bar{q}_3$ denote this quark or diquark pair. The cluster then experiences a two-body decay to hadrons h_1 and h_2 of flavours $q_1\bar{q}_3$ and $q_3\bar{q}_2$, respectively

$$C_l(q_1\bar{q}_2) \rightarrow h_1(q_1\bar{q}_3) + h_2(q_3\bar{q}_2) \quad (2.58)$$

where C_l denotes the decaying cluster. An exception to this decay rule occurs for about 0.5 per cent of the clusters, which are too light to decay into two hadrons and which are thus transformed into a single particle. The decay eq. (58) provides a mechanism for heavy quark production because the flavour q_3 is limited only by the phase space which is available to the hadron daughters. Thus q_3 could in principle be a light (d , u or s) quark or diquark, a charm quark, a bottom quark or even a top quark. In practice only light quark, light diquark and charm quark pairs are produced in cluster decay, however, with the Herwig default parameter set. About 0.4 per cent of all Herwig events possess an additional charm quark pair because of this $c\bar{c}$ production mechanism in cluster decay.

The particle species in which these heavy quarks and antiquarks appear is determined by selecting hadrons h_1 and h_2 from a table containing particles of the correct flavour content for the decay eq. (58). A random number is then tested against the value of the phase space factor

$$(2S_1 + 1)(2S_2 + 1)P_{rest} \quad (2.59)$$

to determine whether the two hadrons h_1 and h_2 will be kept; else a new selection of daughter candidates is made from the tables. The factors S_1 and S_2 in eq. (59) are the spins of h_1 and h_2 ; P_{rest} is the magnitude of their 3-momenta in the rest frame of the decaying cluster. Thus P_{rest} is the kinematic phase space factor for the decay. The charmed and bottomed hadrons which are implemented in the model and which are thereby candidates to be cluster decay daughters are listed in table Tab. 2.9. The production rates for these hadrons as predicted by Herwig is discussed below.

0^{-+} charmed	D^+	D^-	D^0	\bar{D}^0	D_s^+	D_s^-	η_c	
1^{--} charmed	D^{*+}	D^{*-}	D^{*0}	\bar{D}^{*0}	D_s^{*+}	D_s^{*-}	J/ψ	ψ'
1^{++} charmed	D_1^{*+}	D_1^{*-}	D_1^{*0}	\bar{D}_1^{*0}	D_{s1}^{*+}	D_{s1}^{*-}	χ_1	
2^{++} charmed	D_2^{*+}	D_2^{*-}	D_2^{*0}	\bar{D}_2^{*0}	D_{s2}^{*+}	D_{s2}^{*-}		
0^{-+} bottomed	B^+	B^-	B^0	\bar{B}^0	B_s^0	\bar{B}_s^0	B_c^+	B_c^-
1^{--} bottomed	$\Upsilon(1S)$							
0^{-+} topped	T^+	T^-	T^0	\bar{T}^0	T_s^0	\bar{T}_s^0		
$s = 1/2$ singly charmed	Σ_c^{*++} $\Xi_c'^{*+}$	Σ_c^{*+} $\Xi_c'^{*0}$	Σ_c^{*0}	Λ_c^0	Ξ_c^{*+}	Ξ_c^{*0}	Ω_c^0	
$s = 3/2$ singly charmed	Σ_c^{*++}	Σ_c^{*+}	Σ_c^{*0}	Ξ_c^{*+}	Ξ_c^{*0}	Ω_c^{*0}		
$s = 1/2$ singly bottomed	Σ_b^{*+}	Σ_b^{*0}	Λ_b^0	Ξ_b^{*0}	Ξ_b^{*-}	Ω_b^{*-}		

Tab. 2.9: Charmed and bottomed hadrons which are implemented inside the Herwig Monte Carlo.

2.3.5. A COMPARISON OF HEAVY QUARK FRAGMENTATION IN JETSET71 AND HERWIG32*

To conclude this section we shall compare the predictions of Jetset version 7.1 with those of Herwig version 3.2 for certain properties of charmed and bottomed quark fragmentation. Jetset is a string-type Monte Carlo which has been widely used at Pep and Petra energies. Herwig is a well known Monte Carlo of the perturbative shower variety. Both Jetset and Herwig are likely to see wide application at Lep. Their basic features and their current status were discussed earlier in this section. More extensive descriptions of these models may be found in the companion book on event generators.

*J.W. GARY

The production rates for direct charmed and bottomed hadrons, as predicted by these two models, are shown in Tabs. 2.10–2.15. By “direct” we mean a hadron whose immediate parent is a string in the case of Jetset or a cluster in the case of Herwig. For the purposes of these comparisons and of all others which we shall present here, events have been generated under the following conditions: default parameter values as specified by the authors and a cm energy of 92 GeV. In particular this means that no simulation for initial-state electromagnetic radiation has been included, for example. The numbers which appear in the tables or which will otherwise be quoted are derived from Monte Carlo samples of 10^5 events each, with a normal flavour mixture of down, up, strange, charm and bottom quark pairs created at the electro-weak vertex. Charmed and bottomed hadrons which do not appear in Tabs. 2.10–2.15 were not produced as direct particles by either model in the event samples which were generated.

Tab. 2.10 presents the predictions of the models for the production rates of direct charmed mesons. The most noticeable feature of Tab. 2.10 is the lack of 1^{++} and 2^{++} mesons in Jetset. In fact these mesons exist as part of the Jetset71 hadron spectrum, but their production is turned off by default. Their production should be allowed in future versions of the program, however. Despite this difference, it may be seen that the ratio of the number of excited mesons to the number of pseudoscalar mesons is approximately the same for the two models, i.e. this ratio is 2.97 in Jetset and 3.17 in Herwig. Similarly, the predictions for the ratio of the number of D_s^+ to the number of D^+ are in rough agreement. Tab. 2.11 presents the analogous predictions for charmed baryons. Here, the most noticeable feature is the large rate for heavy charmed baryons which is predicted by Herwig. The rate for the direct production of the Ω_c^{*0} is more than sixty times larger in Herwig than it is in Jetset, for example. In total, about forty-four percent of the direct charmed baryons produced by Jetset are the lightest state Λ_c^+ ; in Herwig this number is only four percent.

There are two important differences between the Jetset and Herwig predictions for the direct charmed hadron production rates, as seen from Tabs. 2.10, 2.11. First, the total cross section for these hadrons is about five percent larger in Herwig than in Jetset, i.e. 39,439 particles are listed in the Herwig columns of Tabs. 2.10, 2.11 as opposed to only 37,510 for Jetset. The excess in Herwig is due to $c\bar{c}$ production in the phase space decays of clusters during the hadronization phase, see Fig. 2.19. No such mechanism for the non-perturbative production of charm exists in Jetset. We note that Herwig and Jetset agree within statistical errors for the rate of charm production through other mechanisms: $c\bar{c}$ pair creation at the electro-weak vertex and in the perturbative shower, see Tabs. 2.12, 2.13. The second important difference between Jetset and Herwig relative to the production rates of direct charmed hadrons is that the baryon fractions differ by

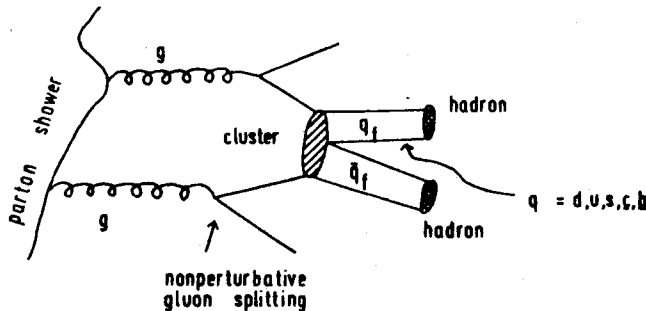
	Jetset vers. 7.1	Herwig vers. 3.2
D^0	3850	3457
D^+	3606	3277
D_s^+	1159	1263
η_c	4	4
D^{*0}	11080	6198
D^{*+}	11188	6235
D_s^{*+}	3358	1770
J/ψ	4	1
D_1^{*0}	-	2275
D_1^{*+}	-	2371
D_{1S}^{*+}	-	953
D_2^{*0}	-	2167
D_2^{*+}	-	2108
D_{2S}^{*+}	-	1277
Total	34249	33356

Tab. 2.10: The number of direct charmed mesons produced in a sample of 10^5 Monte Carlo Events generated at a cm energy of 92 GeV. The production of 1^{++} and 2^{++} mesons is not allowed by default in version 7.1 of Jetset.

	Jetset vers. 7.1	Herwig vers. 3.2
$d\bar{d}$	21922	22011
$u\bar{u}$	17144	16939
$s\bar{s}$	21960	21852
$c\bar{c}$	16982	17148
$b\bar{b}$	21992	22050

Tab. 2.12: The number of quark pairs of flavour $q_f\bar{q}_f$ produced at the electro-weak vertex in a sample of 10^5 Monte Carlo events generated at a cm energy of 92 GeV.

a factor of two, i.e. about eighteen percent of all charm generated in Herwig appears in baryons vs. only about nine percent in Jetset.



	Jetset vers. 7.1	Herwig ver. 3.2
Λ_c^+	1425	260
Ξ_c^0	160	179
Ξ_c^+	160	197
Σ_c^0	171	559
Σ_c^+	162	234
Σ_c^{++}	164	654
$\Xi_c'^0$	14	144
$\Xi_c'^+$	10	156
Ω_c^0	0	245
Σ_c^{*0}	308	1026
Σ_c^{*+}	330	436
Σ_c^{*++}	295	1087
Ξ_c^{*0}	21	247
Ξ_c^{*+}	35	275
Ω_c^{*0}	6	384
Total	3261	6083

Tab. 2.11: The number of direct charmed baryons produced in a sample of 10^5 Monte Carlo Events generated at a cm energy of 92 GeV.

	Jetset vers. 7.1	Herwig ver. 3.2
$d\bar{d}$	9473	24143
$u\bar{u}$	9575	23840
$s\bar{s}$	8453	10975
$c\bar{c}$	1784	1706
$b\bar{b}$	158	316

Tab. 2.13: The number of quark pairs of flavour $q_f\bar{q}_f$ produced in the perturbative shower in a sample of 10^5 Monte Carlo events generated at a cm energy of 92 GeV.

Fig. 2.19: The mechanism for $c\bar{c}$ or $b\bar{b}$ pair production in the phase space decay of clusters in Herwig.

The predictions of the models for the direct production rates of bottomed hadrons are presented in Tabs. 2.14, 2.15. Here, the differences between models are dominated by the limited number of bottomed hadrons which are implemented in Herwig. It is to be hoped that a more complete spectrum of such hadrons will be included in the future. Despite this difference, the predictions of the models may be said to be similar in that the total production rates, the partial rates to baryons and the ratios of the numbers of B_s^0 to the numbers of B^0 agree. The non-perturbative production of $b\bar{b}$ pairs in Herwig, through the mechanism of cluster decay, is suppressed by the lack of phase space (with the default Herwig parameter values). Thus the agreement between models for the total bottomed hadron cross section is no surprise. Note however that significantly more $b\bar{b}$ pairs are created perturbatively in the Herwig parton shower than are in the Jetset parton shower Tab. 2.13; however this mechanism is not important enough to affect the overall prediction for the bottomed hadron rate to a large extent. For bottom, Herwig demonstrates the same tendency toward heavy baryons which it does for charm: only about twenty-four percent of the direct bottomed hadrons appear as the Λ_b^0 in Herwig as opposed to almost forty-five percent in Jetset.

We next examine the energy spectra of direct charmed and bottomed hadrons as predicted by Jetset and Herwig. Fig. 2.20 show the scaled energy distributions for the particles of Tabs. 2.10–2.15, for which hadrons in each of the four categories charmed mesons, charmed baryons, bottomed mesons and bottomed baryons are displayed separately. Hadron species within each category possess spectra which differ little from that which is shown for its class. These energy spectra may be characterized by the value of the average scaled energy $\langle x_E \rangle$, defined by

$$\langle x_E \rangle = \left\langle \frac{2E_{hadron}}{E_{cms}} \right\rangle$$

The values of the average scaled energy $\langle x_E \rangle$ for the distributions in Fig. 2.20 are listed in Tab. 2.16. We also include in Tab. 2.16 the value of $\langle x_E \rangle$ for charged pions, for purposes of comparison with the heavy hadrons. The statistical errors on the numbers in Tab. 2.16 are less than 0.002 in all cases.

For charged pions, the predictions of the two models for $\langle x_E \rangle$ are essentially the same. For charmed and bottomed hadrons, the Jetset predictions are about 25% larger than those of Herwig, however. This hardness of the Jetset fragmentation function for heavy quark hadrons, relative to that of Herwig, is apparent from Fig. 2.20. Experimental data tend to support the softer spectra of Herwig as opposed to the harder ones of Jetset, as discussed in the previous section. In addition it may be seen that, for Herwig, heavy baryons possess a softer spectrum than do heavy mesons of the same heavy quark type, presumably because of the smaller phase space which is available to them on average

	Jetset vers. 7.1	Herwig vers. 3.2
B^0	4448	17707
B^+	4379	17868
B_s^0	1260	5093
B_c^+	2	0
η_B	0	-
B^{*0}	13403	-
B^{*+}	13115	-
B_s^{*0}	3817	-
B_c^{*+}	12	-
$\Upsilon(1S)$	0	0
Total	40436	40668

Tab. 2.14: The number of direct bottomed mesons produced in a sample of 10^5 Monte Carlo Events generated at a cm energy of 92 GeV. A dash in the Herwig column indicates that the meson is not implemented in version 3.2.

	Jetset vers. 7.1	Herwig ver. 3.2
Λ_b^0	1732	961
Ξ_b^-	176	313
Ξ_b^0	198	305
Σ_b^-	157	1061
Σ_b^0	181	-
Σ_b^+	196	1311
$\Xi_b'^-$	12	-
$\Xi_b'^0$	15	-
Ω_b^-	0	113
Σ_b^{*-}	366	-
Σ_b^{*0}	367	-
Σ_b^{*+}	393	-
Ξ_b^{*-}	42	-
Ξ_b^{*0}	24	-
Ω_b^{*-}	5	-
Total	3864	4064

Tab. 2.15: The number of direct bottomed baryons produced in a sample of 10^5 Monte Carlo Events generated at a cm energy of 92 GeV. A dash in the Herwig column indicates that the baryon is not implemented in version 3.2.

	Jetset vers. 7.1	Herwig vers. 3.2
π^+	0.059	0.058
charmed mesons	0.505	0.428
charmed baryons	0.529	0.421
bottomed mesons	0.757	0.631
bottomed baryons	0.761	0.607

Tab. 2.16: The mean scaled energy value $\langle x_E \rangle$ predicted for various hadrons classes by Jetset and Herwig at a cm energy of 92 GeV.

in cluster decay, because of their larger masses. In contrast, for Jetset, heavy baryons possess a harder energy spectrum than do the corresponding heavy mesons, due to the nature of the Jetset fragmentation function which becomes harder as the particle mass increases.

2.4. PARTICLE FLOW BETWEEN JETS*

The complexity of quark/gluon fragmentation did not allow us so far to describe the development of jets in a unified way from very small to very large distances. The general discussion in the preceding section on heavy quark fragmentation has demonstrated how

*V. KHOZE, P.M. ZERWAS

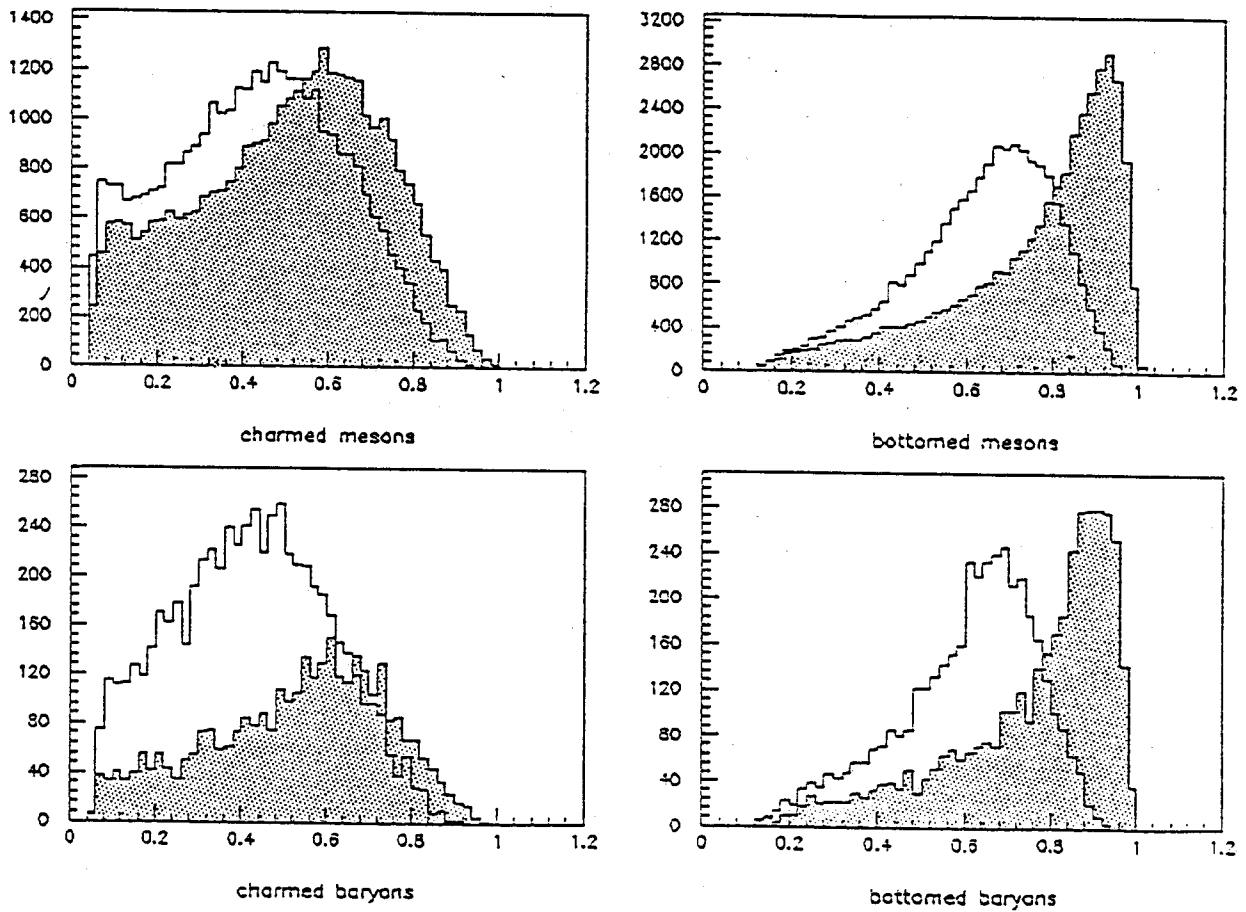


Fig. 2.20: The scaled energy distribution $x_E = 2E_{\text{hadron}}/E_{\text{cms}}$ for direct charmed and bottomed mesons and baryons as predicted by Jetset version 7.1 (filled histograms) and by Herwig version 3.2 (open histograms) at a cm energy of 92 GeV.

perturbative and nonperturbative QCD elements must be intertwined in order to draw a physically acceptable picture. As an example, let us recall the string effect [4] which was predicted as a result of the Lorentz boost exerted by a gluon on the *nonperturbative* string stretched between quarks. However, the effect may also be understood as a *perturbative* radiation effect [28]. In this approach it is a consequence of colour coherence among the gluon waves radiated from 3-parton $q\bar{q}g$ configurations.

The experimental investigation of the large variety of subtle perturbative QCD predictions and their confrontation with nonperturbative fragmentation models are often hampered by the fact that quark and gluon jets can in general not be separated on an event-by-event basis. However, the large number of charm and bottom decays of Z bosons in which the heavy quark jet can be identified by hard prompt leptons, specific final state particles, vertex detection, etc., opens new vistas on this problem. In the following we shall briefly comment on the most important points in this context without elaborating details that are discussed by other study groups.

Tests of QCD coherence phenomena and their discrimination from nonperturbative

effects require precise analyses of the particle flow in three-jet events [19]. Detailed investigations of these events should make it possible to reliably distinguish the perturbative predictions from non-perturbative string fragmentation schemes. Of particular interest are correlation measurements:

- depletion of the cone [half-aperture $\sim \gamma^{-1}$] surrounding a heavy hadron, from light hadrons;
- correction of the particle flow between jets by $1/N_c^2$ interference terms [$N_c = 3$ is the number of quark colours] and the energy dependence of the radiation pattern;
- string-string interaction;
- $1/N_c^2$ corrections to the azimuthal asymmetry of quark jets;
- oblateness of gluon jets.

While the profile of heavy quark jets has been elaborated before, we discuss here correlation measurements in which the quantum mechanical collective nature of perturbative gluon emission manifests itself. Interference effects lead to the screening of the $q\bar{q}g$ antennae, and correlations among the particles emitted between the jets are predicted, that modify the independent string fragmentation in the canonical Lund models.

Most of our points are made on the quark-gluon level, and therefore somewhat qualitative in nature by invoking local parton-hadron duality to justify the application to multi-hadron final states. More quantitative investigations, e.g. based on dipole Monte Carlos [21], are called for in the future.

2.4.1. PARTICLE FLOW IN 3-JET EVENTS

For a given $q\bar{q}g$ configuration the kinematics of which is fixed by the tagged heavy quarks as shown in Fig. 2.21, the angular distribution of the particle flow between the jets can be written as [28]

$$\frac{dN^{q\bar{q}g}}{d\vec{n}} \propto [gq] + [g\bar{q}] - \frac{1}{N_c^2}[q\bar{q}] \quad (2.60)$$

where

$$[ij] = \frac{a_{ij}}{a_i a_j} \quad \begin{cases} a_i = 1 - \cos \vartheta_i & \vartheta_i = \angle[\vec{n}, \vec{n}_i] \\ a_{ij} = 1 - \cos \vartheta_{ij} & \vartheta_{ij} = \angle[\vec{n}_i, \vec{n}_j] \end{cases}$$

(For small angles ϑ_i a more elaborate formula may be found in Ref. 29.) The first two terms agree with the celebrated string effect while the last negative term is the result of interference effects between the radiation from the q , \bar{q} and g antennae, not accounted for by independent string fragmentation. These interference effects enhance the asymmetry of particle yields between quark/gluon and quark/antiquark jets, a consequence of the repulsive force between q and \bar{q} in a colour octet state. (Note also that the particle flow increases with energy). The results can best be illustrated for 3-fold symmetric $q\bar{q}g$ events

($\theta_{q\bar{q}} = \theta_{qg} = \theta_{g\bar{q}} = 120^\circ$). The ratio of the multiplicity flows projected on the $q\bar{q}g$ plane in the sectors introduced in Fig. 2.21, are:

$$\frac{N_{III}}{N_{IV}} \simeq \frac{5 - 1/N_c^2}{2 - 4/N_c^2} = \begin{cases} 3.14 & \text{with interference} \\ 2.5 & \text{without } [N_c \rightarrow \infty] \end{cases}$$

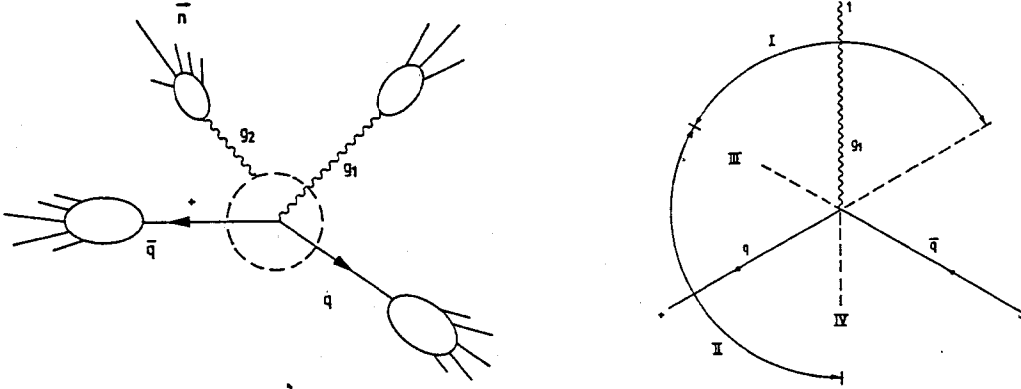


Fig. 2.21: The kinematics of soft particle distributions in $e^+e^- \rightarrow q\bar{q}g$ events and sectors in the $q\bar{q}g_1$ plane for a symmetric configuration.

Thus with interference this ratio is markedly different from the prediction of non-interacting strings. [Note that in the case of untagged jets the ratio is considerably diminished due to the smearing caused by the misidentification of quark and gluon jets.]

The coherence effect can seemingly be enhanced by normalizing the multiplicity of $q\bar{q}\gamma$ events in the region IV to $q\bar{q}g$ events

$$\frac{dN^{q\bar{q}\gamma}}{d\vec{n}} \propto \frac{8}{9}[q\bar{q}] \quad (2.61)$$

and

$$\frac{N_{IV}^{q\bar{q}g}}{N_{IV}^{q\bar{q}\gamma}} \simeq \frac{1 - 2/N_c^2}{2 - 2/N_c^2} = 0.44$$

This enhancement, however, does not teach us much. Any fragmentation model, including IJF models, would boost the particles into the sector between the q and the \bar{q} lines in photon events.

A final remark ought to be added on the fat gluon jet which is easy to isolate in three-jet events involving heavy quarks. Denoting the average multiplicity in a 120° sector, Fig. 2.21, for light $q\bar{q}g$ events by $\langle N \rangle$, one finds for the multiplicity in the gluon sector of heavy $Q\bar{Q}g$ events the ratio

$$\frac{N_I}{\langle N \rangle} \simeq 1.4$$

i.e. a strong increase of the particle yield. It is only slightly less than the canonical ratio $\frac{9}{4}/\frac{1}{3}[\frac{9}{4} + 1 + 1] = \frac{27}{17} \simeq 1.6$, the difference being partly due to the interference between gluon emission from q and \bar{q} lines.

2.4.2. CORRELATIONS OF INTERJET PARTICLE FLOWS / STRING-STRING INTERACTIONS

An interesting manifestation of the QCD wave nature of hadronic particle flows arises from studying the double-inclusive correlations of the interjet flows (see Fig. 2.22). Correlations result from the mutual influence of different colour antennae [29] on each other. These effects are not incorporated in orthodox string models in which the string segments fragment independently.

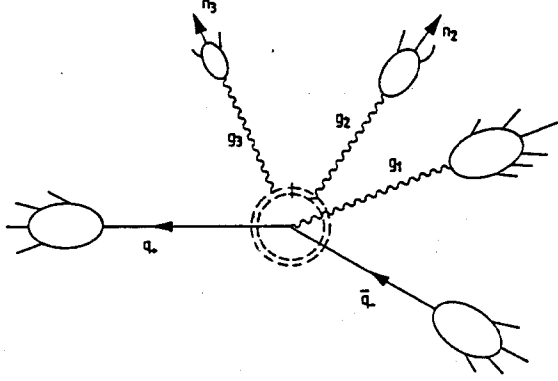


Fig. 2.22: Double-inclusive correlation of multiplicity flows in events with $q\bar{q}g_1$ topology.

These correlations bear the information on the colour shielding of the $q\bar{q}g_1$ antennae by the field of a second gluon g_2 that has been produced in a cascade, but preceding the emission of a third gluon g_3 . The energies are ordered in the sequence $E_3 \ll E_2 \ll E_1 \sim E_+ \sim E_- \sim \sqrt{s}/3$. The angular distribution of particles in the directions of the secondary jets g_2 and g_3 is given by terms coming from the independent emission plus a contribution that links the two gluons:

$$\frac{d^2 N}{d\vec{n}_2 d\vec{n}_3} \propto [g_3; g_2 g_1] [g_2; g_1 q] + [g_3; g_2 q] [g_2; g_1 q] + q \rightarrow \bar{q} \quad (2.62)$$

+ individual jet contributions

$$[i; jk] = a_{jk} / (a_{ij} a_{ki})$$

To quantify the correlation effects we compare the ratio of the single inclusive particle flow between the jets,

$$r_1 = \frac{dN}{d\vec{n}_{gq}} / \frac{dN}{d\vec{n}_{q\bar{q}}}$$

with the ratio of the double-inclusive flow,

$$r_2 = \frac{d^2 N}{d\vec{n}_{gq} d\vec{n}_{g\bar{q}}} / \frac{d^2 N}{d\vec{n}_{q\bar{q}} d\vec{n}_{g\bar{q}}}$$

The pair ij denotes the directions midway between the partons i and j . In the picture of independent fragmentation of the string segments the additional measurement of the

particle flow in the region $(g\bar{q})$ does not affect the ratio $(gq)/(q\bar{q})$ so that $r_2 = r_1$ in this model. However, the mutual influence of the antennae renders r_2 different from r_1 . For example, in the case of 3-fold symmetric events these ratios are

$$r_1 = 2.42 \quad r_2 = 2.06$$

if the particle flows are projected onto the event plane. This effect is by no means small. It is a fundamental prediction of string-string interactions. For present LEP energies this perturbative picture of QCD radiophysics is tied to the validity of local duality and must thus be subject to experimental scrutiny.

2.4.3. AZIMUTHAL ASYMMETRY OF QUARK JETS ...

The structure of final states given by the string picture coincides with the perturbative QCD radiation pattern only up to $1/N_c^2$ corrections. However, in a few cases $1/N_c$ terms could become sizeable or even dominating [30].

The radiation pattern of a tagged quark jet in $q\bar{q}g$ events follows from eq. (60). If all angles are large, the third term in eq. (60), resulting from colour coherence, leads to a sizeable 10% decrease of the first two terms describing the independent string formation. If the direction \vec{n} is chosen close to the quark axis \vec{n}_q , a noticeable asymmetry of the particle flow is predicted. The azimuthal distribution of particles produced inside a cone of half-aperture θ_0 (Fig. 2.23a) may be characterized by the asymmetry parameter

$$A(\theta_0) = \frac{N^{-g}(\theta < \theta_0) - N^{-\bar{q}}(\theta < \theta_0)}{N_{tot}(\theta < \theta_0)} \quad (2.63)$$

For small θ_0 the asymmetry parameter reads

$$A(\theta_0) = \frac{2\theta_0}{\pi} G \sqrt{4N_c \frac{\alpha_s(E\theta_0)}{2\pi}}$$

$$\frac{8}{3}G = N_c \cot \frac{\theta_{gq}}{2} + \frac{1}{N_c} \cot \frac{\theta_{q\bar{q}}}{2} \quad (2.64)$$

The first colour-favored term in eq. (64) describes the Lund-motivated asymmetry due to the "boosted string" connecting the q and the g directions. The corresponding asymmetry vanishes with increasing θ_{gq} as the string straightens. Here however the second coherence term stops the decrease, Fig. 2.23b, and forces the asymmetry to rise again. This behaviour may be interpreted as an additional repulsion between particles from two neighboring q and \bar{q} jets in a colour octet state.

To study this effect one has to select $q\bar{q}g$ events where the hard gluon moves in the direction opposite to the quasi-collinear $q\bar{q}$ pair. In the case of heavy quarks the opening half-angle θ_0 must be taken bigger than $\gamma^{-1} = m_q/E$ ($= 6^\circ, 2^\circ$ for b, c respectively). The asymmetry can be extracted as a function of the relative angle between the q and

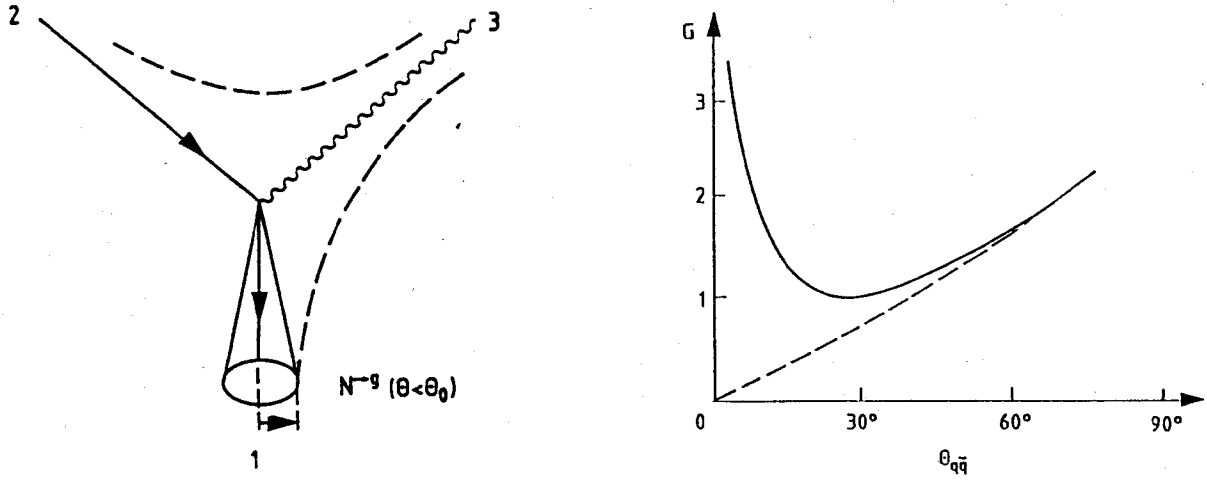


Fig. 2.23: (a) The azimuthal asymmetry of the quark jet in $e^+e^- \rightarrow q\bar{q}g$. Geometry in the event plane: dashed lines show the topology of the colour strings.

(b) QCD (solid) vs. "string" (dashed) prediction for the G factor.

\bar{q} jets from Fig. 2.23b. The increase of A is of comfortable size at moderate $\theta_{q\bar{q}}$ angles. Of course, before this different behaviour of orthodox string models and perturbative QCD radiophysics can be studied in detail, the asymmetry itself must be established experimentally.

2.4.4. ... AND GLUON JETS

All the subtle coherence effects discussed in the previous subsections are a consequence of the fact that gluons carry colour charges enabling them to emit gluons themselves. The existence of the triple-gluon coupling is the basis of asymptotic freedom in QCD. It is therefore of utmost importance to search for effects that are a direct consequence of this self-coupling. Azimuthal asymmetries, with respect to a transverse gluon polarization axis, in the splitting of virtual gluons into gluons [31] are of opposite sign to those where gluons split into quark-antiquark pairs. The angular dependence of the splitting functions [32] is given by

$$D_{g \rightarrow gg}(z, \chi) = \frac{6}{2\pi} \left\{ \frac{(1-z+z^2)^2}{z(1-z)} + z(1-z) \cos 2\chi \right\} \quad (2.65)$$

$$D_{g \rightarrow q\bar{q}}(z, \chi) = \frac{1}{2\pi} \left\{ \frac{1}{2} [z^2 + (1-z)^2] - z(1-z) \cos 2\chi \right\} \quad (2.66)$$

z denotes the energy fraction carried by one of the child partons. Quark jets accumulate perpendicular to the polarization vector [33] with a maximal asymmetry $\sim [1 - \cos 2\chi]$ for $z = 1/2$. The asymmetry for gluons is less pronounced $\sim [1 + \frac{1}{9} \cos 2\chi]$ for $z = 1/2$. The magnitude of the asymmetries is illustrated as a function of z in Fig. 2.24.

The gluons in $e^+e^- \rightarrow q\bar{q}g$ 3-jet events are linearly polarized to a high degree in the event plane, $P = 2(1-x_g)/(x_q^2 + x_{\bar{q}}^2)$. We therefore expect that tagged charm and bottom

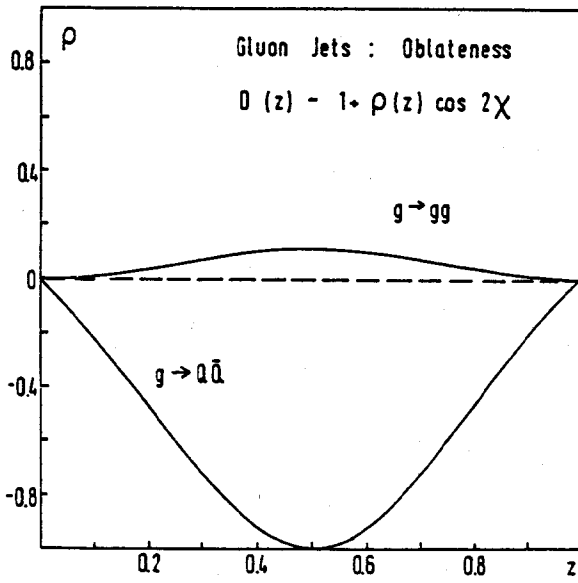


Fig. 2.24: Azimuthal asymmetries in the fragmentation of gluons to a pair of gluons or quarks.

quarks from the cascade $g \rightarrow Q\bar{Q}$ are emitted preferentially out of the event plane. On the other hand, due to the dominating $g \rightarrow gg$ gluon splitting, the hadrons should in general be almost isotropically distributed about the g direction. [Adding up gluons plus three light quarks without tagging, the oblateness of the g jet vanishes [34]]. It has been shown that the difference between the quark and gluon asymmetries survives if the analysis is based on clear 4-jet events evolving from short distances in the femto-universe [35]. The polar angles of the low energy jets with respect to the high energy jets are large for $q\bar{q}Q\bar{Q}$ final states while they are small for $q\bar{q}gg$ events [36]. Another useful observable is the jet alignment discussed in [37]. Detailed analyses demonstrate that the 3-gluon coupling can be explored experimentally under the generally accepted orthodox conditions for applying perturbative QCD.

2.5. INCLUSIVE PRODUCTION OF J/ψ , Υ AND B_c^*

In addition to the resonant production of spin 1 quarkonia at low energies these states will also be produced in Z decays through the processes depicted in Fig. 2.25a.

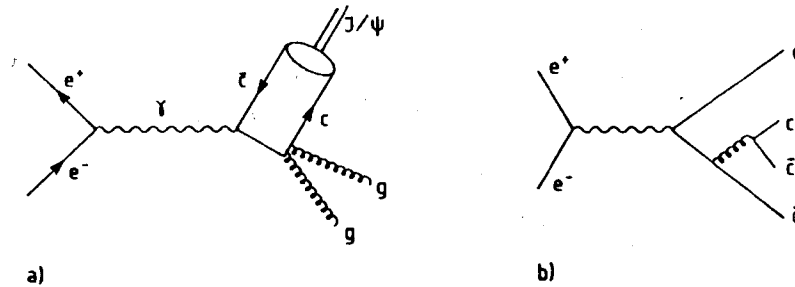


Fig. 2.25: Diagrams that contribute to inclusive J/ψ production.

The reaction $e^+e^- \xrightarrow{\gamma^*} J/\psi + gg$ has been studied in [38]. The analytic result can

*J.H. KÜHN AND P.M. ZERWAS

easily be converted to the corresponding rate for $Z \rightarrow J/\psi + gg$. Normalized relative to μ pairs one finds

$$\frac{\Gamma(Z \rightarrow J/\psi gg)}{\Gamma(Z \rightarrow \mu^+ \mu^-)} \approx \frac{v_c^2}{a_\mu^2 + v_\mu^2} \frac{1}{Q_c^2} \frac{2}{3\pi} \left(\frac{\alpha_s}{\alpha}\right)^2 \frac{\Gamma(J/\psi \rightarrow e^+ e^-)}{m_\psi} \mu^2 \left[\ln^2\left(\frac{\mu^2}{4}\right) + 2 \ln(256\mu^2) - 18 \right]$$

and correspondingly for Υ . As a result one finds branching ratios of $2 \cdot 10^{-7}$ for Υ and $6 \cdot 10^{-8}$ for J/ψ . (See also Ref. 39.)

The situation is more favourable for charmonium production through the diagram depicted in Fig. 2.25b. The fraction of the cross section for $e^+e^- \rightarrow q\bar{q} + c\bar{c}$ where the invariant mass of the $c\bar{c}$ system lies between $2m_c$ and $2m_D$, is via local duality identified with the cross section for charmonium production [40] (Fig. 2.26).

About a fraction of 10^{-2} of hadronic Z decays will contain a charmonium state and perhaps $3 \cdot 10^{-3}$ contain J/ψ . Tagging J/ψ through its e^+e^- and $\mu^+\mu^-$ mode one would find about 300 of these events in a sample of $10^6 Z$ — a non-negleageable background for B tagging through its J/ψ -decays. The corresponding fractions for $b\bar{b}$ production are $0.3 \cdot 10^{-2}$ for all bound states below threshold, 10^{-3} for Υ and about 60 $\Upsilon \rightarrow e^+e^-$ or $\mu^+\mu^-$ events in a sample of $10^6 Z$.

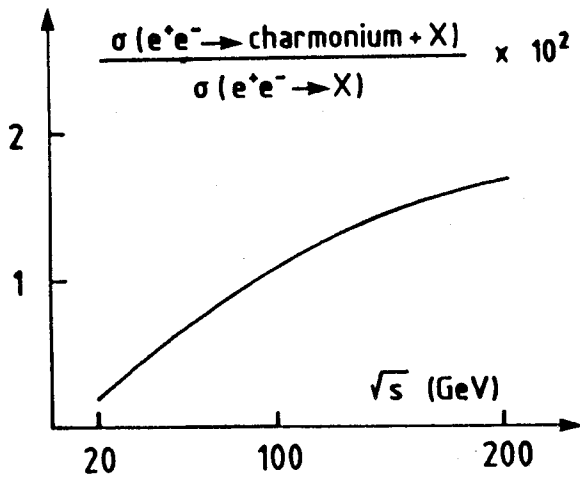


Fig. 2.26: Inclusive charmonium production rate as estimated in [40].

Charmed bottom mesons B_c can be produced at an appreciable rate only through $(\bar{b}c) \rightarrow B_c$ fusion in perturbatively generated $Z \rightarrow b\bar{b}c\bar{c}$ final states. [Spontaneous non-perturbative $c\bar{c}$ pair creation in a gluonic flux tube is suppressed at a level of 10^{-11}]. Folding the 4-quark production amplitude with the $b\bar{c}$ quark-antiquark bound-state wave function, a branching ratio for $Z \rightarrow B_c$ of order 10^{-4} to 10^{-5} has been estimated in [41] so that order 100 to 1,000 B_c are expected in $10^7 Z$ decays. The final state has a remarkable signature: an isolated B_c meson plus 2 jets. The lifetime of the B_c meson is determined by the lifetime of the charmed quark, shorter by a factor 1/3 to 1/4 than the average b -hadron lifetime. Decay signatures are therefore $B_c \rightarrow B + K's$ and $\pi's$.

REFERENCES

- [1] R.D. Field and R.P. Feynman, *Nucl. Phys. B* **136** (1978) 1.
- [2] P. Hoyer, P. Osland, H.G. Sander, T.F. Walsh and P.M. Zerwas, *Nucl. Phys. B* **161** (1979) 349.
- [3] A. Ali, E. Pietarinen, G. Kramer and J. Willrodt, *Phys. Lett.* **93 B** (1980) 155.
- [4] B. Andersson, G. Gustafson, G. Ingelman and T. Sjöstrand, *Phys. Rep. C* **97** (1983) 33.
- [5] G. Marchesini and B.R. Webber, *Nucl. Phys. B* **310** (1988) 461.
- [6] J.D. Bjorken, *Phys. Rev. D* **17** (1978) 171.
- [7] M. Suzuki, *Phys. Lett.* **71 B** (1977) 139.
- [8] V. A. Khoze, Ya.I. Azimov and L.L. Frankfurt, Proceedings, Conference on High Energy Physics, Tbilisi 1976.
- [9] I. Bigi, Yu. Dokshitzer, J. Kühn and P. Zerwas, *Phys. Lett.* **181 B** (1986) 157.
- [10] C. Peterson, D. Schlatter, I. Schmitt and P.M. Zerwas, *Phys. Rev. D* **27** (1983) 105.
- [11] P. Collins and T. Spiller, *J. Phys. G* **11** (1985) 1289.
- [12] V.G. Kartvelishvili, A.G. Likhoded and V.A. Petrov, *Phys. Lett.* **78 B** (1978) 615
- [13] F. Amiri and C.R. Ji, *Phys. Lett.* **195 B** (1987) 593.
- [14] B. Andersson, G. Gustafson and B. Söderberg, *Z. Phys. C* **20** (1983) 317.
- [15] M.G. Bowler, *Z. Phys. C* **11** (1981) 169.
- [16] D.A. Morris, *Nucl. Phys. B* **313** (1989) 634.
- [17] X. Artru and G. Mennessier, *Nucl. Phys. B* **70** (1974) 93.
- [18] D. Morris, private communication.
- [19] Yu.L. Dokshitzer, V.A. Khoze, A.H. Mueller and S.I. Troyan, *Rev. Mod. Phys.* **60** (1988) 373.
- [20] M. Bengtsson and T. Sjöstrand, *Nucl. Phys. B* **289** (1987) 810.
- [21] G. Gustafson, *Phys. Lett.* **176 B** (1986) 453.
- [22] Yu.L. Dokshitzer, V.A. Khoze and S.I. Troyan, Proceedings, 6th International Conference on Physics in Collision, (World Scientific, 1987).
- [23] G. Fox, Untangling Jets from Hadronic Final States, SLAC Summer Institute 1981.
- [24] S. Bethke, *Z. Phys. C* **29** (1985) 175.
- [25] J. Chrin, *Z. Phys. C* **36** (1987) 163.
- [26] J. Chrin, *Annals New York Academy of Sciences* **535** (1988) 131.
- [27] S. Bethke, Proceedings, The International Symposium on The Production and Decay of Heavy Hadrons, Heidelberg 1986.
- [28] Ya. Azimov, Yu.L. Dokshitzer, V.A. Khoze and S.I. Troyan, *Phys. Lett.* **165 B** (1985) 147.
- [29] Yu.L. Dokshitzer, V.A. Khoze and S.I. Troyan, *Sov. Journal Nucl. Phys.* **47** (1988) 881.
- [30] Yu. Dokshitzer, V.A. Khoze and S.I. Troyan, Leningrad Report LNPI-1372.
- [31] G. Altarelli and G. Parisi, *Nucl. Phys. B* **126** (1977) 298.
- [32] K. Koller, K.H. Streng, T.F. Walsh and P.M. Zerwas, *Nucl. Phys. B* **206** (1982) 23 .
- [33] S.J. Brodsky, T. DeGrand and R. Schwitters, *Phys. Lett.* **79 B** (1978) 225.
- [34] A. Smilga and H. Vysotsky, *Pis'ma Zh. Eksp. Teor. Fiz.* **29** (1979) 251.
- [35] M. Bengtsson and P.M. Zerwas, *Phys. Lett.* **208 B** (1988) 306.
- [36] O. Nachtmann and A. Reiter, *Z. Phys. C* **16** (1982) 45.
- [37] J.G. Körner, G. Schierholz and J. Willrodt, *Nucl. Phys. B* **185** (1981) 365.
- [38] J.H. Kühn and H. Schneider, *Z. Phys. C* **11** (1981) 263.
- [39] K.J. Abraham, Bottomium Production at LEP, Preprint NIKHEF, 1989.
- [40] G.C. Branco, H.P. Nilles and K.H. Streng, *Phys. Lett.* **85 B** (1979) 269.
- [41] F. Amiri and C.R. Ji, *Phys. Rev. D* **35** (1987) 3318.

2.6. HEAVY FLAVOUR LIFETIMES

2.6.1. THEORETICAL SUMMARY*

The typical momentum transfer in weak decays of hadrons which are composed of a heavy quark Q and light quark constituents is of the order of the mass m_Q . Thus, for sufficiently large values of m_Q , inclusive decay properties such as total lifetimes and semileptonic branching ratios should mainly reflect the dynamics at short distances. In particular, the light constituents are expected to play a passive role. This approximation, known as the spectator model [1], implies that the lifetimes of all weakly decaying states containing Q are equal and essentially determined by the intrinsic lifetime of Q . The latter is given by theory similarly as the lifetimes of the μ and τ leptons. Indeed, the observed average charm lifetime can be understood on the basis of the Fermi constant G_F , the charm quark mass $m_c \simeq 1.6$ GeV, the Cabibbo angle $|V_{cs}| \simeq \cos \theta_c \simeq 1$, and the number of Cabibbo-allowed decay channels:

$$\tau_c \simeq \left[5 \frac{G_F^2 m_c^5}{192 \pi^3} \right]^{-1} \simeq \frac{1}{5} \left(\frac{m_\mu}{m_c} \right)^5 \tau_\mu \simeq 6 \times 10^{-13} s \quad (2.67)$$

Here, the mode $c \rightarrow s u \bar{d}$ is counted three times because of colour, and $\tau_\mu \simeq 2.2 \times 10^{-6} s$ is the μ lifetime. For bottom decays, taking $m_b \simeq 4.5$ GeV and $|V_{cb}| \simeq \sin^2 \theta_c \simeq 0.05$, one obtains

$$\tau_b \simeq \frac{1}{5} \frac{1}{|V_{cb}|^2} \left(\frac{m_\mu}{m_b} \right)^5 \tau_\mu \simeq 1 \times 10^{-12} s \quad (2.68)$$

which nicely reproduces the magnitude of the observed B meson lifetime. In eq. (68), the channels with two heavy particles in the final state, i.e. $b \rightarrow c s \bar{c}$ and $c \tau \bar{\nu}_\tau$, have been disregarded because of phase space suppression. We see that the free quark picture which emerges in the limit $m_Q \rightarrow \infty$ already makes sense for charm decays despite of the relatively light charm quark mass. Therefore, it appears well justified to use the spectator model in bottom decays.

On the other hand, the observed lifetime differences of charmed particles clearly indicate the existence of sizeable preasymptotic corrections to the spectator model approximation. These corrections have their origin in non-spectator mechanisms such as W -exchange [2, 3] and quark interference [4, 5]. Yet, m_b is considerably larger than m_c so that non-spectator effects should be less important in bottom decays than in charm decays. This expectation is corroborated by semi-quantitative estimates obtained from the empirical charm lifetime pattern by means of reasonable scaling arguments. One expects corrections of the order of about 10% [6]. However, because of the lack of a complete

*R. RÜCKL

quantitative understanding of the charm data, one cannot absolutely trust these extrapolations. It is certainly desirable to clarify the role of non-spectator corrections in bottom decays experimentally by separate measurements of the lifetimes of the B^\mp , B_d^0 , and B_s^0 mesons as well as of bottom baryons such as the Λ_b^0 . This would not only help to develop a reliable theoretical framework, but also put the extraction of the quark mixing parameters V_{cb} and V_{ub} from the inclusive semileptonic decays [7] and the analysis of $B - \bar{B}$ oscillations [8] on a more solid basis.

The present tractate is mainly concerned with the bottom lifetime as predicted in the spectator model and with the qualitative lifetime hierarchy generated by non-spectator corrections. Also discussed are order of magnitude estimates for the lifetime differences of bottom hadrons. Since these expectations are based on ideas and results stemming from the study of charm decays, it is useful to begin with a brief recapitulation of theoretical interpretations of the charm lifetime pattern.

Résumé of Charm Lifetimes

The common starting point in current theoretical treatments of inclusive decays is an effective weak hamiltonian H_W which includes renormalization effects due to gluon exchanges with momentum $p \gtrsim m_Q$ [9]. Inclusive decay widths are then computed from the formal expression

$$\Gamma(h \rightarrow \text{anything}) = \frac{1}{M_h} \text{Im} \langle h | i \int d^4x T(H_W(x) H_W^\dagger(0)) | h \rangle \quad (2.69)$$

using the concept of quark-hadron duality [6]. This eventually leads to an expansion of Γ in powers of m_Q^{-1} . The “leading” contributions represent the spectator model approximation, while the terms suppressed by the heavy quark mass m_Q constitute preasymptotic corrections related to non-spectator processes. Taking for granted the implicit assumptions of this approach, one is left with the following problems. Firstly, the spectator model predictions depend on various parameters, in particular, effective quark masses which are not precisely known and thus give rise to considerable uncertainties [10]. Secondly, the non-spectator corrections involve QCD bound state properties and nonperturbative effects, and are therefore even more difficult to estimate reliably. Having no better alternative, one usually resorts to additional assumptions and phenomenological bound state models [2–6, 10, 11]. As a result of the uncertainties in the spectator approximation, on the one side, and in the model calculations of non-spectator effects, on the other side, some aspects of the charm lifetimes are still controversial or at least unclear.

Unquestioned is the importance of non-spectator corrections after the experimental discovery of considerable differences in the lifetimes of charmed particles, to wit [12]

$$\tau(D^+) : \tau(D^0) : \tau(D_s^+) : \tau(\Lambda_c^+) : \tau(\Xi_c^+) : \tau(\Omega_c^0) \simeq 2.5 : 1 : 1 : 0.5 : 1.3 : 1.9 \quad (2.70)$$

Furthermore, there is consensus on the mechanisms which, from a purely qualitative point of view could explain the observed lifetime hierarchy. The suspected mechanisms include

- (i) the W -exchange processes [2, 3] $c\bar{u} \rightarrow s\bar{d}$ and $cd \rightarrow su$,
- (ii) the weak annihilation processes [2] $c\bar{s} \rightarrow u\bar{d}$ and $c\bar{s} \rightarrow \bar{l}\nu_l$, and
- (iii) Pauli interference [4, 5] of constituent quarks or antiquarks with identical quark species produced in the decay $c \rightarrow sud$.

The remaining questions concern the absolute and relative magnitude of the effects induced by the above mechanisms. A natural parameter characterizing the size of non-spectator effects is given by [6]

$$4\pi^2 \left(\frac{f_D}{m_c} \right)^2 \approx 0(1) \quad (2.71)$$

Here, the decay constant $f_D \approx 200$ MeV reflects the suppression due to the necessary spatial overlap of the charm quark with a light constituent quark in a non-spectator process, while the numerical factor accounts for the difference in phase space of spectator decays (3-body) and non-spectator mechanisms (effectively 2-body). In the light of eq. (71), one can qualitatively understand the overall magnitude of the observed lifetime differences. Thus, the main controversial issue is the relative importance of the non-spectator mechanisms (i) – (iii). In order to examine this question one has to make further assumptions.

Similarly as in many other weak processes, it is instructive to use vacuum saturation or valence quark descriptions as a first approximation. One can then straightforwardly evaluate the hadronic matrix elements appearing in the expansion of eq. (69) in terms of local operators. This leads to the following results [6, 10]. In the case of D mesons, the largest non-spectator correction comes from destructive interference of the two \bar{d} -quarks in the decay $D^+ \rightarrow sud\bar{d}$. The size of this effect is as anticipated in eq. (71). In contrast, the non-spectator processes $D^0 \rightarrow s\bar{d}$ and $D_s^+ \rightarrow u\bar{d}$ give much smaller contributions of the order of

$$4\pi^2 \frac{f_D^2 m_q^2}{m_c^2 m_c^2} \ll 1 \quad (2.72)$$

m_q being the mass of the heaviest final state quark. As well-known, the additional suppression factor m_q^2/m_c^2 is enforced by helicity conservation in $V - A$ interactions. Thus, vacuum saturation suggests to attribute the $D^+ - D^0$ lifetime difference to quark interference, while it predicts almost equal lifetimes for the D^0 and D_s^+ :

$$\tau(D^+) > \tau(D^0) \simeq \tau(D_s^+) \quad (2.73)$$

This pattern is in nice agreement with the recent data [12].

A quite different picture emerges for baryon decays since here W -exchange is not suppressed by helicity conservation. On the contrary, using quark model wave-functions

one finds that the non-spectator processes $\Lambda_c^+ \rightarrow suu$ and $\Xi_c^0 \rightarrow sus$ are comparable in strength to the spectator model decays [3, 5, 11]. In the nonrelativistic limit, the relative magnitude is described by the parameter

$$48\pi^2 \frac{|\psi_{cq}(0)|^2}{m_c^3} \approx O(1) \quad (2.74)$$

where $\psi_{cq}(0)$ denotes the wavefunction at the origin of the weakly interacting constituents in the initial bound state. Eq.(74) is equivalent to eq. (71) if the nonrelativistic relation $f_D^2 \simeq 12|\psi_{c\bar{q}}(0)|^2/m_c$ is used. The best evidence for the importance of W -exchange in baryon decays is provided by the observed inequality $\tau(\Lambda_c^+) < \tau(D^0)$. Furthermore, similarly as in the meson case, one estimates sizeable shifts in the baryon lifetimes due to quark interference [5, 11]. These corrections are also of the type characterized by eq. (74), however, the sign can be positive or negative. Whereas the u -quark from the decay $c \rightarrow su\bar{d}$ interferes destructively with a u -constituent in the baryons, the corresponding interference of s -quarks is constructive. Together, the non-spectator effects generate a rather intricate lifetime hierarchy [5]*:

$$\tau(\Omega_c^0) \simeq \tau(\Xi_c^0) < \tau(\Lambda_c^+) < \tau(\Xi_c^+) \quad (2.75)$$

So far, only the last inequality is verified experimentally, while the prediction for the Ω_c^0 seems to be at variance with the experimental result quoted in eq. (70). Considering the large error of the Ω_c^0 lifetime measurement [12] and the lack of data on the Ξ_c^0 lifetime, it may however be too early to draw a definite conclusion.

Qualitatively, the modifications of the uniform spectator model lifetime due to non-spectator effects are determined by the general properties of H_W and the valence quark structure of the charmed hadrons. Therefore, one can rather reliably predict the lifetime hierarchy resulting from a given non-spectator mechanism. On the other hand, the actual size of the various corrections is subject to large uncertainties connected with the bound state wavefunctions, the influence of gluons, and so forth. These uncertainties leave room for speculations which lead to quite different scenarios.

In particular, it has been argued [2] that the presence of gluons in hadronic bound states may render valence quark approximations and vacuum saturation inappropriate. For instance, D meson bound states might contain sizeable components in which the valence quarks form a spin-one configuration with the $c\bar{q}$ spin being balanced by a gluonic system. In this configuration, W -exchange and weak annihilation would not be prohibited by helicity conservation. Consequently, non-spectator processes such as $D^0 \rightarrow s\bar{d} + X_{glue}$

*Taking into account further corrections, the authors of ref. [11] argue in favour of $\tau(\Omega_c^0) < \tau(\Xi_c^0) < \tau(\Lambda_c^+) \simeq \tau(\Xi_c^+)$.

and $D_s^+ \rightarrow u\bar{d} + X_{glue}$ should occur with rates of the order of $4\pi^2 \tilde{f}_D / m_c^2$ relative to the spectator mechanism. The difficult part is to estimate the parameter \tilde{f}_D which is related to the $c\bar{q}$ wavefunction in the spin-one configuration and which replaces the decay constant f_D in the valence quark approximation discussed before. At present, one cannot calculate \tilde{f}_D reliably because of the nonperturbative nature of the problem. If one nevertheless treats the gluon background perturbatively, considering one-gluon bremsstrahlung from a nonrelativistic $(c\bar{q})$ -bound state, one obtains (M. Bander et al. [2])

$$\tilde{f}_D^2 = \frac{\alpha_s}{54\pi} \left(\frac{m_c}{m_q} \right)^2 f_D^2 \quad (2.76)$$

where m_q is the mass of the light constituent quark. In spite of the enhancement factor $(m_c/m_q)^2 \approx 30(10)$ for $m_u \approx 300\text{MeV}$ ($m_s \approx 500\text{MeV}$), this estimate yields too small a value of \tilde{f}_D for W -exchange and weak annihilation to have a major influence on the D meson lifetimes.

However, one can argue that the perturbative result, eq. (76), is not trustful and assume [2] instead $\tilde{f}_D = O(f_D)$ in which case

$$4\pi^2 \frac{\tilde{f}_D^2}{m_c^2} \approx O(1) \quad (2.77)$$

This is the principal assumption of the so-called annihilation models which attribute the $D^+ - D^0$ and $D^+ - D_s^+$ lifetime differences to W -exchange and weak annihilation processes, respectively, accompanied by gluons, while quark interference effects are considered less important. The strongest support for this conjecture comes from the small semileptonic branching ratio of the D^0 , namely $B_{sl}(D^0) \simeq 7.5\%$ [13]. This number seems to be smaller than what one can obtain within the spectator model from the QCD short distance enhancement of nonleptonic decays induced by H_W [9] and the suppression of semileptonic decays due to radiative gluon effects [14]. On the other hand, the equality of the D_s^+ and D^0 lifetimes, a natural consequence of interference dominance, appears rather accidental in annihilation models. Moreover, weak annihilation should not only induce nonleptonic D_s^+ decays but also contribute to the semileptonic width of the D_s^+ via $D_s^+ \rightarrow \bar{l}\nu_l + X_{glue}$. Obviously, similar channels do not exist for D^0 decays via W -exchange. Therefore, one expects $B_{sl}(D_s^+) > B_{sl}(D^0)$, in contrast to $B_{sl}(D_s^+) = B_{sl}(D^0)$ as implied by the interference interpretation of the $D^+ - D^0$ lifetime difference. In other words, the D_s^+ semileptonic branching ratio provides a good way to discriminate between the two competing pictures [10]. Finally, if the soft gluon background plays a decisive role in meson decays, it presumably has also some effects on baryon decays. Making the assumption that the shifts of baryon lifetimes due to W -exchange completely dominate the quark interference modifications contrary to the expectation on the basis of quark

model estimates, one arrives at

$$\tau(\Xi_c^0) \simeq \tau(\Lambda_c^+) < \tau(\Xi_c^+) \simeq \tau(\Omega_c^0) \quad (2.78)$$

Comparison with the lifetime hierarchy, eq. (75), obtained in the valence quark approximation using conventional quark model wavefunctions shows that accurate data on the Ω_c^0 and Ξ_c^0 lifetimes can clarify the issue. Clearly, a confirmation of the existing rough measurement of the Ω_c^0 lifetime would speak against strong interference effects, and thus indirectly support annihilation models.

To conclude, in inclusive approaches leading asymptotically to the spectator model it is possible to qualitatively reproduce the observed lifetime hierarchy, eq. (70), of charmed particles by taking into account quark interference (D^+ , Λ_c^+ , Ξ_c^+ , Ξ_c^0 , Ω_c^0), and/or W -exchange (D^0 , Λ_c^+ , Ξ_c^0) and weak annihilation (D_s^+). However, a clear quantitative explanation of the data has so far been prevented by calculational uncertainties. This problem exists in particular for the W -exchange and annihilation mechanisms in D -decays where one has to invoke nonperturbative gluon dynamics in order to circumvent helicity suppression.

In my opinion there is growing evidence in favour of quark interference as the main origin of the $D^+ - D^0$ lifetime difference [6, 10]. This belief relies substantially on the results of advanced studies of exclusive D decays. Experimentally, the two-body channels including resonances are found to constitute a large fraction of all non-leptonic D^\pm and D^0 decays [13]. Therefore, the correct theory of exclusive decays should simultaneously explain the D meson lifetime difference. Without going into further details I just recall some important results. Firstly, the main features of the observed two-body branching ratios can be described *without* annihilation and W -exchange [15], provided one consistently works in the large N_c limit [16] (N_c being the number of colour degrees of freedom). It should be noted that for $N_c \rightarrow \infty$, the usually assumed factorization of weak matrix elements holds strictly. Direct calculation of the total two-body D decay widths $\Gamma_2(D)$ then yields the ratio [15]

$$\frac{\Gamma_2(D^0)}{\Gamma_2(D^+)} \approx 3 \quad (2.79)$$

Together with the semileptonic widths $\Gamma_{sl}(D^+) \simeq \Gamma_{sl}(D^0)$ this result essentially explains the total $D^+ - D^0$ lifetime ratio quoted in eq. (70). Secondly, final state interactions turn out to be important. Among other effects, they feed, via rescattering, annihilation-type decay channels such as $D^0 \rightarrow \bar{K}^0 \phi$ [15, 17]. Thirdly, annihilation and W -exchange enter through non-factorizable matrix elements. The latter are non-leading in the sense of a formal expansion in $1/N_c$, and have been estimated using QCD sum rule methods [18]. According to these estimates, the D^0 and D_s^+ lifetimes are shortened only by about 20%

in contrast to the large effect of quark interference in D^+ decays apparent from eq. (79). In summary, studies of exclusive D decays lend substantial support to the valence quark approximations for inclusive decays described at the beginning of this section.

Spectator Model Predictions on the Bottom Lifetime

In the spectator model inclusive nonleptonic and semileptonic widths of heavy quark states are replaced by the corresponding free quark decay rates. The estimates made in eqs.(67) and (68) are very rough approximations of this kind. These estimates can be refined by taking into account

- (i) phase space corrections due to finite quark and lepton masses [19],
- (ii) QCD corrections [9, 14, 20, 21] arising from virtual gluon exchanges and real gluon emission, and
- (iii) smearing effects due to the Fermi motion of the constituents inside the decaying bound states (Altarelli et al. [14]; see also ref. [22]).

The corrections (i) and (ii) are comprised in the following expressions for semileptonic and nonleptonic decay rates:

$$\Gamma_{sl}(Q \rightarrow q\bar{l}\nu_l) = |V_{qQ}|^2 I(r_q, r_l, 0) \eta_{sl} \frac{G_F^2 m_Q^5}{192\pi^3} \quad (2.80)$$

$$\Gamma_{nl}(Q \rightarrow q_1 q_2 \bar{q}_3) = |V_{q_1 Q}|^2 |V_{q_3 q_2}|^2 I(r_{q_1}, r_{q_2}, r_{q_3}) \eta_{nl} 3 \frac{G_F^2 m_Q^5}{192\pi^3} \quad (2.81)$$

Here, V_{ab} are elements of the CKM matrix, $I(r_a, r_b, r_c)$ with $r_a = \frac{m_a}{m_Q}$ are phase space factors, and η_{sl} and η_{nl} are QCD correction factors. Explicit formulas for the phase space functions $I(r_a, r_b, r_c)$ can be found, for example, in ref. [19]. For massless final states one obviously has $I(0, 0, 0) = 1$. Similarly, the normalization of the QCD factors is such that $\eta_{sl} \rightarrow 1$ and $\eta_{nl} \rightarrow 1$ when the strong interactions are switched off. Virtual gluon corrections to the effective weak hamiltonian only affect four-quark operators, but not local operators consisting of a product of a quark current and a leptonic current. Therefore, $\eta_{sl} \neq 1$ is solely due to radiative corrections to the Born approximation of $\Gamma_{sl}(Q \rightarrow q\bar{l}\nu_l)$. In lowest order and neglecting the lepton masses, one has

$$\eta_{sl} = 1 - \frac{2\alpha_s(m_Q^2)}{3\pi} \left(\pi^2 - \frac{25}{4} \right) f(r_q) \quad (2.82)$$

where $f(0) = 1$, while the coefficient $f(r_q)$ for a massive final state quark can be obtained from ref. [14]. In contrast, η_{nl} generally receives contributions from the renormalization of the nonleptonic hamiltonian H_{nl} as well as from radiative corrections to the decay rate for $Q \rightarrow q_1 q_2 \bar{q}_3$ derived from H_{nl} . In leading logarithmic approximation (LLA) only the short-distance QCD effects on H_{nl} enter yielding [9]

$$\eta_{nl} = \frac{1}{3} (2c_+^2 + c_-^2) \quad (2.83)$$

For bottom decays, the short-distance coefficients c_{\pm} are given by

$$c_{\pm} = \left(\frac{\alpha_s^{(6)}(m_t^2)}{\alpha_s^{(6)}(m_W^2)} \right)^{\frac{d_{\pm}}{2b_6}} \left(\frac{\alpha_s^{(5)}(m_b^2)}{\alpha_s^{(5)}(m_t^2)} \right)^{\frac{d_{\pm}}{2b_5}} \quad (2.84)$$

where $d_- = -2d_+ = 8$ and $\alpha_s^{(f)}(Q^2)$ is the running QCD coupling constant for f effective massless flavours:

$$\alpha_s^{(f)}(Q^2) = \frac{4\pi}{b_f \ln \frac{Q^2}{\Lambda_f^2}} \quad (2.85)$$

with $b_f = 11 - \frac{2}{3}f$ and Λ_f being the relevant QCD Λ -parameter. Continuity of $\alpha_s^{(f)}(Q^2)$ is ensured by the relation $\Lambda_6 = \Lambda_5(\Lambda_5/m_t)^{\frac{2}{21}}$. Strictly speaking, eq. (84) holds for $m_b \ll m_t \ll m_W$. The next-to-leading order (NLLA) corrections have been calculated in the massless limit taking for the number f of excited flavours some effective value between 4 and 6 [21]. The resulting QCD factor η_{nl} can be written in the form

$$\eta_{nl} = \frac{1}{3}(2c_+^2 + c_-^2) \left(1 + \frac{2\alpha_s^{(f)}(m_Q^2)}{3\pi} h_f \right) \quad (2.86)$$

where $c_{\pm} = (\alpha_s^{(f)}(m_Q^2)/\alpha_s^{(f)}(m_W^2))^{d_{\pm}/2b_f}$ and $\alpha_s^{(f)}(Q^2)$ is the running QCD coupling in two-loop approximation. The coefficient h_f contains contributions from the two-loop anomalous dimensions of the relevant four-quark operators as well as from $O(\alpha_s)$ radiative corrections to $Q \rightarrow q_1 q_2 \bar{q}_3$. The latter are discussed separately in ref. [20]. Numerically, h_f turns out to be of order unity in the c and b mass range, and decreases as m_Q increases. The normal size of the NLLA effects and the tendency to corroborate the nonleptonic enhancement found in LLA demonstrate the reliability of the QCD corrections in eqs.(80) and (81). Evaluating η_{sl} and η_{nl} from eqs.(82) and (86) for $b \rightarrow c$ transitions, using $m_b = 4.8\text{GeV}$, $m_c = 1.35\text{GeV}$, $f = 5$ and $\Lambda_{\overline{MS}} = 150$ (300) MeV, one obtains

$$\eta_{sl} = 0.89(0.87) \text{ and } \eta_{nl} = 1.11(1.18). \quad (2.87)$$

As expected from asymptotic freedom, the QCD corrections to the free quark predictions for bottom decays are considerable smaller than in the charm case [6, 10].

Finally, the spectator model can be further improved by taking into account the Fermi motion of the constituents inside the initial heavy hadrons. The corrections are mainly important for decay spectra, in particular, for the endpoint region of the charged lepton spectrum from semileptonic B decays which is used to determine the ratio of the $b \rightarrow u$ versus $b \rightarrow c$ couplings. For integrated semileptonic and nonleptonic widths this bound state effect is less essential. Nevertheless, following the procedure suggested by Altarelli et al. [14] for D and B mesons one can reduce the uncertainties in the spectator model

prediction, eq. (80), on the semileptonic width $\Gamma_{sl}(Q \rightarrow ql\bar{\nu}_l)$ coming from the uncertain values of the quark masses m_Q and m_q . The trick is essentially to exploit the constraints on m_Q and m_q provided by the measured shape of the lepton energy spectrum. Consider the desintegration of a $(Q\bar{q}_{sp})$ -bound state P induced by the decay $Q \rightarrow ql\bar{\nu}_l$ in which the spectator antiquark \bar{q}_{sp} is emitted as an on-shell particle with mass m_{sp} and momentum \vec{p} . The heavy quark Q must then be off-shell because of energy-momentum conservation. In the restframe of P , its invariant mass is given by

$$W_Q^2 = M_P^2 + m_{sp}^2 - 2M_P\sqrt{m_{sp}^2 + |\vec{p}|^2} \quad (2.88)$$

where M_P is the physical meson mass. Moreover, Q carrying the momentum $-\vec{p}$ decays in flight. Hence, the energy spectrum of the lepton l in the restframe of P is obtained by folding the appropriately boosted spectrum from $Q \rightarrow ql\bar{\nu}_l$ with the distribution in $|\vec{p}|$. The latter is usually assumed to be gaussian:

$$\phi(|\vec{p}|) = \frac{4}{\sqrt{\pi}p_F^3} \exp\left(-\frac{|\vec{p}|^2}{p_F^2}\right); \int_0^\infty \phi(p)p^2 dp = 1 \quad (2.89)$$

where p_F characterizes the average Fermi momentum, i.e. $p_F \lesssim 300\text{MeV}$. The final lepton spectrum is thus parametrized in terms of the spectator mass m_{sp} , the Fermi momentum p_F , and the mass m_q of the final quark. These parameters are to be suitably chosen or fitted to the experimental spectrum. The heavy quark mass m_Q does not appear as an independent parameter, but is replaced by the average effective mass $\langle W_Q \rangle$ determined for a given value of m_{sp} by the fitted value of p_F . A recent analysis of the electron spectrum from B decays has lead to the following values for the effective b and c quark masses [7]:

$$m_b = (4.93 \pm 0.05)\text{GeV}, \quad m_c = (1.56 \pm 0.06)\text{GeV} \quad (2.90)$$

$$m_b - m_c = (3.37 \pm 0.03)\text{GeV}.$$

Obviously, the semileptonic width Γ_{sl} can be obtained directly by integrating the theoretical lepton spectrum resulting from the fit. Alternatively, one may use the spectator model formula, eq. (80), together with the above mass values and η_{sl} from eq. (87) to find

$$\Gamma_{sl}(b \rightarrow ce^- \bar{\nu}_e) = |V_{cb}|^2 \frac{0.43}{10^{-14}\text{s}} \quad (2.91)$$

It is important to note that this prediction is not too sensitive to the precise values of m_b and m_c as long as the mass difference $m_b - m_c$ is fixed. For illustration, taking $m_b - m_c$ from eq. (90) and varying m_b from 4.8 GeV to 5.2 GeV, the numerical coefficient in eq. (91) varies only from 0.41 to 0.48.

Combining the improved spectator model result eq. (91) with the world averages of the semileptonic branching ratio and total B lifetime (ref. [23] and Kleinknecht [7]),

$$B_{sl}(B) = (10.9 \pm 0.8)\% \quad (2.92)$$

$$\tau(B) = (1.15 \pm 0.14) \times 10^{-12}\text{s}$$

and neglecting $\Gamma_{sl}(b \rightarrow ul\bar{\nu}_l) (< 0.04\Gamma_{sl}(b \rightarrow cl\bar{\nu}_l) [7])$, one obtains

$$|V_{cb}| \simeq \left(\frac{10^{-14}s}{0.43} \times \frac{B_{sl}(B)}{\tau(B)} \right)^{1/2} \simeq 0.047 \pm 0.005 \quad (2.93)$$

where the error estimate is taken from Schubert [7].

It is of course also interesting and necessary to check whether the experimental results on B_{sl} and τ given in eq. (92) and used in eq. (93) can be understood within the spectator model. This requires the calculation of the total nonleptonic width $\Gamma_{nl}(b \rightarrow c)$. Again, $\Gamma_{nl}(b \rightarrow u)$ is practically negligible since $\Gamma_{nl}(b \rightarrow u)/\Gamma_{nl}(b \rightarrow c) \simeq \Gamma_{sl}(b \rightarrow u)/\Gamma_{sl}(b \rightarrow c) < 0.04$. Nevertheless, in the following the $b \rightarrow u$ contributions are included assuming the maximum allowed value $|\frac{V_{ub}}{V_{cb}}|^2 = 0.02$. Below, I present numerical predictions on the B lifetime and semileptonic branching ratio derived from eqs.(80) and (81) for two rather extreme choices of quark masses and for QCD corrections as estimated in eq. (87):

$$\tau(B) \times \frac{|V_{cb}|^2}{10^{-15}s} = \begin{cases} 2.9(2.8) & (I) \\ 3.1(3.0) & (II) \end{cases} \quad (2.94)$$

$$B_{sl}(B) = \begin{cases} 0.13(0.12) & (I) \\ 0.16(0.15) & (II) \end{cases} \quad (2.95)$$

Here, (I) and (II) refer to the two sets of quark masses $(m_b, m_c, m_s, m_{u,d}) = (4.8, 1.4, 0.15, 0)$ GeV (I) and $(5.2, 1.8, 0.5, 0.3)$ GeV (II), while the two numbers given for each mass assumption correspond to $\Lambda_{\overline{MS}} = 150\text{MeV}$ (300 MeV). In the spirit of the spectator model, the above expectations apply to all weakly decaying bottom hadrons. Substituting the experimental B lifetime from eq. (92) in eq. (94) one gets

$$|V_{cb}| \simeq 0.049 \text{ to } 0.052. \quad (2.96)$$

Some comments are in order:

- (i) The total bottom lifetime expected in the spectator model is consistent with the measured B lifetime and the value of $|V_{cb}|$ derived from inclusive semileptonic B decays.
- (ii) Similarly as the semileptonic width also the total nonleptonic width does not depend very sensitively on the precise values of the input quark masses provided the difference of the two heavy masses $m_b - m_c$ is kept fixed. More definitely, $\Gamma_{nl}(b \rightarrow c)$ decreases by about 20% when changing the masses from set (I) to set (II) and taking $m_b - m_c = 3.4$ GeV as suggested by experiment (see eq. (90)). Moreover, this decrease is largely compensated in $\Gamma_{tot}(b \rightarrow c)$ by the corresponding increase of $\Gamma_{sl}(b \rightarrow c)$ so that the total lifetime given in eq. (94) varies by less than 10%.
- (iii) The semileptonic branching ratio varies more strongly under the same variation of quark masses. Comparison of the theoretical and experimental results given in eqs.(95)

and (92), respectively, clearly shows that small quark masses and large QCD corrections lead to a better agreement.

(iv) The present world average of $B_{sl}(B)$, eq. (92), seems to lie slightly below the lowest value of $B_{sl}(B)$ resulting from the spectator model in the parameter range considered in eq. (95). Although the discrepancy is not very significant, it is reminiscent of the situation in D decays. There, the measured D^0 and D^\pm branching ratios, $B_{sl}(D^0) \simeq 7.5\%$ and $B_{sl}(D^\pm) \simeq 17\%$ [13], yield on average $B_{sl}(D) \simeq 12\%$, whereas the spectator model typically predicts about 15%.

Suppose one would not know the individual semileptonic branching ratios of the D^0 and D^\pm . The above discrepancy could then seemingly be cured by taking into account in the calculation of $B_{sl}(D)$ only the leading order contributions in a formal $1/N_c$ expansion of the inclusive rates [11,16]. One may argue that since not all non-leading in $1/N_c$ terms can be calculated at present, but only those with factorizable matrix elements, the contributions from higher orders in $1/N_c$ should be dropped altogether for consistency. This argument is supported by the successful description of the two-body D decays in a conventional valence quark model after removing the non-leading in $1/N_c$ terms (with the exception of final state interactions) [15,16]. In the inclusive case, the above prescription implies the replacement of the usual short-distance factor $\frac{1}{3}(2c_+^2 + c_-^2)$ assumed in the previous discussion (see eq. (83) by the factor $\frac{1}{2}(c_+^2 + c_-^2)$. This modification leads to a stronger nonleptonic enhancement, since

$$\frac{\frac{1}{2}(c_+^2 + c_-^2)}{\frac{1}{3}(2c_+^2 + c_-^2)} \simeq \begin{cases} 1.3 & c - \text{decay} \\ 1.2 & b - \text{decay} \end{cases} \quad (2.97)$$

and consequently to lower semileptonic branching ratios. Considering only the average value $B_{sl}(D) = \frac{1}{2}(B_{sl}(D^0) + B_{sl}(D^\pm))$, the additional nonleptonic enhancement factor, eq. (97), suffices to reconcile the spectator model to experiment. However, knowing the individual D^0 and D^\pm semileptonic branching ratios we can of course not accept this as a solution of the problem. In addition, one has to invoke non-spectator effects in order to explain the difference in $B_{sl}(D^0)$ and $B_{sl}(D^\pm)$ (see discussion in preceding section). Nevertheless, it is interesting to observe that the situation improves considerably as compared to the original spectator model treatment if one restricts oneself to the leading order in $1/N_c$. Firstly, the disagreement between the experimental value $B_{sl}(D^0) \simeq 7.5\%$ and the original spectator model prediction $B_{sl}(D) \approx 15\%$ is reduced by a factor 2. Secondly, the equivalent decrease in $B_{sl}(D^+)$ is compensated by a reinforcement of the Pauli interference effect shifting $B_{sl}(D^+)$ back to the experimental value $B_{sl}(D^+) \simeq 17\%$. The remaining discrepancy in $B_{sl}(D^0)$ may indicate the presence of sizeable contributions to the nonleptonic width $\Gamma_{nl}(D^0)$ from higher orders in $1/N_c$ [18], from di-quark correlations [24], or from W -exchange contrary to valence quark estimates [6,10].

Returning to B decays, one finds that the modification of the spectator model estimates, eqs.(94) and (95), according to eq. (97) gives perfect agreement between theory and experiment. It should be emphasized that the rule of keeping only the leading order in $1/N_c$ contributions is also supported by the study of two-body B decays, in particular, the channels $B \rightarrow J/\psi K$ and $J/\psi K^*$ [15]. Yet, the experience with charm decays shows that from the successful calculation of the average B^0 and B^\pm lifetime and semileptonic branching ratio alone one cannot conclude that higher order in $1/N_c$ corrections and non-spectator contributions are completely negligible. In order to clarify this point it is essential to look for differences in lifetimes and semileptonic branching fractions of the various bottom hadrons. Theoretical expectations are discussed in the next section using the implications from charm decays summarized in the previous section as a guidance.

Non-Spectator Corrections and Lifetime Differences of Bottom Hadrons

The degeneracy of lifetimes which exists in the spectator model is lifted by preasymptotic effects involving the spectator quarks. As recapitulated in second section, the charmed lifetime hierarchy most likely results from quark interference and, in the case of baryons, in addition from W -exchange processes. For meson decays, annihilation type processes seem to play a less significant role. Considering the flavour structure of the bottom hadrons and the pattern of the Cabibbo-Kobayashi-Maskawa matrix [7] one can immediately single out those few non-spectator processes which could in principle have noticeable effects on the bottom lifetimes [6, 10]. In the following discussion I concentrate on the B^- , \bar{B}_d^0 , \bar{B}_s^0 , and Λ_b^0 particles (and their charge conjugates), and refer to the other weakly decaying bottom hadrons only in a few scattered comments. The very interesting states containing also a charm quark such as the $B_c^- (b\bar{c})$ or the (bcc) -baryon are not considered here.

Quark interference occurs dominantly in the channels

$$B^-(b\bar{u}) \rightarrow c\bar{u}d\bar{u} \quad (2.98)$$

$$\Lambda_b^0(bud) \rightarrow c\bar{u}dud \quad (2.99)$$

All other B^- and Λ_b^0 channels leading to identical (anti)-quark pairs are suppressed either by the Cabibbo angle, or the very small $b \rightarrow u$ coupling, or by phase space. Frequently, one has two of the above suppression factors at the same time. Illustrative examples are $B^- \rightarrow c\bar{u}s\bar{u}$, $\Lambda_b^0 \rightarrow u\bar{u}dud$, and $\Lambda_b^0 \rightarrow c\bar{c}dud$. Concerning other bottom hadrons, it should be stressed that \bar{B}_d^0 and \bar{B}_s^0 decays are not at all affected by quark interference. However, important decay modes of other baryons such as $\Xi_b^-(bsd) \rightarrow c\bar{u}dsd$, $\Xi_b^0(bsu) \rightarrow c\bar{c}ssu$, and $\Omega_b^0(bss) \rightarrow c\bar{c}sss$ are subject to Pauli interference. Furthermore, similarly as for the D^+ and Λ_c^+ one finds for the B^- and Λ_b^0 that the interference is destructive. Hence, the lifetimes of the B^- and Λ_b^0 tend to be lengthened and the semileptonic branching

ratios tend to be increased in comparison to the spectator model predictions given in the preceding section. While for the Λ_b^0 this expectation is a direct consequence of the Pauli principle, in the case of the B^- the hard gluon corrections to H_{nl} making $c_-^2 > 2c_+^2$ are essential [4, 5, 11]. Without these corrections, $c_- = c_+ = 1$ and the interference effect on $\tau(B^-)$ would have the opposite sign!

In the presence of a positively charged valence quark or antiquark, besides the b -quark, a bottom hadron can also decay via W -exchange. This condition is fulfilled for the \bar{B}_d^0, \bar{B}_s^0 and Λ_b^0 . The relevant channels are indicated below:

$$\bar{B}_d^0(b\bar{d}) \rightarrow c\bar{u} \quad (2.100)$$

$$\bar{B}_s^0(b\bar{s}) \rightarrow c\bar{c} \quad (2.101)$$

$$\Lambda_b^0(bud) \rightarrow cdd \quad (2.102)$$

All other W -exchange modes are Cabibbo suppressed or involve the tiny $b \rightarrow u$ coupling, and can therefore be neglected when considering total lifetimes. Obviously, the above processes tend to shorten the \bar{B}_d^0, \bar{B}_s^0 and Λ_b^0 lifetimes and to decrease the corresponding semileptonic branching ratios with respect to the spectator model expectations, quite in analogy to what is the case for the D^0 and Λ_c^+ . However, following the arguments given in the second section, the effect is completely negligible in meson decays, unless the presence of gluons in hadronic bound states catalyzes this mechanism by circumventing, in some way, the suppression due to helicity conservation. In contrast, W -exchange contributions to the nonleptonic width of the Λ_b^0 (and also the Ξ_b^0) are not helicity suppressed and, therefore, more likely.

Finally, *weak annihilation* can only take place in B^- and B_c^- decays. In the first case, it is suppressed by the small $b \rightarrow u$ coupling, and thus irrelevant for the B^- lifetime. The second case resembling weak annihilation in D_s^+ decays is rather special, since the B_c^- can make transitions to ordinary B mesons via the decay of the charm quark (rather than the bottom quark), and the emission of pseudoscalar or vector octet mesons. Note in this respect that $\tau_c \simeq 6 \cdot 10^{-12} s$ and $\tau_b \simeq 10^{-12} s$ are not very different.

The above survey of possible non-spectator processes in bottom decays leads to a unique qualitative hierarchy of lifetimes and inclusive semileptonic branching ratios:

$$\tau(B^-) > \tau(\bar{B}_s^0) \geq \tau(\bar{B}_d^0) > \tau(\Lambda_b^0) \quad (2.103)$$

$$B_{sl}(B^-) > B_{sl}(\bar{B}_s^0) \geq B_{sl}(\bar{B}_d^0) > B_{sl}(\Lambda_b^0) \quad (2.104)$$

One should note that the relation of $\tau(\bar{B}_s^0)$ and $\tau(\bar{B}_d^0)$ in eq. (103) takes into account the phase space suppression of the W -exchange process (101) relative to the process (100).

Moreover, since there is only the spectator model route to semileptonic final states, the semileptonic branching ratios in eq. (104) follow exactly the lifetime pattern. This is different from charm decays where $D_s^+ \rightarrow l^+ \nu_l X$ may also proceed via weak annihilation as emphasized in the chapter on charm lifetimes.

Reliable estimates of the actual magnitude of the differences in lifetimes and semileptonic branching ratios are not necessarily easier for bottom hadrons than they have been for charmed hadrons. On the contrary, in the bottom case one cannot approach the problem in an exclusive way by studying all two-body decay modes, since the latter constitute only a rather small fraction of the nonleptonic decay width and do therefore not allow conclusions on the total widths. This possibility exists in the charm case and has led to some clarification as already mentioned. Nevertheless, a reasonable order of magnitude estimate of the inequalities given in eqs.(103) and (104) can be obtained by using the scaling laws for non-spectator processes in the nonrelativistic valence quark model, i.e. eqs.(71) and (74), and extrapolating the experimental $D^+ : D^0 : \Lambda_c^+$ lifetime ratios shown in eq. (70) to the bottom mass range. One then finds

$$\begin{aligned} \frac{\tau(B^-)}{\tau(\bar{B}_d^0)} &\simeq 1 + r_{\text{QCD}} \left(\frac{f_B}{f_D} \right)^2 \left(\frac{m_c}{m_b} \right)^2 \left[\frac{\tau(D^+)}{\tau(D^0)} - 1 \right] \\ &\simeq \begin{cases} 1.15 & \text{for } f_B \simeq f_D \\ 1.06 & \text{for } f_B/f_D \simeq \sqrt{m_c/m_b} \end{cases} \end{aligned} \quad (2.105)$$

and, similarly,

$$\begin{aligned} \frac{\tau(\bar{B}_d^0)}{\tau(\Lambda_b^0)} &\simeq 1 + r_{\text{QCD}} \frac{|\psi_{bu}(0)|^2}{|\psi_{cd}(0)|^2} \left(\frac{m_c}{m_b} \right)^3 \left[\frac{\tau(D^0)}{\tau(\Lambda_c^+)} - 1 \right] \\ &\simeq \begin{cases} 1.10 & \text{for } |\psi_{bu}/\psi_{cd}| \simeq \sqrt{m_b/m_c} \\ 1.04 & \text{for } |\psi_{bu}| \simeq |\psi_{cd}| \end{cases} \end{aligned} \quad (2.106)$$

where the two alternative assumptions on the meson decay constants and the baryon wavefunctions correspond to each other. The ratio r_{QCD} of the relevant QCD short-distance factors is set to 1 in the above numerical estimates. Actually, the decrease of the hard gluon corrections when going from m_c to m_b suppresses the influence of quark interference and W -exchange on B^- and Λ_b^0 decays further by roughly a factor of 3 and 1.5, respectively [10]. Thus, the valence quark description of inclusive decays suggests that the lifetime differences among bottom hadrons should not exceed 10%.

A similar conclusion is reached in annihilation models invoking a strong nonperturbative gluon enhancement of W -exchange and weak annihilation processes. Assuming eq. (77) one basically reproduces the result of eq. (105). On the other hand, if one follows

the perturbative estimate (Bander et al. [2]) leading to eq. (76), one obtains

$$\begin{aligned} \frac{\Gamma(\bar{B}_d^0 \rightarrow c\bar{u}g)}{\Gamma(\bar{B}_d^0 \rightarrow c\bar{u}d\bar{d})} &\simeq \frac{2\pi\alpha_s(m_b^2)(c_+ + c_-)^2}{27(2c_+^2 + c_-^2)} \left(\frac{f_B}{m_d}\right)^2 \\ &\simeq 0.02 \left(\frac{f_B}{0.15 \text{ GeV}}\right)^2 \left(\frac{0.3 \text{ GeV}}{m_d}\right)^2 \end{aligned} \quad (2.107)$$

that is again a very small effect on the \bar{B}_d^0 lifetime.

Sometimes it is argued that the low value of the experimental semileptonic branching ratio $B_{sl}(B) \simeq 10.9\%$ (see eq. (92)), which is an average over $B_{sl}(B^\pm)$ and $B_{sl}(B^0)$, indicates sizeable W -exchange contributions to B^0 decays, and thus implies a considerable B meson lifetime difference. The essence of this argument can be illustrated by the following simple numerical example. Starting from the upper range of the spectator model predictions on $B_{sl}(B)$ given in eq. (95)(II), i.e. $B_{sl}(B) \simeq 15\%$, and allowing for non-spectator decays of the B^0 , one has

$$\begin{aligned} B_{sl}^{\text{exp}}(B) &\simeq \frac{1}{2}(B_{sl}(B^\pm) + B_{sl}(B^0)) \\ &\simeq \frac{1}{2}\left(0.15 + \frac{0.15}{1 + \gamma}\right) \end{aligned} \quad (2.108)$$

where $\gamma = \Gamma_{nl}^{\text{nonspect}}/\Gamma_{tot}^{\text{spect}}$. The experimental result $B_{sl}^{\text{exp}}(B) \simeq 11\%$ then requires

$$\frac{\Gamma_{nl}^{\text{nonspect}}}{\Gamma_{tot}^{\text{spect}}}(B^0) \simeq 1 \quad (2.109)$$

and, hence, implies

$$\frac{\tau(B^\pm)}{\tau(B^0)} \simeq 1 + \frac{\Gamma_{nl}^{\text{nonspect}}}{\Gamma_{tot}^{\text{spect}}}(B^0) \simeq 2 \quad (2.110)$$

This possibility is not yet excluded by experiment which so far only provides the bound [25]

$$0.5 < \frac{\tau(B^\pm)}{\tau(B^0)} < 2.5 \quad (2.111)$$

However, the above argument is based on a prejudice concerning the spectator model value of $B_{sl}(B)$, and moreover contradicts quite reasonable and general theoretical considerations. In fact, starting from the lower value $B_{sl}^{\text{spect}}(B) \simeq 12\%$ obtainable from the spectator model, one would derive $\Gamma_{nl}^{\text{nonspect}}/\Gamma_{tot}^{\text{spect}} \simeq 0.2$ instead of eq. (109), and thus conclude

$$\frac{\tau(B^\pm)}{\tau(B^0)} \simeq 1.2 \quad (2.112)$$

This number is in qualitative agreement with the theoretical scenarios outlined earlier in this section.

We see that the non-spectator corrections to bottom decays should be rather small: of the order of a few to may be ten percent. Correspondingly, the lifetimes of the different bottom hadrons and their inclusive semileptonic branching ratios should be shifted from the uniform spectator model values by a similarly small amount. Moreover, the shifts should produce the hierarchy exhibited in eqs. (103,104). Finally, while the lifetime difference of the mass eigenstates of the neutral $B_d^0 - \bar{B}_d^0$ system is also expected to be very small, the lifetime difference of the $B_s^0 - \bar{B}_s^0$ mass eigenstates may reach 30%, and thus be the largest lifetime difference among all weakly decaying bottom hadrons [26], with the possible exception of $(b\bar{c})$ - and (bcc) -states.

Conclusions

The spectator model is expected to provide an appropriate framework for the description of inclusive weak decay properties of bottom hadrons. Non-spectator corrections which are found to be of order unity in charm decays are estimated to drop to a level of or below 10% in bottom decays. Accordingly, the total lifetimes and inclusive semileptonic branching ratios for all weakly decaying bottom hadrons should be equal within a few to ten percent. An interesting exception may be the mass eigenstates of the $B_s^0 - \bar{B}_s^0$ system the lifetimes of which may differ by a larger amount.

The quantitative predictions of the spectator model are subject to uncertainties arising mainly from uncertain values of the effective initial and final state quark masses, and to a lesser extent from the Fermi motion of the heavy quark and from gluon corrections. Some of the parameters can be fixed or constrained by fitting the theoretical decay lepton spectra to the experimental distributions. Using then the result as input in the evaluation of nonleptonic widths one can also predict the total bottom lifetime and semileptonic branching ratio with a considerably reduced uncertainty of about 30%. It is fair to say that the current data on $\tau(B)$ and $B_{sl}(B)$ can be well accommodated in the spectator model (with $|V_{cb}|$ taken from inclusive or exclusive semileptonic decays and $|V_{ub}| \ll |V_{cb}|$). However, it should also be stressed that a semileptonic branching ratio $B_{sl}(B) \simeq 10\%$ as obtained in the most recent ARGUS and CLEO measurements [12] with an error of about 1% becomes difficult to be understood within the spectator model. If this result is confirmed with a smaller error one may have to reconsider the question of non-spectator corrections.

At any rate, in the absence of a clear and absolutely reliable answer from theory, it is very important to exploit every possibility which might exist at LEP of measuring the lifetimes and inclusive semileptonic branching ratios separately for the various bottom hadrons.

2.6.2. EXPERIMENTAL ASPECTS*

The inclusive mean B lifetime, averaging the results from the PEP and PETRA experiments, is measured to be $\tau_B = 13.1^{+1.4}_{-1.3} 10^{-13}$ s [27]. What are the prospects at LEP for improving this measurement? Can we go beyond and measure individual B_d^0, B_u^+, B_s^0 and Λ_b^0 lifetimes? As seen in the theory section, the theoretical expectation for the B^0, B^+ lifetime difference is at most 30%. Can we reach the interesting level of 10% precision on individual lifetimes?

Inclusive B lifetime measurement

The method of measuring the impact parameter of leptons coming from semileptonic decays presents several advantages (see Fig. 2.27 for definition). The mean impact parameter does not depend, in first approximation, on the energy of the B meson and hence on the precise knowledge of the fragmentation function. The residual dependence of the mean impact parameter on the B meson energy, as seen in Fig. 2.27, is smaller at LEP than it was at PEP and PETRA energies.

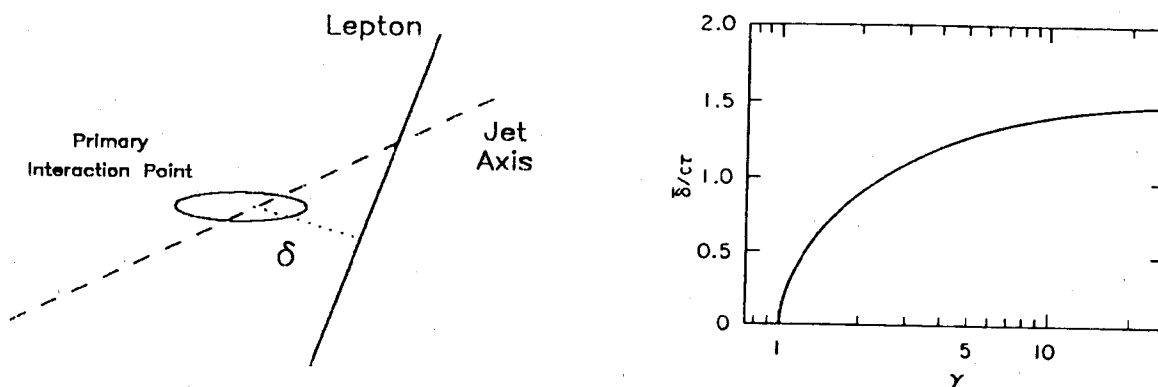


Fig. 2.27: Definition of the impact parameter and variation of the average impact parameter as a function of γ_B . From Ref. 28.

Selecting leptons with high momentum and high p_T with respect to the jet axis allows tagging of B mesons with typical efficiencies of 10% (where efficiency is defined as the number of tagged $B\bar{B}$ events over the total number of $B\bar{B}$ events) and purities of 70 – 80%. The background consists of cascade $b \rightarrow c \rightarrow l$ decays, primary $c \rightarrow l$ decays and $u, d, s \rightarrow l$ decays or misidentified hadrons. The lepton spectrum being rather well known, one can estimate those background with a good accuracy.

The mean impact parameter for a B lifetime of 13×10^{-13} s is $350\mu m$ in space or $230\mu m$ projected in the plane perpendicular to the beam axis. The resolution on impact parameters expected in the LEP experiments [29] with their foreseen vertex detectors and the present design of the beam pipe will be typically 30 – $40\mu m$ at momentum above

*M. BOSMAN in collaboration with H.-G. MOSER, B. VAN EIJK, P. MÄTTIG

10 GeV while the multiple scattering in the beam pipe and the detector itself leads to a resolution of $50\mu m$ ($200\mu m$) at 5 GeV (1 GeV). This could be improved by reducing the beam pipe radius. The knowledge of the primary vertex is determined first by the beam crossing profile. One expects at LEP $\sigma_x \sim 15\mu m$ and $\sigma_y \sim 350\mu m$ in the plane perpendicular to the beam direction. Reconstruction of the primary vertex on an event by event basis can further constrain σ_y to about $100\mu m$. Hence, we will know the primary vertex with an average precision of about $50\mu m$ to be combined with the $30 - 50\mu m$ precision on the impact parameter of the lepton in the momentum range considered. The precision on the lifetime measurement will be:

$$\frac{\sigma_\tau}{\tau} \sim \frac{\sqrt{1 + (\frac{\sigma_{i.p.}}{i.p.})^2}}{\sqrt{N_{lepton}}} \sim \frac{\sqrt{1 + (0.3)^2}}{\sqrt{N_{lepton}}} \sim \frac{1.05}{\sqrt{N_{lepton}}}$$

For $10^5 Z^0$, i.e. 30K B mesons, we expect about 3000 selected leptons and a 2% statistical error on the lifetime. Systematic errors were estimated at PEP and PETRA to be of the order of 20% [30] with contributions from the subtraction of the background, knowledge of the fragmentation function and understanding of the detector resolution. Given the high statistics available at LEP, one could reduce the background by more restrictive selection of the lepton and correspondingly reducing their contribution to the systematic error. As mentioned already, the residual dependence of the mean impact parameter on the fragmentation function is smaller at LEP. So, altogether, a smaller systematic error should be obtained at LEP.

Exclusive B lifetime measurement

To identify the B mesons, fully reconstructed hadronic decays are natural candidates. Tab. 2.17 summarizes branching fractions for low multiplicity exclusive decays and the expected number of events per $10^6 Z^0$ before selection criteria assuming the LUND 6.3 or Webber Monte Carlo "prediction" of $B_s^0 : B_d^0 : B_u^+ \sim 1. : 3.6 : 3.6$ and 9% baryon production.

The number of events in exclusive hadronic decay modes are small. One has to consider that the numbers presented in Tab. 2.17 are further reduced by the acceptance of the vertex detectors and reconstruction efficiency, i.e. a factor 2-3. Decays to J/ψ are expected to give a clean sample while decays to D mesons + hadrons may suffer from higher combinatorial background. The precision on the reconstructed decay vertex is of the order of $200 - 300\mu m$ along the flight path to be compared to an average decay length of 2.5 mm. In fully reconstructed decays, the momentum of the B meson is measured, so we have $\frac{\delta t}{\tau} \sim 10\%$ and hence $\frac{\delta \tau}{\tau} \sim \frac{1}{\sqrt{N_B}}$. The systematic error will come mainly from understanding systematic effects in reconstructing the flight path. For $10^7 Z^0$, with the

Decay Channel	ARGUS	CLEO	THEORY	Nb B/ $10^6 Z^0$
$B_d^0 \rightarrow D^{*-} \pi^+$ $D^{*-} \rightarrow \bar{D}^0 + \pi^+$ $\bar{D}^0 \rightarrow K^+ \pi^-$	$0.35 \pm 0.18 \pm 0.13$	$0.16 \pm 0.12 \pm 0.10$	0.15	10
$B_d^0 \rightarrow D^+ \pi^-$ $D^- \rightarrow K^+ \pi^- \pi^-$	$0.31 \pm 0.13 \pm 0.10$	$0.60^{+0.32+0.15}_{-0.28-0.12}$	0.58	55
$B_u^+ \rightarrow \bar{D}^0 \pi^+$	$0.19 \pm 0.10 \pm 0.06$	$0.51^{+0.17+0.11}_{-0.15-0.07}$	0.37	17
$B_s^0 \rightarrow D_s^- \pi^+$ $D_s^- \rightarrow \phi \pi^-$ $\phi \rightarrow K^+ K^-$			0.5	3
$B_d^0 \rightarrow J/\Psi \bar{K}^{*0}$ $J/\Psi \rightarrow l^+ l^-$ $\bar{K}^{*0} \rightarrow K^+ \pi^-$	0.33 ± 0.18	0.06 ± 0.03	0.39	43
$B_u^+ \rightarrow J/\Psi K^+$ $J/\Psi \rightarrow l^+ l^-$	0.07 ± 0.04	0.05 ± 0.02	0.09	15
$B_s^0 \rightarrow J/\Psi \phi$ $J/\Psi \rightarrow l^+ l^-$ $\phi \rightarrow K^+ K^-$			0.3	7

Tab. 2.17: The expected number of B mesons per $10^6 Z^0$ are calculated with the theoretical values of the B branching fractions [31]. No acceptance or efficiency factors are included. For D mesons and light mesons branching fractions the PDG [27] values are assumed, except for $Br(D_s \rightarrow \phi \pi)$ where 4% is used. The experimental values of the B mesons branching fractions are taken from Ref. 32. [Branching fractions in %].

present knowledge of the branching fractions, one should gather enough statistics to reach the 10% statistical error on individual lifetime.

To find decay modes with higher branching fractions, one has to turn to semileptonic decay channels: $Br(B \rightarrow e + \nu + \text{hadrons}) = 12.3 \pm 0.8\%$ and $Br(B \rightarrow \mu + \nu + \text{hadrons}) = 11.0 \pm 0.9\%$ [27]. Decays $Br(B \rightarrow l + D + \nu)$ and $Br(B \rightarrow l + D^* + \nu)$ are expected to be dominant and in the ratio $D^*/D \sim 3$ [33].

The following pattern is obtained :

$$\begin{aligned}
B_u^+ &\rightarrow \ell^+ \bar{D}^0 \\
\bar{D}^{*0} &\rightarrow \bar{D}^0 + (\pi^0, \gamma) \quad 100\% \\
B_d^0 &\rightarrow \ell^+ \bar{D}^- \\
D^{*-} &\rightarrow \bar{D}^0 + \pi^- \quad 50\% \\
D^- &+ (\pi^0, \gamma) \quad 50\% \\
B_s^0 &\rightarrow \ell^+ D_s^- \\
\bar{D}_s^{*-} &\rightarrow D_s^- + \gamma \quad 100\%
\end{aligned}$$

Pairs $l^+ D^-$, $l^+ D^{*-}$ and $l^+ D_s^-$ are unambiguous signatures for B_d^0 and B_s^0 respectively,

while pairs $l^+\bar{D}^0$ come 60% from B_u^+ , 40% from B_d^0 if the cascade $D^{*-} \rightarrow \bar{D}^0 + \pi^-$ is not identified in the event. Clean samples are expected for $B_d^0 \rightarrow l^+ D^{*-}$ and $B_s^0 \rightarrow l^+ D_s^-$ thanks to the small combinatorial background for the $D^{*-} \rightarrow \bar{D}^0 \pi^-$ cascade and the $D_s^- \rightarrow \phi \pi^-$ decay. Expected number of events for $10^6 Z^0$ before selection criteria are 410 B_d^0 and 160 B_s^0 , an order of magnitude more than for the hadronic decay modes.

The precision on the position of the decay vertex should be of the order of $300 \mu\text{m}$ but, because of the missing ν , the momentum of the B is not known. The momentum of the B meson p_B can be estimated from the ratio $\frac{p_{\text{visible}}/m_{\text{visible}}}{p_B/m_B}$. This ratio is expected to be close to 1 and independent of p_B . This method results in a precision of about 20% on p_B [34]. Hence, we obtain $\frac{\sigma_t}{\tau} \sim \sqrt{(\frac{\sigma_l}{l_0})^2 + (\frac{t}{\tau})^2 (\frac{\sigma_p}{p})^2} \sim 22\%$ which is only slightly better than measuring the lifetime via the lepton impact parameter. With about $10^6 Z^0$, the level of 10% statistical error on individual B mesons should be reached.

For what concerns Λ_b^0 , the semileptonic decay mode $\Lambda_b^0 \rightarrow l^+ + \bar{\Lambda}_c$ or hadronic decay modes to charmed particles like $\bar{p} \bar{D}^0 \pi^+$ are good candidates. It is difficult to predict the ability of the experiments to discriminate those signals from the combinatorial background or reflections from other resonances due to particle identification ambiguities.

REFERENCES

- [1] For early discussions see
M.K. Gaillard, B.W. Lee, J.L. Rosner, *Rev. Mod. Phys.* **47** (1975) 277;
J. Ellis, M.K. Gaillard, D.V. Nanopoulos, *Nucl. Phys. B* **100** (1975) 313;
J. Ellis, M.K. Gaillard, D.V. Nanopoulos, S. Rudaz, *Nucl. Phys. B* **131** (1977) 285.
- [2] W. Bernreuther, O. Nachtmann, B. Stech, *Z. Phys. C* **4** (1980) 257;
S.P. Rosen, *Phys. Rev. Lett.* **44** (1980) 4;
M. Bander, D. Silverman, A. Soni, *Phys. Rev. Lett.* **44** (1980) 7, 962 (Erratum);
H. Fritzsch, P. Minkowski, *Phys. Lett.* **90 B** (1980) 455.
- [3] V. Barger, J.P. Leveille, P.M. Stevenson, *Phys. Rev. Lett.* **44** (1980) 226;
J.L. Cortes, J. Sanchez-Guillen, *Phys. Rev. D* **24** (1981) 2982.
- [4] B. Guberina, S. Nussinov, R.D. Peccei, R. Rückl, *Phys. Lett.* **89 B** (1979) 111;
Y. Koide, *Phys. Rev. D* **20** (1979) 1739;
K. Jagannathan, V.S. Mathur, *Phys. Rev. D* **21** (1980) 3165;
R.D. Peccei, R. Rückl, *Proc. Ahrenschoop Symp. on Special Topics in Gauge Field Theories* (Akademie der Wissenschaften der DDR, Zeuthen, GDR, 1981) p. 8;
T. Kobayashi, N. Yamazaki, *Prog. Theor. Phys.* **65** (1981) 775.
- [5] R. Rückl, *Phys. Lett.* **120 B** (1983) 449;
B. Guberina, R. Rückl, J. Trampetić, *Z. Phys. C* **33** (1986) 297.
- [6] M.A. Shifman, *Proc. Int. Symp. on Production and Decay of Heavy Hadrons, Heidelberg, 1986*, ed. by K.R. Schubert, R. Waldi (DESY, Hamburg, 1986), and *Proc. Int. Symp. on Lepton and Photon Interactions at High Energies, Hamburg, 1987*, ed. by W. Bartel, R. Rückl, *Nucl. Phys. B (Proc. Suppl.)* **3** (1988) 289.
- [7] K.R. Schubert, *Talk at Conf. on Phenomenology in High Energy Physics, ICTP, Trieste, 1988*, University of Karlsruhe, IEKP-KA/88-4 (1988);
K. Kleinknecht, *Proc. XXIV. Int. Conf. on High Energy Physics, Munich, 1988*, ed. by R. Kotthaus, J.H. Kühn (Springer-Verlag, Berlin Heidelberg, 1989) p. 98.
- [8] J.-M. Gérard, this report;
K.R. Schubert, *Prog. Part. and Nucl. Phys.* **21** (1988) 3.

- [9] G. Altarelli, N. Cabibbo, L. Maiani, *Nucl. Phys. B* **88** (1975) 285;
R.L. Kingsley, S.B. Treiman, F. Wilczek, A. Zee, *Phys. Rev. D* **11** (1975) 1919;
J. Ellis, M.K. Gaillard, D.V. Nanopoulos, *Nucl. Phys. B* **100** (1975) 313.
For the analogous octet enhancement in strange particle decays see
M.K. Gaillard, B.W. Lee, *Phys. Rev. Lett.* **33** (1974) 108;
G. Altarelli, L. Maiani, *Phys. Lett.* **52 B** (1974) 351.
- [10] R. Rückl, Weak Decays of Heavy Flavours (Habilitationsschrift, University of Munich, 1983), CERN print (1983), and Proc. XXII. Int. Conf. on High Energy Physics, Leipzig, 1984, ed. by A. Meyer, E. Wieczorek (Akad. der Wissenschaften der DDR, Zeuthen, GDR, 1984) p. 135.
- [11] M.A. Shifman, M.B. Voloshin, *Yad. Fiz.* **41** (1985) 187, *ZhETF* **91** (1986) 1180.
- [12] H. Schröder, Proc. XXIV. Int. Conf. on High Energy Physics, Munich, 1988, ed. by R. Kotthaus, J.H. Kühn (Springer-Verlag, Berlin Heidelberg, 1989) p. 73.
- [13] D. Hitlin, Proc. Int. Symp. on Lepton and Photon Interactions at High Energies, Hamburg, 1987, ed. by W. Bartel, R. Rückl, *Nucl. Phys. B (Proc. Suppl.)* **3** (1988) 179.
- [14] N. Cabibbo, L. Maiani, *Phys. Lett.* **79 B** (1978) 109;
M. Suzuki, *Nucl. Phys. B* **145** (1978) 420;
A. Ali, E. Pietarinen, *Nucl. Phys. B* **154** (1979) 519;
N. Cabibbo, G. Corbo, L. Maiani, *Nucl. Phys. B* **155** (1979) 93;
G. Altarelli, N. Cabibbo, G. Corbo, L. Maiani, G. Martinelli, *Nucl. Phys. B* **208** (1982) 365;
G. Corbo, *Phys. Lett.* **116 B** (1982) 298, *Nucl. Phys. B* **212** (1983) 99;
M. Jezabek, J.H. Kühn, *Phys. Lett.* **207 B** (1988) 91, *Nucl. Phys. B* **320** (1989) 20.
- [15] M. Bauer, B. Stech, M. Wirbel, *Z. Phys. C* **34** (1987) 103;
for a review see
M. Wirbel, *Prog. Part. and Nucl. Phys.* **21** (1988) 33.
- [16] A.J. Buras, J.-M. Gérard, R. Rückl, *Nucl. Phys. B* **268** (1986) 16.
- [17] J.F. Donoghue, *Phys. Rev. D* **33** (1986) 1516.
- [18] B. Blok, M.A. Shifman, *Yad. Fiz.* **45** (1987) 211, 478, 841.
- [19] J.L. Cortes, X.Y. Pham, A. Tounsi, *Phys. Rev. D* **25** (1982) 188.
- [20] B. Guberina, R.D. Peccei, R. Rückl, *Phys. Lett.* **91 B** (1980) 116, *Nucl. Phys. B* **171** (1980) 333.
- [21] G. Altarelli, G. Curci, G. Martinelli, S. Petrarca, *Phys. Lett.* **99 B** (1981) 141, *Nucl. Phys. B* **187** (1981) 461.
- [22] C.S. Kim, A.D. Martin, University of Durham, DTP/89/10 (1989);
V. Barger, C.S. Kim, R.J.N. Phillips, University of Madison, MAD/PH/501 (1989);
A. Bareiss, E.A. Paschos, University of Dortmund, DO-TH 89/1 (1989).
- [23] D. Muller, Proc. XXIV. Int. Conf. on High Energy Physics, Munich, 1988, ed. by R. Kotthaus, J.H. Kühn (Springer-Verlag, Berlin Heidelberg, 1989) p. 884.
- [24] B. Stech, *Phys. Rev. D* **36** (1987) 975;
M. Neuberg, B. Stech, Talk at the 2. Int. Symp. on the 4th Family of Quarks and Leptons, Santa Monica, 1989, University of Heidelberg, HD-THEP-89-11 (1989).
- [25] Particle Data Group, *Phys. Lett.* **204 B** (1988) 1.
- [26] A. Datta, E.A. Paschos, U. Türke, *Phys. Lett.* **196 B** (1987) 382;
A. Datta, E.A. Paschos, Y.L. Wu, University of Dortmund, DO-TH 88/3 (1988);
V.A. Khoze, M.A. Shifman, N.G. Uraltsev, M.B. Voloshin, *Yad. Fiz.* **46** (1987) 181.
- [27] Particle Data Group, *Phys. Lett.* **204 B** (1988) 1.
- [28] J.A. Jaros, SLAC-PUB-3569, 1985.
- [29] R. Settles in Physics at LEP, CERN86-02.
- [30] S.L. Wu, Proceedings, Lepton Photon Conference, Hamburg 1987.
- [31] M. Bauer, B. Stech and M. Wirbel, *Z. Phys. C* **34** (1987) 103.
- [32] H. Schroeder, Spectroscopy and Decays of Heavy Quarks in Proc. of the XXIV Int. Conf. on High Energy Physics, Eds: R. Kotthaus and J. Kühn, Springer-Verlag Heidelberg 1989.
- [33] M. Wirbel, DO-TH 88/2.
- [34] B. Franek, RAL-95-026, 1985.

2.7. B DECAYS

2.7.1. SEMILEPTONIC DECAYS

(a) Electron and Muon Final States *

Semileptonic decays of hadrons play an important role for our understanding of the interplay between weak and strong interactions: They are essential for testing the Standard Model and determining its fundamental parameters. They also provide valuable information on the bound state structure of hadrons not yet calculable from QCD.

Inclusive semileptonic B decays

Semileptonic decays of B mesons have therefore been extensively studied experimentally [1-7] as well as theoretically [8-27]. In the *spectator model* they proceed through the decay of the heavy b quark to a c or a u quark and the emission of a virtual W^- boson which couples** to $(l\bar{\nu}_l)$. The strength of the $b \rightarrow c$ and of the $b \rightarrow u$ transitions is determined by the Kobayashi-Maskawa matrix elements V_{cb} and V_{ub} , respectively. The determination of these matrix elements from the observed decay rates and spectra is, however, afflicted with large theoretical uncertainties which will be discussed below.

We start the analysis of semileptonic decays of B mesons at the quark level where the heavy b quark decays while the light spectator quark goes along unaffected. As long as we are not interested in separating exclusive final states, a free quark calculation may be adopted with the total semileptonic width

$$\Gamma(b \rightarrow \bar{q}l^-\bar{\nu}) = \frac{G_F^2 m_b^5}{192\pi^3} |V_{ub}|^2 F\left(\frac{m_q}{m_b}\right) \quad (2.113)$$

$$F(x) = 1 - 8x^2 + 8x^6 - x^8 - 24x^4 \ln x$$

The total rates, as well as the shape of the lepton spectrum, depend on unknown quark masses in the amplitude and – most important – which determine the allowed phase space. In addition, the simple quark model has to be modified by taking into account radiative corrections due to the emission of virtual and real gluons [28]. One obtains for the semileptonic width

$$\Gamma_{sl} = \frac{G_F^2 m_b^5}{192\pi^3} \left[f_c |V_{cb}|^2 + f_u |V_{ub}|^2 \right] \quad (2.114)$$

where f_c and f_u are products of phase space and QCD correction factors. Values for f_c and f_u are given in the following table for constituent masses $m_b = 5.2$ GeV, $m_c =$

*M. WIRBEL

**Only massless leptons will be studied in this part of the report.

mode	current masses	constituent masses
$b \rightarrow c \ell^- \bar{\nu}_\ell$	$f_c = 0.56$	0.42
	$f_c = 0.48$	0.36
$b \rightarrow u \ell^- \bar{\nu}_\ell$	$f_u = 1.00$	0.97
	$f_u = 0.87$	0.84

Tab. 2.18: Correction factors f_c and f_u defined in eq. (114) [from Table 7 of Ref. 29]. The upper values are for $\alpha_s = 0$, the lower values include next-to-leading-log corrections.

1.8 GeV, $m_u = 0.34$ GeV) and current masses $m_b = 4.8$ GeV, $m_c = 1.35$ GeV, $m_u = 0.006$ GeV).

The predictions for the semileptonic width are also modified considerably by bound state effects for the initial meson. In Ref. 8, for example, a non-relativistic model has been used. The light spectator quark has a fixed mass m_{SP} but the decaying b quark is off-shell because of energy-momentum conservation; its invariant mass given by

$$W^2 = m_B^2 + m_{SP}^2 - 2m_B \sqrt{\vec{p}^2 + m_{SP}^2}$$

m_B being the mass of the B meson and \vec{p} the momentum of the spectator quark. A Gaussian distribution for $|\vec{p}|$ with an adjustable width p_F has been assumed. The lepton spectrum and the total width then result from folding this distribution with the decay spectrum of the heavy b quark with effective mass W . The allowed phase space thus depends on the mass of the spectator quark and the Fermi momentum p_F , as well as on the mass of the final quark.

A model which is complementary to the non-relativistic quark model in many respects has been recently proposed in Ref. 12. There, the calculation of the decay probability is carried out in a frame where the B meson moves with infinite momentum. The decay probability of the mesons is the incoherent sum of the decay probabilities of free b quarks carrying a fraction z of the B meson momentum $p_{b\mu} = zp_{B\mu}$. The width of the B meson is then obtained by calculating the decay of a quasi-free b quark folded with the probability to find a b quark carrying a fraction z of the longitudinal momentum of the B meson. The distribution function of b quarks in the infinite momentum frame is identified with the fragmentation function of b -quarks to B -mesons*.

The uncertainties of the theoretical calculations may be summarized by comparing the results for f_c defined in eq. (114). Ref. 12 give values for f_c which range from $f_c = 0.24$ for $m_c = 1.3$ GeV to $f_c = 0.15$ for $m_c = 1.8$ GeV with $m_b = m_B$ in eq. (114). QCD corrections are included. (From Table 4 of [12] with the central value of the parameter ϵ which determines the distribution function.) Typical results for f_c using the model of

*Many other models (see for example [9–11]) have been suggested to describe inclusive semileptonic B meson decays, which cannot be described in detail.

Ref. [8] are the following:

$$f_c = 0.23 \quad \text{for} \quad m_{SP} = 0.15 \text{ GeV}, \quad p_F = 0.30 \text{ GeV},$$

and

$$f_c = 0.29 \quad \text{for} \quad m_{SP} = 0.15 \text{ GeV}, \quad p_F = 0.15 \text{ GeV},$$

including QCD corrections. We note that those models which include bound state corrections predict values for f_c which are considerably smaller than those obtained in the free quark model. The corresponding values for $|V_{cb}|$ will therefore be larger with, however, large uncertainties between different models and the variation of parameters within the models.

Exclusive semileptonic B decays

The inclusive approach described above is appropriate if the final hadronic state consists of a 'continuum' of hadrons, which is probably the case for the $b \rightarrow u$ decays. The semileptonic $b \rightarrow c$ decays, however, seem to be dominated by few exclusive channels as indicated experimentally by the ARGUS result [4]

$$Br(\bar{B} \rightarrow D^* l^- \bar{\nu}_l) = (7.0 \pm 1.2 \pm 1.9)\% \quad (2.115)$$

compared to the inclusive semileptonic branching ratio [7]:

$$Br(\bar{B} \rightarrow l^- X) = (11.5 \pm 0.9)\% \quad (2.116)$$

We will therefore present some details on exclusive semileptonic B meson decays in this chapter.

In an exclusive treatment the decay distributions are given by the matrix elements of the weak currents between initial and final meson states $J_\mu \equiv \langle X | J_\mu(0) | \bar{B} \rangle$. $J_\mu(0)$ is the weak $V - A$ current and X is the final meson. We will consider the transitions involving a pseudoscalar ($X = P$) or a vector meson ($X = V$). From Lorentz invariance one finds the decomposition of the hadronic matrix element in terms of unknown form factors:

$$\langle P | J_\mu(0) | \bar{B} \rangle = t_{P\mu} F_1(q^2) + \frac{m_B^2 - m_P^2}{q^2} q_\mu F_0(q^2) \quad (2.117)$$

where

$$t_{P\mu} = (p_B + p_P)_\mu - \frac{m_B^2 - m_P^2}{q^2} q_\mu \quad q_\mu = (p_B - p_P)_\mu \quad (2.118)$$

and (assuming asymptotic current conservation) $F_1(0) = F_0(0)$.

$$\begin{aligned} \langle V | J_\mu(0) | \bar{B} \rangle &= \epsilon_{\mu\nu\alpha\beta} p_B^\nu p_V^\alpha \epsilon^{*\beta} \frac{2}{m_B + m_V} V(q^2) \\ &+ i t_{V\mu} + i \frac{\epsilon^* \cdot q}{q^2} q_\mu \frac{2}{m_V} A_0(q^2) \end{aligned} \quad (2.119)$$

where

$$t_{V\mu} = \epsilon_\mu^*(m_B + m_V)A_1(q^2) - \frac{\epsilon^* \cdot q}{m_B + m_V}(p_B + p_V)_\mu A_2(q^2) - \frac{\epsilon^* \cdot q}{q^2} q_\mu 2m_V A_3(q^2) \quad (2.120)$$

$A_3(q^2)$ is an abbreviation for

$$A_3(q^2) = \frac{1}{2m_V}[(m_B + m_V)A_1(q^2) - (m_B - m_V)A_2(q^2)]$$

with (assuming asymptotic current conservation) $A_3(0) = A_0(0)$. The form factor decomposition has been written in such a way that $q^\mu t_{P\mu} = q^\mu t_{V\mu} = 0$. The transition matrix elements squared, including the lepton currents, take the following simple form [22, 25]:

$$|A_{sl}(\bar{B} \rightarrow P)|^2 = \frac{G_F^2}{2} |V_{qb}|^2 4q^2(1 - z^2) |H|^2 \quad (2.121)$$

$$|A_{sl}(\bar{B} \rightarrow V_{transv})|^2 = \frac{G_F^2}{2} |V_{qb}|^2 2q^2 \times \{(1 - z)^2 |H_-|^2 + (1 + z)^2 |H_+|^2\} \quad (2.122a)$$

$$|A_{sl}(\bar{B} \rightarrow V_{long})|^2 = \frac{G_F^2}{2} |V_{qb}|^2 4q^2(1 - z^2) |H_0|^2 \quad (2.122b)$$

V_{transv} and V_{long} denote transversely and longitudinally polarized vector mesons, respectively. z can be identified with the cosine of the angle between the final meson and the charged lepton l^- in the $(l^- \bar{\nu})$ rest frame; it can be expressed by

$$z = \frac{1}{2m_B K}(m_B^2 - m_X^2 + q^2 - 4m_B E_l) \quad (2.123)$$

where E_l and K are the energy of the charged lepton and the momentum of the final meson X in the B meson restframe:

$$K = \frac{1}{2m_B}[(m_B^2 - m_X^2 - q^2)^2 - 4m_X^2 q^2]^{1/2} \quad (2.124)$$

The helicity amplitudes introduced above are related to the form factors in the following way:

$$H(q^2) = \frac{2m_B K}{\sqrt{q^2}} F_1(q^2) \quad (2.125a)$$

$$H_0(q^2) = \frac{1}{2m_V \sqrt{q^2}} [(m_B^2 - m_V^2 - q^2)(m_B + m_V)A_1(q^2) - \frac{4m_B^2 K^2}{m_B + m_V} A_2(q^2)] \quad (2.125b)$$

$$H_\pm(q^2) = (m_B + m_V)A_1(q^2) \mp \frac{2m_B K}{m_B + m_V} V(q^2) \quad (2.125c)$$

Various approaches have been suggested to estimate the form factors [13–26]. We will concentrate on the results obtained by two models which use quite different assumptions to calculate the rates and spectra:

i) The *BSW model* [15] assumes nearest pole dominance for the q^2 -dependence of the form factors*

$$F_1(q^2) = \frac{h_1}{1 - q^2/m_1^2} \quad \text{etc.}$$

The unknown residues h_i – i.e. the form factors at $q^2 = 0$ – are estimated by describing the mesons as relativistic bound states of a quark-antiquark pair in the infinite-momentum limit. The h_i are then given by overlap integrals of the wave functions of the initial and final meson. A quite successful description of D and B meson decay data has been achieved this way [15, 25, 30, 31]. This method has the advantage of using a fully relativistic formalism, but there are also several difficulties connected with this model: For example, it is difficult to define J^P eigenstates using infinite-momentum-frame wave functions.

ii) The *GISW model* [16, 26] adopts the non-relativistic quark potential method to make a correspondence between the Lorentz-invariant form factors and those appearing in a quark-model calculation (‘mock-meson method’). These form factors are identified near zero recoil, i.e. at maximal $q_{max}^2 = (m_B - m_X)^2$. Variational solutions of the Schrödinger equation based on the usual Coulomb plus linear potential have been chosen for the wave functions of the initial and final mesons. Away from zero-recoil the q^2 dependence of the form factors is not calculable accurately and terms of order $(q_{max}^2 - q^2)^2$ had to be dropped. This procedure results in an exponential q^2 dependence of the form factors.

The two models described above differ considerably in their assumptions and therefore give an estimate of the theoretical uncertainties connected with the predictions of semileptonic rates and spectra. The theoretical results for the total semileptonic decay rates of D and B mesons are summarized in the Tables below and compared with experimental data so far as available. It is evident from these tables that the predictions roughly agree with each other except for the $\bar{B} \rightarrow \pi l^- \bar{\nu}$ and $\bar{B} \rightarrow \rho l^- \bar{\nu}$ decays which are most important for the determination of the so far unknown Kobayashi Maskawa matrix element $|V_{ub}|$. Of some concern is the disagreement between the theoretical predictions for the $D \rightarrow K^* e \nu$ decay and the experimental results. However, the experimental results still disagree on the size of the nonresonant $D \rightarrow (K\pi) l^- \nu$ decays, i.e. $(K\pi)$ pairs not coming from $D \rightarrow K^* l^- \nu \rightarrow (K\pi) l^- \nu$ [31–33].

*The model of Körner and Schuler [22] is very similar to the BSW model. The main difference is that monopole and dipole form factors are used in this model.

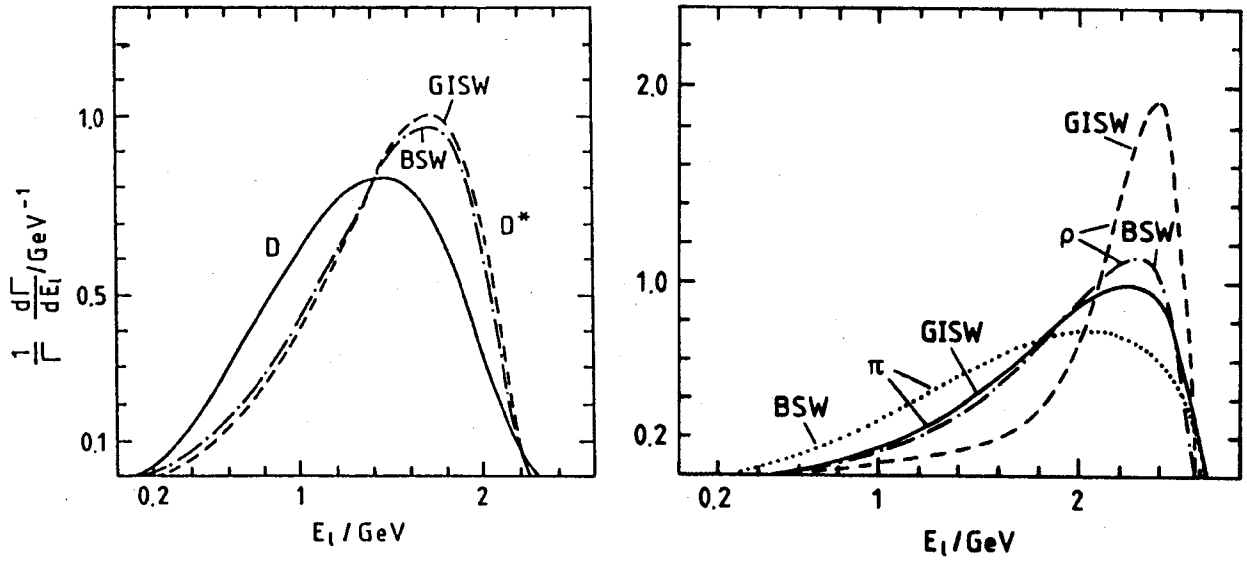


Fig. 2.28: a) Energy spectra of the charged lepton in semileptonic $\bar{B} \rightarrow D l^- \bar{\nu}$ and $\bar{B} \rightarrow D^* l^- \bar{\nu}$ decays as predicted by the BSW and GISW models (in the B rest frame). The results for $\bar{B} \rightarrow D l^- \bar{\nu}$ are nearly identical.

b) Energy spectra of the charged lepton in semileptonic $\bar{B} \rightarrow \pi l^- \bar{\nu}$ and $\bar{B} \rightarrow \rho l^- \bar{\nu}$ decays as predicted by the BSW and GISW models (in the B rest frame).

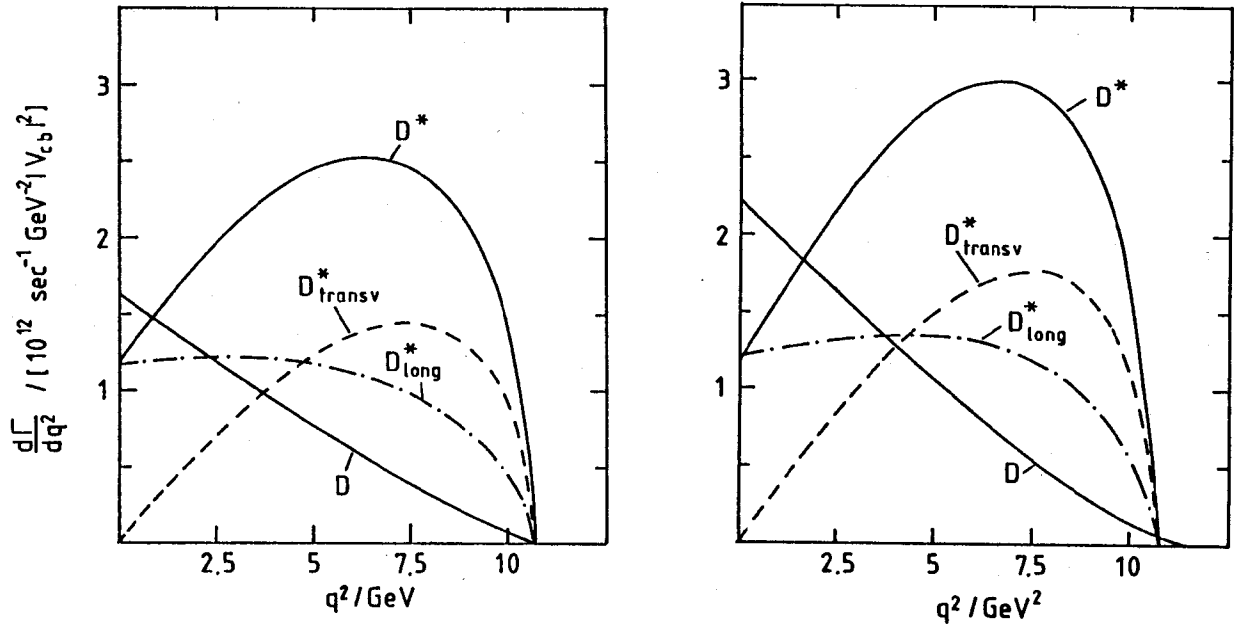


Fig. 2.29: q^2 dependence of the semileptonic decays $\bar{B} \rightarrow D l^- \bar{\nu}$ and $\bar{B} \rightarrow D^* l^- \bar{\nu}$ in the a) BSW and b) GISW model, respectively. D_{transv}^* and D_{long}^* denote the contribution of transversely and longitudinally polarised D^* mesons.

Measuring V_{ub}

Limits on $|V_{ub}/V_{cb}|$ have been obtained in the past by a study of the endpoint region of the lepton momentum spectrum [7, 6, 34]. The theoretical predictions for the energy spectra of the charged lepton in semileptonic $\bar{B} \rightarrow D, D^*$ and $\bar{B} \rightarrow \pi, \rho$ decays are shown in Fig. 2.28a and b respectively (in the B rest frame). The BSW and GISW models not

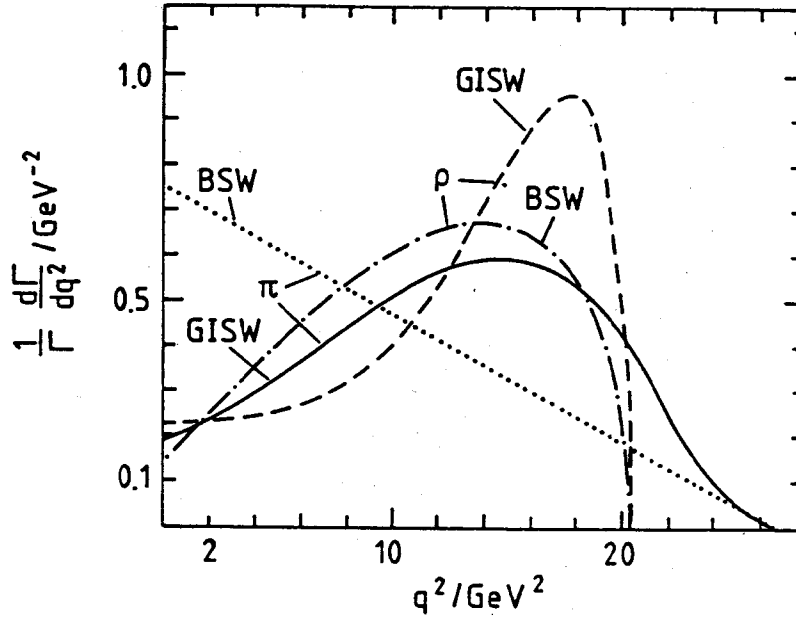


Fig. 2.30: q^2 dependence of the semileptonic decays $\bar{B} \rightarrow \pi l^- \bar{\nu}$ and $\bar{B} \rightarrow \rho l^- \bar{\nu}$ in the BSW and GISW models.

Tab. 2.19: Semileptonic decay rates of D and B mesons. All rates are given in units of 10^{10}sec^{-1} . $|V_{cb}| = 0.05$ has been used.

Decay mode	BSW	GISW	Experiment
$D^0 \rightarrow K^- e^+ \nu_e$	8.3	8.4	$9.0 \pm 1.1 \pm 1.2$ [32]
$D^+ \rightarrow \bar{K}^0 e^+ \nu_e$	9.5	9.1	$4.1 \pm 0.7 \pm 0.5$ [32]
$D^0 \rightarrow \pi^- e^+ \nu_e$	0.7	0.4	$0.9 \pm 0.7 \pm 0.2$ [34]
$D^0 \rightarrow \rho^- e^+ \nu_e$	0.7	0.5	-----
$D^0 \rightarrow X l^+$			17.8 ± 3.9 [33]
$D^+ \rightarrow X l^+$			15.6 ± 1.9 [33]
(inclusive)			
Decay mode	BSW	GISW	Experiment
$\bar{B} \rightarrow D l^- \bar{\nu}_l$	2.0	2.8	-----
$\bar{B} \rightarrow D^* l^- \bar{\nu}_l$	5.5	6.2	$5.8 \pm 1.0 \pm 1.6$ [4]
$\bar{B}^0 \rightarrow \pi^+ l^- \bar{\nu}_l$	$1.9 V_{ub}/V_{cb} ^2$	$0.5 V_{ub}/V_{cb} ^2$	-----
$\bar{B}^0 \rightarrow \rho^+ l^- \bar{\nu}_l$	$6.5 V_{ub}/V_{cb} ^2$	$2.1 V_{ub}/V_{cb} ^2$	< 0.2 [7]
$\bar{B} \rightarrow l^- X$			9.6 ± 0.8 [7]
(inclusive)			

only predict different rates but also the form of the spectrum is quite different for the $b \rightarrow ul^- \bar{\nu}$ transitions. Assuming $|V_{ub}/V_{cb}| = 0.1$ and choosing $|V_{cb}| = 0.05$ the predicted

rates are of the order

$$\Gamma_{sl}(\bar{B}^0 \rightarrow \pi^+) \sim (0.5 - 2)10^8 \text{sec}^{-1} \quad Br_{sl}(\bar{B}^0 \rightarrow \pi^+) \sim (0.6 - 2.4) \cdot 10^{-4}$$

and

$$\Gamma_{sl}(\bar{B}^0 \rightarrow \rho^+) \sim (2 - 7) \cdot 10^8 \text{sec}^{-1} \quad Br_{sl}(\bar{B}^0 \rightarrow \rho^+) \sim (2.4 - 8.4) \cdot 10^{-4}.$$

The upper limit on $|V_{ub}/V_{cb}|$ obtained by this method therefore depends significantly on the theoretical model and it is very difficult to guess the theoretical error. A conservative estimate of the upper limit [7, 31] is $|V_{ub}/V_{cb}| < 0.21$. The q^2 dependence of the $b \rightarrow cl^- \bar{\nu}$ and $b \rightarrow ul^- \bar{\nu}$ decays is shown in Figs. 2.29, 2.30. The predictions for $\bar{B} \rightarrow \pi l^- \bar{\nu}$ and $\bar{B} \rightarrow \rho l^- \bar{\nu}$ again differ considerably in the BSW and GISW approach – in contrast to the results for the $\bar{B} \rightarrow Dl^- \bar{\nu}$ and $\bar{B} \rightarrow D^* l^- \bar{\nu}$ decays which agree very nicely. In Fig. 2.29 we have included the q^2 dependence of the production of transversely and longitudinally polarized D^* mesons. The polarization of the D^* can be determined by measuring the angular distribution of the strong decay $D^* \rightarrow D\pi$: $d\Gamma_{sl}(\bar{B} \rightarrow D^* \rightarrow D\pi)/d\cos\theta^* \sim (1 + \alpha_B \cos^2\theta^*)$ where α_B measures the ratio of longitudinal to transverse polarization. The theoretical predictions [26, 22, 25, 35] agree nicely with the experimental results [5].

The cleanest signal presumably for a $b \rightarrow u$ transition would be the purely leptonic decay of the B meson: $B^- \rightarrow \tau^- \bar{\nu}_\tau$. However, the branching ratio is quite small as can be easily estimated by rescaling the known decay rate for $K \rightarrow \mu\nu$:

$$\Gamma(B^- \rightarrow \tau^- \bar{\nu}) = \left(\frac{m_\tau}{m_\mu}\right)^5 \frac{m_B}{m_K} \left(\frac{1 - m_\tau^2/m_B^2}{1 - m_\mu^2/m_K^2}\right) \left(\frac{f_B}{f_K}\right)^2 |V_{ub}/V_{us}|^2 \times \Gamma(K \rightarrow \mu\nu) \quad (2.126)$$

From this we obtain

$$Br(B^- \rightarrow \tau^- \bar{\nu}) \simeq 0.16 \left(\frac{f_B}{f_K}\right)^2 |V_{ub}/V_{us}|^2 \simeq 8 \cdot 10^{-3} \left(\frac{f_B}{f_K}\right)^2 |V_{ub}/V_{cb}|^2 \quad (2.127)$$

and the branching ratio will be of the order 10^{-4} for $|V_{ub}/V_{cb}| = 0.1$ and $f_B \simeq f_K$.

(b) τ Final States *

Decays of B mesons into final states containing a $\tau \bar{\nu}_\tau$ pair constitute a significant fraction of all semileptonic B decays. These decays have an intrinsic interest, as they can probe certain form factors characterizing the matrix elements $\langle D | J_\mu | B \rangle$, $\langle D^* | J_\mu | B \rangle$ etc. which produce effects proportional to m_l^2 that are inaccessible in the $e \bar{\nu}_e$ and $\mu \bar{\nu}_\mu$ decay modes [36]. In addition, the decay $B \rightarrow \tau \bar{\nu}_\tau X$ followed by $\tau \rightarrow \nu_\tau e \bar{\nu}_e$ or $\tau \rightarrow \nu_\tau \mu \bar{\nu}_\mu$ act as sources of secondary leptons that constitute a background to the spectrum of primary electrons and muons emitted in B decays.

*L. SEHGAL in collaboration with P. HEILIGER

Quark Model Guidelines

The decay widths associated with $B \rightarrow X l \nu_l$ for $l = \tau$ and $l = e$ can be simply estimated on the basis of the quark transitions $b \rightarrow c l \nu_l$ or $b \rightarrow u l \nu_l$:

$$\Gamma_l = \frac{G_F^2 m_b^5}{192\pi^3} \left\{ |V_{cb}|^2 I\left(\frac{m_c}{m_b}, \frac{m_l}{m_b}, 0\right) + |V_{ub}|^2 I\left(\frac{m_u}{m_b}, \frac{m_l}{m_b}, 0\right) \right\} \quad (2.128)$$

Here $I(x, y, 0)$ is a phase space factor given by [37]

$$\begin{aligned} I(x, y, 0) = & \sqrt{1 - 2(x^2 + y^2) + (x^2 - y^2)^2} (1 - 7(x^2 + y^2) + 6x^2 y^2 \\ & - 2(x^2 + y^2)^2 - 6x^2 y^2 (x^2 + y^2) + (x^2 - y^2)(x^4 - y^4 + 5y^2 - 5x^2)) \\ & + 12(x^4 + y^4 - 2x^2 y^2) \ln \frac{1 - x^2 - y^2 + \sqrt{1 - 2(x^2 + y^2) + (x^2 - y^2)^2}}{2xy} \\ & + 12(x^4 - y^4) \ln \frac{x^2 + y^2 - (x^2 - y^2)^2 - (x^2 - y^2)\sqrt{1 - 2(x^2 + y^2) + (x^2 - y^2)^2}}{2xy} \end{aligned} \quad (2.129)$$

Special cases of interest are

$$\begin{aligned} I(x, x, 0) = & \sqrt{1 - 4x^2} (1 - 14x^2 - 2x^4 - 12x^6) + 24x^4 (1 - x^4) \ln \frac{1 + \sqrt{1 - 4x^2}}{1 - \sqrt{1 - 4x^2}} \\ I(x, 0, 0) = & I(0, x, 0) = 1 - 8x^2 + 8x^6 - x^8 - 24x^4 \ln x \end{aligned} \quad (2.130)$$

Taking $m_c/m_b \approx m_\tau/m_b \approx 1/3$ and neglecting m_u or m_e we obtain

$$\frac{\Gamma_\tau}{\Gamma_e} = \frac{|V_{cb}|^2 I(\frac{1}{3}, \frac{1}{3}, 0) + |V_{ub}|^2 I(0, \frac{1}{3}, 0)}{|V_{cb}|^2 I(\frac{1}{3}, 0, 0) + |V_{ub}|^2 I(0, 0, 0)} \quad (2.131)$$

Using the fact that $|V_{ub}|^2/|V_{cb}|^2 < 0.04$ [38] and the phase space factors $I(\frac{1}{3}, \frac{1}{3}, 0) = 0.119$, $I(0, \frac{1}{3}, 0) = I(\frac{1}{3}, 0, 0) = 0.447$, $I(0, 0, 0) = 1$,

$$\Gamma_\tau/\Gamma_e \approx 0.266 \quad (2.132)$$

The energy spectrum of the τ given by the transition $b \rightarrow c \tau^- \bar{\nu}_\tau$ is [39]

$$\frac{d\Gamma}{dx} = \frac{G_F^2 m_b^5}{96\pi^3} |V_{cb}|^2 \lambda^{\frac{1}{2}}(1, y, \delta) (4xyA + \{(1 - \delta)^2 - y^2\}B)$$

where

$$x = E_\tau/m_b, \quad \delta = (m_\tau/m_b)^2, \quad y = 1 - 2x + \delta$$

$$\lambda(x, y, z) = x^2 + y^2 + z^2 - 2xy - 2yz - 2zx$$

$$A = \lambda^{\frac{3}{2}}(1, \frac{m_c^2}{m_b^2} y, 0)$$

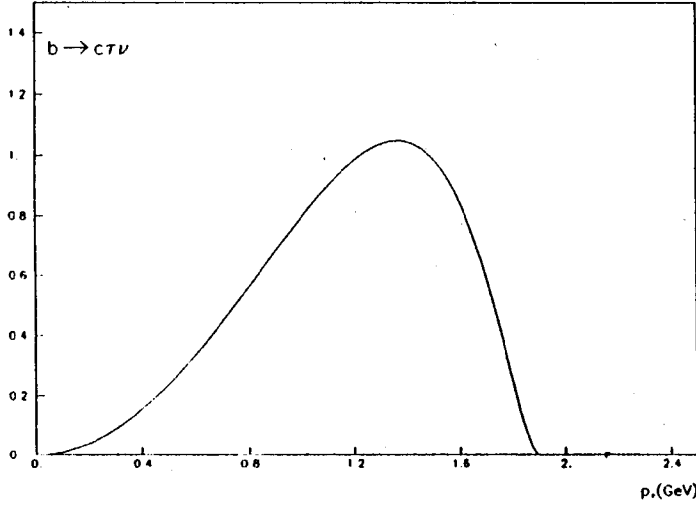


Fig. 2.31: The spectrum of the τ lepton in the spectator model.

$$B = 2\lambda^{\frac{1}{2}}(1, \frac{m_c^2}{m_b^2 y}, 0) \left(1 + \frac{m_c^2}{m_b^2 y} - 2(\frac{m_c^2}{m_b^2 y})^2\right) \quad (2.133)$$

Assuming $m_c/m_b \approx m_\tau/m_b = 1/3$, the spectrum of the τ lepton is shown in Fig. 2.31

Finally the longitudinal polarization of the τ^- in the decay $b \rightarrow c\tau^- \bar{\nu}_\tau$ is

$$P_\tau = -\frac{v}{c} \frac{1}{1 - \frac{m_\tau^2}{m_b E_\tau} \frac{g(E_\tau)}{f(E_\tau)}} \quad (2.134)$$

where

$$g(E_\tau) = m_b(m_b - E_\tau) \left(1 + \frac{2m_c^2}{m_b^2 + m_\tau^2 - 2m_b E_\tau}\right)$$

$$f(E_\tau) = .5(m_b^2 - 2m_b E_\tau + m_\tau^2 - m_c^2) + g(E_\tau)$$

v being the velocity of the τ in the b rest frame.

Exclusive Decay $B \rightarrow D\tau\nu_\tau$

The matrix element of $B \rightarrow D l \nu_l$ is characterized by two form factors defined by

$$\langle D(p') | V_\mu | B(p) \rangle = f_+(q^2)(p + p')_\mu + f_-(q^2)(p - p')_\mu \quad (2.135)$$

where $q = p - p'$. The contribution of f_- to the decay rate is proportional to m_l^2 and hence negligible for $l = e$ or μ , but significant for $B \rightarrow D\tau\nu_\tau$. The double differential spectrum in the energies of the lepton and the D meson is [40]

$$\frac{d^2\Gamma}{dE_l dE_D} = \frac{G_F^2}{4\pi^3} |V_{cb}|^2 (|f_+|^2 A + \text{Re} f_+^* f_- B + |f_-|^2 C)$$

where

$$A = m_D[2E_l E_\nu - m_D(W_0 - E_D)] + \frac{1}{4}m_l^2(W_0 - E_D) - m_l^2 E_\nu$$

$$B = m_l^2[E_\nu - \frac{1}{2}(W_o - E_D)] \quad C = \frac{1}{4}m_l^2[W_o - E_D]$$

with

$$W_o = (m_B^2 + m_D^2 - m_l^2)/(2m_B) \quad E_\nu = m_B - E_D - E_l \quad (2.136)$$

For the form factors $f_\pm(q^2)$ we have considered two hypotheses:

- (a) The parametrization of Bauer, Stech and Wirbel (BSW) according to which [30]

$$f_i(q^2) = \frac{h_i}{1 - q^2/m_i^2} \quad i = 0, 1 \quad (2.137)$$

where f_0 and f_1 are related to f_\pm by

$$f_+(q^2) = f_1(q^2), \quad f_-(q^2) = \frac{m_B^2 - m_D^2}{q^2}(f_0(q^2) - f_1(q^2)) \quad (2.138)$$

The pole-residues are $h_0 = h_1 = 0.69$, the pole-positions being $m_0 = 6.8 \text{ GeV}$ and $m_1 = 6.34 \text{ GeV}$.

- (b) The parametrization of Altomari and Wolfenstein [41] (AW) in which the normalization of f_\pm at $q^2 = q_{max}^2 = (m_B - m_D)^2$ is determined with the help of the quark model

$$f_\pm(q_{max}^2) \approx \frac{m_D \pm m_B}{2\sqrt{m_D m_B}} \quad (2.139)$$

and the q^2 -dependence is given by a pole at a mass of 6.8 GeV .

A comparison of the two parametrizations shows that f_-/f_+ is much smaller for BSW as compared to AW.

We now summarize the main results concerning the decay $B \rightarrow D\tau\nu_\tau$.

- (i) The ratio of $B \rightarrow D\tau\nu_\tau$ to $B \rightarrow De\nu_e$ is

$$\frac{\Gamma_\tau(B \rightarrow D)}{\Gamma_e(B \rightarrow D)} = \begin{cases} 0.25 & \text{(AW)} \\ 0.30 & \text{(BSW)} \end{cases} \quad (2.140)$$

These numbers bracket the quark model value given in eq. (132).

- (ii) The momentum spectrum of the D meson, derived from eq. (136), is shown in Fig. 2.32a for the two choices of form factors. The BSW spectrum is slightly softer.
- (iii) The momentum spectrum of the τ is shown in Fig. 2.32c and is practically indistinguishable for the AW and BSW cases.
- (iv) The longitudinal polarization of the τ is depicted in Fig. 2.32e, where the quark model result is also shown for comparison.

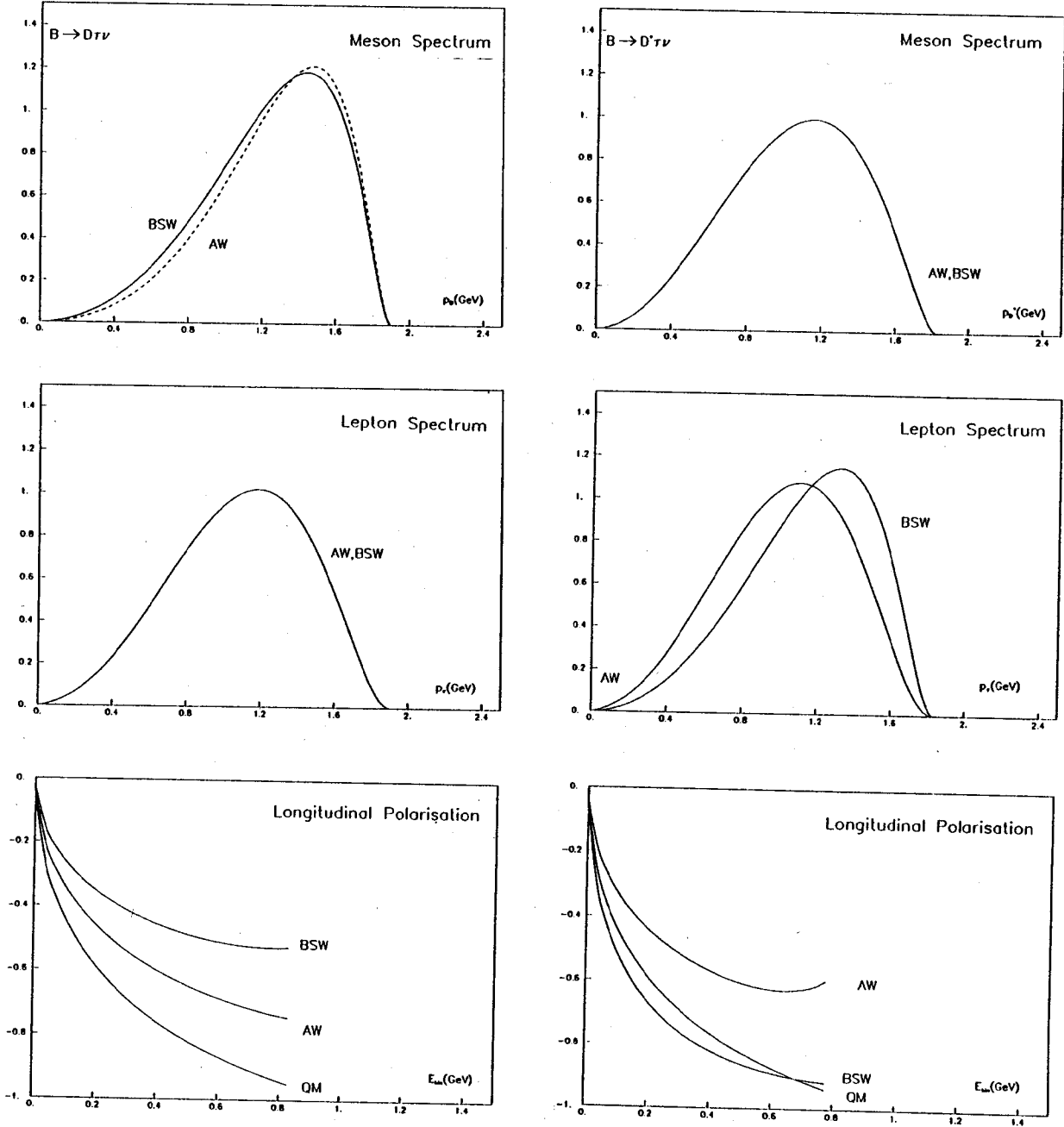


Fig. 2.32: (a),(b) The momentum spectrum of the D and D^* -meson.
(c),(d) The momentum spectrum of the τ in D and D^* final states.
(e),(f) The longitudinal polarization of the τ in D and D^* final states.

Exclusive Decay $B \rightarrow D^ \tau \nu_\tau$*

The matrix element $\langle D^* | J_\mu | B \rangle$ is characterized by four form factors, defined by

$$\begin{aligned} \langle D^*(\epsilon) | J^\mu | B \rangle = & f(q^2) \epsilon^\mu + a_+(q^2) (p_B + p_D)^\mu \epsilon \cdot p_B + a_-(q^2) (p_B - p_D)^\mu \epsilon \cdot p_B \\ & + i g \epsilon^{\mu\nu\rho\sigma} \epsilon_\nu (p_B + p_D)_\rho (p_B - p_D)_\sigma \end{aligned} \quad (2.141)$$

The quark model prescription of Altomari and Wolfenstein [41] yields, for $q^2 = q_{max}^2$,

$$f \approx \sqrt{4m_B m_{D^*}} \quad g \approx \frac{1}{2m_D} \sqrt{\frac{m_{D^*}}{m_B}}$$

$$a_+ \approx \frac{-1}{\sqrt{4m_D m_B}} \left[1 + \frac{m_{D^*}}{m_B} \left(1 - \frac{m_{D^*}}{m_B} \right) \right] \quad a_- = a_+ + \frac{1}{\sqrt{m_{D^*} m_B}} \quad (2.142)$$

The extrapolation to other q^2 -values follows a pole hypothesis with a pole mass of 6.8 GeV. The form factor a_- contributes to the decay rate in proportion to m_l^2 . In the AW model a_- is close to zero, a feature which remains valid in the BSW ansatz. (For details see the previous section.) The double differential cross section in the lepton and D^* energies is given in the Appendix.

The principal results for the decay $B \rightarrow D^* \tau \nu_\tau$ are as follows.

- (i) The decay width of $B \rightarrow D^* \tau \nu_\tau$ compared to the electron mode is

$$\frac{\Gamma_\tau(B \rightarrow D^*)}{\Gamma_e(B \rightarrow D^*)} = \begin{cases} 0.26 & \text{(AW)} \\ 0.24 & \text{(BSW)} \end{cases} \quad (2.143)$$

- (ii) The D^* momentum spectrum is shown in Fig. 2.32b and is essentially the same for the BSW and AW form factors.
- (iii) The lepton momentum spectrum is exhibited in Fig. 2.32d. Here we note a significant difference, the BSW prescription giving a harder spectrum.
- (iv) The τ -lepton polarization as a function of the τ energy, is shown in Fig. 2.32f.
- (v) The decay width of $B \rightarrow D_{long}^* \tau \nu$ compared to $B \rightarrow D_{trans}^* \tau \nu$ (where the subscripts denote longitudinal and transverse polarization) is

$$\frac{\Gamma_\tau(B \rightarrow D_{long}^*)}{\Gamma_\tau(B \rightarrow D_{trans}^*)} = \begin{cases} 0.77 & \text{(AW)} \\ 0.79 & \text{(BSW)} \end{cases} \quad (2.144)$$

whereas in the case of electron emission we get

$$\frac{\Gamma_e(B \rightarrow D_{long}^*)}{\Gamma_e(B \rightarrow D_{trans}^*)} = \begin{cases} 0.91 & \text{(AW)} \\ 1.07 & \text{(BSW)} \end{cases} \quad (2.145)$$

Summary

- (i) Decays of the B meson into $D \tau \nu_\tau$ should occur with a probability (25 – 30)% compared to the decay $B \rightarrow D e \nu_e$.
- (ii) Decays into $D^* \tau \nu_\tau$ should occur with a probability (24 – 26)% relative to $B \rightarrow D^* e \nu_e$.
- (iii) Decays with higher mass D-states may be reasonably approximated by the quark model $b \rightarrow c l \nu_l$, which gives a $\tau : e$ ratio of 27%.
- (iv) The exclusive branching ratios $B \rightarrow D(D^*) \tau \nu_\tau$ depend slightly on the choice of form factors. This dependence is also present in the meson and lepton spectra as displayed in Fig. 2.32a-f.

$$\frac{d^2\Gamma}{dE_l dE_{D^*}} = \frac{G_F^2 |V_{cb}|^2}{16\pi^3 m_B} \left[f^2 A_1 + 2m_B f a_+ A_2 + 2m_l^2 f a_- A_3 - 8fg A_4 \right. \\ \left. + a_+^2 A_5 B_1 + 2m_l^2 a_+ a_- A_6 B_1 + m_l^2 a_-^2 A_7 B_1 + 8g^2 A_8 \right]$$

where

$$\begin{aligned} A_1 &= \frac{1}{2}(m_B^2 + m_{D^*}^2 - m_l^2) - m_B E_{D^*} \\ &\quad + \frac{2}{m_{D^*}^2} \left\{ \left(-\frac{1}{2}(m_B^2 + m_{D^*}^2 + m_l^2) + m_B(E_l + E_{D^*}) \right) \left(\frac{1}{2}(m_B^2 - m_{D^*}^2 + m_l^2) - m_B E_l \right) \right\} \\ A_2 &= m_B^2(-4E_l - 3E_{D^*} + m_B) + m_B(4E_l E_{D^*} + 4E_l^2 + m_{D^*}^2) - m_l^2(E_l - \frac{1}{2}E_{D^*}) \\ &\quad + \frac{1}{m_{D^*}^2} m_B E_{D^*} \left\{ m_B^2(4E_l - m_B + 2E_{D^*}) - m_B(4E_l^2 + 4E_l E_{D^*} + \frac{3}{2}m_l^2) \right. \\ &\quad \left. + m_l^2(3E_l - \frac{1}{2}\frac{m_l^2}{m_B} + 2E_{D^*}) \right\} \\ A_3 &= -m_B^2 + m_B(E_{D^*} + E_l) \\ &\quad + \frac{1}{m_{D^*}^2} m_B E_{D^*} \left\{ m_B(E_l + 2E_{D^*}) + \frac{1}{2}(m_B^2 - m_{D^*}^2 + m_l^2) \right\} \\ A_4 &= m_B E_{D^*} \left(-\frac{1}{2}(m_B^2 + m_{D^*}^2 + m_l^2) + m_B(2E_l + E_{D^*}) \right) \\ &\quad - m_{D^*}^2 m_B E_l + \frac{1}{2}m_B^2(m_B^2 + m_{D^*}^2 + m_l^2) - m_B^3(E_l + E_{D^*}) \\ A_5 &= m_B^2(-2m_B^2 - 2m_{D^*}^2 - \frac{3}{2}m_l^2 + 8m_B E_l + 4m_B E_{D^*} - 8E_l^2 - 8E_l E_{D^*}) \\ &\quad + m_B(3m_l^2 E_{D^*} + 4m_l^2 E_l) + \frac{1}{2}m_{D^*}^2 m_l^2 - \frac{1}{2}m_l^4 \\ A_6 &= \frac{1}{2}(3m_B^2 - m_{D^*}^2 + m_l^2) - m_B(2E_l + E_{D^*}) \\ A_7 &= \frac{1}{2}(m_B^2 + m_{D^*}^2 - m_l^2) - m_B E_{D^*} \\ A_8 &= (m_B^2 E_{D^*}^2 - m_B^2 m_{D^*}^2) \left(\frac{1}{2}(m_B^2 + m_{D^*}^2 + m_l^2) - m_B E_{D^*} \right) \\ &\quad + 2m_B^2 E_{D^*} E_l \left(\frac{1}{2}(m_B^2 + m_{D^*}^2 + m_l^2) - m_B(E_l + E_{D^*}) \right) \\ &\quad + m_B^2 \left(-\frac{1}{2}(m_B^2 + m_{D^*}^2 + m_l^2) + m_B(E_l + E_{D^*}) \right)^2 \\ &\quad + m_{D^*}^2 m_B^2 E_l^2 \\ B_1 &= -m_B^2 + \frac{1}{m_{D^*}^2} m_B^2 E_{D^*}^2 \end{aligned}$$

2.7.2. NONLEPTONIC DECAYS*

The interplay between weak and strong interactions at short and long distances has been studied for a long time in strange quark decays. Many features of strange quark decays, e.g. ' $\Delta I = 1/2$ ' rule, have never been fully understood and the disagreement between theoretical predictions and experimental results has been attributed to the unknown long distance corrections. The situation is more encouraging in charm and bottom decays

*M. WIRBEL

where the mass of the decaying quark may be large enough that long distance corrections become unimportant for the understanding of the decay dynamics. It turned out that this is essentially the case, although hadronization still plays a more important role in charm decays than anticipated. The best known example is the problem of the lifetime difference between the various charmed mesons. Bottom decays seem to be dominated by short distance dynamics and they are therefore a very important laboratory for testing the Standard Model and looking for new physics. [For overview articles and many references see, for example [42, 29, 31].]

In the standard model for electromagnetic and weak interactions the Lagrangian for flavour changing interactions is given by

$$\mathcal{L} = -\frac{G_F}{\sqrt{2}} J_\mu^\dagger(0) \cdot J^\mu(0) + \text{h.c.} \quad (2.146)$$

where

$$J_\mu = (\bar{u}, \bar{c}, \bar{t}) \gamma_\mu (1 - \gamma_5) V \begin{pmatrix} d \\ s \\ b \end{pmatrix}$$

V is the Cabbibo-Kobayashi-Maskawa matrix that relates the mass eigenstates to the weak eigenstates. In order to take into account strong interaction effects we have to rely on assumptions concerning the decay dynamics :

- Short distance effects arise from the exchange of hard gluons. They modify the effective Hamiltonian and can be calculated using the well known short distance techniques of QCD. As a result the Hamiltonian is given by a sum of local operators O_i with scale dependent short distance coefficients $c_i(\mu)$,

$$\mathcal{H}_{eff} = -G_F/\sqrt{2} \sum_i c_i(\mu) O_i \quad (2.147)$$

- Long distance effects are responsible for the binding of quarks and gluons into hadrons. They include the exchange of soft gluons, the creation of quark-antiquark pairs from the vacuum, and final state interaction. We assume that all long distance effects can be absorbed in the initial and final hadronic states.

Following these assumptions the amplitudes for the weak decay of a meson M into final hadrons X_i is determined by the matrix element of the effective Hamiltonian between asymptotic initial and final states :

$$\begin{aligned} A(M \rightarrow X_1 + X_2 + \dots) &= \langle X_1, X_2, \dots | \mathcal{H}_{eff} | M \rangle \\ &= -G_F/\sqrt{2} \sum_i c_i(\mu) \langle X_1, X_2, \dots | O_i | M \rangle \end{aligned} \quad (2.148)$$

It is clear that the matrix elements in eq. (148) cannot be calculated from first principles since they include all long distance aspects of QCD. On the other hand, the calculation of

short distance coefficients is straightforward and can be done perturbatively. The $O(\alpha_s)$ corrections introduce new operators in the effective Hamiltonian [43], which is given by

$$\begin{aligned}\mathcal{H}_{eff} = & -G_F/\sqrt{2}V_{cb}\left\{c_1(m_b)\left[(\bar{c}b)(\bar{d}'u) + (\bar{c}b)(\bar{s}'c)\right]\right. \\ & \left.+ c_2(m_b)\left[(\bar{d}'b)(\bar{c}u) + (\bar{s}'b)(\bar{c}c)\right]\right\} \\ & - G_F/\sqrt{2}V_{ub}\left\{c_1(m_b)\left[(\bar{u}b)(\bar{d}'u) + (\bar{u}b)(\bar{s}'c)\right]\right. \\ & \left.+ c_2(m_b)\left[(\bar{d}'b)(\bar{u}u) + (\bar{s}'b)(\bar{u}c)\right]\right\} + \text{h.c.}\end{aligned}\quad (2.149)$$

Here we have introduced the following notation:

$$d' = d \cos \Theta_c + s \sin \Theta_c \quad s' = -d \sin \Theta_c + s \cos \Theta_c \quad (2.150)$$

with Θ_c the Cabbibo angle, and

$$(\bar{q}_2 q_1) = \sum \bar{q}_{2\alpha} \gamma_\mu (1 - \gamma_5) q_{1\alpha} \quad (2.151)$$

where α is the colour index. c_1 and c_2 are the short distance coefficients. At the scale of the decaying b quark they take the following values [29]:

$$c_1(m_b) \simeq 1.13 \quad c_2(m_b) \simeq -0.29 \quad (2.152)$$

Note that Penguin type operators have been neglected in the effective Hamiltonian. They lead to flavour changing neutral $b \rightarrow s$ decays which will not be discussed in this part of the report.

Two Particle Decays of B Mesons

The effective Hamiltonian responsible for weak b quark decays is of the (current) \times (current) type. The currents are either charged, terms proportional to c_1 , or neutral, terms proportional to c_2 in eq. (149). The basic assumption now consists in making a factorization ansatz where the amplitude for $\bar{B} \rightarrow M_1 M_2$ is approximated by products of one-particle matrix elements:

$$\langle M_1 | J_\mu(0) | 0 \rangle \langle M_2 | J^\mu(0) | \bar{B} \rangle \quad \text{or} \quad \langle M_2 | J_\mu(0) | 0 \rangle \langle M_1 | J^\mu(0) | \bar{B} \rangle$$

i.e. one of the final mesons is directly generated by a current [44, 45]. In this approximation the matrix elements for the decay $\bar{B}^0 \rightarrow D^+ \pi^-$, $\bar{B}^0 \rightarrow \bar{K}^0 J/\psi$ and $B^- \rightarrow D^0 \pi^-$, for example are given by:

$$\begin{aligned}\langle D^+ \pi^- | \mathcal{H}_{eff} | \bar{B}^0 \rangle &= -G_F/\sqrt{2}V_{cb} \cos \Theta_c a_1 \langle \pi^- | (\bar{d}u) | 0 \rangle \langle D^+ | (\bar{c}b) | \bar{B}^0 \rangle \\ \langle \bar{K}^0 J/\psi | \mathcal{H}_{eff} | \bar{B}^0 \rangle &= -G_F/\sqrt{2}V_{cb} \cos \Theta_c a_2 \langle J/\psi | (\bar{c}c) | 0 \rangle \langle \bar{K}^0 | (\bar{s}b) | \bar{B}^0 \rangle \\ \langle D^0 \pi^- | \mathcal{H}_{eff} | B^- \rangle &= -G_F/\sqrt{2}V_{cb} \cos \Theta_c \left[a_1 \langle \pi^- | (\bar{d}u) | 0 \rangle \langle D^0 | (\bar{c}b) | B^- \rangle \right. \\ &\quad \left. + a_2 \langle D^0 | (\bar{c}u) | 0 \rangle \langle \pi^- | (\bar{d}b) | B^- \rangle \right]\end{aligned}\quad (2.153)$$

The one-particle matrix elements are given in terms of decay constants, for example

$$\langle \pi^- | (\bar{d}u) | 0 \rangle = -if_\pi p_{\pi\mu}$$

and form factors, for example

$$\langle D^+ | (\bar{c}b) | \bar{B}^0 \rangle = (p_B + p_D)_\mu f_+(q^2) + q_\mu f_-(q^2).$$

The form factors can only be estimated at the moment using a model for the bound state structure of the mesons. The relativistic model of Bauer et al. [15, 46, 47] will be employed in the following to give predictions for branching ratios for nonleptonic B decays.

New, scale independent parameters a_1 and a_2 have been introduced in eq. (153) [48] which take the place of the scale dependent short distance coefficients c_1, c_2 in eq. (149). Comparing eq. (149) and eq. (153) one would guess

$$\begin{aligned} a_1 &= c_1(m_b) + \zeta c_2(m_b) \\ a_2 &= c_2(m_b) + \zeta c_1(m_b) \end{aligned} \tag{2.154}$$

with $\zeta = 1/3$ from counting the different colour combinations. However, one has to keep in mind that the long distance dynamics – exchange of soft gluons – may easily destroy completely the colour structure and therefore a_1 and a_2 will be treated as free parameters in the following.

The predictions obtained in the approach described above are summarized in Tabs. 2.20 - 2.22 and compared with the available experimental data. $|V_{cb}| = 0.05$ and the universal lifetime $\tau_B = 1.2 \cdot 10^{-12}$ sec have been used. One may try the following assumptions for the parameters a_1, a_2 at the scale of the decaying b quark mass:

i) $\zeta = 1/3$, as suggested by colour counting. In this case a_1 and a_2 take the values:

$$a_1 \simeq 1.03 \quad \text{and} \quad a_2 \simeq 0.09 \tag{2.155}$$

ii) $\zeta = 0$, in this case one finds:

$$a_1 \simeq 1.13 \quad \text{and} \quad a_2 \simeq -0.29 \tag{2.156}$$

It has been possible [48, 30] to obtain a reasonable good fit to about 20 two-particle decay modes of D and D_s mesons using the factorization approximation together with the $\zeta = 0$ rule. $\zeta = 0$ also follows in leading order of the $1/N_c$ expansion [50], where N_c is the number of colours. It is also supported by an analysis of D meson decays using QCD sum rules [51] where non-factorizable contributions cancel to a large extent against nonleading terms in the $1/N_c$ expansion.

Decay mode	Theory [30, 47]	ARGUS [49]	CLEO [49]
$\bar{B}^0 \rightarrow D^+ \pi^-$	$0.48 a_1^2$	$0.33 \pm 0.12 \pm 0.10$	$0.60^{+0.32+0.15}_{-0.28-0.12}$
$\bar{B}^0 \rightarrow D^+ \rho^-$	$1.25 a_1^2$	$2.3 \pm 1.0 \pm 0.9$	
$\bar{B}^0 \rightarrow D^{*+} \pi^-$	$0.37 a_1^2$	$0.35 \pm 0.18 \pm 0.13$	$0.46 \pm 0.12 \pm 0.10$
$\bar{B}^0 \rightarrow D^{*+} \rho^-$	$1.18 a_1^2$		
$\bar{B}^0 \rightarrow D^+ D_s^-$	$0.67 a_1^2$		
$\bar{B}^0 \rightarrow D^+ D_s^{*-}$	$0.73 a_1^2$		
$\bar{B}^0 \rightarrow D^{*+} D_s^-$	$0.30 a_1^2$		
$\bar{B}^0 \rightarrow D^{*+} D_s^{*-}$	$2.03 a_1^2$		
$\bar{B}^0 \rightarrow \pi^+ \pi^-$	$0.17 a_1^2 V_{ub}/V_{cb} ^2$	< 0.04	< 0.009
$\bar{B}^0 \rightarrow \pi^+ \rho^-$	$0.46 a_1^2 V_{ub}/V_{cb} ^2$		< 0.61
$\bar{B}^0 \rightarrow \rho^+ \pi^-$	$0.11 a_1^2 V_{ub}/V_{cb} ^2$		
$\bar{B}^0 \rightarrow \rho^+ \rho^-$	$0.37 a_1^2 V_{ub}/V_{cb} ^2$		
$\bar{B}^0 \rightarrow \pi^+ D_s^-$	$0.28 a_1^2 V_{ub}/V_{cb} ^2$		
$\bar{B}^0 \rightarrow \pi^+ D_s^{*-}$	$0.40 a_1^2 V_{ub}/V_{cb} ^2$		
$\bar{B}^0 \rightarrow \rho^+ D_s^-$	$0.13 a_1^2 V_{ub}/V_{cb} ^2$		
$\bar{B}^0 \rightarrow \rho^+ D_s^{*-}$	$0.82 a_1^2 V_{ub}/V_{cb} ^2$		
$\bar{B}^0 \rightarrow \pi^0 D^0$	$0.13 a_2^2$		
$\bar{B}^0 \rightarrow \pi^0 D^{*0}$	$0.19 a_2^2$		
$\bar{B}^0 \rightarrow \rho^0 D^0$	$0.07 a_2^2$		
$\bar{B}^0 \rightarrow \rho^0 D^{*0}$	$0.38 a_2^2$		
$\bar{B}^0 \rightarrow \bar{K}^0 J/\psi$	$1.02 a_2^2$		0.04 ± 0.03
$\bar{B}^0 \rightarrow \bar{K}^{*0} J/\psi$	$4.36 a_2^2$	0.33 ± 0.18	0.06 ± 0.03
$\bar{B}^0 \rightarrow D^+ D^-$	$4 \cdot 10^{-2} a_1^2$		
$\bar{B}^0 \rightarrow D^{*+} D^{*-}$	$4 \cdot 10^{-2} a_1^2$		
$\bar{B}^0 \rightarrow D^0 \bar{K}^0$	$2 \cdot 10^{-2} a_2^2$		
$\bar{B}^0 \rightarrow D^{*0} \bar{K}^0$	$2 \cdot 10^{-2} a_2^2$		

Tab. 2.20: Branching ratios (given in %) for two-particle decay modes of \bar{B}^0 .

The two choices, $\zeta = 0$ or $\zeta = 1/3$, lead to substantially different predictions for the B decay rates proportional to a_2^2 . The branching ratios for $\bar{B}^0 \rightarrow \bar{K}^{*0} J/\psi$ and $\bar{B}_s^0 \rightarrow \phi J/\psi$, for example, vary from 0.37% and 0.25% for $\zeta = 0$ to 0.04% and 0.02% for $\zeta = 1/3$, respectively. The rates proportional to a_1^2 or those involving both parameters are on the other hand quite insensitive to these two choices.

A second important issue in nonleptonic standard B decays is the determination of

Decay mode	Theory [30, 47]	ARGUS [49]	CLEO [49]
$B^- \rightarrow D^0 \pi^-$	$0.48(a_1 + 0.75a_2)^2$	$0.21 \pm 0.10 \pm 0.06$	$0.51^{+0.17+0.11}_{-0.15-0.07}$
$B^- \rightarrow D^0 \rho^-$	$1.25(a_1 + 0.34a_2)^2$	$2.1 \pm 0.8 \pm 0.9$	
$B^- \rightarrow D^{*0} \pi^-$	$0.37(a_1 + 1.04a_2)^2$		
$B^- \rightarrow D^{*0} \rho^-$	$1.18(a_1 + 0.79a_2)^2$		
$B^- \rightarrow D^0 D_s^-$	$0.67a_1^2$		
$B^- \rightarrow D^0 D_s^{*-}$	$0.73a_1^2$		
$B^- \rightarrow D^{*0} D_s^-$	$0.30a_1^2$		
$B^- \rightarrow D^{*0} D_s^{*-}$	$2.02a_1^2$		
$B^- \rightarrow \pi^0 \pi^-$	$0.08(a_1 + 1.00a_2)^2 V_{ub}/V_{cb} ^2$		< 0.23
$B^- \rightarrow \pi^0 \rho^-$	$0.23(a_1 + 0.50a_2)^2 V_{ub}/V_{cb} ^2$		
$B^- \rightarrow \rho^0 \pi^-$	$0.06(a_1 + 2.01a_2)^2 V_{ub}/V_{cb} ^2$	< 0.07	< 0.015
$B^- \rightarrow \rho^0 \rho^-$	$0.19(a_1 + 1.00a_2)^2 V_{ub}/V_{cb} ^2$		
$B^- \rightarrow \pi^0 D_s^-$	$0.13a_1^2 V_{ub}/V_{cb} ^2$		
$B^- \rightarrow \pi^0 D_s^{*-}$	$0.19a_1^2 V_{ub}/V_{cb} ^2$		
$B^- \rightarrow \rho^0 D_s^-$	$0.07a_1^2 V_{ub}/V_{cb} ^2$		
$B^- \rightarrow \rho^0 D_s^{*-}$	$0.41a_1^2 V_{ub}/V_{cb} ^2$		
$B^- \rightarrow K^- J/\psi$	$1.01a_2^2$	0.07 ± 0.04	0.05 ± 0.02
$B^- \rightarrow K^{*-} J/\psi$	$4.33a_2^2$		

Tab. 2.21: Branching ratios (given in %) for two-particle decay modes of B^- .

$|V_{ub}|$ from $b \rightarrow u$ transitions. Unfortunately the same reservations have to be made as in semileptonic B decays: The theoretical uncertainties in predicting the matrix elements involving the B meson and one light meson, like $\langle \pi | (\bar{u}b) | B \rangle$, introduce an uncertainty of at least a factor 2 in the determination of $|V_{ub}/V_{cb}|$. One way to avoid these uncertainties to a large extent is to study clever ratios of branching ratios as has been suggested by Shifman [52]. $\text{Br}(B^- \rightarrow K^- \bar{D}^{*0}) / \text{Br}(B^- \rightarrow K^- J/\psi)$ appears to be the best example since most of the theoretical uncertainties cancel in the ratio:

$$\text{Br}(B^- \rightarrow K^- \bar{D}^{*0}) = (0.5 \pm 0.1) |V_{ub}/V_{cb}|^2 \text{Br}(B^- \rightarrow K^- J/\psi) \quad (2.157)$$

where the coefficient (0.5 ± 0.1) takes into account possible errors. In order to estimate the number of B decays needed to obtain $|V_{ub}/V_{cb}|$, the branching ratio for $B^- \rightarrow K^- \bar{D}^{*0}$ has to be estimated:

$$\begin{aligned} \text{Br}(B^- \rightarrow K^- \bar{D}^{*0}) &= 0.48a_2^2 |V_{ub}/V_{cb}|^2 \% \\ &\simeq \begin{cases} 4 \cdot 10^{-3} |V_{ub}/V_{cb}|^2 \% \\ 4 \cdot 10^{-2} |V_{ub}/V_{cb}|^2 \% \end{cases} \end{aligned} \quad (2.158)$$

Decay mode	Theory [30, 47]	Decay mode	Theory [30, 47]
$\bar{B}_s^0 \rightarrow D_s^+ \pi^-$	$0.44 a_1^2$	$\bar{B}_s^0 \rightarrow K^0 D^0$	$0.19 a_2^2$
$\bar{B}_s^0 \rightarrow D_s^+ \rho^-$	$0.32 a_1^2$	$\bar{B}_s^0 \rightarrow K^{*0} D^0$	$0.11 a_2^2$
$\bar{B}_s^0 \rightarrow D_s^{*+} \pi^-$	$0.32 a_1^2$	$\bar{B}_s^0 \rightarrow K^0 D^{*0}$	$0.28 a_2^2$
$\bar{B}_s^0 \rightarrow D_s^{*+} \rho^-$	$1.14 a_1^2$	$\bar{B}_s^0 \rightarrow K^{*0} D^{*0}$	$0.50 a_2^2$
$\bar{B}_s^0 \rightarrow D_s^+ D_s^-$	$0.61 a_1^2$	$\bar{B}_s^0 \rightarrow K^0 J/\psi$	$0.03 a_2^2$
$\bar{B}_s^0 \rightarrow D_s^{*+} D_s^-$	$0.28 a_1^2$	$\bar{B}_s^0 \rightarrow K^{*0} J/\psi$	$0.13 a_2^2$
$\bar{B}_s^0 \rightarrow D_s^+ D_s^{*-}$	$0.67 a_1^2$	$\bar{B}_s^0 \rightarrow \phi J/\psi$	$2.93 a_2^2$
$\bar{B}_s^0 \rightarrow D_s^{*+} D_s^{*-}$	$1.79 a_1^2$	$\bar{B}_s^0 \rightarrow \eta J/\psi$	$0.4 a_2^2$
$\bar{B}_s^0 \rightarrow K^+ \pi^-$	$0.12 a_1^2 V_{ub}/V_{cb} ^2$	$\bar{B}_s^0 \rightarrow \eta' J/\psi$	$0.3 a_2^2$
$\bar{B}_s^0 \rightarrow K^{*+} \pi^-$	$0.08 a_1^2 V_{ub}/V_{cb} ^2$	$\bar{B}_s^0 \rightarrow D_s^+ K^-$	$3 \cdot 10^{-2} a_1^2$
$\bar{B}_s^0 \rightarrow K^+ \rho^-$	$0.34 a_1^2 V_{ub}/V_{cb} ^2$	$\bar{B}_s^0 \rightarrow D^0 \phi^-$	$5 \cdot 10^{-3} a_2^2$
$\bar{B}_s^0 \rightarrow K^{*+} \rho^-$	$0.49 a_1^2 V_{ub}/V_{cb} ^2$	$\bar{B}_s^0 \rightarrow K^0 \pi^0$	$6 \cdot 10^{-2} a_2^2 V_{ub}/V_{cb} ^2$
		$\bar{B}_s^0 \rightarrow \phi^0 \rho^0$	$6 \cdot 10^{-3} a_2^2 V_{ub}/V_{cb} ^2$
		$\bar{B}_s^0 \rightarrow K^0 \rho^0$	$0.2 a_2^2 V_{ub}/V_{cb} ^2$

Tab. 2.22: Branching ratios (given in %) for two-particle decay modes of \bar{B}_s^0 .

Final State	$B \rightarrow D$	$B \rightarrow D^*$	$\frac{B \rightarrow D_{long}^*}{B \rightarrow D_{transv}^*}$
$e\bar{\nu}_e + \mu\bar{\nu}_\mu$	4.1 (4.1)	11.0 (11.0)	1.07 (1.07)
$\tau\bar{\nu}_\tau$	0.6 (0.6)	1.4 (1.4)	0.80 (0.80)
X_u	7.4 (6.8)	19.9 (17.9)	1.07 (1.03)
X_c	3.6 (2.0)	8.6 (4.2)	0.87 (0.74)
X	15.7 (13.4)	40.9 (34.4)	1.01 (0.99)

Tab. 2.23: Rates for inclusive $B \rightarrow DX$ and $B \rightarrow D^*X$ decays in units of $10^{10}/\text{sec}$ for $|V_{cb}| = 0.05$. Current (constituent) quark masses have been used.

where $a_2 = 0.09$ and $a_2 = -0.29$ have been chosen, respectively. The branching ratio will therefore be of order $5 \cdot 10^{-5}$ to $5 \cdot 10^{-4}\%$ for $|V_{ub}/V_{cb}| \simeq 0.1$.

Inclusive B Decays*

Information on the dynamics of B decays and matrix elements can be obtained not only from exclusive semileptonic and nonleptonic decays but also from inclusive $B \rightarrow DX$ and $B \rightarrow D^*X$ decays, where X can be any leptonic or hadronic final state. Measurements of these decays have been performed by the ARGUS and CLEO collaborations (see, for

*The results presented in this part of the report have been obtained in collaboration with Y. - L. Wu [53].

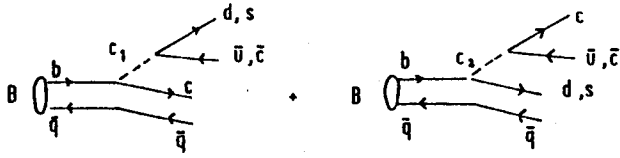


Fig. 2.33: Diagrams contributing to $b \rightarrow c$ transitions in nonleptonic B decays.

example, Ref. 6, 54). They find the following branching ratios:

$$\text{Br}(B \rightarrow D^0 X) = \begin{matrix} (0.466 \pm 0.071 \pm 0.063)\% & \text{ARGUS} \\ (0.5 \pm 0.061 \pm 0.067)\% & \text{CLEO} \end{matrix}$$

$$\text{Br}(B \rightarrow D^+ X) = \begin{matrix} (0.208 \pm 0.046 \pm 0.031)\% & \text{ARGUS} \\ (0.209 \pm 0.049 \pm 0.031)\% & \text{CLEO} \end{matrix}$$

$$\text{Br}(B \rightarrow D^{*+} X) = (0.35 \pm 0.07 \pm^{+0.11}_{-0.06})\% \quad \text{CLEO}$$

The number of D^* mesons produced per B decay is therefore roughly (0.7 ± 0.2) since $\text{Br}(B \rightarrow D^{*+} X)$ should be equal to $\text{Br}(B \rightarrow D^{*0} X)$. The corresponding number for semileptonic decays only is about the same [54]:

$$\text{Br}(B \rightarrow D^* l^- \bar{\nu}) \simeq (0.6 \pm 0.2) \text{Br}(B \rightarrow X l^- \bar{\nu})$$

The last result agrees with the theoretical description which has been developed in the last few years [15, 16, 22, 26, 55, 56]. According to these models the semileptonic B decays are saturated to more than 80% by only two channels: $\bar{B} \rightarrow D l^- \bar{\nu}_l$ and $\bar{B} \rightarrow D^* l^- \bar{\nu}_l$.

In nonleptonic decays the $b \rightarrow c$ transition occurs via the diagrams shown in Fig. 2.33. Assuming again factorization the amplitude is given by:

$$\begin{aligned} \langle q_1 \bar{q}_2 \bar{q} c | \mathcal{H}_{eff} | \bar{B} \rangle &\simeq G_F / \sqrt{2} V_{cb} \\ &\times \left\{ a_1 \langle q_1 \bar{q}_2 | (\bar{q}_1 q_2) | 0 \rangle \langle \bar{q} c | (\bar{c} b) | \bar{B} \rangle \right. \\ &\left. + a_2 \langle c \bar{q}_2 | (\bar{c} q_2) | 0 \rangle \langle \bar{q} q_1 | (\bar{q}_1 b) | \bar{B} \rangle \right\} \end{aligned} \quad (2.159)$$

The next step to determine inclusive D and D^* production is to assume that the matrix element $\langle \bar{q} c | (\bar{c} b)_\mu | \bar{B} \rangle$ is saturated by D and D^* only:

$$\langle \bar{q} c | (\bar{c} b)_\mu | \bar{B} \rangle \simeq \langle D | (\bar{c} b)_\mu | \bar{B} \rangle + \langle D^* | (\bar{c} b)_\mu | \bar{B} \rangle \quad (2.160)$$

and to neglect the second term in eq. (159) since we expect that $|a_2| \ll |a_1|^*$. The matrix element for inclusive D (D^*) production is then given by:

$$\langle X D (D^*) | \mathcal{H}_{eff} | \bar{B} \rangle \simeq \frac{G_F}{\sqrt{2}} V_{cb} a_1 \langle q_1 \bar{q}_2 | (\bar{q}_1 q_2) | 0 \rangle \langle D (D^*) | (\bar{c} b) | \bar{B} \rangle \quad (2.161)$$

corresponding to Fig. 2.34a. Contributions from Fig. 2.34b to d are probably small and are neglected. Of course the contribution from semileptonic decays $B \rightarrow D (D^*) l^- \bar{\nu}$ have still to be added to eq. (161).

* We have estimated the contribution from Fig. 2.34c alone using the free quark model for $\langle \bar{q} d | (\bar{d} b) | B \rangle$. We found that this process contributes only 2 to 3% for $|a_2| = 0.3$.

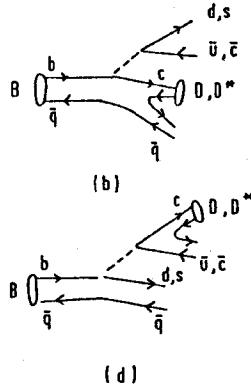
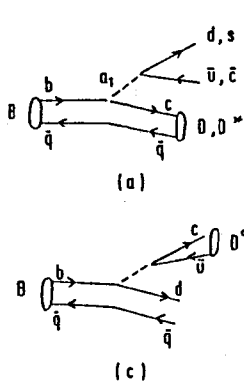


Fig. 2.34: Diagrams contributing to non-leptonic $B \rightarrow DX$ and $B \rightarrow D^*X$ decays.

The differential decay rate for $B \rightarrow D(D^*) X$ can now be calculated using the form factor expansion for the $B \rightarrow D(D^*)$ matrix element:

$$\frac{d\Gamma}{dq^2}(B \rightarrow D X) = \frac{G_F^2}{32\pi m_B} |V_{cb}|^2 \lambda^{1/2}(m_B^2, m_D^2, q^2) \times \{H_T^2(q^2) \rho_T(q^2) + H_L^2(q^2) \rho_L(q^2)\} \quad (2.162)$$

and

$$\begin{aligned} \frac{d\Gamma}{dq^2}(B \rightarrow D^* X) &= \frac{G_F^2}{32\pi m_B} |V_{cb}|^2 \lambda^{1/2}(m_B^2, m_{D^*}^2, q^2) \\ &\times \frac{q^2}{m_B^2} \left\{ [H_+^2(q^2) + H_-^2(q^2) + H_{0T}^2(q^2)] \rho_T(q^2) \right. \\ &\quad \left. + H_{0L}^2(q^2) \rho_L(q^2) \right\} \end{aligned} \quad (2.163)$$

with [57]

$$\begin{aligned} H_T(q^2) &= \frac{1}{m_B} \lambda^{1/2}(m_B^2, m_D^2, q^2) F_1(q^2) \\ H_L(q^2) &= \frac{1}{m_B} \lambda^{1/2}(m_B^2, m_D^2, 0) F_0(q^2) \\ H_{\pm}(q^2) &= (m_B + m_{D^*}) A_1(q^2) \mp \frac{\lambda^{1/2}(m_B^2, m_{D^*}^2, q^2)}{m_B + m_{D^*}} V(q^2) \\ H_{0T}(q^2) &= \frac{m_B + m_{D^*}}{2m_{D^*} \sqrt{q^2}} \left[(m_B^2 - m_{D^*}^2 - q^2) A_1(q^2) - \frac{\lambda(m_B^2, m_{D^*}^2, q^2)}{(m_B + m_{D^*})^2} A_2(q^2) \right] \\ H_{0L}(q^2) &= \frac{1}{\sqrt{q^2}} \lambda^{1/2}(m_B^2, m_{D^*}^2, q^2) A_0(q^2) \end{aligned}$$

and

$$\lambda(x, y, z) = (x - y - z)^2 - 4yz \quad (2.164)$$

The transverse and longitudinal spectral functions $\rho_T(q^2)$ and $\rho_L(q^2)$ are defined by

$$\begin{aligned} (2\pi)^3 \sum_X \delta^4(q - P_X) \langle 0 | J_\mu^\dagger(0) | X \rangle \langle X | J_\nu(0) | 0 \rangle \\ = (-g_{\mu\nu} q^2 + q_\mu q_\nu) \rho_T(q^2) + q_\mu q_\nu \rho_L(q^2) \end{aligned} \quad (2.165)$$

and receive contributions from leptonic and hadronic final states. The estimation of the hadronic part of the spectra function is clearly model dependent [58, 59]. We have used the free quark model, where ρ_T and ρ_L can be easily calculated:

$$\begin{aligned}\rho_T(q^2) &= \frac{N_c c^2}{3(2\pi)^2 q^6} \lambda^{1/2}(m_1^2, m_2^2, q^2) \left[2q^4 - (m_1^2 + m_2^2) q^2 - (m_1^2 - m_2^2)^2 \right] \\ \rho_L(q^2) &= \frac{N_c c^2}{(2\pi)^2 q^6} \lambda^{1/2}(m_1^2, m_2^2, q^2) \left[(m_1^2 + m_2^2) q^2 - (m_1^2 - m_2^2)^2 \right]\end{aligned}\quad (2.166)$$

where $N_c = 3$ is the number of colours and $c = a_1$ is the parameter defined in eq. (159). m_1 and m_2 are the masses of the quark-antiquark pair. We use two sets of parameters for the quark masses:

current masses: $m_u = m_d = 0$, $m_s = 0.15\text{GeV}$, $m_c = 1.4\text{GeV}$

constituent masses: $m_u = m_d = 0.35\text{GeV}$, $m_s = 0.55\text{GeV}$, $m_c = 1.7\text{GeV}$.

The relations eq. (166) of course also hold for the leptonic contribution to the spectral function with $N_c = 1$ and $c = 1$.

The results are summarized in Tab. 2.23 and in Fig. 2.35. D_{long}^* and D_{tr}^* denote longitudinally and transversely polarized D^* mesons, respectively. In order to compare with experiment the production of neutral and charged D mesons can be determined from the results of Tab. 2.23. Using $\text{Br}(D^{*+} \rightarrow D^0 \pi^+)$ and $\text{Br}(D^{*+} \rightarrow D^+ \pi^0 + D^+ \gamma) \simeq 50\%$ and $\text{Br}(D^{*0} \rightarrow D^0 \pi^0 + D^0 \gamma) \simeq 100\%$ [38] we find:

$$\begin{aligned}\text{Br}(B \rightarrow D^+ X) &\simeq 0.5 [\text{Br}(B \rightarrow D X) + 0.5 \text{Br}(B \rightarrow D^* X)] \\ &\simeq (18 - 22)\%\end{aligned}\quad (2.167)$$

and

$$\begin{aligned}\text{Br}(B \rightarrow D^0 X) &\simeq 0.5 [\text{Br}(B \rightarrow D X) + 1.5 \text{Br}(B \rightarrow D^* X)] \\ &\simeq (40 - 46)\%\end{aligned}\quad (2.168)$$

in agreement with the experimental results. Contributions from Figs. 2.34b to d and from higher resonances like D^{**} can therefore contribute only at the level of 20% or less inclusive D^0 and D^+ production.

2.7.3. RARE B DECAYS: STANDARD MODEL AND BEYOND*

In this section rare B decays due to loop-induced FCNC transitions will be discussed, namely $b \rightarrow s \gamma$, $b \rightarrow s g^*$, $b \rightarrow s \ell^+ \ell^-$, Within the Standard Model, probably only $b \rightarrow s \gamma$ can be studied, but vertex detectors may improve the chances for disentangling the other modes semi-inclusively. Beyond the SM, a 4th generation, extra Higgs, low

*G.W.-S. HOU, A. MASIERO

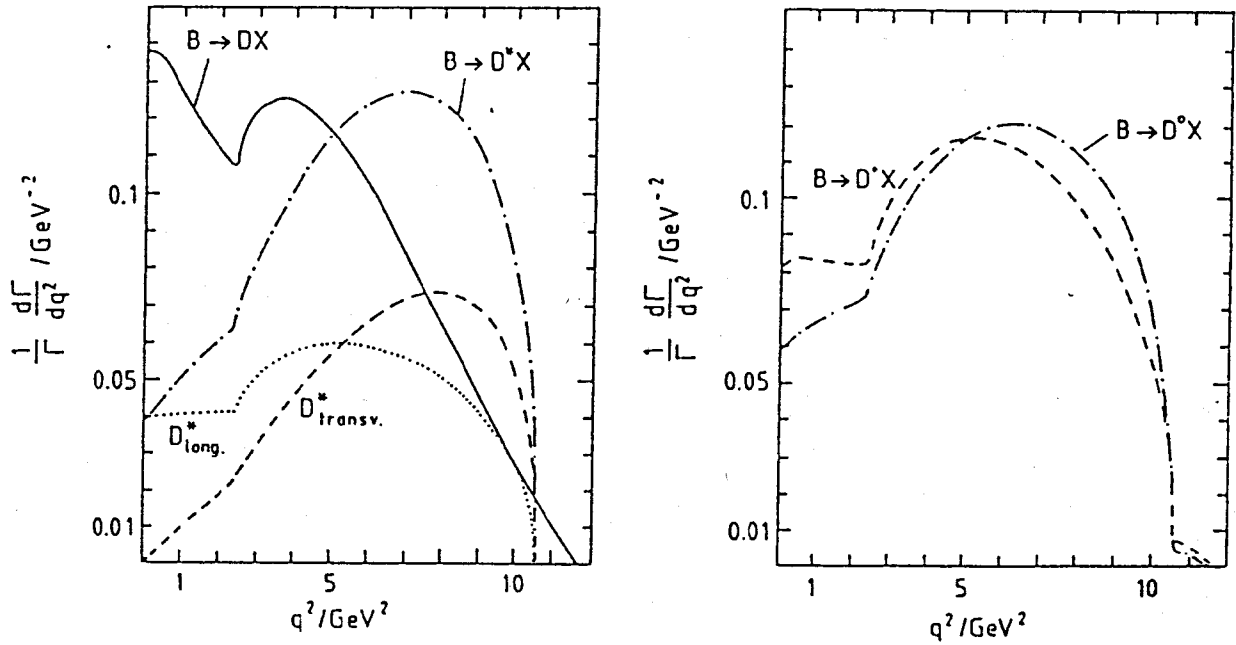


Fig. 2.35: (a) Normalized q^2 distribution for inclusive $B \rightarrow DX$ and $B \rightarrow D^*X$ decays. The dashed and dotted lines show the contributions of transversely and longitudinally polarized D^* mesons to $B \rightarrow D^*X$. The free quark model with current quark masses has been used.

(b) Normalized q^2 distribution for $B \rightarrow D^0X$ and $B \rightarrow D^+X$ decays. The free quark model with current quark masses has been used.

energy SUSY etc. could lead to sizeable enhancements of some or all of these modes, which are therefore sensitive probes for physics beyond the SM.

With $10^5 - 10^6$ B 's per year, LEP is not the best place for studying rare B decays. However, with the B 's moving very fast, vertex detectors provide an extra handle for studying B physics at LEP which is not available in symmetric B factories at Υ energies. In the following discussion, we highlight our current understanding of various rare B decay modes, in the standard model (SM), and possible effects of the simplest extensions beyond SM. Aside from sheer numbers, we try to keep in mind the potentially different role LEP may play in looking for these rare modes.

We concentrate on loop-induced flavor-changing neutral currents (FCNC). The effective $\bar{s}bV^0$ ($V^0 = Z^0, \gamma, g$) coupling is

$$J_\mu = \bar{s}\{\gamma_\mu F L + i\sigma_{\mu\nu}q_\nu m_b F_T R\}b$$

F will be referred to as the charge, and F_T as the dipole form factor (f.f.). L and R denote the left and right projection operators. For γ and g , current conservation implies $F \equiv q^2 F_1$, therefore it vanishes with q^2 ; thus, the charge f.f. does not contribute in case of "on-shell" photons and gluons. However, in this case, $F_T \equiv F_2$ has a power GIM

cancellation in the absence of QCD corrections (in contrast, F_1 suffers from only “mild”, logarithmic GIM suppression), leading to drastic suppressions of the $b \rightarrow s\gamma$ rate for low top mass. Interestingly, QCD corrections restore a “mild”, logarithmic GIM suppression for F_2 at $\mathcal{O}(\alpha_s)$, leading to a sizeable enhancement [60], making $b \rightarrow s\gamma$ into perhaps the first FCNC b decay that will be observed in nature. For $V^0 = Z^0$, $F \equiv G_Z$ is strongly m_Q dependent ($Q = t, t', \dots$), growing with m_Q in much the same way as the familiar box diagrams for K and B meson mixing (for similar reasons as well).

These effective couplings, with real or virtual gauge bosons, lead to the decay processes $b \rightarrow s\gamma$, $b \rightarrow sg^*$, $b \rightarrow s\ell^+\ell^-$ and $b \rightarrow s\nu\bar{\nu}$. For the latter two there are also box diagram contributions. Aside from the standard model, we consider some very simple, or well motivated extensions: i) models with a fourth fermionic generation; ii) models with two Higgs doublets; iii) low energy supersymmetry; iv) left-right symmetric models;

$b \rightarrow s\gamma$

The study of $b \rightarrow s\gamma$ is likely to represent the most promising chance for LEP to say something new on FCNC rare B decays.

In the SM a fascinating and surprising QCD enhancement of $BR(b \rightarrow s\gamma)$ occurs [60], as stated already in the above. This enhancement is not from intrinsically “large” corrections, but because the “leading”, purely electroweak effect is suppressed (power vs. logarithmic GIM). Thus, $\mathcal{O}(\alpha_s)$ corrections enhance $(b \rightarrow s\gamma)$ roughly by one order of magnitude, and $BR(b \rightarrow s\gamma) \gtrsim 10^{-4}$ is expected; the dependence on m_t is, however, very mild.

We immediately run into one of the main difficulties for experimental rare B decay studies. The inclusive rate above looks promising. However, we do not (at present) have a good handle on inclusive studies, and have to rely on exclusive, few body modes. The most accessible exclusive channel is $B \rightarrow K^*\gamma$. Although the estimate of $\Gamma(B \rightarrow K^*\gamma)/\Gamma(b \rightarrow s\gamma)$ is rather controversial, it seems likely that this ratio should not be much more than 10%. Thus, in order to probe the SM result one should push the bound on $BR(B \rightarrow K^*\gamma)$ down to $\mathcal{O}(10^{-5})$. Presently, the ARGUS [61] bound is $BR(B \rightarrow K^*\gamma) < 2.4 \times 10^{-4}$. It remains to be seen whether the vertex separation capabilities (for both B and D) can lead to improvements on this dilemma.

Aside from this, for LEP the relevant question might be: is there new physics which can enhance $BR(b \rightarrow s\gamma)$ up to $\mathcal{O}(10^{-3})$?

If a heavy fourth generation exists, there is the possibility [62] of having $BR(b \rightarrow s\gamma)$ as large as few times 10^{-3} . For this to occur two conditions must be met: i) the fourth up-quark, t' , must be heavy compared to top, $m_{t'} > 150 \text{ GeV}$ and ii) large mixing of t' with b and s must occur: $|V_{t'b}V_{t's}|$ of order of the Cabibbo angle. Such a large mixing cannot

be presently ruled out, but seems unlikely. One interesting extra is that, due to the fact that only one single f.f. contributes to the decay, the t' contribution may cancel against the others, leading to a suppression of the $b \rightarrow s\gamma$ rate. Thus, $BR(b \rightarrow s\gamma) < 10^{-4}$ could also be an indication of presence of 4th generation. If the B_s meson exhibits “maximal” mixing, not much can be said about $V_{t's}$, but a nonmaximal B_s mixing would imply $V_{t's}$ to be not too large, and 4th generation effects on $b \rightarrow s\gamma$ have to be small.

Another potential source of enhancement [63,64] for $b \rightarrow s\gamma$ is the presence of one additional Higgs doublet. Of particular physical interest is the situation where one doublet (H_1) gives mass to the up-quark sector, whilst the other doublet (H_2) is responsible for the down-quark masses. In this case no tree level scalar mediated FCNC arise. The charge Higgs boson effects always add constructively to the SM contribution, leading to enhancements. Denoting by v_1 and v_2 the vacuum expectation values of H_1 and H_2 , we distinguish the two cases: i) $v_1 > v_2$, which is a “natural hierarchy” given that $m_t > m_b$; ii) $v_1 < v_2$, the “unnatural hierarchy”, which is technically feasible provided that the Yukawa couplings are conveniently tuned. In this latter case, extraordinarily large enhancements of $BR(b \rightarrow s\gamma)$ are possible. Indeed, some extreme values are already excluded by the ARGUS bound. On the contrary, in a situation of “natural” hierarchy only moderate enhancements are possible, typically, one obtains $BR(b \rightarrow s\gamma)$ between 10^{-4} and 10^{-3} . To keep an open mind, however, one should not preclude the possibility that extra Higgs bosons can enhance the $b \rightarrow s\gamma$ rate beyond the 10^{-3} level. Indeed, in a second type of a two Higgs doublet model, though lacking in motivation, the enhancement factor can be even greater (while suppression also becomes possible) [63].

The first type of a two Higgs model mentioned above is a natural ingredient in minimal SUSY models, and the previous discussion is applicable. However, in SUSY the real novelty concerning FCNC phenomena is that they can be generated in the strong interaction sector through gluino-squark-quark vertices [65]. $BR(b \rightarrow s\gamma) \sim \mathcal{O}(10^{-3})$ is likely to require squark and gluino masses below $\sim 70 - 80 \text{ GeV}$ (at least in the simplest, “minimal” SUSY version of SM) [66] so that this possibility seems to be ruled out by the present upper limits on $m_{\tilde{g}}$ and $m_{\tilde{q}}$ from the Tevatron. However, the direct bounds that one derives at the hadronic colliders are subject to theoretical uncertainties (jet analysis, assumption on the dominant decay channels of squarks and gluinos, degeneracy of squark masses, ...) and, thus, the search for indirect effects of SUSY particles in $b \rightarrow s\gamma$ is still an interesting challenge.

In left-right (LR) symmetric extensions of SM, there are two new parameters whose values is decisive in establishing the strength of FCNC: the mass of right-handed gauge bosons W_R^\pm and their mixing ξ with the ordinary left-handed W_L^\pm of SM. In those LR extensions where the mixing angles in the right-handed charged current sector coincide

with their left-handed counterparts, i.e. the entries of the familiar Kobayashi-Maskawa matrix, very stringent bounds on M_{W_R} and ξ hold, leading to only very minor changes [67] in the prediction of the rates for $b \rightarrow s$ FCNC decays, in particular $b \rightarrow s\gamma$. However, the equality of the Cabibbo-Kobayashi-Maskawa mixings in the left- and right-handed sectors is by no means a general property of LR symmetric schemes, and in the most generic cases the left and right mixing are unrelated. Then, much milder bounds on M_{W_R} and ξ apply, roughly $M_{W_R} > 300 \text{ GeV}$ and ξ less than few percent. If such is the case, LR symmetric models can also provide sizeable enhancements to FCNC rare B decays through one-loop diagrams where a $W_L - W_R$ mixing takes place.

In conclusion:

- i) observation of $b \rightarrow s\gamma$ with a $BR \sim 10^{-3}$ would unambiguously signal the presence of new physics. To be sure, this should be some kind of “non-canonical” new physics, namely some extension of the minimal supersymmetric standard model, a two Higgs doublet model with “unnatural hierarchy” of v_1 , and v_2 (or the perhaps even more unappealing second type of model), or a fourth generation model with very large mixing between the fourth and the second and third families.
- ii) observation of $b \rightarrow s\gamma$ with $10^{-4} < BR < 10^{-3}$ would signal some possible more canonical new physics.
- iii) detection of $b \rightarrow s\gamma$ with $BR = (2-3) \cdot 10^{-4}$ would prove that, indeed, impressively large QCD corrections are present in SM.
- iv) detection of $b \rightarrow s\gamma$ below 10^{-4} would indicate the presence of a fourth generation, or the rather “non-canonical” second type of two Higgs doublet models.

$b \rightarrow sg^*$

In the SM, $BR(b \rightarrow sg^*)$, with the q^2 of the gluon g positive, i.e. $b \rightarrow sq\bar{q}$, sgg , is at the 1 – 2% level, and the dependence on m_t is mild [68]. This is a rather large “rare” branching ratio. Unfortunately, this inclusive level rate is very hard to measure, while exclusively, there is in general a three order of magnitude suppression factor (three “parton” final states vs. one in the $b \rightarrow s\gamma$ case) for two body modes, i.e. down to the 10^{-5} level.

Further enhancement is possible in SUSY models where the gluon line can be attached to the internal gluino line with a characteristic color enhancement factor [69]. For the second type of the two Higgs models, drastic enhancements are allowed by the B mixing constraint [63]. Because of the insensitivity towards large t' masses, one does not expect enhancements from a fourth fermion generation, even if the conditions of large $m_{t'}$ and large $V_{t'b}$ and $V_{t's}$ mixing angles are met. In the first two cases the enhancements can

result in values of $BR(b \rightarrow sg^*)$ as large as $\sim 10 - 20\%$, consistent with present “charm deficit” limits.

Our earlier remark regarding B vertex separation and vetoing against charm is still valid, except that one does not have a photon as a clean signal anymore. However, if semi-inclusive studies are possible, the rate seems rather large even in the SM case. Vertex detectors should be able to distinguish between an s produced at the primary b vertex and an s from the secondary vertex $b \rightarrow c + X \rightarrow s + X$. In general, the penguin modes will lead to a very large multiplicity, with all particles coming from one single vertex consistent with a B decay vertex, which could lend an additional handle. Another possible way to put a bound on $b \rightarrow sg^*$ is to look just for limits on charmless b decays. Since the large enhancements mentioned above push $BR(b \rightarrow sg^*)$ up to $10 - 20\%$, this second possibility should be feasible.

$b \rightarrow s\ell^+\ell^-$ and $b \rightarrow s\nu\bar{\nu}$

The BR 's for these FCNC semileptonic decays are rather small in the SM [70], although strongly dependent on m_t . Aside from the tree level resonance contribution $b \rightarrow s\psi \rightarrow s\ell^+\ell^-$, which is at the 10^{-3} level, the short distance (therefore m_t dependent) contribution gives a rate (off the ψ , ψ' resonances) between 10^{-6} and 10^{-5} , depending on the value of m_t . $b \rightarrow s\nu\bar{\nu}$ comes purely from short distance contributions and ranges from $10^{-6} - 10^{-4}$, growing with m_t rather rapidly.

For $b \rightarrow s\ell^+\ell^-$, since one would readily study $b \rightarrow s\psi$ by tagging on the $\ell^+\ell^-$ pair, the short distance effect should show up in the off resonance $\ell^+\ell^-$ mass spectrum. The main problem is statistics. $b \rightarrow s\nu\bar{\nu}$, at first sight, looks hopeless because of the missing energy. However, the rate is very similar to the one expected for $B \rightarrow \tau\nu_\tau$ (which is relevant for measuring $V_{ub} \times f_B$), and if this mode can be studied, so can the loop induced mode. One knows that the τ lepton mainly decays to one-prong, non-strange hadrons, so it should be quite distinguishable from the loop induced mode, which should have strangeness one in the final state, and have higher multiplicity. We remark that if the top is very heavy (close to 200GeV), it will take a while for it to be discovered, and one of the ways to study its indirect effect is via the modes discussed here.

In SUSY, due to the lack of the characteristic large logs of the super GIM mechanism, no enhancement is present. With two Higgs doublets with the “inverted” hierarchy $v_1 < v_2$, an enhancement up to 10^{-5} is possible if the top is light [63], a consequence of the measured B_d mixing. For the even less canonical second type of models, even larger enhancements are possible [63], but only if $b \rightarrow sg^*$ and $b \rightarrow s\gamma$ are greatly enhanced as well (so far the best bound on $b \rightarrow s\ell^+\ell^-$ has been obtained by CLEO [71], with $BR(B \rightarrow \ell^+\ell^- + X) < 1.2 \cdot 10^{-3}$).

Because of the strong dependence on heavy internal quark masses, these modes are ideal places to search for heavy t' effects [70]. In general, the rates can get enhanced by an order of magnitude if $m_{t'}$ is several hundred GeV , even with modest $V_{t's}$ values. Increasing the latter to the size of the Cabibbo angle can lead to enhancements by another order of magnitude. Thus, $b \rightarrow s\ell^+\ell^-$ at the 10^{-4} order and $b \rightarrow s\nu\bar{\nu}$ at the 10^{-3} order is quite possible.

	$b \rightarrow s\gamma$	$b \rightarrow sg^*$	$b \rightarrow s\ell^+\ell^-$	$b \rightarrow s\nu\bar{\nu}$
SM	10^{-4}	10^{-2}	$10^{-6} - 10^{-5}$	$10^{-6} - 10^{-4}$
SUSY	$\lesssim 10^{-3}$	$\lesssim 15\%$	$\sim SM$	$\sim SM$
2 Higgs	$10^{-4} - 10^{-3}$ $0 - 10^{-2}$	$\sim SM$ $\lesssim 15\%$	$\lesssim 10^{-5}$ $\lesssim 10^{-4}$	$\sim SM$
4th gen.	$0 - 10^{-3}$	$\sim SM$	$\lesssim 10^{-4}$	$\lesssim 10^{-3}$

Tab. 2.24: Allowed ranges (inclusive) at present for various models. For discussion of the limits, and the assumptions involved, see the text. Exclusive modes are typically one order of magnitude lower, while two body exclusive modes for $b \rightarrow sg^*$ are typically 3 orders of magnitude lower than the inclusive (even more in the case of large enhancements in the SUSY and 2 Higgs models). The two sets of numbers for 2 Higgs models refer to model I and II. The left-right model is omitted since its predictions are similar to the SM.

In conclusion, we think that it is not easy for LEP (with $10^5 - 10^6$ B 's per year) to probe the FCNC rare B decays that we considered with rates at the SM level. However, in view of the significant enhancements that could occur in several extensions of the SM, and the possibility for exploiting vertex detectors in the study of B physics, we think that it is worthwhile for LEP experiments to devise strategies to study rare B decays, in particular the modes $b \rightarrow s\gamma$ and $b \rightarrow s\ell^+\ell^-$, at least after a first set of results concerning B physics has been obtained. If techniques are developed to veto against charm, the not-so-rare penguin mode $b \rightarrow sg^*$ may also be studied, while $b \rightarrow s\nu\bar{\nu}$ should be studied concurrently if one plans to study $B \rightarrow \tau\nu_\tau$. A final remark should be made regarding the prospects of having LEP as a Z factory, with 10^8 Z 's per year. In that case, one would have roughly 3×10^7 B mesons per year. Although CP violation may still elude us, the prospect of seeing most of the rare decay modes discussed here, even within the standard model, becomes rather good. The high energy environment at the Z pole is certainly complimentary to the environment at the $\Upsilon(4S)$.

REFERENCES

- [1] G. Levman et al., *Phys. Lett.* **141 B** (1984) 271.
- [2] S. Behrends et al., *Phys. Rev. Lett.* **59** (1987) 407.
- [3] K. Wachs et al., DESY preprint, DESY 88-111 (1988).
- [4] H. Albrecht et al., *Phys. Lett.* **197 B** (1987) 452.
- [5] H. Albrecht et al., *Phys. Lett.* **219 B** (1989) 121.
- [6] E.H. Thorndike and R.A. Poling, *Physics Reports* **157** (1988) 183.
- [7] H. Schröder, Preprint, DESY 88-101 (1988).
- [8] G. Altarelli, N. Cabibbo, G. Corbo, L. Maiani and G. Martinelli, *Nucl. Phys. B* **208** (1982) 365.
- [9] M. Suzuki, *Phys. Lett.* **155 B** (1985) 112.
- [10] L. Angelini, L. Nitti, M. Pellicoro and G. Preparata, *Phys. Lett.* **172 B** (1986) 447.
- [11] J.L. Basdevant, I. Bediaga and E. Predazzi, *Nucl. Phys. B* **294** (1987) 1054.
- [12] A. Bareiss and E.A. Paschos, Dortmund Preprint DO-TH 89/1 (1989).
- [13] A. Ali, *Z. Phys. C1* (1979) 25.
- [14] A. Ali, D.G. Körner, G. Kramer and J. Willrodt, *Z. Phys. C1* (1979) 269.
- [15] M. Wirbel, B. Stech and M. Bauer, *Z. Phys. C* **29** (1985) 637.
- [16] B. Grinstein, M.B. Wise and N. Isgur, *Phys. Rev. Lett.* **56** (1986) 298.
- [17] F. Schöberl and H. Pietschmann, *Europhysics Letters* **2** (1986) 583.
- [18] M. Shifman and M. Voloshin, ITEP-64 (1987).
- [19] S. Nussinov and W. Wetzel, *Phys. Rev. D* **36** (1987) 130.
- [20] T. Altomari and L. Wolfenstein, *Phys. Rev. Lett.* **58** (1987) 1583 and CMU-HEP-86-17.
- [21] B. Grinstein and M. Wise, *Phys. Lett.* **197 B** (1987) 249.
- [22] J.G. Körner and G.A. Schuler, *Z. Phys. C38* (1988) 511; *Z. Phys. C41* (1989) 690.
- [23] M. Suzuki, *Phys. Rev. D* **37** (1988) 239.
- [24] C.A. Dominguez and N. Paver, *Z. Phys. C41* (1988) 217.
- [25] M. Bauer and M. Wirbel, *Z. Phys. C* **42** (1989) 671.
- [26] B. Grinstein, N. Isgur, D. Scora and M. Wise, *Phys. Rev. D* **39** (1989) 799.
- [27] J.M. Cline, W.F. Palmer and G. Kramer, DESY 89-029 (1989).
- [28] N. Cabibbo and L. Maiani, *Phys. Lett.* **79 B** (1978) 109;
N. Cabibbo, G. Corbo and L. Maiani, *Nucl. Phys. B* **155** (1979) 93;
G. Corbo, *Nucl. Phys. B* **212** (1983) 99;
M. Suzuki, *Nucl. Phys. B* **145** (1978) 420;
A. Ali and E. Pietarinen, *Nucl. Phys. B* **154** (1979) 519.
- [29] R. Rückl, Weak Decays of Heavy Flavours, CERN (1983).
- [30] M. Bauer, B. Stech and M. Wirbel, *Z. Phys. C* **34** (1987) 103.
- [31] M. Wirbel, *Progress in Particle and Nuclear Physics* **21** (1988) 33.
- [32] J.C. Anjos et al., *Phys. Rev. Lett.* **62** (1989) 722.
- [33] R.H. Schindler, Proc. of the XXIV Int. Conf. on High Energy Physics, München (1988).
- [34] K. Wachs et al., DESY 88-111 (1988); T. Jensen, *Nucl. Phys. B* **1** (Proc. Suppl.) (1988) 81.
- [35] J.G. Körner and G.A. Schuler, Mainz preprint MZ-TH/89-01 and DESY 89-015 (1989).
- [36] P. Heiliger and L.M. Sehgal, to be published.
- [37] J.L. Cortes, X.Y. Pham and A. Tounsi, *Phys. Rev. D* **25** (1982) 188.
- [38] Particle Data Group, *Phys. Lett.* **204 B** (1988) 1.
- [39] Similar to the e spectrum in μ -decay with a massive ν_μ : e.g. R.E. Shrock, *Phys. Rev. D* **24** (1981) 1275.

- [40] This is the analog of the well known result for K_{l3} decay. See, e.g., R.E. Marshak, Riazuddin and C.P. Ryan, "Theory of Weak Interactions in Particle Physics", Wiley-Interscience (1969).
- [41] T. Altomari and L. Wolfenstein, *Phys. Rev. Lett.* **58** (1987) 1583;
see also B. Grinstein, N. Isgur, D. Scora and M. Wise, *Phys. Rev. D* **39** (1989) 799.
- [42] E.A. Paschos and U. Türke, *Phys. Rep.* **C 178** (1989) 145.
- [43] G. Altarelli and L. Maiani, *Phys. Lett.* **52 B** (1974) 351;
M.K. Gaillard and B.W. Lee, *Phys. Rev. Lett.* **33** (1974) 108.
- [44] D. Fakirov and B. Stech, *Nucl. Phys.* **B 133** (1978) 315.
- [45] N. Cabibbo and L. Maiani, *Phys. Lett.* **73 B** (1978) 418.
- [46] M. Bauer, B. Stech and M. Wirbel, *Z. Phys.* **C 34** (1987) 103.
- [47] M. Bauer, Ph.D. Thesis, Heidelberg (1987).
- [48] M. Bauer and B. Stech, *Phys. Lett.* **152 B** (1985) 380.
- [49] H. Schröder, Proc. of The XXIV Int. Conf. on High Energy Physics, München 1988.
- [50] A.J. Buras, J.-M. Gerard and R. Rückl, *Nucl. Phys.* **B 268** (1986) 16.
- [51] B. Blok and M.A. Shifman, *Yad. Fiz.* **45** (1987) 211, 478, 841; and ITEP Reports 9, 17, 37 (1986).
- [52] M.A. Shifman, *Nucl. Phys. B (Proc. Suppl.)* **3** (1988) 289 and *J. of Mod. Phys.* **3A** (1988) 2769.
- [53] M. Wirbel and Y.-L. Wu, DO-TH 89/6.
- [54] H. Schroeder, Physics of B Mesons, DESY 88-101.
- [55] M.A. Shifman and H. Voloshin, *Yad. Fiz.* **47**(1987)801.
- [56] N. Isgur, *Phys. Rev. D* **40** (1989) 101.
- [57] For the definition of various form factors see e. g. Ref. 15 and the section on semileptonic B decays.
- [58] H. Pietschmann and H. Rupertsberger, *Z. Phys.* **C 27** (1985) 73.
- [59] H. Grotch and K. Schilcher, *Phys. Rev. D* **37** (1988) 137.
- [60] S. Bertolini, F. Borzumati and A. Masiero, *Phys. Rev. Lett.* **59** (1987) 180;
N.G. Deshpande, P. Lo, J. Trampetic, G. Eilam and P. Singer, *Phys. Rev. Lett.* **59** (1987) 183;
B. Grinstein, R. Springer and M.B. Wise, *Phys. Lett.* **202 B** (1988) 138;
R. Grigjanis, P.J. O'Donnell, M. Sutherland and H. Navelet, *Phys. Lett.* **213 B** (1988) 355.
- [61] ARGUS collab. H. Albrecht et al., *Phys. Lett.* **210 B** (1988) 258;
see also CLEO collab., P. Avery et al., *Phys. Lett.* **223 B** (1989) 470.
- [62] W. S. Hou, A. Soni and H. Steger, *Phys. Lett.* **192 B** (1987) 441;
J.L. Hewett, *Phys. Lett.* **193 B** (1987) 327.
- [63] W.S. Hou and R.S. Willey, *Phys. Lett.* **202 B** (1988) 591 and *Nucl. Phys.* **B** to appear.
- [64] B. Grinstein and M.B. Wise, *Phys. Lett.* **201 B** (1988) 274;
T.D. Nguyen and G.C. Joshi, *Phys. Rev. D* **37** (1988) 3220.
- [65] M.J. Duncan, *Nucl. Phys.* **B 221** (1985) 285;
J.F. Donoghue, H.P. Nilles and D. Wyler, *Phys. Lett.* **128 B** (1983) 55;
A. Bouquet, J. Kaplan and C. Savoy, *Phys. Lett.* **148 B** (1984) 69.
- [66] S. Bertolini, F. Borzumati and A. Masiero, *Phys. Lett.* **192 B** (1987) 437;
A. Masiero and G. Ridolfi, *Phys. Lett.* **212 B** (1988) 171.
- [67] D. Cocolicchio, G. Costa, G. Fogli, J.H. Kim and A. Masiero, CERN-TH 5110/88.
- [68] W. S. Hou, A. Soni and H. Steger, *Phys. Rev. Lett.* **59** (1987) 1521;
W. S. Hou, *Nucl. Phys.* **B 308** (1988) 561.
- [69] S. Bertolini, F. Borzumati and A. Masiero, *Nucl. Phys.* **B 294** (1987) 321.
- [70] W.S. Hou, R.S. Willey and A. Soni, *Phys. Rev. Lett.* **58** (1987) 1608.
- [71] CLEO collab., A. Bean et al., *Phys. Rev. D* **35** (1987) 3533.

2.7.4. HEAVY FLAVOUR DECAYS: EURODEC*

We report on a recent attempt to classify and model the decays of hadrons containing heavy quarks. A detailed analysis is presented in which we compare our model with several experimental distributions. Special attention is paid to the inclusive and exclusive semileptonic decay distributions of charmed and bottom hadrons which are of major importance in the analysis of weak mixing in the bottom sector at both hadron collider experiments and LEP.

We extensively discuss exclusive and inclusive hadronic decay modes and compare with experimentally obtained decay rates. Cabibbo suppression is explicitly accounted for.

Although the experimental input is in many cases still rather poor we find good agreement between the distributions obtained with our model and recent measurement of $J/\psi, \psi'$ and baryon production in the decays of bottom mesons. We briefly discuss kinematical correlations in the decay of light mesons.

Appropriate matrix elements for both heavy and light flavour hadrons are included in the EURODEC Monte Carlo program for the fragmentation of partons and decays of particles. This program is part of the larger EUROJET package for the simulation of hard partonic interactions. The decay program makes use of a detailed particle decay table which can be easily modified according to the needs of the user.

Basis

Charged weak currents play a dominant role in the description of flavour changing phenomena. In the Standard three family $SU(2)_L * U(1)$ Model the charged weak currents are governed by a unitary $3 * 3$ matrix. The charged current part of the Lagrangian in the Standard Model was first written down by Kobayashi and Maskawa [1]:

$$J_\mu^\pm \sim g(\bar{u}, \bar{c}, \bar{t})\gamma_\mu(1 - \gamma_5) \begin{pmatrix} d' \\ s' \\ b' \end{pmatrix} + h.c., \text{ with: } \begin{pmatrix} d' \\ s' \\ b' \end{pmatrix} = V \begin{pmatrix} d \\ s \\ b \end{pmatrix} \quad (1)$$

with the gauge coupling constant g and assuming three doublets: $(u, d')_L, (c, s')_L, (t, b')_L$. Since the Cabibbo-GIM sector is by now well established, experiments concentrate on resolving the 'third family sector' in the CKM mixing matrix:

$$V \equiv \begin{pmatrix} V_{ud} & V_{us} & V_{ub} \\ V_{cd} & V_{cs} & V_{cb} \\ V_{td} & V_{ts} & V_{tb} \end{pmatrix} \quad (2)$$

*B. VAN EIJK in collaboration with K. BOS

that is the matrix elements expressing the magnitude of mixing between u, d, s and c quarks and the bottom or top quark.

Except for the b -lifetime, almost everything we have learned about the bottom hadron sector has come from e^+e^- -experiments. Measurements with colliding beams tuned at the $\Upsilon(4S)$ have produced a wealth of information on inclusive and exclusive B -hadron decay properties. Since there is no strong signal for charmless bottom decays, previous (and continuing) measurements at the $\psi''(3770)$ are of great importance in the analysis of both semileptonic and hadronic bottom decays.

Although the top quark turns out to be a difficult family member to trace [2], experimental data on the bottom quark sector have provided us with information from which one is able to derive limits on the top quark mixing matrix elements. Using the unitarity bound together with $m_b < m_t < M_W$ and the reported observations of mixing in both B^0 sector (ARGUS [3]) and B_s^0 sector (UA1 [4]), fairly strong limits on $|V_{td}|$ and $|V_{ts}|$ may be calculated [5, 6, 7, 8, 9]. Uncertainties in these calculations mainly stem from hadronic corrections to the box diagram picture describing the weak mixing between particle and antiparticle and the unknown top quark mass ($\sim 60 \text{ GeV}/c^2 < m_t < \sim 200 \text{ GeV}/c^2$).

The outline of this paper is as follows. First we will discuss our model for heavy flavour decays and its Monte Carlo (EURODEC, see Ref. 10) implementation. In the third section we focus on charmed meson and charmed baryon decays, the first mainly measured at the $\psi''(3770)$. We summarize experimentally obtained inclusive and exclusive decay rates and compare experimental distributions with the distributions produced by our model. In the next section we review the experimental situation on the bottom sector, describe our model and compare inclusive and exclusive quantities and distributions. Special emphasis is put on semileptonic heavy flavour decays, ‘hidden charm’ and baryon production. In the fifth section we cover the modelling of top (and ‘fourth family’ member) decays. Finally we briefly summarize the decay matrix elements we have included to achieve a correct kinematical description of the decays of specific ‘light flavour’ hadrons and draw conclusions. The modelling of the production and decay of onium states is reviewed in more detail elsewhere [11].

Heavy flavour decay models and their Monte Carlo implementation

Let us concentrate on three-body decays of charm, bottom and heavier quarks. We have assumed a pure $V - A$ structure of the weak charged current in the weak hadronic decays $Q \rightarrow q\bar{f}f$, where all fermions Q, q, f and \bar{f} may have arbitrary masses. The matrix element squared reads [12]:

$$|M|^2 = C \times \frac{8[p_q \cdot p_f * (p_Q + m_Q s) \cdot p_{\bar{f}}]}{m_Q^4} \quad (3)$$

with p and m the four-vector (momentum and energy) and mass of the indicated particles (C contains the propagator and coupling constants while s describes the polarization of Q . Both quantities will be discussed later). The generalization to a flexible admixture of vector (g_v) and axial (g_a) couplings is purely technical and the program implementation may easily be taken care of by the user if desired [13]:

$$\begin{aligned}
|M|^2 = \frac{C^*}{m_Q^4} * (g_v + g_a)^2 [p_q \cdot p_f \times (p_Q + m_Q s) \cdot p_{\bar{f}}] \\
+ (g_v - g_a)^2 [p_q \cdot p_{\bar{f}} * (p_Q - m_Q s) \cdot p_f] \\
+ (g_v^2 - g_a^2) (-p_f \cdot p_{\bar{f}} m_Q m_q + p_Q \cdot p_f s \cdot p_{\bar{f}} - p_Q \cdot p_{\bar{f}} s \cdot p_f)
\end{aligned} \tag{4}$$

If we sum over polarizations and treat the decay of Q in its rest-frame, eq.(3) reduces to a very simple expression:

$$|M|^2 = \frac{16C}{m_Q^4} * (p_q \cdot p_f * m_Q E_{\bar{f}}) \tag{5}$$

with $E_{\bar{f}}$ the energy of the antifermion.

The semileptonic decays $X \rightarrow l\nu_l Y$, with X charmed or bottom pseudoscalar particles (the strong decay of charm and bottom vectors will take place at a much shorter time scale than their weak decay) and Y respectively predominantly strange or charm pseudoscalar particles, are governed by the same matrix element (5), whereas decays $X \rightarrow l\nu_l Y^*$ with Y^* a vector particle are described assuming a pure vector current. The matrix element for this type of decays has been derived by A. Ali [14]. The normalized lepton energy distribution can be written as

$$\frac{1}{\Gamma} \frac{d\Gamma}{dE_l} = \frac{96}{m_X^5 f} * \frac{E_l^2 (m_X^2 - m_{Y^*}^2 - 2m_X E_l)^2 * (m_X^2 + 2m_{Y^*}^2 - 2m_X E_l)^2}{(m_X^2 - 2m_X E_l)^2} \tag{6}$$

with m and E the appropriate mass and energy of the particles (index) and f the usual phase space factor [14].

Although the effect of the W propagator may safely be neglected in case of charm decays, it has to be included in the decay of third family quarks. The effect becomes extreme important for top quarks with mass $m_t \sim M_W$ and larger ! This will be discussed in some more detail in section 5.

The Monte Carlo program presented here relies heavily on earlier work [15]. However, we have completely reviewed and improved the procedure of the implementation of decays, which now goes along the following lines. Depending on the particle masses involved in a specific decay mode, the maximum phase space weight is calculated. In the next step the kinematics for the particles is generated following the well-known procedure that the n -dimensional phase space (n means here the number of particles) may be treated

as $n - 1$ two-body decays. The invariant mass of each (virtual) two particle system is bound by the mass of the parent (or remaining energy of the previous two-body decay) and the sum of physical masses of the decay particles. More explicit for the three-body decay $P \rightarrow D_1 D_2 D_3$ (in the P rest-frame) a virtual invariant mass is generated for the remaining two-body system $D_2 - D_3$, with $m_2 + m_3 < m_{virtual} < m_P$. The kinematics of D_1 and the virtual intermediate state are then fixed. The probability for a certain value of $m_{virtual}$ depends entirely the masses involved in the decay. Finally the kinematics for D_2 and D_3 are generated in the rest-frame of the virtual 'particle' (followed by a Lorentz transformation) by letting the virtual state decay. The probability for a certain value of $m_{virtual}$ may be translated into a weight for this specific phase space configuration and can now be compared with the maximum phase space weight. A simple rejection algorithm ensures that each surviving decay configuration is generated with equal probability. Since kinematics are now fixed, the matrix element squared can be calculated and introduces an additional weighting procedure. We have normalized all the matrix elements such that their maximum weight never exceeds 1.

Two-body heavy flavour decays (decay ratios mainly taken from experimental data) are treated according to pure phase space. Angular correlations are not but may easily be included.

Charm decay properties

The ψ'' (3770) is believed to decay dominantly into $D\bar{D}$. Charged particle momentum distributions [16] and the analysis of di-lepton and single lepton rates [17] at the ψ'' compared with continuum measurements indicate the correctness of this statement. However, the assumption made in many earlier analyses of exclusive D decay ratios that $BR(\psi'' \rightarrow D\bar{D}) \approx 100\%$ is too strong a statement. Most of the analysis have been redone assuming $\sim 22\%$ charmless ψ'' decays. The bulk of the experimental values we use to compare our model with are derived using this percentage.

Although the experimental errors in the measurement of the lepton momentum spectrum in D decays are still rather large, we have performed a comparison with our semileptonic D decay model. The Monte Carlo results for $D \rightarrow e\nu_e X$ are presented together with the inclusive $\psi'' \rightarrow DX \rightarrow e\nu_e X'$ measurement from DELCO [18] at SPEAR in figures 1 (D^0) and 2 (D^+). It turns out that these distributions are rather sensitive on the choice of the admixture of strangeless D decays on one hand and the ratio between vector and pseudoscalar particles on the other. The Monte Carlo distributions were obtained assuming the branching ratios listed in table 1. The result is satisfactory whereas our assumptions are also in agreement with most model calculations. The individual contributions to the decay $\psi'' \rightarrow DX \rightarrow \mu(e)\nu_{\mu(e)}X'$ are displayed in fig. 3 (D^0) and fig. 4 (D^+).

The list of all decay modes for all charmed particles (including spin 1/2 and spin 3/2 baryons) as included in our program is too lengthy to be presented here. The charm decays are modelled with at most three particles (allowing for all sorts of resonances) in the final state. Subsequent decays increase both charged and neutral particle multiplicities. Decay rates have been modelled using experimental data, the matrix elements from the Cabibbo sector in the KM-matrix (including Cabibbo suppression), phase space suppression factors and particle symmetries in the comparison with experimentally measured decay modes. Roughly 22% (D^+) and 39% (D^0) of the decays are two-body modes. Non trivial decay channels originating from final state interactions, annihilation processes etc. have been included ad hoc.

In tables 2 and 3 we present a comparison for exclusive and inclusive D^0 and D^+ hadronic branching ratios respectively as obtained by EURODEC and an average over a set of experimentally obtained decay rates. Since some experiments do not provide details about systematic errors in their numbers for these specific decay ratios, we have been extremely conservative in deriving averages. We have used an unweighted average over the best measurements (mainly in terms of statistical errors). Finally we have used reported systematical errors to derive a rough combined error by adding systematical and statistical errors in quadrature. It turns out that the majority of experimental results lie within 1σ from our calculated mean value, probably indicating that we have been too conservative in our error estimates. For a more precise and more detailed discussion of errors and averages see Refs. 19, 20. Both tables 2 and 3 show a good agreement between Monte Carlo and experimental data.

In conclusion, the charged particle multiplicity distributions in D^0 and D^+ decays are presented in figures 5 and 6. Excellent overall agreement with experimental data [21, 22, 23] and [24] is obtained. There is a surprisingly good agreement among the inclusive measurements of MARK II [21], LGW [22] and LEBC [24] (topological) and the exclusive measurement ($\sim 90\% D^0$ and $\sim 80\% D^+$ reconstructed [19]) by MARK III [23]. Predictions for total multiplicities in D^0 and D^+ decays which are only of academic interest due to experimental complications, are shown for completeness in fig. 7 and fig. 8. As at present there seems to be no urgent need for the modelling of exclusive $n > 3$ body decays. The user of the program may easily modify the decay table to include 4- and/or 5-body decays if desired.

Bottom decay properties

Within the framework of the Standard Model, the fundamental quantities to be obtained from b -decays are the Kobayashi-Maskawa matrix elements V_{ub} and V_{cb} . The values for the bottom meson lifetimes, semileptonic branching fractions and the ratio $\Gamma(b \rightarrow u)/\Gamma(b \rightarrow c)$

are key ingredients indispensable for pinning down the V_{xb} sector.

Many e^+e^- -collider experiments have determined branching ratios for $B \rightarrow e\nu X$ and $B \rightarrow \mu\nu X$. Within experimental errors, measurements at both $\Upsilon(4S)$ and continuum agree indicating that either all B mesons have comparable semileptonic branching ratios or that the mix of flavours at the $\Upsilon(4S)$ and continuum are not too different. In the continuum and at the $\Upsilon(4S)$, leptons from b -decays can rather easily be separated from leptons from charm decays. This is due to the larger phase space available in the decay $B \rightarrow l\nu X$. In turn, the analysis of the inclusive lepton energy spectrum from b -decays shows that the upper end of the spectrum is fully populated by leptons from direct semileptonic b -decays. The end-point of the spectrum is therefore an obvious place to search for $B \rightarrow l\nu X_u$ contributions, since $m_{X_u} \ll m_{X_c}$.

We will concentrate on inclusive lepton energy distributions as measured by several experiments at the $\Upsilon(4S)$ and test our ansatz for decay matrix elements and branching fractions we have introduced in EURODEC. Particle masses and lifetimes are taken from Ref. 20. The $\Upsilon(4S)$ resonance is ideal to study b -decays since the resonance is just ($\sim 20 \text{ MeV}/c^2$) above $B\bar{B}$ threshold and decays entirely into B mesons whereas there is no room for additional fragmentation of the primordial b quarks. Along the lines sketched in the previous section, we set up the phase space bounded by the physical particle masses involved in the decay channel. The semileptonic channels are selected with the probabilities given in table 4. We have simulated the full process $\Upsilon(4S) \rightarrow B\bar{B} \rightarrow lX$ (see also table 5) accounting for the Lorentz boost of the B mesons. In the decays $B \rightarrow lDX$ the D kinematics are constructed using the formula of eq. (5) (unpolarised B -meson assumed, pseudoscalars!), whereas the prompt lepton spectrum in the D^* channel $B \rightarrow lD^*X$ is described by eq. (6). Both kinematics and decay matrix elements are calculated using physical particle masses instead of the constituent fermion masses. Secondary leptons (from charm decays) are generated as described in the previous section. This modified parton picture results in a description for charmless B -decays which is very close to the spectator quark model of Altarelli et al. [25]. However, the two free parameters in their model, the Fermi momentum factor and the c/u quark mass, are absent in our approach! Although again small, the effect of the W propagator is folded in.

Figures 9 - 13 display inclusive lepton momentum spectra as measured with the Crystal Ball [26], ARGUS [27] and CLEO [28] detectors together with the prediction from our model. In the plots individual contributions from leptons from b -, c - and τ decays are shown together with the inclusive spectrum. From all experimental distributions the continuum contribution was subtracted and the data were corrected for detector efficiency. The end-point spectrum is described correctly, which is not very surprising since we found

that our model gives results not very different from the spectator quark model of Ref. 25. We do not expect large deviations from valence quark models (non-relativistic [29] or relativistic bound state wave functions [30, 31]) provided all (most) of the possible resonances are explicitly taken into account in the Monte Carlo simulation. For a detailed discussion of the end-point spectrum and the retrieval of limits on $|V_{ub}|$, see Ref. 26. Clearly, the predictive power of our model with respect to semileptonic branching ratios is limited and they should preferably be taken either from experiment or the calculations of for instance [29] or [30].

Before we arrive at the discussion of exclusive hadronic decay modes, we have made some comparisons with charged particle multiplicity measurements. Figure 14 shows the charged particle multiplicity of $B\bar{B}$ events in the CLEO experiment [32]. The experimental distribution is not corrected for detector efficiency and γ -conversions in the beam pipe etc., therefore the Monte Carlo prediction comes out slightly shifted towards higher values. Since these measurements performed at the $\Upsilon(4S)$, the multiplicity distributions are not obscured by b quark fragmentation effects. The only distortion may be caused by uncertainties in subtracting continuum events. However, we expect that this uncertainty is rather small and becomes even smaller after requiring at least one prompt lepton. Figures 15 and 16 show the data for these multiplicities from the CLEO detector together with the predictions from our model.

CLEO has developed a method to correct for detector inefficiencies and they are able to derive a value for the average number of charged particles in hadronic B -decays $\langle N_{had} \rangle = 5.75 \pm 0.10 \pm 0.10$ [33]. The mean number in semileptonic B -decays is determined as well: $\langle N_{lep} \rangle = 3.84 \pm 0.10 \pm 0.10$ [33]. In nearly 100% of the b -decays a D or D^* will be produced (see table 5). If one subtracts the mean charged multiplicity of such a particle, assuming a reasonable mixture of D and D^* , the number of charged particles in addition to the lepton and D or D^* in semileptonic B -decays becomes very small (0.24 ± 0.15 [34]). This result and the experimentally reconstructed recoil mass of $\sim 2 \text{ GeV}/c^2$ support the ansatz that spectator fragmentation in $B \rightarrow l\nu D$ is suppressed. The average values for the multiplicities compare well with the EURODEC numbers: $\langle N_{had} \rangle = 5.85$ and $\langle N_{lep} \rangle = 3.75$, whereas the shape of the distributions are also in good agreement.

About 62% of the B -decay modes are modelled as two-body and three-body decays (including resonances) in EURODEC. The other $\sim 38\%$ is modelled according to the decay $B \rightarrow D, D^* u\text{-quark } d\text{-quark}$ allowing both quarks to fragment, forcing the total multiplicity to be larger than 3 particles in the final state (again including possible resonances!). The branching ratios are chosen with care using phase space constraints and particle decay symmetries. In tables 5, 6 and 7 we present a comparison of our model

with experimentally measured exclusive and inclusive decay rates. We conclude that EURODEC B -decay multiplicities, inclusive and exclusive decay rates are well in agreement with experimental data. Of academic interest is the total particle multiplicity distribution as depicted in figure 17.

Although EURODEC describes the electron and muon inclusive momentum spectra well at $p_e, p_\mu \geq 1.5$ GeV/ c , a direct comparison at low momentum is more difficult due to lacking experimental data. However, we can get an indirect measure for the inclusive lepton spectrum in this region. Since the low end of the spectrum is dominated by charm particle decays as shown before, the convolution of the D^0 and D^+ momentum spectrum with their semileptonic decay distributions (as described in section 4) may provide us a good indication. The inclusive D^0, D^+ and D^{*+} momentum distributions at the $\Upsilon(4S)$ have been analysed by CLEO [35] and have undergone a considerable evolution with increase of statistics (D^0 [36], $D^{*\pm}$ [37]). The experimental data points from Ref. 35 are shown in figures 18 (D^0, \bar{D}^0) and 19 (D^{*+}, D^{*-}) together with the Monte Carlo predictions. The dashed line in both figures indicates the contribution due to semileptonic b -decays. Table 5 contains the predicted inclusive D^0 and D^+ rates in comparison with the experimental values. We interpret the good agreement with the data as additional evidence for correctly modelling the inclusive lepton spectrum.

The decay channel $D_s^\pm \rightarrow \phi\pi^\pm (\phi \rightarrow K^+K^-)$ has been explored by CLEO [38] and ARGUS [39] to study D_s^\pm production in B -meson decays. Although there is a phase space suppression factor, the dominance of the b -to- c coupling ensures a substantial probability ($\sim 15\%$) for the decay $b \rightarrow cW^- \rightarrow c\bar{c}s$. So one may expect final states of the form $B \rightarrow D_s DX$. The contributions from the W exchange diagram (B^0) and $s\bar{s}$ popping between the charm quark and b -spectator antiquark are predicted to be less important and may be disentangled from the D_s momentum spectrum. The decay $B^0 \rightarrow D_s^+ K^-$ will lead to a very hard D_s momentum spectrum, whereas $s\bar{s}$ popping will mainly contribute to the low end of the D_s momentum spectrum.

In figure 20 the CLEO and ARGUS data points are shown. CLEO does not observe any significant signal in the momentum region from 2.0 to 2.5 GeV/ c supporting the theoretical calculations that the contribution from the W -exchange diagram is small. Both experiments confirm the prediction for a large fraction of two-body decays ($\approx 50\%$) [40]. The histogram is the result of our model calculations. We assume that the decays $B \rightarrow DD_s, D^*D_s, DD_s^*$ and $D^*D_s^*$ saturate the two-body decay modes. The rest of the spectrum is described via decays of the type $B \rightarrow D_s X$ (X -multiplicity ≥ 2), $D_s DX'$, where D_s and D may either be a pseudoscalar or a vector. Although phase space suppressed, the decay $B \rightarrow D_s D_s X$ is assumed to contribute as well. The comparison between the EURODEC and experimental inclusive D_s rate can be found in table 5.

The uncertainty in the experimental decay ratio is mainly determined by the uncertainty on the $D_s^\pm \rightarrow \phi\pi^\pm$ -branching fraction ($\sim 3.5 - 5\%$).

In 1979 Fritzsche [41] suggested that the decay $B \rightarrow J/\psi X$ could be one of the most favourable modes for reconstructing B -mesons. First (weak) experimental evidence for this decay channel was reported by CLEO [42]. Since then statistics have steadily increased and both CLEO [43], [44] and ARGUS [45] have confirmed the observation on a more solid basis. The J/ψ momentum distribution (fig. 21) suggests a large two-body decay contribution on one hand and hard gluon emission or J/ψ production through the decay of ψ' and/or χ_c^1 on the other. It is only recently that the ARGUS collaboration [46] has succeeded in explicitly reconstructing the ψ' through its semileptonic decay ($\psi' \rightarrow l^+l^- \approx 0.9\%$) and via the decay channel $\psi' \rightarrow J/\psi\pi^+\pi^-$ ($\psi' \rightarrow J/\psi X \approx 55\%$).

In figure 21 we have plotted the CLEO [44] and ARGUS [46] data together with our prediction for the inclusive J/ψ momentum spectrum. The bin size chosen in the analysis of experimental data (statistics !) is crucial for disentangling direct and indirect J/ψ production. In fig. 22 we have indicated the EURODEC prediction for *indirect* J/ψ production (dotted line). The spectrum receives contributions from $\psi' \rightarrow J/\psi X$ and $\psi' \rightarrow \chi_c^0, \chi_c^1, \chi_c^2 X \rightarrow J/\psi X'$. We have not explicitly taken into account $B \rightarrow \chi_c^1 X \rightarrow J/\psi X'$ although this contribution may still be relatively sizeable as suggested by Kühn et al. [47]. The $B \rightarrow \psi X$ decay ratios as derived by the CLEO and ARGUS experiments are in excellent agreement and are averaged over in the comparison with EURODEC rates (see table 5).

The last topic of this section concerns the observation of baryons in B -meson decays. Simple phase space arguments indicate a 5 - 10% branching fraction for B -meson \rightarrow (charmed) baryon X [48]. However, the calculation of exclusive branching ratios remains a theoretically unresolved enterprise. The first *direct* observation of Λ_c^\pm in B -meson decays was reported by ARGUS [49] via the reconstruction of the decay chain: $B \rightarrow \Lambda_c^+ X \rightarrow pK^-\pi^+$ (and charge conjugate channel). Earlier studies by both ARGUS [50] and CLEO [51] gave *indirect* evidence for charmed baryon production via baryon-correlations through the observation of protons and Λ 's [52]. Both experiments observe a relatively high multiplicity in these decays. Our interpretation is that other charmed baryons than Λ_c^\pm must play a role. Decay chains like for instance $B^- \rightarrow \Sigma_c^0 X \rightarrow \Lambda_c^+ X'$ and $\bar{B}^0 \rightarrow \Sigma_c^0 X \rightarrow \Lambda_c^+ X'$ in general enhance the average multiplicity. Other charmed baryons like Ξ_c^0 may be produced as well but do not lead to a Λ_c^\pm intermediate state while the Λ signal is enhanced significantly.

In EURODEC we have introduced a variety of B -decays into (charmed) baryons. For the total baryonic charm decay rate we have assumed $\sim 9\%$. In table 5 the resulting inclusive Λ_c^+ branching ratio is compared with the measurements from CLEO and ARGUS

at the $\Upsilon(4S)$. The Λ_c^\pm momentum distribution is shown in figure 23. The data points are taken from [49] and seem to indicate a preference for a relatively soft Λ_c^\pm momentum spectrum. However, the experimental errors are still too large to draw conclusions whether our model is fully compatible with the data. For instance the soft part of the momentum distribution seems to indicate that we may have underestimated the particle multiplicity in a subset of the baryonic decay modes. More illuminating are Lambda and proton momentum spectra (figs. 24 and 25). Both ARGUS [27] and CLEO [51] measurements are in good agreement and are well explained by our model.

Finally we would like to remark that EURODEC includes the possibility to simulate $D^0 - \bar{D}^0$, $B^0 - \bar{B}^0$ and $B_s^0 - \bar{B}_s^0$ mixing with probabilities defined by the user.

The sixth quark and beyond

As pointed out in section 2, the effect of the W propagator plays an important role in the weak process $Q \rightarrow q\bar{f}f$ when the mass of the heavy quark Q approaches or exceeds physical mass of the W and $m_Q \gg m_q$. This becomes more clear when we analyse the Breit-Wigner expression for the W propagator:

$$\text{B.W.} \sim \frac{1}{[M_W^2 - (p_f + p_{\bar{f}})^2]^2 + m_W^2 \Gamma_W^2} \quad (7)$$

with M_W, Γ_W the physical mass and width of the W^\pm and $(p_f + p_{\bar{f}})^2$ the virtual W mass. The upper and lower limits on the virtual mass are fixed by the masses of the particles involved in the decay. The function in eq. (7) will strongly peak if the virtual mass gets close to or exceeds the physical W mass. Ergo for a heavy top quark or heavy fourth generation particles, the Breit-Wigner will dominate the decay distributions. The Monte Carlo implementation can be pursued in two ways. Since the kinematical boundaries are fixed for each decay, the maximum value for function (7) can be calculated. The actual value is determined by the three-body kinematics as set-up by the phase space generator (see section 2). A simple accept/reject algorithm ensures the correct weight distribution for the surviving events. A more elaborate procedure may be followed by slightly modifying the phase space generator. Due to the sequential treatment of the three-body phase space (see section 2), the generation of the invariant mass of the $f\bar{f}$ system can be forced to follow the distribution of eq. (7). Consequently, no rejection algorithm has to be applied, which improves the efficiency of the method considerably. In the next section we sketch the analytical procedure in the discussion of particle mass smearing.

Obviously, the hadronic decays of very heavy flavours will be dominated by a large jet multiplicity. Both f and \bar{f} will give rise to one or more jets of particles. Additional fragmentation of the resulting quark ' q ' may indeed also occur. In our model each of the

$f - \bar{f}$ and q -spectra for quark/diquark systems are treated as colour-neutral objects.

Kinematical correlations in the decays of non-heavy flavoured hadrons

To complete the description of the decay models in EURODEC we briefly discuss the set of additional matrix elements used in the treatment of non-heavy flavour particles. The kinematics of the decay products in the decay $\omega, \phi \rightarrow \pi^+ \pi^- \pi^0$ is well described [53] by convoluting the phase space with:

$$|M|^2 = C * |\mathbf{p}_{\pi^+} \times \mathbf{p}_{\pi^-}|^2 \quad (8)$$

Similarly, the complete kinematics of the Dalitz decays of the π^0 and $\eta(\pi^0, \eta \rightarrow \gamma e^+ e^-)$ is correctly described by applying the Kroll-Wada procedure [54] in which one generates a properly distributed virtual mass for the $e^+ e^-$ -pair.

Pseudoscalar particles PS_2 and PS_3 produced in the decay chain $PS_0 \rightarrow PS_1$ Vector $\rightarrow PS_1 PS_2 PS_3$ will have the following decay angular distribution in the rest frame of vector 'V':

$$|M|^2 \sim \cos^2 \theta_{02} \quad (9)$$

where θ_{02} is the opening angle between the PS_2 and PS_0 momentum vectors [55]. A discussion on τ -lepton decay matrix elements can be found in Ref. 56.

By default, the physical particle masses are taken from the particle table as read by the EURODEC program at initialisation time. However, the user may introduce a physical width (optional) which is at present set to twice the full width half maximum ($\sim \pm \Gamma$) of a Breit-Wigner distribution, thus assuming the narrow width approximation is a sufficiently good approximation for the mass distribution. Γ is calculated from the particle lifetimes which are tabulated in the particle table as well. The smeared mass is then generated according to:

$$\begin{aligned} m_{smear} &= \sqrt{m_{phys} * \{m_{phys} + \Gamma * \tan[(up - low) * x + low]\}} \\ up &= \text{atan} \left[\frac{(m_{phys} + \Gamma)^2 - m_{phys}^2}{m_{phys} \Gamma} \right] \\ low &= \text{atan} \left[\frac{(m_{phys} - \Gamma)^2 - m_{phys}^2}{m_{phys} \Gamma} \right] \end{aligned} \quad (10)$$

with x uniformly random at $0 < x < 1$. The expression for m_{smear} is a straight forward inversion of the analytical integration of the Breit-Wigner formula [6].

Conclusions

We have given an extensive description of the EURODEC treatment of heavy flavour (charm and bottom) decays and have performed a detailed comparison between the predictions by our model and available experimental data. We have discussed the generalization to four families as well. Some special features like mass smearing and kinematical correlations in the decay of non-heavy flavour particles are reviewed. Exclusive and inclusive decay properties are adequately described and we find in many cases excellent agreement between our model and experimentally measured quantities. We therefore conclude that EURODEC could serve as an important tool in the analysis of both LEP and collider data.

REFERENCES

- [1] M. Kobayashi and K. Maskawa, *Progr. Theor. Phys.* **49** (1973) 652.
- [2] 'Top Quark Search', presentations at CERN by the CDF, UA2 and UA1 Collaborations, April 18 (1989). Conclusion: Assuming the Standard Model (no charged Higgses!) most likely $m_t > 60 \text{ GeV}/c^2$.
- [3] H. Albrecht et al. (ARGUS), *Phys. Lett.* **192 B** (1987) 245.
- [4] C. Albajar et al. (UA1), *Phys. Lett.* **186 B** (1987) 247.
- [5] A. Ali, B. van Eijk and I. ten Have, *Phys. Lett.* **198 B** (1987) 354.
- [6] B. van Eijk, Ph.D. Thesis, University of Amsterdam, unpublished (1987).
- [7] A. Ali in Physics at LEP, CERN Report 86-02 (1986).
- [8] K. Kleinknecht and B. Renk, *Z. Phys. C* **16** (1982) 7,
K. Kleinknecht and B. Renk, *Z. Phys. C* **20** (1983) 67,
K. Kleinknecht, Dortmund Report UNIDO 84/2S1 (1984).
- [9] E.A. Paschos and U. Türke, *Phys. Lett.* **176 B** (1986) 185,
G. Altarelli and P.J. Franzini, *Z. Phys. C* **37** (1988) 271.
- [10] B. van Eijk, 'EURODEC User Manual, Version 2.3', DELPHI Report DELPHI 89-39 PHYS 41 PROG 136 and DD Long Program Write-up (1989); and Ref. Manual, in prep.
- [11] B. van Eijk and R. Kinnunen, *Z. Phys. C* **41** (1988) 489,
E. Barberio and B. van Eijk, DELPHI Report, in preparation (1989).
- [12] See e. g.: J. Ellis, M.K. Gaillard, D.V. Nanopoulos and S. Rudaz, *Nucl. Phys. B* **131** (1977) 285.
- [13] See e. g.: S. Jadach and J.H. Kühn, Max Planck Report München MPI-PAE/PTh 64/86 (1986).
- [14] A. Ali, *Z. Phys. C* **25** (1979) 41.
- [15] A. Ali, B. van Eijk and E. Pietarinen, 'EUROJET, a Monte Carlo Generator for hard Partonic Interactions' (unpublished); A. Ali, B. van Eijk and I. ten Have, *Nucl. Phys. B* **292** (1987) 1.
- [16] J.M. Feller, Ph.D. Thesis University of California, Berkeley (1979 unpublished).
- [17] W. Bacino et al. (DELCO Collaboration), *Phys. Rev. Lett.* **45** (1980) 329.
- [18] W. Bacino et al. (DELCO Collaboration), *Phys. Rev. Lett.* **43** (1979) 1073.
- [19] D.G. Hitlin, 'Weak Decays of Charmed Particles'. Talk given at the Erice Workshop on Heavy Flavours, to appear in the Conference Proceedings, D.G. Hitlin, CALTEC Report, CALT-68-1472.
- [20] Particle Data Group, *Phys. Lett.* **204 B** (1988) 1.
- [21] R.H. Schindler et al. (MARK II Collaboration), *Phys. Rev. D* **24** (1981) 78.
- [22] V. Vuillemin et al. (Lead Glass Wall Collaboration), *Phys. Rev. Lett.* **41** (1978) 1149.
- [23] J. Adler et al. (MARK III Collaboration), *Phys. Rev. Lett.* **60** (1988) 89,
R.M. Baltrusaitis et al. (MARK III Collaboration), *Phys. Rev. Lett.* **56** (1986) 2140.

- [24] M. Aguilar-Benitez et al. (LEBC Collaboration), *Z. Phys. C* **41** (1988) 191.
- [25] G. Altarelli, N. Cabibbo, G. Corbo, L. Maiani and G. Martinelli, *Nucl. Phys. B* **208** (1982) 365.
- [26] K. Wachs, DESY Report DESY 87-084 (1987),
K. Wachs et al. (Crystal Ball Collaboration), DESY Report DESY 88-111 (1988).
- [27] H. Schröder, 'Results from ARGUS', Talk given at the 1988 Erice Workshop on Heavy Flavours, to appear in the Conference Proceedings.
- [28] S. Behrends et al., *Phys. Rev. Lett.* **59** (1987) 407.
- [29] B. Grinstein, M.B. Wise and N. Isgur, *Phys. Rev. Lett.* **56** (1986) 298.
- [30] M. Wirbel, B. Stech and M. Bauer, *Z. Phys. C* **29** (1985) 637.
- [31] J.G. Körner and G.A. Schuler, *Z. Phys. C* **38** (1988) 511; *Z. Phys. C* **41** (1989) 690.
- [32] M.S. Alam et al. (CLEO Collaboration), *Phys. Rev. Lett.* **49** (1982) 357.
- [33] D.S. Riley et al. (CLEO Collaboration), *Bull. Am. Phys. Soc.* **31** (1986) 790.
- [34] E.H. Thorndike and R.A. Poling, *Physics Reports* **157** (1988) 183.
- [35] D. Bortoletto et al. (CLEO Collaboration), *Phys. Rev. D* **35** (1987) 19.
- [36] M.S. Alam et al. (CLEO Collaboration), *Phys. Rev. D* **30** (1984) 2279.
- [37] M.S. Alam et al. (CLEO Collaboration), *Phys. Rev. Lett.* **54** (1985) 1894.
- [38] M.S. Alam et al. (CLEO Collaboration), *Phys. Rev. Lett.* **56** (1986) 2781.
- [39] H. Albrecht et al. (ARGUS Collaboration), DESY Report, DESY 87-001 (1987).
- [40] A. Ali, J.G. Körner and G. Kramer, *Z. Phys. C* **1** (1979) 269,
F. Hussain and M. Scadron, *Phys. Rev. D* **30** (1984) 1492.
- [41] H. Fritzsch, *Phys. Lett.* **86 B** (1979) 164; *Phys. Lett.* **86 B** (1979) 343.
- [42] R. Giles et al. (CLEO Collaboration), *Phys. Rev. D* **30** (1984) 2279.
- [43] P. Haas et al. (CLEO Collaboration), *Phys. Rev. Lett.* **55** (1985) 1248.
- [44] M.S. Alam et al. (CLEO Collaboration), *Phys. Rev. D* **34** (1986) 3279.
- [45] H. Albrecht et al. (ARGUS Collaboration), *Phys. Lett.* **162 B** (1985) 395.
- [46] H. Albrecht et al. (ARGUS Collaboration), DESY Report DESY 87-111.
- [47] J.H. Kühn, S. Nussinov and R. Rückl, *Z. Phys. C* **5** (1980) 117.
- [48] I.I. Bigi, *Phys. Lett.* **106 B** (1981) 510.
- [49] H. Albrecht et al. (ARGUS Collaboration), DESY Report DESY 88-012 (1988).
- [50] R. Ammar, Proc. of the Int. Europhysics Conf., Uppsala (1987) 360.
- [51] M.S. Alam et al. (CLEO Collaboration), *Phys. Rev. Lett.* **59** (1987) 22.
- [52] M.S. Alam et al. (CLEO Collaboration), *Phys. Rev. Lett.* **51** (1983) 1143.
- [53] R.H. Dalitz, 'Strange Particles and Strong Interactions' London, Oxford University Press (1962).
- [54] N. Kroll and I. Wada, *Phys. Rev.* **98** (1955) 1355.
- [55] K. Gottfried and J.D. Jackson, *Nuovo Cim.* **33** (1964) 309,
G.F. Wolters, Proc. Koninklijke Academie van Wetenschappen, B67 (1964) 192.
- [56] B. van Eijk and J. Fuster, DELPHI Report DELPHI 89-45 PHYS 42 (1989).

Table 1: Semileptonic (electron) charm decay branching ratios as included in the EURODEC decay table.

exclusive decay mode				EURODEC branching ratio (%)
D^0	\rightarrow	K^-	$e^+ \nu_e$	4.94
		K^-	$e^+ \nu_e$	1.97
		π^-	$e^+ \nu_e$	0.42
		ρ^-	$e^+ \nu_e$	0.17
D^+	\rightarrow	\bar{K}^0	$e^+ \nu_e$	11.85
		\bar{K}^0	$e^+ \nu_e$	4.75
		π^0	$e^+ \nu_e$	1.00
		ρ^0	$e^+ \nu_e$	0.40

Table 2: Comparison between D^0 exclusive decay modes and inclusive rates as proposed in the EURODEC particle decay table and experimental data.

exclusive decay mode				EURODEC branching ratio (%) ¹⁾	Experiment (%) ²⁾
D^0	\rightarrow	K^-	π^+	4.30	4.2 ± 0.7
		K^-	ρ^+	10.79	10.8 ± 1.7
		\bar{K}^0	π^0	2.18	2.5 ± 0.9
		\bar{K}^0	ϕ	0.99	0.92 ± 0.36
		\bar{K}^0	ω	3.78	3.2 ± 1.5
		\bar{K}^0	η	1.79	1.5 ± 0.7
		\bar{K}^0	ρ^0	1.31	0.75 ± 0.5
		K^-	π^+	5.20	5.2 ± 1.5
		\bar{K}^0	π^0	2.41	2.6 ± 0.8
		π^-	π^+	0.20	0.26 ± 0.1
		K^-	K^+	0.61	0.54 ± 0.13
		\bar{K}^0	K^0	0.00	0.3 ± 0.3
		\bar{K}^0	K^0	0.00	<0.55 @ 90% CL
		K^-	K^+	0.99	0.8 ± 0.5
		K^-	$\pi^+ \pi^0$	2.11	1.2 ± 0.63
		\bar{K}^0	$K^+ K^-$	1.00	2.1 ± 0.8
		π^-	$\pi^+ \pi^0$	1.00	1.1 ± 0.4
inclusive decay mode				EURODEC branching ratio (%)	Experiment (%)
D^0	\rightarrow	K^-	$\pi^+ \pi^0$	15.31	14.9 ± 5.2
		\bar{K}^0	$\pi^+ \pi^-$	7.88	6.7 ± 2.1
		K^-	$\pi^+ \pi^- \pi^+$	8.99	8.5 ± 2.2
		\bar{K}^0	$\pi^+ \pi^- \pi^0$	14.00	11.5 ± 3.6
		K^-	$\pi^+ \pi^0 \pi^0$	12.98	14.9 ± 4.8
		π^-	$\pi^+ \pi^- \pi^+$	2.01	1.5 ± 0.6

Table 3: Comparison between D^* exclusive decay modes and inclusive rates as proposed in the EURODEC particle decay table and experimental data.

exclusive decay mode				EURODEC branching ratio (%) ³⁾	Experiment (%) ²⁾			
D^+	\rightarrow	\bar{K}^0	π^+	3.27	3.3 ± 0.9			
		\bar{K}^0	p^+	8.19	6.9 ± 2.4			
		\bar{K}^0	π^+	5.90	5.9 ± 3.1			
		\bar{K}^0	K^+	1.09	0.9 ± 0.4			
		π^+	π^0	0.00	$<0.48 @ 90\% CL$			
		ϕ	π^+	0.99	0.85 ± 0.2			
		\bar{K}^0	K^+	0.51	0.56 ± 0.2			
		ρ^0	π^+	0.20	0.2 ± 0.09			
		K^-	π^+	π^+	7.18	7.2 ± 1.9		
		\bar{K}^0	π^+	π^0	1.31	1.3 ± 1.1		
		π^+	π^+	π^-	0.40	0.37 ± 0.14		
		K^-	K^+	π^+	0.50	0.50 ± 0.15		
inclusive decay mode				EURODEC branching ratio (%)	Experiment (%)			
D^+	\rightarrow	K^-	π^+	π^+	11.13	8.9 ± 1.5		
		\bar{K}^0	π^+	π^0	11.46	14.4 ± 5.0		
		K^-	K^+	π^+	1.33	0.8 ± 1.7		
		K^-	π^+	π^+	π^0	4.95	4.2 ± 1.7	
		\bar{K}^0	π^+	π^+	π^+	7.50	8.7 ± 2.8	
		ϕ	π^+	π^+	π^+	0.00	$<0.09 @ 90\% CL$	
		K^-	π^+	π^+	π^+	π^-	0.96	<i>seen</i>
		K^-	π^+	π^+	π^0	π^0	2.18	2.2 ± 4.7
		\bar{K}^0	π^+	π^+	π^+	π^0	4.90	4.4 ± 0.7

Table 4: Semileptonic (electron) bottom decay branching ratios as included in the EURODEC decay table.

exclusive decay mode			EURODEC branching ratio (%)
\bar{B}^0	\rightarrow	$D^+ e^- \bar{\nu}_e$	2.3
		$D^{*+} e^- \bar{\nu}_e$	9.3
B^-	\rightarrow	$D^0 e^- \bar{\nu}_e$	2.3
		$D^{*0} e^- \bar{\nu}_e$	9.3

Table 5: Comparison between $\Upsilon(4S)$ exclusive decay modes and inclusive rates as proposed in the EURODEC particle decay table and experimental data.

exclusive decay mode			EURODEC branching ratio (%) ⁴⁾	Experiment (%) ²⁾	
$\Upsilon(4S)$	\rightarrow	$B^0 \quad \bar{B}^0$	44.98	-	
		$B^- \quad B^+$	55.02	-	
inclusive decay mode			EURODEC branching ratio (%)	Experiment (%)	
B	\rightarrow	$D^0 \quad X$	63.35	63.	$\pm 13.$
		$D^+ \quad X$	28.78	28.	$\pm 10.$
		$D_s^+ \quad X$	9.97	11.	$\pm 4.$
		$\Lambda_c^+ \quad X$	7.39	7.	$\pm 3.$
		$J/\psi \quad X$	1.11	1.07	± 0.003
		$\psi' \quad X$	0.0047	0.005	± 0.003
Total			~ 110	~ 110	

Table 6: Comparison between B^- exclusive decay modes and inclusive rates as proposed in the EURODEC particle decay table and experimental data.

exclusive decay mode				EURODEC branching ratio (%) ⁵⁾	Experiment (%) ²⁾
B ⁻	→	D ⁰	π ⁻	0.28	0.29 ± 0.18
		D ⁰	ρ ⁻	2.23	2.9 ± 1.8
		J/ψ	K ⁻	0.07	0.07 ± 0.04
		ψ'	K ⁻	0.11	0.22 ± 0.17
		D ^{*+}	π ⁻ π ⁻	0.59	0.6 ± 0.4
		D ⁺	π ⁻ π ⁻	0.39	0.42 ± 0.3
inclusive decay mode				EURODEC branching ratio (%)	Experiment (%)
B ⁻	→	D ^{*+}	π ⁻ π ⁻ π ⁰	0.1	5.6 ± 3.8
		J/ψ	K ⁻ π ⁺ π ⁻	0.14	0.11 ± 0.7
		D ⁰	X	87.20	-
		D ⁺	X	4.96	-
		D _s ⁺	X	9.94	-
		Λ _c ⁺	X	7.38	-
		J/ψ	X	1.10	-
		ψ'	X	0.46	-

Table 7: Comparison between \bar{B}^0 exclusive decay modes and inclusive rates as proposed in the EURODEC particle decay table and experimental data.

		exclusive decay mode	EURODEC branching ratio (%) ⁶⁾	Experiment (%) ²⁾
\bar{B}^0	\rightarrow	$D^{*+} \pi^-$	0.41	0.35 ± 0.2
		$D^{*+} \rho^-$	3.39	2.0 ± 1.4
		$D^+ \pi^-$	0.28	0.41 ± 0.2
		$D^+ \rho^-$	2.23	2.8 ± 1.6
		$J/\psi K^{*0}$	0.33	0.33 ± 0.18
		$D^{*+} \pi^- \pi^0$	0.00	2.0 ± 1.4
		inclusive decay mode	EURODEC branching ratio (%)	Experiment (%)
\bar{B}^0	\rightarrow	$D^{*+} \pi^- \pi^+ \pi^-$	9.35	4.3 ± 2.3
		$D^0 X$	34.18	-
		$D^+ X$	57.92	-
		$D_s^+ X$	10.00	-
		$\Lambda_c^+ X$	7.41	-
		$J/\psi X$	1.11	-
		$\psi' X$	0.47	-

- 1) As obtained from Monte Carlo run with $4 \cdot 10^8$ D^0 events
- 2) See text for explanation
- 3) As obtained from Monte Carlo run with $4 \cdot 10^8$ D^+ events
- 4) As obtained from Monte Carlo run with $2 \cdot 10^8$ $\Upsilon(4S)$ events
- 5) As obtained from Monte Carlo run with $2.2 \cdot 10^8$ B^+ events
- 6) As obtained from Monte Carlo run with $1.8 \cdot 10^8$ \bar{B}^0 events

Fig. 1: Electron momentum spectrum from D (D^0 and D^+ and charge conjugates) decays at the $\psi''(3770)$ as measured by the DELCO Collaboration at SPEAR [19] compared with the EURODEC $\psi'' \rightarrow D^0 X \rightarrow e \nu_e X'$ prediction.

Fig. 2: Electron momentum spectrum from D (D^0 and D^+ and charge conjugates) decays at the $\psi''(3770)$ as measured by the DELCO Collaboration at SPEAR [19] compared with the EURODEC $\psi'' \rightarrow D^+ X \rightarrow e \nu_e X'$ prediction.

Fig. 3: Inclusive muon momentum spectrum from D^0 (\bar{D}^0) decays at the $\psi''(3770)$ as predicted by EURODEC. The contributions from the different charm decay channels are drawn separately. No experimental data could be found in the literature.

Fig. 4: Inclusive muon momentum spectrum from D^+ (D^-) decays at the $\psi''(3770)$ as predicted by EURODEC. As in figure 3 the contributions from the different charm decay channels are drawn separately.

Fig. 5: Charged particle multiplicity in events from D^0 (\bar{D}^0) decays at the $\psi''(3770)$ as measured by the MARK II- [22], LGW- [23], MARK III- [24] and LEB- [25] Collaborations compared with the EURODEC prediction.

Fig. 6: Charged particle multiplicity in events from D^+ (or charge conjugate) decays at the $\psi''(3770)$ as determined by the MARK II- [22], LGW- [23], MARK III- [24] and LEB- [25] Collaborations compared with the EURODEC prediction.

Fig. 7: Total particle multiplicity in events from D^0 (\bar{D}^0) decays at the $\psi''(3770)$ as predicted by EURODEC. No experimental data is available (yet).

Fig. 8: Sum of charged and neutral particle multiplicity in events from D^+ (D^-) decays at the $\psi''(3770)$ as predicted by EURODEC. Experimental data is still lacking.

Fig. 9: Inclusive momentum spectrum of electrons from semileptonic B -meson decays at the $\Upsilon(4S)$ as measured by the Crystal Ball Collaboration [27] at the e^+e^- storage ring DORIS II compared with EURODEC predictions. The dashed, dotted and dash-dotted lines indicate the individual contribution from semileptonic b , c and τ decays to the inclusive spectrum.

Fig. 10: Inclusive electron momentum spectrum from semileptonic B decays at the $\Upsilon(4S)$ as measured by the ARGUS Collaboration [28] at the DORIS II e^+e^- storage ring compared with the EURODEC predictions.

Fig. 11: Comparison of the EURODEC prediction for the inclusive muon momentum spectrum from the decay of B-mesons at the $\Upsilon(4S)$ and measurements by the ARGUS Collaboration [28] (DORIS II).

Fig. 12: Inclusive electron momentum spectrum at the $\Upsilon(4S)$ as predicted by EURODEC and measured by the CLEO Collaboration [29] at CESR. Individual contributions from semileptonic charm, bottom and τ decays are indicated as well.

Fig. 13: Comparison of the inclusive muon momentum spectrum in semileptonic B-meson decays as measured at the $\Upsilon(4S)$ at CESR (CLEO [29]) and EURODEC predictions.

Fig. 14: Charged particle multiplicity distribution in $B\bar{B}$ events at the $\Upsilon(4S)$ as obtained by the CLEO Collaboration [33] together with the EURODEC prediction.

Fig. 15: Charged particle multiplicity distribution in $B\bar{B}$ events at the $\Upsilon(4S)$ with at least one observed prompt electron as measured by the CLEO Collaboration [33] compared with the EURODEC prediction.

Fig. 16: EURODEC prediction for the charged particle multiplicity distribution in $B\bar{B}$ events at the $\Upsilon(4S)$ with at least one prompt muon together with the measurement by the CLEO [33].

Fig. 17: Total particle multiplicity distribution for $B\bar{B}$ events at the $\Upsilon(4S)$ as predicted by EURODEC.

Fig. 18: Inclusive D^0 momentum spectrum from B decay as measured by the CLEO Collaboration [36] at CESR at the $\Upsilon(4S)$ compared with EURODEC predictions. The contribution from semileptonic B-meson decays is indicated by a dashed line.

Fig. 19: EURODEC prediction for the total inclusive D^{*+} momentum distribution in B-meson decays at the $\Upsilon(4S)$ compared with CLEO measurements [36]. The dashed line indicates the contribution from semileptonic B decays

Fig. 20: Inclusive D_s momentum spectrum from B-meson decay at the $\Upsilon(4S)$ as measured by ARGUS [40] and CLEO [39]. The EURODEC prediction is indicated as well.

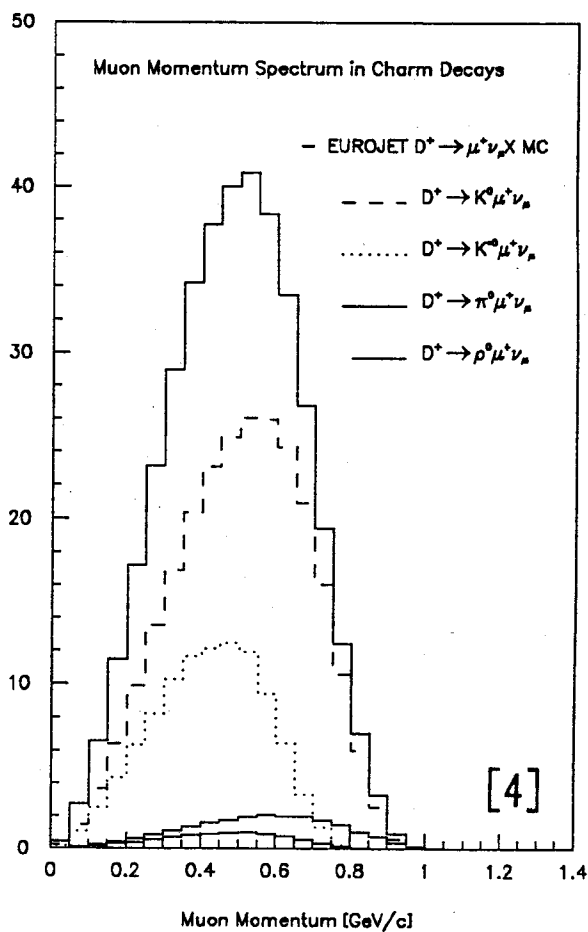
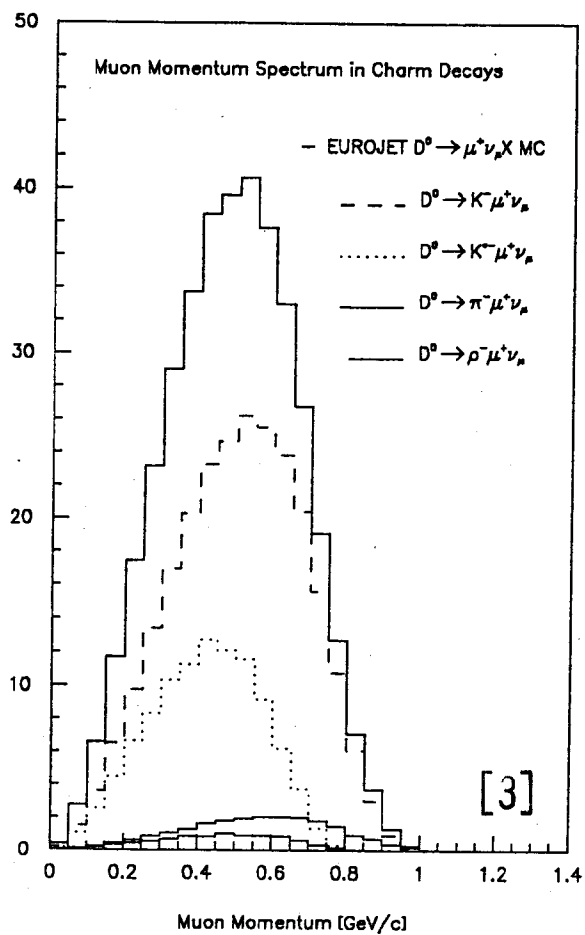
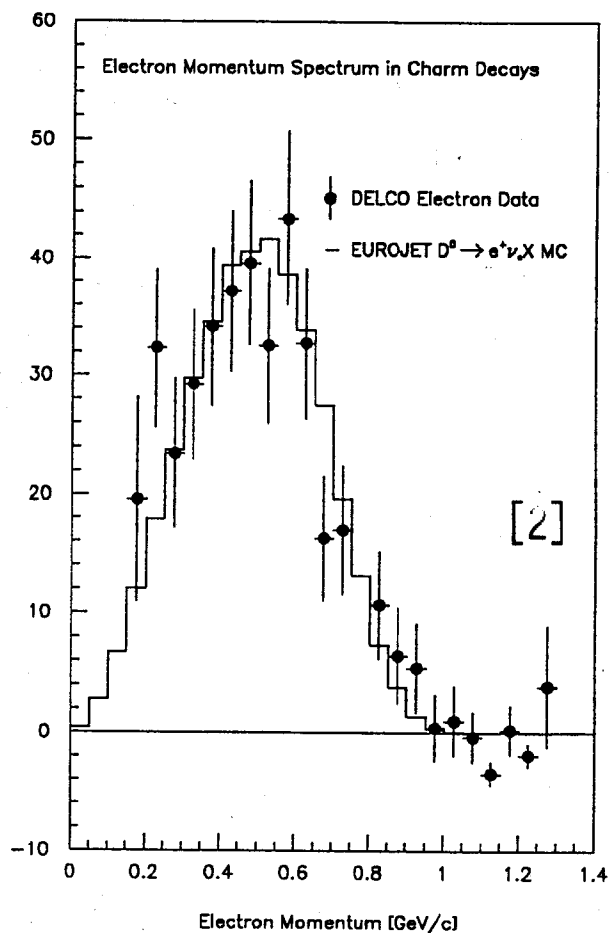
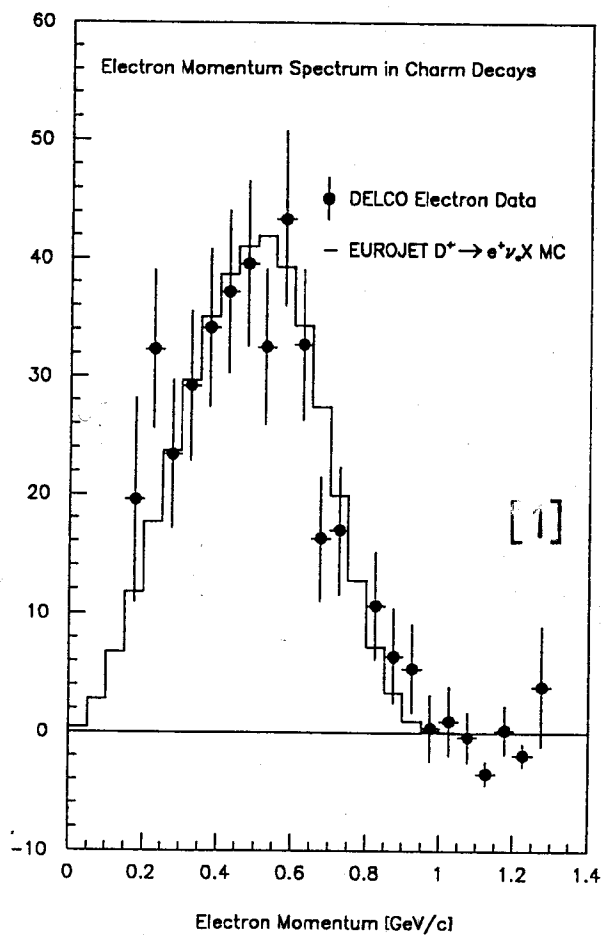
Fig. 21: J/ψ momentum distribution in B decays as measured at the $\Upsilon(4S)$ by the ARGUS Collaboration [47] at the e^+e^- storage ring DORIS II and the CLEO Collaboration [45] at the CESR. The histogram reflects the EURODEC prediction.

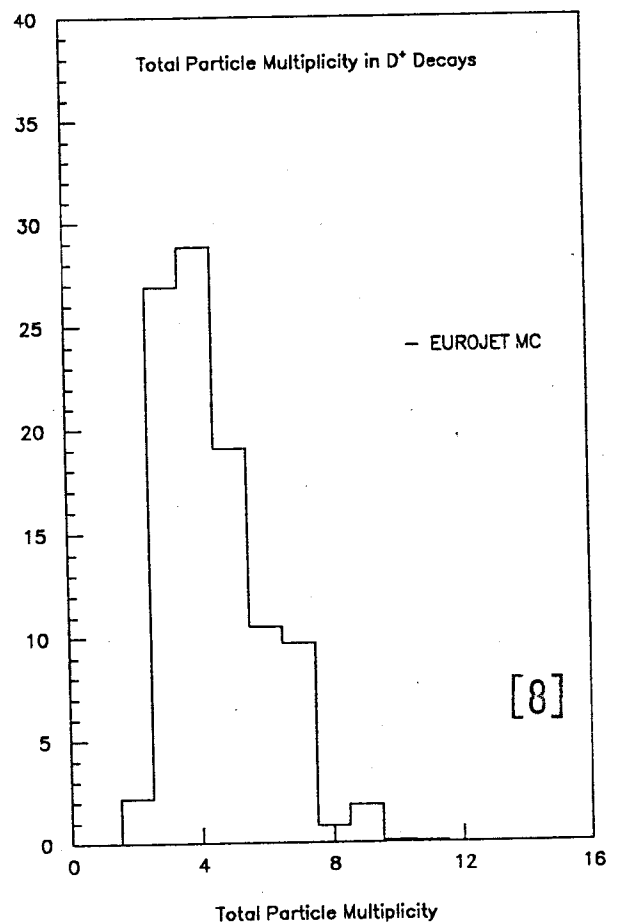
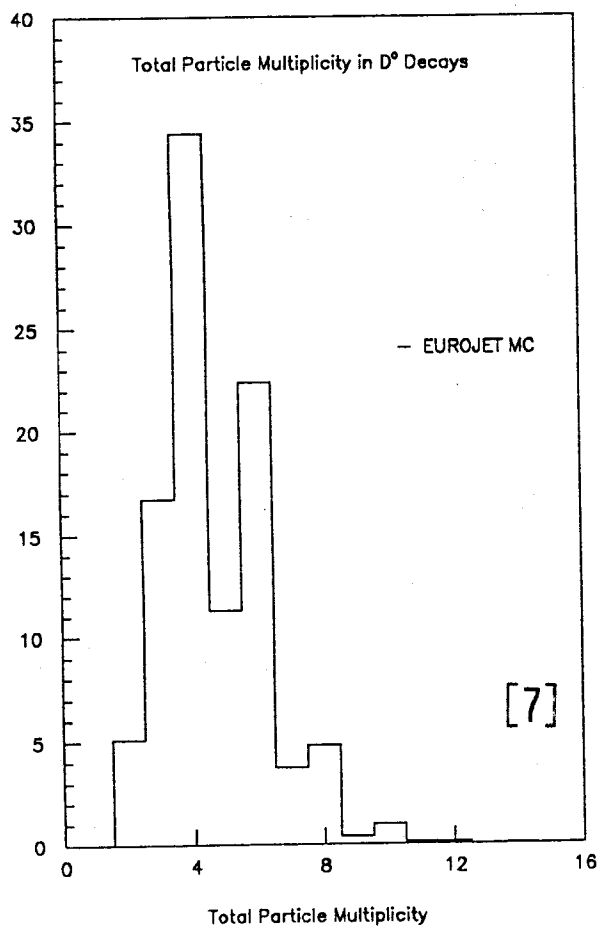
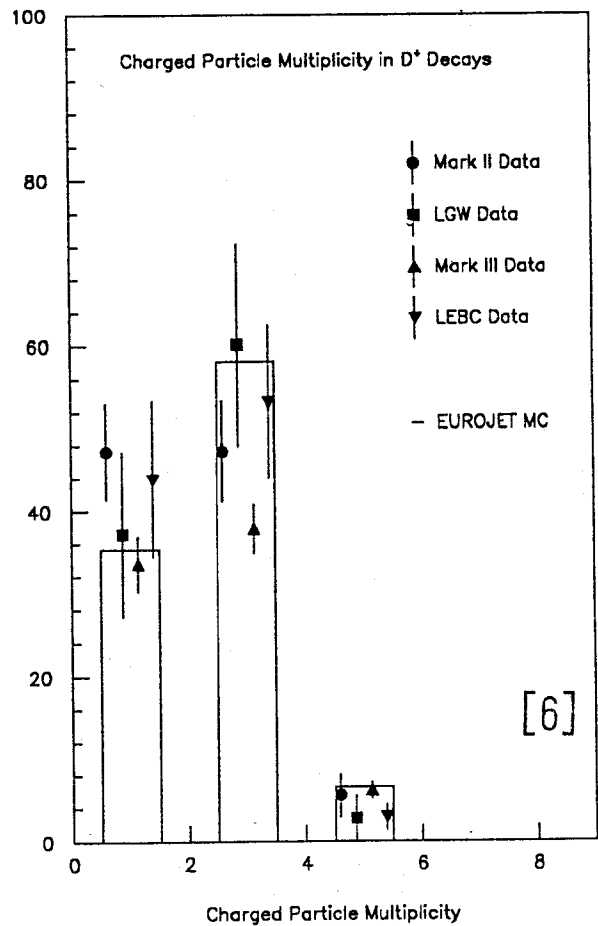
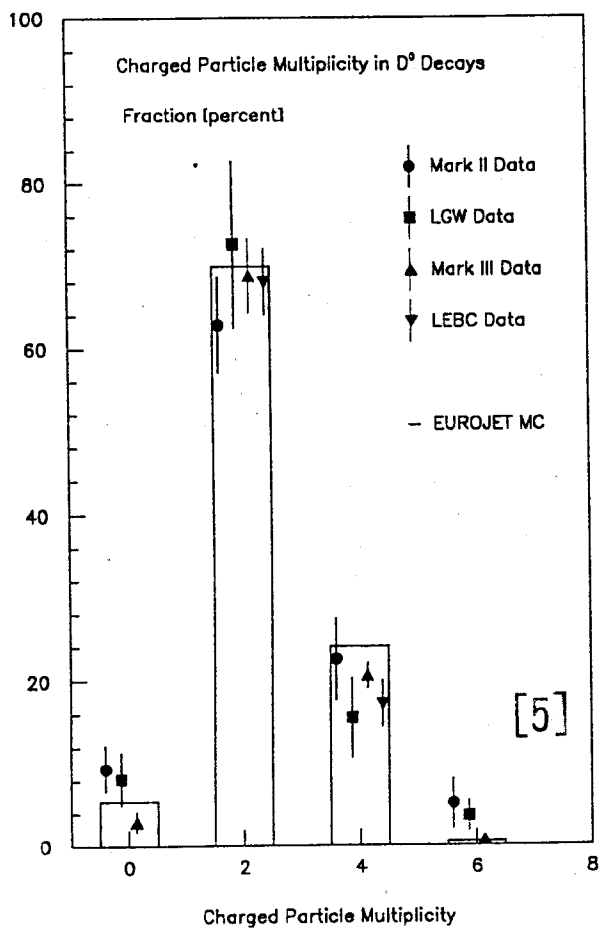
Fig. 22: Momentum distribution of ψ mesons in B decays at the $\Upsilon(4S)$ as predicted by the EURODEC Monte Carlo program. The contribution from $\psi' \rightarrow J/\psi X$ is shown separately (dashed histogram). The experimental data on the inclusive J/ψ spectrum is depicted in Fig. 21. The experimental reconstruction of the ψ' momentum spectrum still suffers from limited statistics.

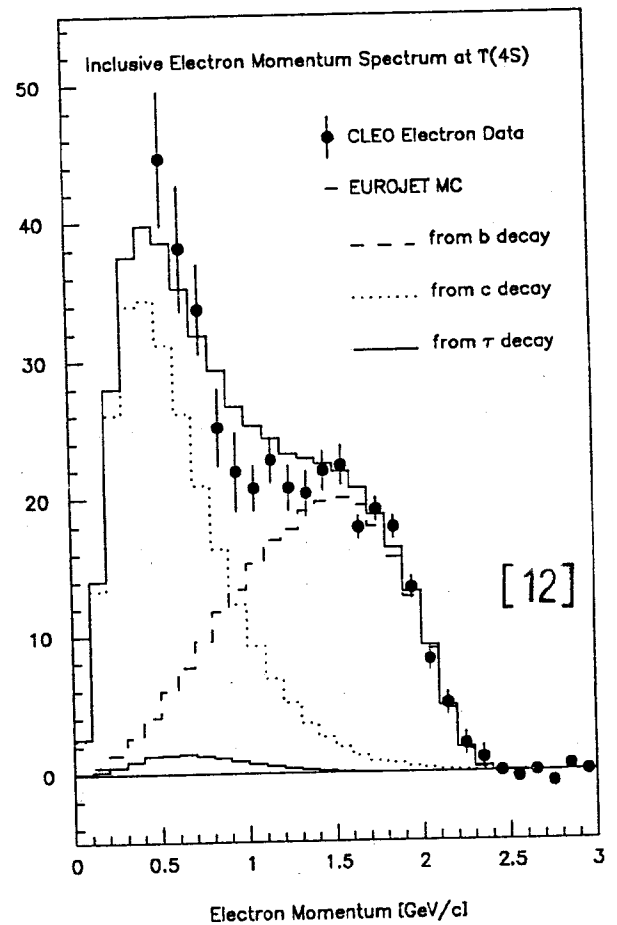
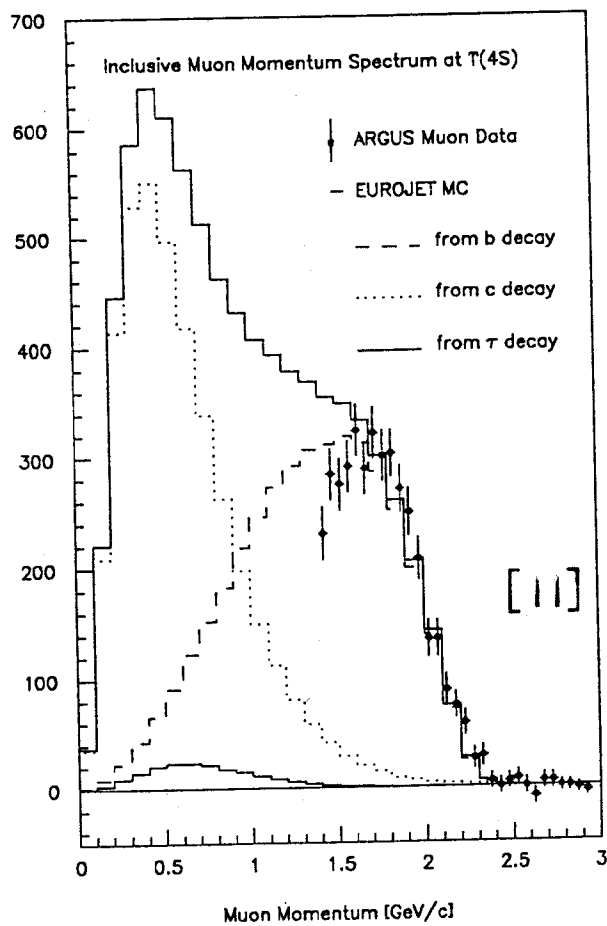
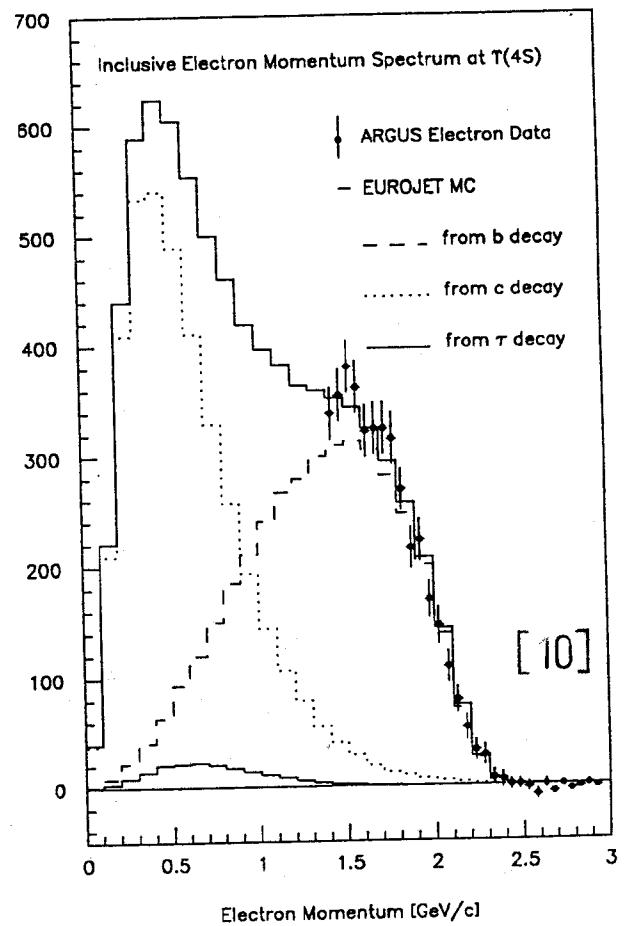
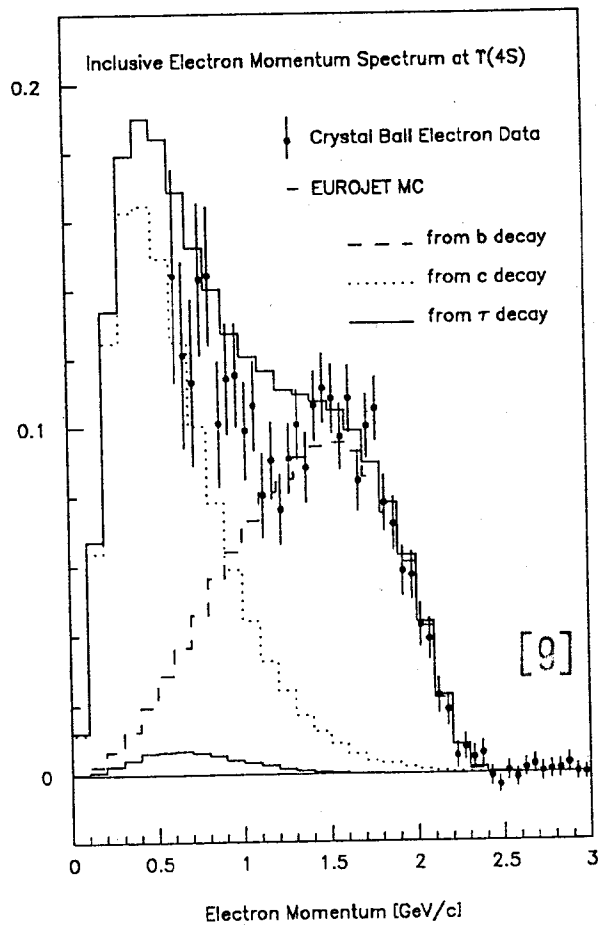
Fig. 23: Inclusive momentum distribution of Λ_c^+ baryons from B-meson decays at the $\Upsilon(4S)$ as measured by the ARGUS Collaboration [50] compared with the EURODEC prediction.

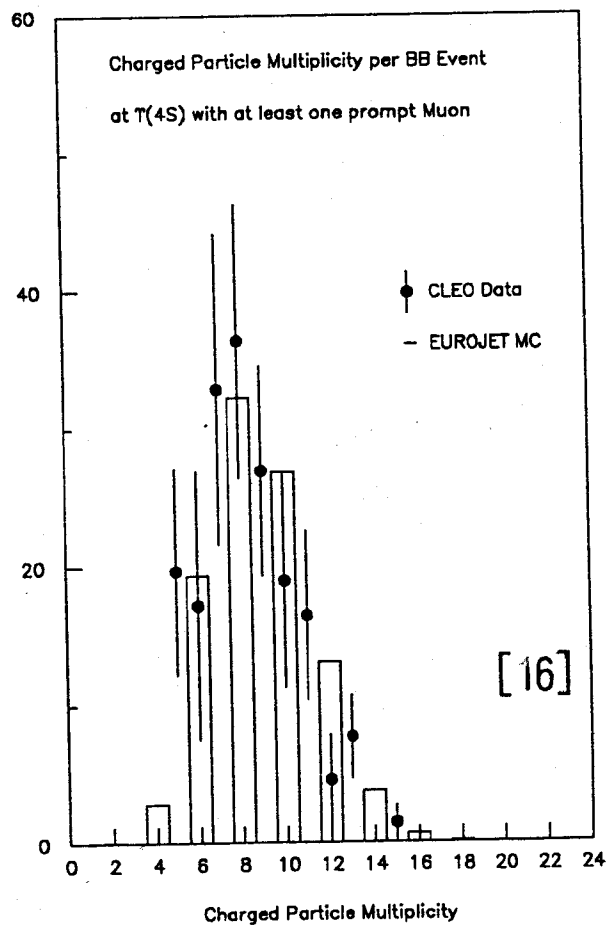
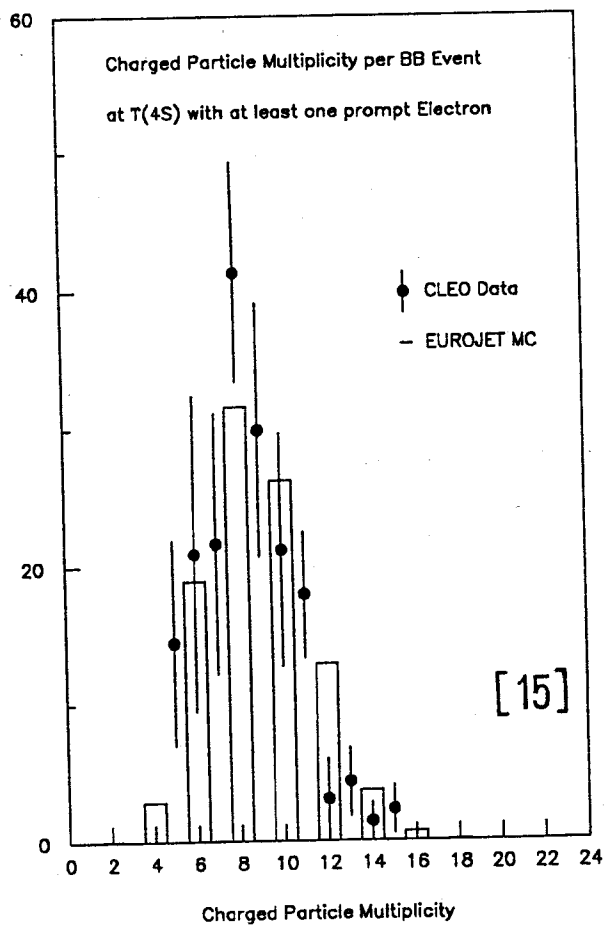
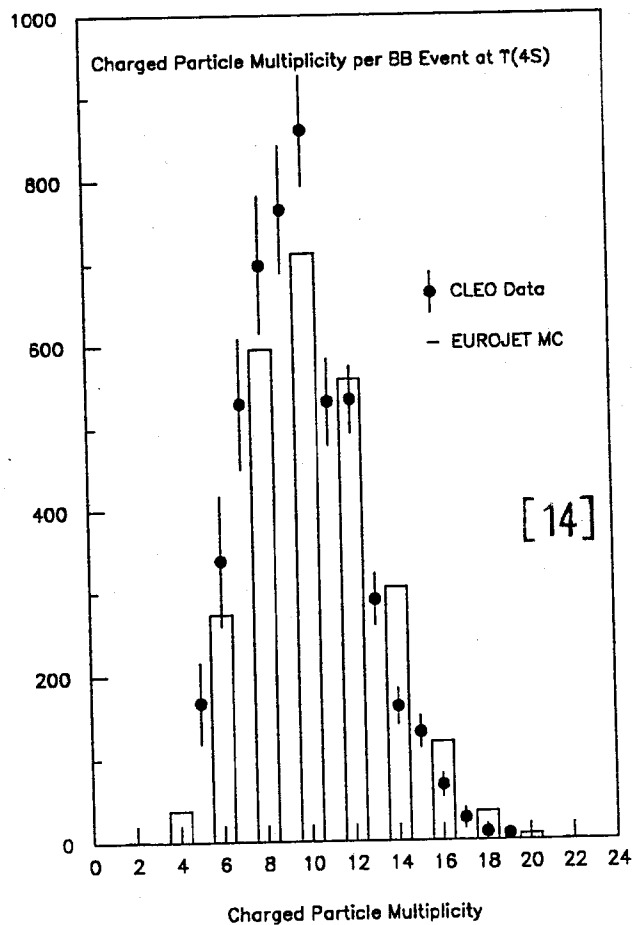
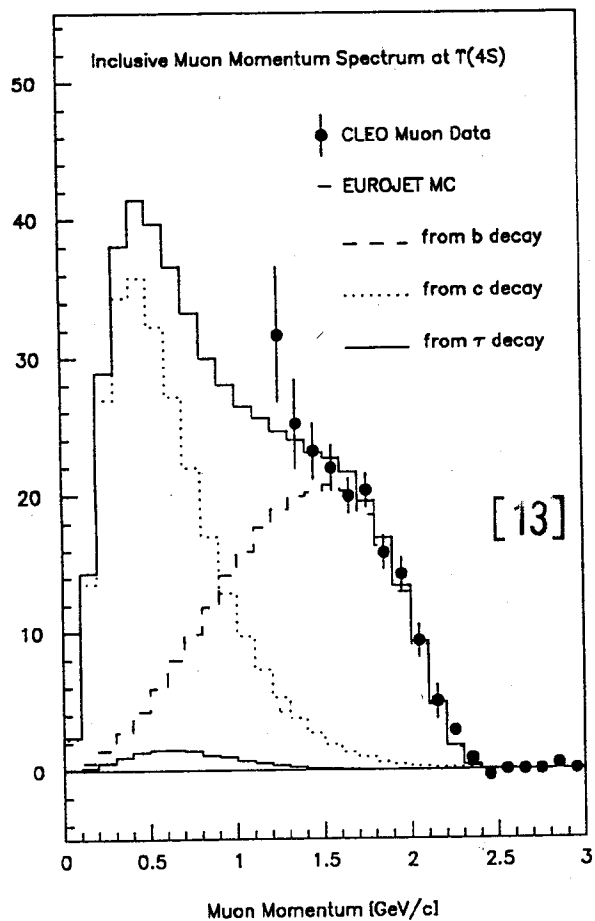
Fig. 24: Λ baryon momentum spectrum from B-meson decays as measured by the ARGUS Collaboration [28] at DORIS II and by CLEO [52] at CESR compared with the EURODEC prediction.

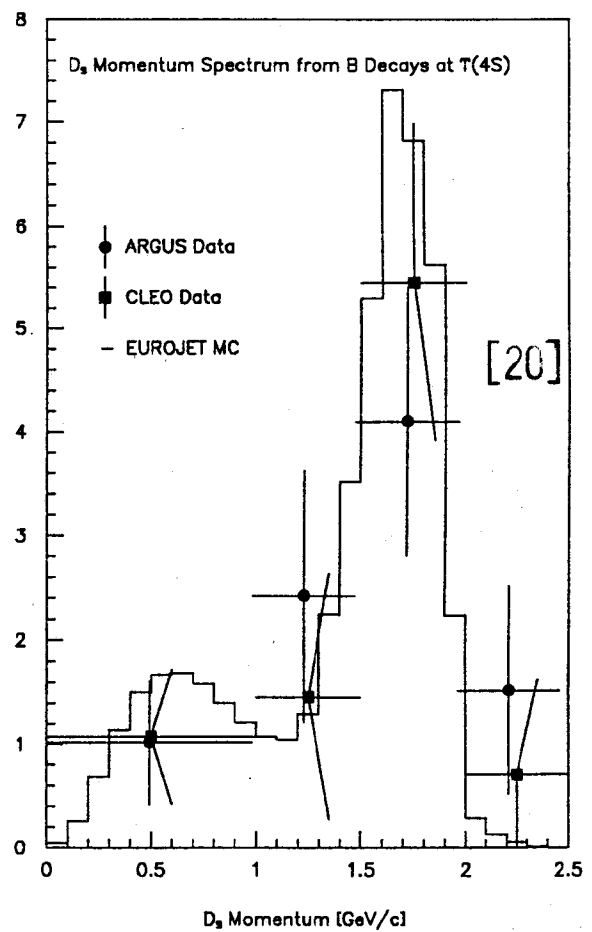
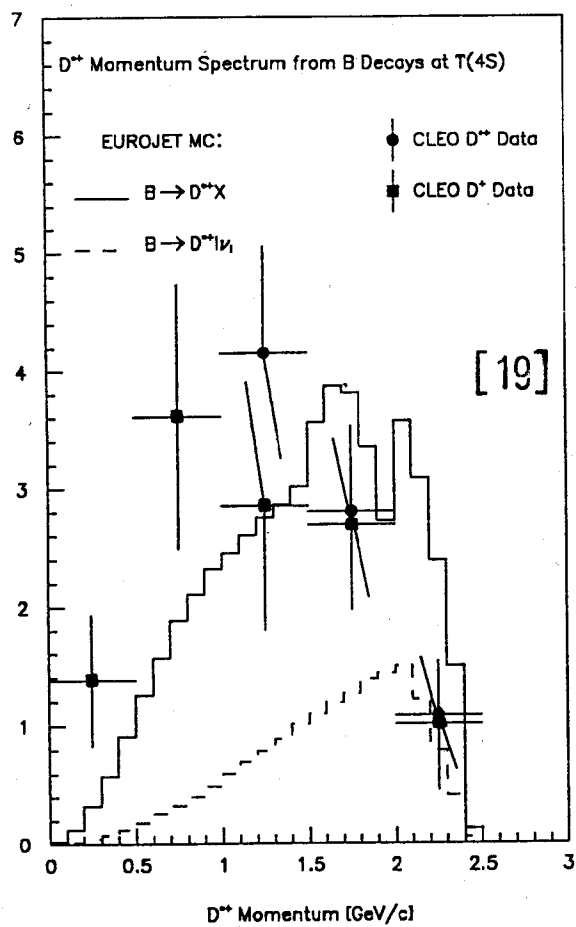
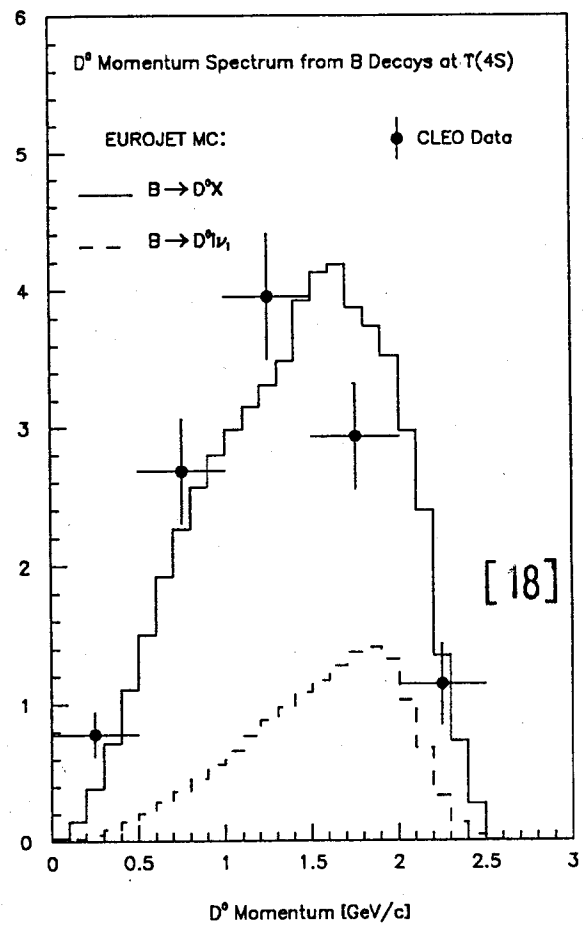
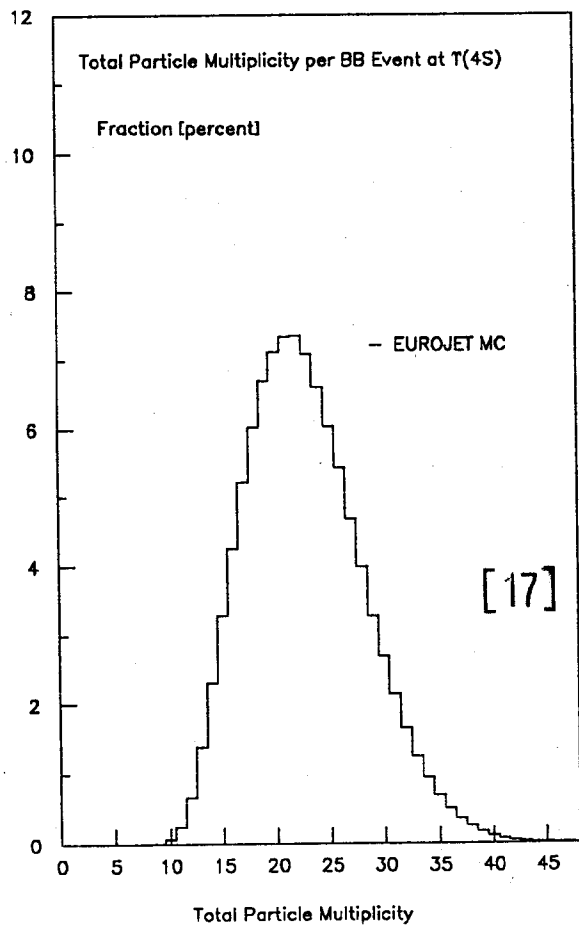
Fig. 25: ARGUS [28] and CLEO [52] measurements of the inclusive proton momentum spectrum in B-meson decays at the $\Upsilon(4S)$ compared with the distribution obtained from the EURODEC Monte Carlo program.

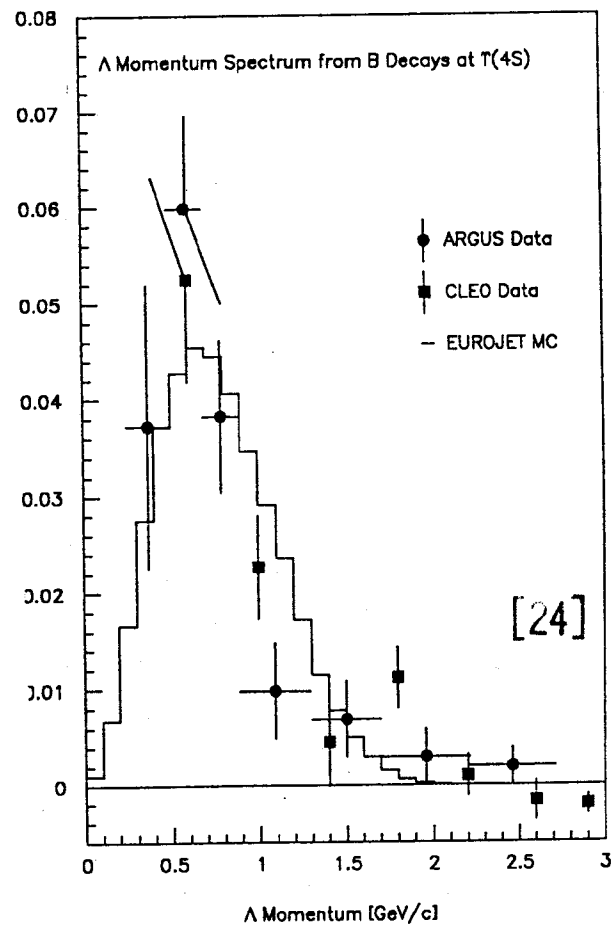
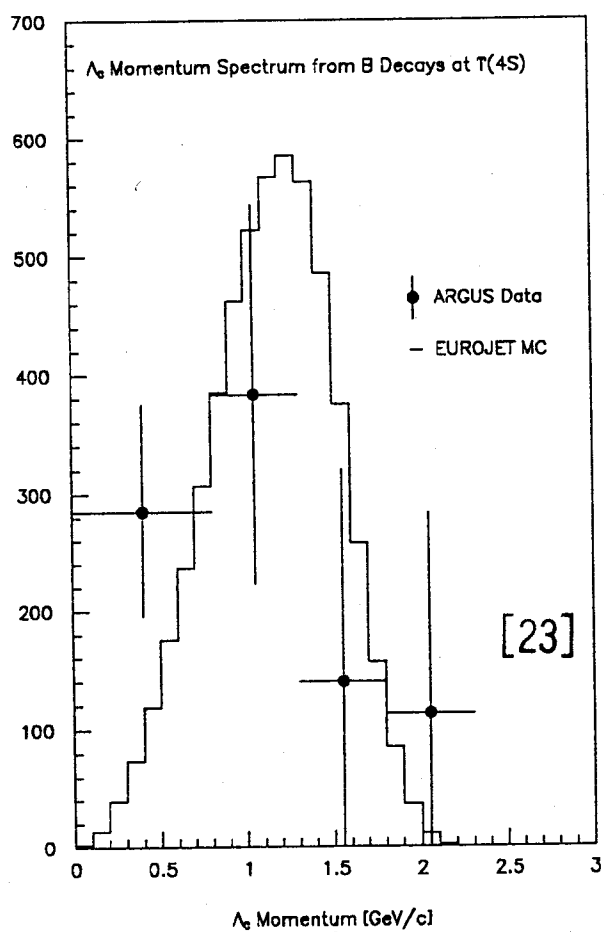
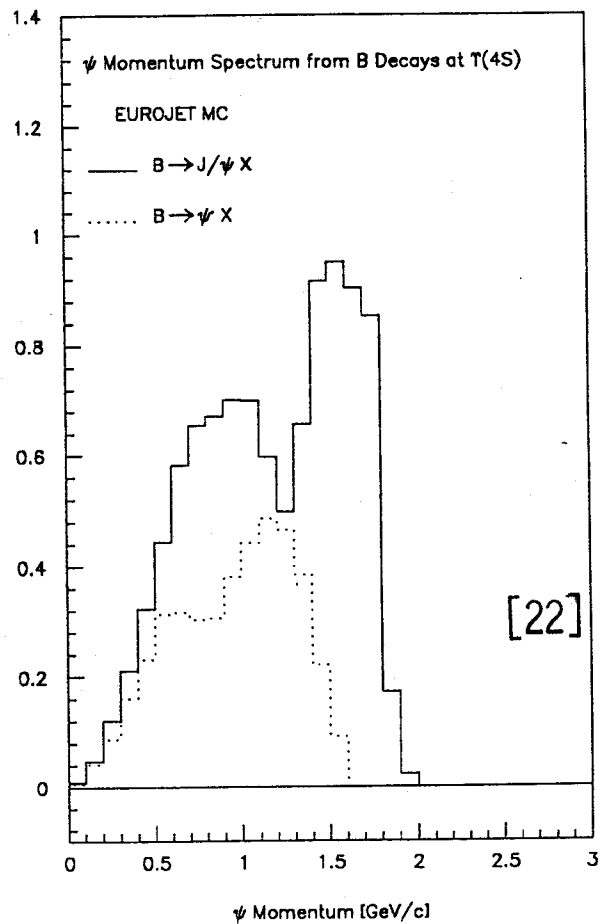
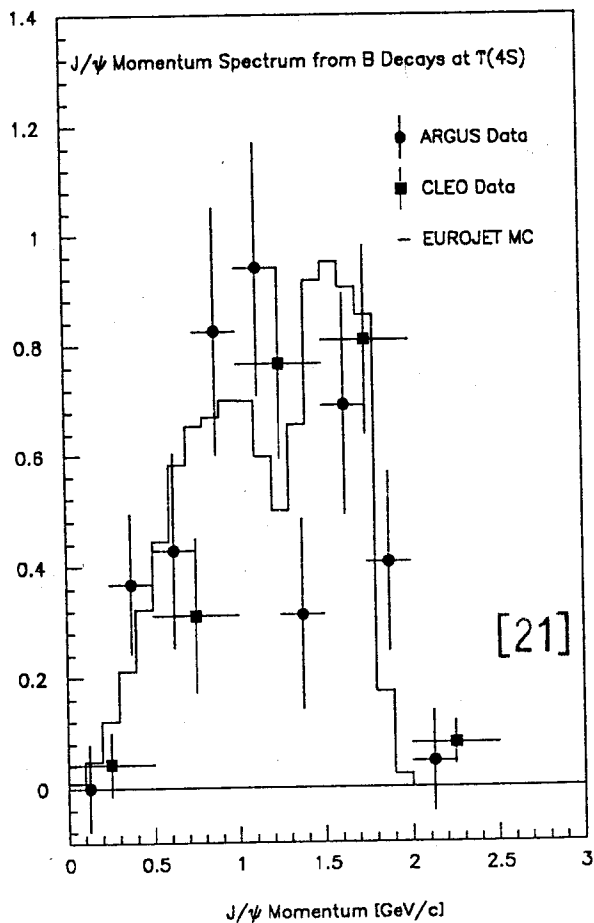


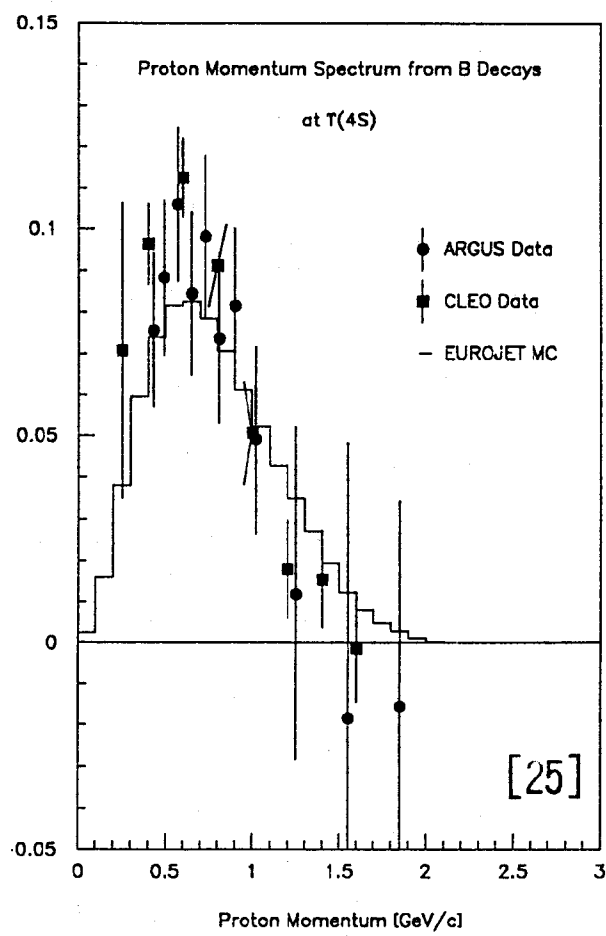












2.8. $B\bar{B}$ MIXING

The recent observation of $B_d^0 - \bar{B}_d^0$ oscillations by the Argus and Cleo collaborations has triggered a revival of interest for heavy flavor mixing. This unexpected large effect together with the measurement of the CP-violating ϵ and ϵ' parameters imply indeed new constraints on the three-generation Cabibbo-Kobayashi-Maskawa (CKM) mixing matrix and on the top quark mass [1]. Therefore, any further information on flavor mixing would provide us with a crucial test for the electroweak standard model itself. In particular, as we will see, the measurement of a rather small $B_s^0 - \bar{B}_s^0$ weak mixing would necessarily require new physics.

Flavor mixing can, in principle, be detected via either time-integrated or time-dependent measurements [2]. For simplicity, we first consider the well-known $K^0 - \bar{K}^0$ system to settle the associated formalisms. We treat then the $D^0 - \bar{D}^0$ and $B^0 - \bar{B}^0$ systems by analogy. Finally, we focus ourselves on the detectability of the $B_s^0 - \bar{B}_s^0$ mixing at LEP.

2.8.1. THEORETICAL FRAMEWORK*

a) Pseudoscalar oscillations

Flavor changing weak interactions induce a mixing between the pseudoscalar K^0 and its conjugate \bar{K}^0 [$CP | K^0 \rangle = - | \bar{K}^0 \rangle$]. Neglecting CP-violation, we obtain the following CP eigenstates:

$$\begin{aligned} K_L &= \frac{1}{\sqrt{2}}(K^0 + \bar{K}^0) & (CP = -1) \\ K_S &= \frac{1}{\sqrt{2}}(K^0 - \bar{K}^0) & (CP = +1) \end{aligned} \quad (2.169)$$

These (unstable) physical states satisfy the usual equation of motion:

$$i \frac{d}{dt} K_{L,S}(t) = \mathcal{H} K_{L,S}(t) = (M - \frac{i}{2}\Gamma)_{L,S} K_{L,S}(t) \quad (2.170)$$

with \mathcal{H} , the diagonal Hamiltonian. A straightforward integration gives then the following time-evolution

$$\begin{aligned} K^0(t) &= g_+(t)K^0(0) + g_-(t)\bar{K}^0(0) \\ \bar{K}^0(t) &= g_-(t)K^0(0) + g_+(t)\bar{K}^0(0) \end{aligned} \quad (2.171)$$

with

$$g_{\pm}(t) = \frac{1}{2}e^{-\Gamma_L t/2} \{1 \pm e^{\Delta\Gamma t/2} e^{i\Delta M t}\} \quad (2.172)$$

The complex factor inside the brackets modifies the usual exponential decay law and induces the oscillation between the K^0 and \bar{K}^0 states. This oscillating behaviour is

*J.-M. GERARD

therefore completely determined by the parameters

$$\Delta\Gamma = \Gamma_L - \Gamma_S \quad \Delta M = M_L - M_S \quad (2.173)$$

An important effect is possible if these quantities are large. The time-integrated probability for K^0 to oscillate into \bar{K}^0 is indeed given by the ratio

$$r \equiv \frac{Pr(K^0 \rightarrow \bar{K}^0)}{Pr(K^0 \rightarrow K^0)} = \frac{\int_0^\infty |g_-(t)|^2 dt}{\int_0^\infty |g_+(t)|^2 dt} = \frac{x^2 + y^2}{2 + x^2 - y^2} \quad (2.174)$$

The mixing r is maximal if $r \rightarrow 1$, i.e.

$$y \equiv \frac{\Delta\Gamma}{2\Gamma} \rightarrow \pm 1 \quad \text{or} \quad x \equiv \frac{\Delta M}{\Gamma} \rightarrow \infty \quad (2.175)$$

with $\Gamma \equiv \frac{1}{2}(\Gamma_L + \Gamma_S)$. On the other hand, the maximal value for the useful quantity

$$\chi = \frac{Pr(K^0 \rightarrow \bar{K}^0)}{Pr(K^0 \rightarrow K^0) + Pr(K^0 \rightarrow \bar{K}^0)} = \frac{r}{1 + r} \quad (2.176)$$

is obviously 1/2.

The first scenario ($y \approx \pm 1$) to get a large mixing turns out to occur in the kaon system for the following simple reason. The quantity $\Delta\Gamma$ receives contributions from self-conjugate on-shell intermediate states

$$\Delta\Gamma \propto \sum_n \langle \bar{K}^0 | H_{\Delta S=1} | n \rangle \langle n | H_{\Delta S=1} | K^0 \rangle. \quad (2.177)$$

The three-body decays being largely phase-space suppressed, we obtain then

$$\Delta\Gamma \simeq \sum_{2\text{-body}} \{\Gamma(K_L \rightarrow n) - \Gamma(K_S \rightarrow n)\} = \Gamma(K_L \rightarrow \pi\pi) - \Gamma(K_S \rightarrow \pi\pi) \simeq -\Gamma_S \quad (2.178)$$

since the $\pi\pi$ final states are CP even. Therefore $y \simeq -1$ and the mixing is almost maximal [3]: $r_K^{exp.} = 0.99284 \pm 0.00003$. In other words, the K_S states decay faster than the K_L ones, leaving then an equal amount of K^0 and \bar{K}^0 irrespectively of the initial conditions.

Such a scenario is of course peculiar to the light $K^0 - \bar{K}^0$ system. For heavier systems, the quantity $\Delta\Gamma$ receives contributions from many CP-even and odd self-conjugate intermediate states. The phase-space suppression argument does not apply anymore and one expects a smaller $\Delta\Gamma/\Gamma$ ratio. This ratio is in addition double-Cabibbo suppressed for the D^0 and B_d^0 systems, the dominant decay channels being not self-conjugate.

Let us therefore consider the case of the B_s^0 system. The self-conjugate inclusive $b(\bar{s}) \rightarrow c\bar{c}s(\bar{s})$ decay contributes to $\Delta\Gamma$. A simple counting of the colour degrees of freedom gives then the constraint $|y_s| < 3/(3 + 3 + 1 + 1 + 1) = 1/3$ namely the bound $1 \leq (\tau_L/\tau_S)_{B_s} < 2$, to be compared with $(\tau_L/\tau_S)_K \simeq 600$. The upper bound given above is in fact quite optimistic. We have indeed neglected the important momentum-mismatch

between the spectator and the hard strange quarks [4] as well as the charm phase-space suppression. One should however keep in mind the possibility [5] of a sizeable lifetime difference effect in a time-dependent study of B_s^0 decay rates.

We have seen that the effect of a lifetime difference can be neglected as far as a time-integrated heavy meson mixing is concerned. This mixing reads then

$$r \simeq \frac{x^2}{2+x^2} \quad x = \frac{\Delta M}{\Gamma}$$

and is large if the oscillation-time (ΔM^{-1}) is small compared to the life-time ($\Gamma^{-1} = \tau$). The D^0 and B lifetimes are well-measured while the spectator model predicts $\tau(B_s) \sim \tau(B_d)$. Consequently, an estimate of the mixing in heavy pseudoscalars requires “only” a theoretical knowledge of the mass splitting ΔM .

b) $D^0 - \bar{D}^0$ oscillations

The $D^0 - \bar{D}^0$ mass difference is dominated [6] by *long-distance* π and K loop contributions and vanishes in the flavor- $SU(3)$ symmetry limit. The surprisingly large $SU(3)$ -breaking observed in two-body Cabibbo-suppressed D -decays:

$$\frac{\Gamma(D^0 \rightarrow K^+ K^-)}{\Gamma(D^0 \rightarrow \pi^+ \pi^-)} \sim 3 \quad (2.179)$$

remaining unexplained, an estimate of the $D^0 - \bar{D}^0$ mixing requires empirical data. Rough estimates give [7] $r_D \sim 10^{-4}$ such that a 1% mixing would definitely signal new physics with large flavor changing neutral currents [8].

The e^+e^- Mark III experiment at the energy of the $\psi(3770)$ has reported three strangeness +2 final state events in the $D^0 \bar{D}^0$ pair decays [9]. Only one such an event is expected from the double-Cabibbo suppressed decay (DCSD) contributions. This result would then imply $r_D \sim 1\%$.

However, the Fermilab photoproduction E691 collaboration has looked for $D^{*+} \rightarrow \pi^+ D^0 \rightarrow \pi^+(K^- \pi^+)$ decays. They used the pion of the D^{*+} decay to tag the charm quantum number and made a time-dependent analysis to reduce the DCSD contributions which fake a mixing. We have indeed the following time-evolution for the wrong sign D^0 decays:

$$\begin{aligned} N(D^0 \rightarrow S = +1) &= N_0 |g_-(t) + \rho t g^2 \theta_c \quad g_+(t)|^2 \\ y &\ll x \\ &\simeq \frac{N_0}{4} e^{-\Gamma t} \{(\Delta M)^2 t^2 + 4 |\rho|^2 t g^4 \theta_c\} \end{aligned} \quad (2.180)$$

with $\rho = \Theta(1)$ and $t g^4 \theta_c \sim 3 \cdot 10^{-3}$, the Cabibbo suppression factor. Applying the cut $t > 2\tau_{D^0}$, 68% ($5e^{-2}$) of the mixing effect (first term) subsists, while only 14% (e^{-2})

of the DCSD effect (second term) remains. With a total of 611 $K^-\pi^+$ events and 375 $K^-\pi^+\pi^+\pi^-$ events, they obtained the limit [10] $r_D < 0.37\%$ at the 90% confidence level.

A similar time-dependent analysis can in principle be carried at LEP. With $10^6 Z^0$, one expects about 750 events $D^{*\pm} \rightarrow \pi^+ D^0 \rightarrow \pi^\pm [K^-\pi^+]$, requiring the D^* to have high momentum to select primary charm, before the lifetime cut and acceptance and reconstruction efficiency factors.

c) $B^0 - \bar{B}^0$ mixing

The $B^0 - \bar{B}^0$ mass difference is induced by the *short distance* box-diagram with the exchange of two heavy top quarks. The recently measured [11, 12] $B_d^0 - \bar{B}_d^0$ mixing implies

$$x_d = 0.70 \pm 0.13 \quad (2.181)$$

and requires [13] a top quark heavier than 50 GeV. In the standard electroweak model with three generations of quarks, the $B_s^0 - \bar{B}_s^0$ mixing is then determined by the following simple relation

$$x_s \sim \left(\frac{f_{B_s}}{f_{B_d}} \right)^2 \left| \frac{V_{ts}}{V_{td}} \right|^2 x_d \quad (2.182)$$

Let us first assume a flavor- $SU(3)$ symmetry for the decay constant f_B . The left-handed CKM mixing matrix V reads

$$V_L \sim \begin{pmatrix} 1 & \lambda & \lambda^3(\rho - i\eta) \\ -\lambda & 1 & \lambda^2 \\ \lambda^3(1 - \rho - i\eta) & -\lambda^2 & 1 \end{pmatrix} \quad (2.183)$$

in the Wolfenstein parametrization [14] based on a mnemonic expansion in the Cabibbo angle $\lambda \simeq 0.22$. The present experimental limit on charmless semi-leptonic B -decays [1]

$$\bar{R} \equiv \frac{\Gamma(b \rightarrow ue\nu)}{\Gamma(b \rightarrow ce\nu)} \leq 6\% \quad (2.184)$$

implies $\rho^2 + \eta^2 \leq (0.8)^2$ and provides the lower bound

$$\left| \frac{V_{ts}}{V_{td}} \right|^2 = \frac{1}{\lambda^2[(1 - \rho)^2 + \eta^2]} > \frac{0.3}{\lambda^2} \sim 6 \quad (2.185)$$

On the other hand [15], for $m_t \leq 130$ GeV, the measured $B_d^0 - \bar{B}_d^0$ mixing strongly favors a negative ρ parameter, while the CP -violating ϵ_K -parameter implies a relatively small η

$$\eta \simeq 0.2[(5/4 - \rho)B_K]^{-1} \left(\frac{m_t}{M_W} \right)^{-4/3} \leq 0.3 \quad (2.186)$$

for $B_K = 0.7$. In that case, $\left| \frac{V_{ts}}{V_{td}} \right|^2 \leq \lambda^{-2}$ and we obtain the range

$$3 \leq x_s \leq 18 \quad (2.187)$$

if one standard deviation is allowed for x_d .

However, $SU(3)$ -breaking effects in the hadronic matrix of the current-current $\Delta B = 2$ weak operator have to be taken into account. The decay constant f_B defines the B -to-vacuum current hadronic matrix element (our normalization corresponds to $f_\pi = 0.132$ GeV):

$$\langle 0 | \bar{b} \gamma_\mu (1 - \gamma_5) q | B_q \rangle \equiv i f_{Bq} p_\mu \quad (2.188)$$

In the non relativistic limit, one has the following scaling

$$f_{Q\bar{q}} \sim \frac{\psi(0)}{\sqrt{m_Q}}. \quad (2.189)$$

If the wave-function and the origin $\psi(0)$ only depends on the reduced mass of the $Q\bar{q}$ system, we obtain

$$f_{B_s}/f_{B_d} \simeq \left(\frac{m_s}{m_d}\right)^{3/2} > 1 \quad (2.190)$$

on dimensional grounds. For the constituent quark masses $m_d = 350$ MeV and $m_s = 500$ MeV, we get then a $SU(3)$ -breaking correction factor of about three in eq. (182). This rough estimate can be compared with the QCD sum rules and lattice predictions listed below:

$f_\pi = 132$ MeV	f_D	f_{D_s}	f_{B_d}	f_{B_s}
QCD sum rules [15]	172 ± 15	~ 220	187 ± 24	—
Lattice:				
UCLA [16]	$174 \pm 26 \pm 46$	$234 \pm 46 \pm 55$	$105 \pm 17 \pm 30$	$155 \pm 31 \pm 48$
ELC [17]	194 ± 15	215 ± 17	—	—

In the QCD sum rules predictions, the naive non-relativistic scaling given in eq. (189) is spoiled by large continuum QCD corrections. This is at variance with preliminary data from the UCLA Lattice collaboration. On the other hand, both non-perturbative methods give a ratio f_{D_s}/f_D larger than one and indicate a sizable $SU(3)$ -breaking effect in weak decay constants. The $SU(3)$ prediction given in eq. (187) should therefore be considered with some caution. The upper bound might be a factor of two larger, but a measured x_s smaller than three would certainly require physics beyond the three-generation standard electroweak model [18].

The simplest extension is of course the introduction of a fourth generation of quarks such that the unitary constraint on V_{td} is relaxed. However, one should keep in mind that any new flavor changing interaction which deviates from the CKM mixing pattern given in (183) could also modify the theoretical prediction (182) on x_s . For example, an $SU(2)_L \times SU(2)_R \times U(1)$ extension of the standard model with the following pattern for

the right-handed CKM mixing matrix [20]

$$V_R \sim \begin{pmatrix} 1 & 0 & 0 \\ 0 & 1 & \lambda^2 \\ 0 & -\lambda^2 & 1 \end{pmatrix} + \mathcal{O}(\lambda^4) \quad (2.191)$$

turns out to be consistent with all existing data, even for $M_{W_R} = \mathcal{O}(M_{W_L})$.

2.8.2. $B\bar{B}$ MIXING MEASUREMENTS*

Experimentally there are two ways of observing the mixing : by measuring time integrated variables, essentially the ratio of mixed BB or $\bar{B}\bar{B}$ pairs with respect to the total number of B pairs or by observing the time evolution of B^0 mesons.

a) Time integrated variables

As we have seen in the introduction both B_d^0 and B_s^0 mix. Experimentally, unless B_d^0 or B_s^0 are exclusively identified, one will observe the combined effect of B_d^0 and B_s^0 mixing. We can distinguish 3 situations : tagging only the b quark sign on each side, identifying a B meson on one side and tagging the sign of the b quark on the other side and finally identifying both B mesons.

Tagging of b quark sign only

By measuring the ratio of same sign leptons over the total number of lepton pairs, one measures

$$X = \frac{l^\pm l^\pm}{ll} = 2\bar{\chi}(1 - \bar{\chi}) \quad (2.192)$$

with

$$\bar{\chi} = f_d \frac{B_d}{\langle B \rangle} \chi_d + f_s \frac{B_s}{\langle B \rangle} \chi_s \quad (2.193)$$

where f_i are the fraction of mesons of type i per jet and $\frac{B_i}{\langle B \rangle}$ is the ratio of the semileptonic branching fraction of meson of type i with respect to the average $\langle B \rangle$ semileptonic branching fraction.

Experimentally the situation is complicated by the presence of background events in addition to the events where both leptons come from $b \rightarrow l$ decays (N_f) : events with one lepton coming from the cascade $b \rightarrow c \rightarrow l$ (N_s), events from primary $c \rightarrow l$ decays (N_c) and background events from $u, d, s \rightarrow l$ decays or misidentified hadrons (N_b). We can write

$$X = \frac{2\bar{\chi}(1 - \bar{\chi}) + [(1 - \bar{\chi})^2 + \bar{\chi}^2]s + \alpha b}{1 + s + c + b} \quad (2.194)$$

*M. BOSMAN in collaboration with H.-G. MOSER, B. VAN EIJK, P. MÄTTIG

with

$$s = \frac{N_s}{N_f}; c = \frac{N_c}{N_f}; b = \frac{N_b}{N_f} \quad (2.195)$$

and α the fraction of N_b giving same sign leptons.

For $10^6 Z^0/s$, one expects about 8000 lepton pairs from b decay before any selection criteria. Assuming a value [11,12] for χ_d of 0.17 and the maximal mixing value for χ_s of 0.5, we obtain $\bar{\chi} = 0.12$. Selection criteria for leptons from b decay ($p_l > \sim 5\text{GeV}$ and p_T^l with respect to the jet axis $> \sim 1\text{GeV}$) and detector acceptance will typically introduce efficiency factors per lepton of ~ 0.5 , reducing the sample to about 2000 $b \rightarrow l$ lepton pairs. Typical values for the background will be $s+c+b$ amounting to $\sim 30\%$ while α will be close to 0.5. With these conditions, the measured value of X will be $X = 0.27 \pm 0.01$ for $10^6 Z^0/s$. The resulting precision on $\bar{\chi}$ will be a statistical error of the order of 10% and a systematic error coming from the control of the background of the same order.

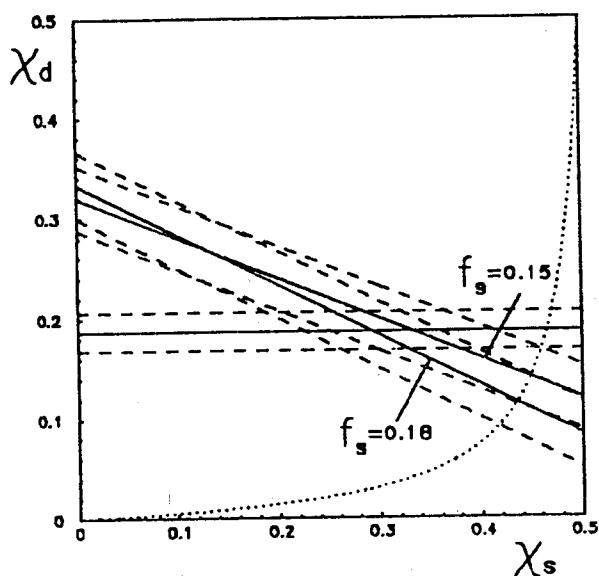


Fig. 2.36: Constraint introduced in the χ_s versus χ_d plane assuming that $\bar{\chi}$ is measured with 10 % precision ($\chi_d = 0.12 \pm 0.012$) for 2 sets of f_s and f_d values : ($f_s = 0.15; f_d = 0.38$) and ($f_s = 0.18; f_d = 0.32$). The intersection of the $\bar{\chi}$ band with the band corresponding to a 10 % precision measurement of χ_d shows the sensitivity of the extracted χ_s value to the f_s fraction. The change of f_s from 0.18 to 0.15 results in $\Delta\chi_s$ of 0.04. The dotted line indicates the values allowed by the standard model.

This measurement provides a constraint in the (χ_d, χ_s) plane (see Fig. 2.36). Introducing the value of χ_d which by then will probably be measured by ARGUS and CLEO with a precision of about 10%, one can extract χ_s . The value of χ_s is quite sensitive, as can be seen in Fig. 2.36, to the fraction f_s .

Identifying B_d^0 or B_s^0 mesons and tagging the sign of the b quark

To access more directly χ_d or χ_s , the B_d^0 or B_s^0 meson has to be identified. As seen in the section on exclusive B meson lifetime measurement, semileptonic decays provide the highest statistics sample of identified B mesons : 410 $B_d^0 \rightarrow l^+ D^{*-}$ and 160 $B_s^0 \rightarrow l^+ D_s^{*-}$ decays for $10^6 Z^0/s$ before selection criteria. Those numbers include the branching fractions of $D^{*-} \rightarrow D^0(K^+\pi^-) + \pi^-$ and of $D_s^{*-} \rightarrow \phi(K^+K^-) + \pi^-$. Requiring the b quark on the other side to decay semileptonically reduces the sample to about 100

lB_d^0 pairs and 40 lB_s^0 pairs. Lepton selection criteria, acceptance and reconstruction efficiencies will typically reduce the sample by an additional factor 3. With $10^7 Z^0$'s, one may envisage this measurement with samples of about 300 lB_d^0 and 120 lB_s^0 reconstructed pairs. The same sign over total number of pairs is given in this case by

$$X = \chi_s(1 - \bar{\chi}) + \bar{\chi}(1 - \chi_s) \quad [\text{or } \chi_d] \quad (2.196)$$

with $\bar{\chi}$ being the mixed parameter discussed in the preceeding section. For $10^7 Z^0$'s, for maximal B_s^0 mixing for example, χ_s would be measured with $\sim 25\%$ statistical error. The advantage of this method is that it is less sensitive to the knowledge of the fraction f_s .

Tagging both B mesons

By identifying $B_u^+ B_s^0$ pairs, one measures directly the mixing :

$$\frac{B_u^+ B_s^0}{B_u^+ B_s^0 + B_u^+ \bar{B}_s^0} = \chi_s \quad (2.197)$$

For $10^7 Z^0$'s, one expects for example 650 $B_u^+ B_s^0$ pairs with the B_s^0 identified via its semileptonic decay $B_s^0 \rightarrow l^+ D_s^- (D_s^- \rightarrow \phi \pi^-)$. Requiring the B_u^+ to be reconstructed in some exclusive decay mode like $\bar{D}^0 \pi^+$ for example, would leave only a few events. One can envisage to identify B_u^+ more inclusively by counting the number of charged tracks in the B vertex. With which efficiency and purity the LEP experiments are able to separate charged from neutral B mesons with such method will determine if this procedure is envisageable or not.

b) Time Evolution

In the limit of no CP violation, the time evolution is given by [$x = \frac{\Delta M}{\Gamma}$]

$$\frac{dP}{dt}(B^0 \rightarrow B^0) = \frac{1}{\tau} e^{-\frac{t}{\tau}} \cos^2\left(\frac{xt}{2\tau}\right) \quad (2.198)$$

$$\frac{dP}{dt}(B^0 \rightarrow \bar{B}^0) = \frac{1}{\tau} e^{-\frac{t}{\tau}} \sin^2\left(\frac{xt}{2\tau}\right) \quad (2.199)$$

To observe the time evolution of B_d^0 or B_s^0 , one needs to identify the B_d^0 or B_s^0 meson, tag the sign of the initial b quark and measure the abundance of B^0 or \bar{B}^0 as a function of the proper time of the decay. The case where the B meson is identified in its leptonic mode on one side and the sign is tagged through a single lepton at the opposite side provides the most abundant sample of tagged B_d^0 or B_s^0 : 300 lB_d^0 and 120 lB_s^0 experimentally reconstructed pairs for $10^7 Z^0$. As discussed in the lifetime chapter, we expect the precision on the proper time to be

$$\frac{\sigma_t}{t} \sim \sqrt{\left(\frac{\sigma_l}{l}\right)^2 + \left(\frac{\sigma_p}{p}\right)^2} \sim 22\% \quad (2.200)$$

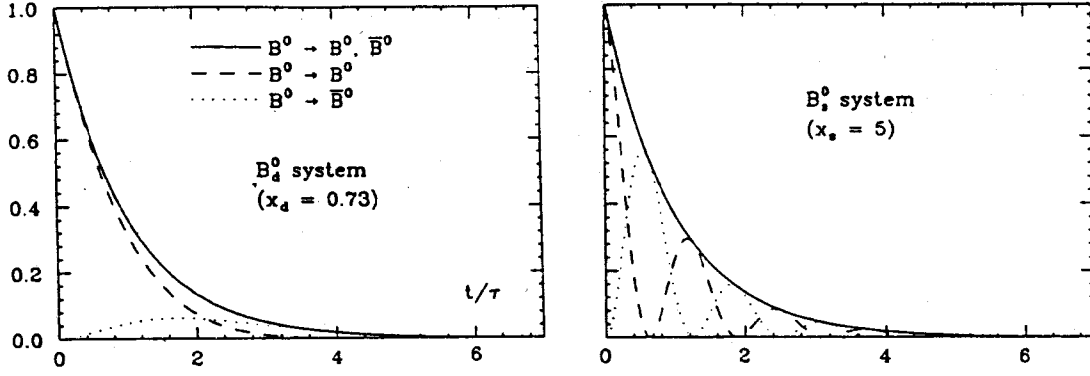


Fig. 2.37: Time evolution for the B_d^0 and B_s^0 system. From [21].

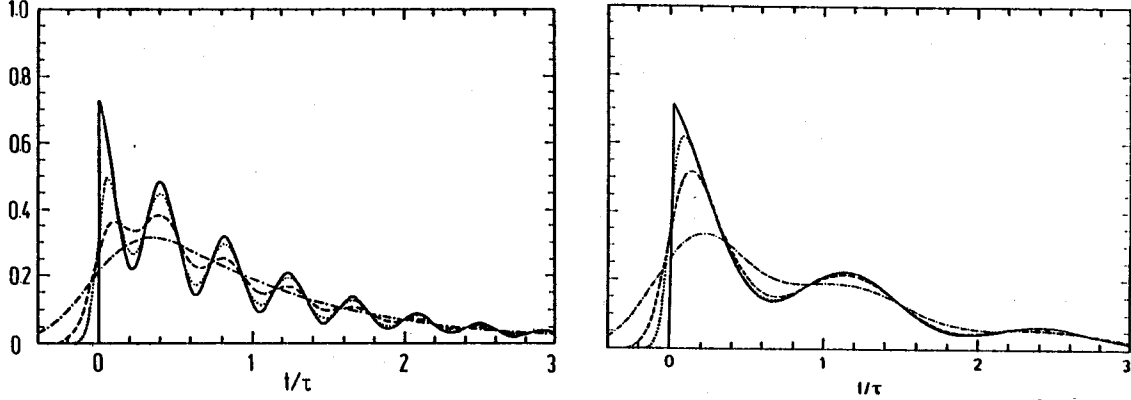


Fig. 2.38: (a) Time evolution for the B_s^0 system for $x_s = 15$ and assuming a 10 % mistagging probability of the sign of the b quark. The full line is the theoretical distribution. The dotted, dashed and dashed-dotted lines are the convolutions with 5, 10 and 25 % experimental resolution on $\frac{\delta t}{\tau}$; from [22]. (b) The same for $x_s = 5$; from [23].

The main contribution comes in the case of semileptonic decays from the uncertainty on the momentum of the B .

Fig. 2.37 shows the corresponding time evolution of B_d^0 mesons. The period of oscillation $T = \frac{2\tau\pi}{x} \sim 9\tau$. After about 2 lifetimes the number of B_d^0 and \bar{B}_d^0 are equal. If one requires the proper decay time to be longer than τ_B , 110 B_d^0 mesons are left. Then the observed mixing is increased and there should be 43 like-sign events. By observing the increasing fraction of mixed events as a function of a cut on the lifetime, one can confirm the time evolution pattern of the B_d^0 meson.

As seen in the theoretical introduction, B_s^0 is expected to be strongly mixed and correspondingly the period of oscillation is expected to be much shorter: $T \sim 1.3\tau$. Fig. 2.37 shows for example the oscillation pattern for $\chi_s = 0.48(x_s = 5)$. The resolution on the proper time becomes a critical parameter to observe those oscillations. Fig. 2.38 shows the expected distribution of events for $\chi_s = 0.498(x_s = 15)$ taking into account a 10 % mistagging probability of the sign of the b quark via the lepton of the other

jet. Fig. 2.38 shows the effect of 5, 10 and 25 % resolution. The resolution expected for semileptonic decays is of the order of 22% which essentially washes out the effect. One has to turn to exclusive hadronic decays for which the momentum of the B is reconstructed and the resolution on the proper time is $\sim 10\%$. $B_s^0 \rightarrow J/\psi \phi$ cannot be used because they do not give the sign of the B. Remain decays like $B_s^0 \rightarrow D_s \pi$. As seen in the lifetime chapter, one expects about 30 such events for $10^7 Z^0$'s. So, how many events can be finally collected will determine what will be the range of sensitivity for the observation of the time evolution pattern in the B_s^0 system.

REFERENCES

- [1] See e.g. K. Kleinknecht, Proceedings of the XXIV International Conference on High Energy Physics (Munich, August 1988);
E.A. Paschos and U. Türke, "Quark mixing and CP violation", to appear in *Phys. Rep.* (1989).
- [2] See e.g. K.R. Schubert, *Progress in Particle and Nuclear Physics*, Vol. 21 (July 1988), and references therein.
- [3] Particle Data Group, *Phys. Lett.* **204 B** (1988) 1.
- [4] J. Hagelin, *Nucl. Phys. B* **193** (1981) 123.
- [5] A. Datta, E.A. Paschos and U. Türke, *Phys. Lett.* **196 B** (1987) 382.
- [6] A. Datta and D. Kumbhakar, *Z. Phys. C* **27** (1985) 515.
- [7] L. Wolfenstein, *Phys. Lett.* **164 B** (1985) 170;
J.F. Donoghue et al., *Phys. Rev. D* **33** (1986) 179;
A.J. Buras and J.-M. Gérard, *Nucl. Phys. B* **264** (1986) 371.
- [8] A. Datta, *Phys. Lett.* **154 B** (1985) 287.
- [9] G.E. Gladding (Mark-III), talk presented at the 2nd Int. Symp. on Production and Decay of Heavy Flavours, Stanford 1987.
- [10] See e.g. S. McHugh, Proceedings of the XXIV International Conference on High Energy Physics (Munich, August 1988).
- [11] H. Albrecht et al. (ARGUS), *Phys. Lett.* **192 B** (1987) 245.
- [12] See e.g. G. Altarelli and P. Franzini, *Z. Phys. C* **37** (1988) 271, and references therein.
- [13] L. Wolfenstein, *Phys. Rev. Lett.* **51** (1983) 1945.
- [14] A.J. Buras and J.-M. Gérard, *Phys. Lett.* **203 B** (1988) 272.
- [15] S. Narison, *Phys. Lett.* **198 B** (1987) 104;
see also C.A. Dominguez and N. Paver, *Phys. Lett.* **197 B** (1987) 423.
- [16] C. Bernard et al., *Phys. Rev. D* **38** (1988) 354.
- [17] M.B. Gavela et al., *Phys. Lett.* **206 B** (1988) 113.
- [18] See e.g. G. Altarelli, CERN preprint TH 4896/87 and references therein.
- [19] J.-M. Gérard, D. London and D. Wyler, in preparation.
- [20] G. Gratta et al., SCIPP88/04.
- [21] P. Krawczyk, D. London and H. Steger, DESY-88-163.
- [22] H. Steger, private communication.

2.9. CP VIOLATION IN B DECAYS*

About 15% of the time, a Z^0 decays into a $b\bar{b}$ final state that evolves into a pair of jets each containing a B-meson or baryon. Such a state may be distinguished from $u\bar{u}$, $d\bar{d}$ and $s\bar{s}$ states by requiring the presence of a prompt lepton in one of the jets, and from $c\bar{c}$ states by requiring that the transverse momentum of the lepton relative to the jet axis be sufficiently large, e.g. $p_\perp > 1\text{GeV}$. Assuming that 50% of the $b\bar{b}$ states survive this cut, and taking 20% as the leptonic branching ratio (e and μ combined) one expects to obtain a sample of 1.5×10^5 leptonically tagged $b\bar{b}$ final states for a total of 10^7 Z^0 's (the statistics aimed for in LEP I), with the charge of the lepton identifying the flavour of the b -quark ($b \rightarrow l^-, \bar{b} \rightarrow l^+$). The question we examine in this note is to what extent this sample might be used to study possible CP violation in the B meson sector.

The Unitarity Triangle

In the standard model with three generations, the nonleptonic Hamiltonian that converts a b -quark into a d -quark may be written as

$$H(b \rightarrow d) = \xi_u H_u + \xi_c H_c + \xi_t H_t \quad (2.201)$$

where $\xi_q = V_{qb} V_{qd}^*$, $q = u, c, t$ and

$$H_q = \frac{G}{\sqrt{2}} [\bar{d}\gamma_\alpha(1 + \gamma_5)q] [\bar{q}\gamma^\alpha(1 + \gamma_5)b]$$

V_{ij} being the elements of the quark mixing matrix. Unitarity of this matrix requires

$$\xi_u + \xi_c + \xi_t = 0 \quad (2.202)$$

which means that the complex numbers ξ_i , treated as vectors in the complex plane, form a closed triangle Fig. 2.39. Knowledge of the length of the three sides (which means knowledge of the moduli $|V_{qb} V_{qd}^*|$ for $q = u, c, t$) fixes the angles of this triangle and hence the relative phase of the coefficients appearing in the Hamiltonian. The occurrence of several pieces in the Hamiltonian with coupling constants complex relative to one another implies CP violation. Invariant measures of the magnitude of CP violation are the sizes of the angles Φ_1, Φ_2, Φ_3 and the area of the triangle

$$\Delta \equiv \frac{1}{2}J = \frac{1}{2}\text{Im}(\xi_c \xi_t^*) = -\frac{1}{2}\text{Im}(\xi_u \xi_t^*) \quad (2.203)$$

In the Wolfenstein representation of the mixing matrix [1],

$$V = \begin{pmatrix} V_{ud} & V_{us} & V_{ub} \\ V_{cd} & V_{cs} & V_{cb} \\ V_{td} & V_{ts} & V_{tb} \end{pmatrix} = \begin{pmatrix} 1 - \frac{1}{2}\lambda^2 & \lambda & A\lambda^3(\rho - i\eta) \\ -\lambda & 1 - \frac{1}{2}\lambda^2 & A\lambda^2 \\ A\lambda^3(1 - \rho - i\eta) & -A\lambda^2 & 1 \end{pmatrix} + O(\lambda^4) \quad (2.204)$$

*L. SEHGAL

and the parameters ξ_i are

$$\xi_c = -A\lambda^3 \quad \xi_u = A\lambda^3(\rho - i\eta) \quad \xi_t = A\lambda^3(1 - \rho + i\eta) \quad (2.205)$$

Thus the unitarity triangle has the form shown in Fig. 2.39, where the sides are measured in units of $A\lambda^3$. The shape of the triangle is defined by the parameters ρ and η . Our empirical knowledge may be summarized in

$$A \approx 1.0 \quad \lambda = 0.22 \quad |\xi_c| = A\lambda^3 \approx 0.01 \quad 0.07 < |\xi_u|/|\xi_c| = \rho + \eta^2 < 1.0$$

where the lower limit in the last line is uncertain. Theoretical attempts to explain CP violation in the K^0 system suggest $\eta \approx 0.4$ (to a factor 2), while attempts to understand the observed $B_d - \bar{B}_d$ mixing show some predilection for $\rho < 0$ [2].

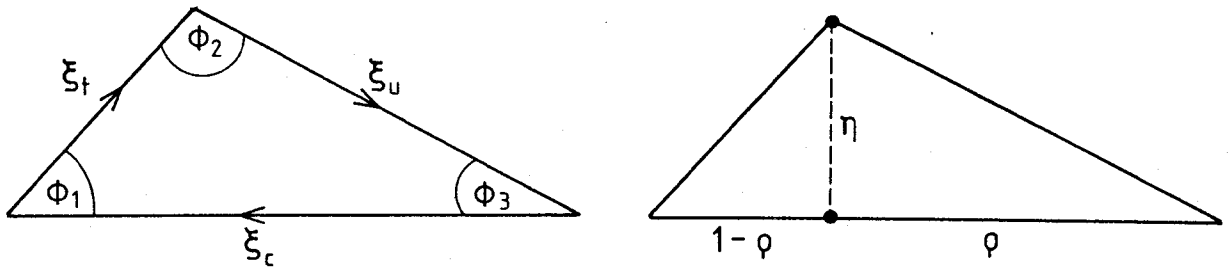


Fig. 2.39: ξ -vectors in the unitarity triangle and Wolfenstein parameters.

CP Violation in the $B^0 - \bar{B}^0$ Mass Matrix

In the presence of CP violation, the mass matrix of the $B^0 - \bar{B}^0$ system has the form

$$\begin{pmatrix} A & p^2 \\ q^2 & A \end{pmatrix} \quad (2.206)$$

with unequal off-diagonal elements, $p \neq q$. As a result, the eigenstates

$$|B_{1,2}\rangle = [p|B^0\rangle \pm q|\bar{B}^0\rangle]/(|p|^2 + |q|^2)^{1/2} \quad (2.207)$$

are not eigenstates of CP. A measure of CP violation in the mass matrix is

$$\langle B_1|B_2\rangle = \frac{|p|^2 - |q|^2}{|p|^2 + |q|^2} \quad (2.208)$$

which is an observable quantity (see next section).

The parameter $\langle B_1|B_2\rangle$ can be calculated with the help of the Bell-Steinberger relation

$$\left(\frac{\Gamma_1 + \Gamma_2}{2} + i \Delta M\right) \langle B_1|B_2\rangle = \sum \langle F|T|B_2\rangle^* \langle F|T|B_1\rangle \quad (2.209)$$

where $\Gamma_{1,2}$ are the widths of $B_{1,2}$ and $\Delta M = M_2 - M_1$.

Taking the imaginary part, we have

$$\Delta M \langle B_1 | B_2 \rangle = \sum 2 \text{Im}(q^* p \bar{A}_F^* A_F) \quad (2.210)$$

where $A_F \equiv \langle F | T | B^0 \rangle$, and where we have used the normalization $|p|^2 + |q|^2 = 1$. Choosing the states F to be CP eigenstates, and anticipating $|p|^2 \approx |q|^2 \approx \frac{1}{2}$,

$$\Delta M \langle B_1 | B_2 \rangle = \sum_F |A_F|^2 \text{Im} \left(\frac{p}{q} \frac{A_F}{A_F^*} \right) \quad (2.211)$$

This equation may be regarded as a sum rule that relates CP violation in the $B^0 - \bar{B}^0$ mass matrix (the parameter $\langle B_1 | B_2 \rangle$) to CP violation in exclusive decay channels. The factors $\text{Im} \left(\frac{p}{q} \frac{A_F}{A_F^*} \right)$ are observables that are related to the asymmetry between exclusive processes $B^0 \rightarrow F$ and $\bar{B}^0 \rightarrow F$ (see Sec.5), and $|A_F|^2$ is the partial decay rate of $B^0 \rightarrow F$. Because of the large number of decay channels F , and the fact that the exclusive asymmetry changes sign from channel to channel, one must expect that the sum in eq. (211) is small.

A theoretical formula for $\langle B_1 | B_2 \rangle$ may be obtained by noting that for CP eigenstates F , the factor $\text{Im} \left(\frac{p}{q} \frac{A_F}{A_F^*} \right)$ is essentially determined by the parameters of the unitarity triangle. Because of the dominance of the top quark contribution to the off-diagonal elements of the $B^0 - \bar{B}^0$ mass matrix, the factor p/q is essentially the phase factor ξ_t/ξ_t^* . Likewise, the factor A_F/A_F^* is a pure phase factor given by [3]

$$\frac{A_F}{A_F^*} = \begin{cases} (\xi_c^*/\xi_c) \eta_F & \text{(A)} \\ (\xi_u^*/\xi_u) \eta_F & \text{(C)} \end{cases} \quad (2.212)$$

where the two results refer to decays induced by the quark transitions $b \rightarrow c + \bar{c} + d$ (class A) and $b \rightarrow u + \bar{u} + d$ (class C). The factor η_F takes values $+1(-1)$ for CP even (odd) final states, and expresses the fact that the exclusive asymmetry changes sign with the CP eigenvalue of the state F . Finally, the contribution of decays which are induced by the quark transitions $b \rightarrow c + \bar{u} + d$ or $b \rightarrow u + \bar{c} + d$ (class B) can be related to that of class A and class C by exploiting the unitarity property

$$\text{Im} \left(\frac{2\xi_u \xi_c}{\xi_t^2} \right) = -\text{Im} \left(\frac{\xi_u}{\xi_t} \right)^2 - \text{Im} \left(\frac{\xi_c}{\xi_t} \right)^2 \quad (2.213)$$

In this manner, Altomari, Wolfenstein and Bjorken (AWB) [4] have derived the result

$$\begin{aligned} \langle B_1 | B_2 \rangle = \frac{\Gamma_0}{\Delta M} & \left[\{ \rho_A \langle CP \rangle_A - \rho_B \langle CP \rangle_B \} |\xi_c|^2 \text{Im} \left(\frac{\xi_t}{\xi_t^*} \frac{\xi_c}{\xi_c^*} \right) \right. \\ & \left. + \{ \rho_C \langle CP \rangle_C - \rho_B \langle CP \rangle_B \} |\xi_u|^2 \text{Im} \left(\frac{\xi_t}{\xi_t^*} \frac{\xi_u}{\xi_u^*} \right) \right] \end{aligned} \quad (2.214)$$

In the above expression ρ_A, ρ_B and ρ_C are (relative) phase space factors describing the three classes of quark decay (with numerical values $\rho_A = 0.12, \rho_B = 0.44, \rho_C = 0.99$) and $\langle CP \rangle_A, \langle CP \rangle_B$ and $\langle CP \rangle_C$ denote the average value of CP in the three classes. The parameter Γ_0 is defined by

$$\Gamma_B = \Gamma_0 |V_{cb}|^2 |V_{ud}|^2 \rho_B \quad (2.215)$$

and may be related to the total decay width Γ by noting that class B decays account for about 55% of all B decays, i.e.

$$\Gamma_0 = \frac{0.55\Gamma}{|V_{cb}|^2 |V_{ud}|^2 \rho_B} \quad (2.216)$$

Using the empirical value $\Delta M/\Gamma = 0.7^*$ deduced from the measurements of $B_d - \bar{B}_d$ mixing, and $|\xi_c|^2/|V_{cb}|^2 = \lambda^2 \approx 0.05$ we get

$$\begin{aligned} \langle B_1|B_2 \rangle = 0.09 & \left[\{ \rho_A \langle CP \rangle_A - \rho_B \langle CP \rangle_B \} \text{Im} \left(\frac{\xi_t \xi_c^*}{\xi_t^* \xi_c} \right) \right. \\ & \left. + \{ \rho_C \langle CP \rangle_C - \rho_B \langle CP \rangle_B \} \left| \frac{\xi_u}{\xi_c} \right|^2 \text{Im} \left(\frac{\xi_t \xi_u^*}{\xi_t^* \xi_u} \right) \right] \end{aligned} \quad (2.217)$$

The factors $\text{Im} \left(\frac{\xi_t \xi_c^*}{\xi_t^* \xi_c} \right)$ and $\text{Im} \left(\frac{\xi_t \xi_u^*}{\xi_t^* \xi_u} \right)$ have a simple interpretation in terms of the angles of the unitarity triangle in Fig. 2.39a or the ρ, η parameters of Fig. 2.39b:

$$\begin{aligned} \text{Im} \left(\frac{\xi_t \xi_c^*}{\xi_t^* \xi_c} \right) &= \sin 2\Phi_1 = 2\eta K \\ \text{Im} \left(\frac{\xi_t \xi_u^*}{\xi_t^* \xi_u} \right) &= \sin 2\Phi_2 = \frac{2\eta}{\eta^2 + \rho^2} (K - 1) \end{aligned} \quad (2.218)$$

with $K = (1 - \rho)/[(1 - \rho)^2 + \eta^2]$. Thus alternative expressions for $\langle B_1|B_2 \rangle$ are

$$\begin{aligned} \langle B_1|B_2 \rangle = 0.09 & \left[\{ \rho_A \langle CP \rangle_A - \rho_B \langle CP \rangle_B \} \sin 2\Phi_1 \right. \\ & \left. + \{ \rho_C \langle CP \rangle_C - \rho_B \langle CP \rangle_B \} \left| \frac{\xi_u}{\xi_c} \right|^2 \sin 2\Phi_2 \right] \end{aligned} \quad (2.219)$$

or

$$\begin{aligned} \langle B_1|B_2 \rangle = 0.18\eta & \left[\{ \rho_A \langle CP \rangle_A - \rho_B \langle CP \rangle_B \} K \right. \\ & \left. + \{ \rho_C \langle CP \rangle_C - \rho_B \langle CP \rangle_B \} (K - 1) \right] \end{aligned} \quad (2.220)$$

The structure of this formula shows that in the limit $m_c \rightarrow m_u$, $\langle B_1|B_2 \rangle$ vanishes, since in that limit all the ρ_i and all the $\langle CP \rangle_i$ become equal.

A calculation of $\langle B_1|B_2 \rangle$ was carried out by Hagelin [5] by considering the absorptive part of the box diagram for the $B^0 - \bar{B}^0$ transition. In such a model, the decays of the

*The sign of $\Delta M/\Gamma$ is not empirically determined.

B -meson into (real) hadronic final states are simulated by two-quark ($B^0 \rightarrow q\bar{q}$) and four-quark ($B^0 \rightarrow q\bar{q}q\bar{q}$) amplitudes. In the notation of eqs. (219, 220), this model yields

$$\rho_A \langle CP \rangle_A - \rho_B \langle CP \rangle_B = -[\rho_C \langle CP \rangle_C - \rho_B \langle CP \rangle_B] = -\frac{m_c^2}{m_b^2} \rho_C \langle CP \rangle_C$$

$$\rho_C \langle CP \rangle_C = 8\pi^2 f_B^2 \frac{m_B}{m_b^3} \quad (2.221)$$

and in consequence

$$\langle B_1 | B_2 \rangle = -0.18\eta(m_c^2/m_b^2)(8\pi^2 f_B^2 \frac{m_B}{m_b^3}) = -0.18\eta(0.11)(0.06) = -1.2\eta * 10^{-3} \quad (2.222)$$

It is clear from the above that the small value of $\langle B_1 | B_2 \rangle$ in the box-diagram calculation is in part the result of a cancellation between the two terms in eqs. (219, 220). In view of this, one can ask whether a more realistic treatment of the hadronic final states can yield a significantly larger value. For an alternative estimate, we assume (with AWB) that the dominant contribution to $\langle B_1 | B_2 \rangle$ comes from class A decays. Because the multi-meson states have alternating CP eigenvalues, they contribute to $\langle B_1 | B_2 \rangle$ with alternating signs. It is thus conceivable that the main contribution is that of the two-body decay channels $B \rightarrow D\bar{D}, B \rightarrow D\bar{D}^*, B \rightarrow \bar{D}D^*$ which are CP even, and $B \rightarrow D^*\bar{D}^*$ which is predominantly so. Referring to eq. (211), we then obtain

$$\langle B_1 | B_2 \rangle = \left(\frac{\Gamma}{\Delta M} \right) \left(\frac{\Gamma(D\bar{D}, D\bar{D}^*, \bar{D}D^*, D^*\bar{D}^*)}{\Gamma} \right) \sin 2\Phi_1$$

$$\approx \left(\frac{1}{0.7} \right) (1.5 * 10^{-3}) \sin 2\Phi_1 \approx 2 * 10^{-3} \sin 2\Phi_1 \quad (2.223)$$

where the two body branching ratio has been taken from Ref. 6. Comparing with eq. (222), we see that while the sign of $\langle B_1 | B_2 \rangle$ is uncertain, $|\langle B_1 | B_2 \rangle| \approx 10^{-3}$ is a reasonable order of magnitude.

Finally we ask what the analogous quantity $\langle B_1 | B_2 \rangle$ is for the $B_s - \bar{B}_s$ system. The essential difference arises from the fact that the factor ΔM appearing in eq. (214) is much larger for B_s than for B_d :

$$(\Delta M)_{B_s} \approx \frac{1}{\lambda^2} (\Delta M)_{B_d} \quad (2.224)$$

The box diagram calculation for $\langle B_1 | B_2 \rangle$ yields [7]

$$\langle B_1 | B_2 \rangle_s \approx -\left| \frac{V_{td}}{V_{ts}} \right|^2 \langle B_1 | B_2 \rangle_d \quad (2.225)$$

suggesting that $\langle B_1 | B_2 \rangle_s$ has an order of magnitude 10^{-4} , and the opposite sign to $\langle B_1 | B_2 \rangle_d$.

Dilepton Asymmetry

As a consequence of CP violation, the probability that a B^0 state evolves into a \bar{B}^0 state differs from the reverse probability for \bar{B}^0 to evolve into B^0 . Integrated over time, these probabilities are

$$\begin{aligned} P &\equiv \text{Prob}(B^0 \rightarrow \bar{B}^0) = \left| \frac{q}{p} \right|^2 \chi \\ \bar{P} &\equiv \text{Prob}(\bar{B}^0 \rightarrow B^0) = \left| \frac{p}{q} \right|^2 \chi \end{aligned} \quad (2.226)$$

where χ is the $B^0 - \bar{B}^0$ mixing parameter given approximately by

$$\chi = \frac{x^2}{2(1+x^2)} \quad x \equiv \frac{\Delta M}{\Gamma} \quad (2.227)$$

For the $B_d - \bar{B}_d$ system, experiments have determined $\chi_d = 0.17$, while for the $B_s - \bar{B}_s$ system, one expects essentially a maximal value $\chi_s \approx 0.5$.

The difference between P and \bar{P} manifests itself in unequal probabilities for like-sign leptons l^+l^+ and l^-l^- emanating from a $B_d\bar{B}_d$ or $B_s\bar{B}_s$ system. The dilepton asymmetry is

$$a_{ll} = \frac{N(l^+l^+) - N(l^-l^-)}{N(l^+l^+) + N(l^-l^-)} = \frac{\bar{P} - P}{\bar{P} + P} = \frac{\left| \frac{p}{q} \right|^2 - \left| \frac{q}{p} \right|^2}{\left| \frac{p}{q} \right|^2 + \left| \frac{q}{p} \right|^2} \approx 2\langle B_1|B_2 \rangle \quad (2.228)$$

and so is just twice the parameter $\langle B_1|B_2 \rangle$ describing CP violation in the mass matrix.

In the LEP experiment, the source of B -mesons is the reaction $e^+e^- \rightarrow b\bar{b}$, in which the b and \bar{b} quarks fragment independently into various species of mesons or baryons. Each of these varieties has a probability of decaying leptonically. In the case of charged B -mesons or b -baryons, the sign of the lepton is uniquely determined by the rule $b \rightarrow l^-$ and $\bar{b} \rightarrow l^+$. For neutral B -mesons (B_d and B_s), however, mixing can result in leptons of the "wrong" sign. Assuming that a \bar{b} -quark fragments into mesons and baryons with the probabilities $[\sum_i f_i = 1]$

$$B_u : B_d : B_s : B_{bary} = f_u : f_d : f_s : f_{bary}$$

and assuming a common semileptonic branching ratio β_{sl} for all species, the number of like sign leptons per produced $b\bar{b}$ is

$$\begin{aligned} \frac{N(l^+l^+)}{N(b\bar{b})} &= (f_d\bar{P}_d + f_s\bar{P}_s)(1 - f_d\chi_d - f_s\chi_s)\beta_{sl}^2 \\ \frac{N(l^-l^-)}{N(b\bar{b})} &= (f_dP_d + f_sP_s)(1 - f_d\chi_d - f_s\chi_s)\beta_{sl}^2 \end{aligned} \quad (2.229)$$

The dilepton asymmetry is therefore

$$a_{ll} = \frac{f_d(\bar{P}_d - P_d) + f_s(\bar{P}_s - P_s)}{f_d(\bar{P}_d + P_d) + f_s(\bar{P}_s + P_s)} \quad (2.230)$$

Using the results eq. (226) and eq. (228), this may be rewritten as

$$a_{ll} \approx a_d W_d + a_s W_s$$

where

$$W_d = \frac{f_d \chi_d}{f_d \chi_d + f_s \chi_s}, \quad W_s = \frac{f_s \chi_s}{f_d \chi_d + f_s \chi_s} \quad (2.231)$$

Using the values $f_d = 0.4$, $f_s = 0.15$, $\chi_d = 0.17$, $\chi_s = 0.5$, we have $W_d = 0.47$, $W_s = 0.53$. Thus the predicted dilepton asymmetry is the average of a_d and a_s with nearly equal weights, with an expected magnitude of about 10^{-3} in the standard theory.

From eq. (229), we see that the expected rate of like sign leptons is

$$\frac{N(l^+ l^+)}{N(b\bar{b})} \approx \frac{N(l^- l^-)}{N(b\bar{b})} = \beta_{sl}^2 \bar{\chi} (1 - \bar{\chi}) \quad (2.232)$$

where $\bar{\chi} = f_d \chi_d + f_s \chi_s$. With a semileptonic branching ratio of 20% (e and μ combined), and taking $N(b\bar{b})/N(Z^0) = 0.15$, we expect for a total of $10^7 Z^0$'s, $N(l^+ l^+) \approx N(l^- l^-) \approx 3600$. Thus the asymmetry accessible at LEP is

$$a_{LEP} = \begin{cases} 1.7\% & (1\sigma) \\ 5\% & (3\sigma) \end{cases} \quad (2.233)$$

where we have assumed the formula $n/\sqrt{N(l^+ l^+)}$ for an $n\sigma$ -effect. While this is an order of magnitude larger than the standard theoretical expectation, it represents a physically interesting goal for CP-violation studies at LEP.

Asymmetries in Exclusive Channels

Neutral B Decays

CP violation can manifest itself as an asymmetry in the exclusive decays of B^0 and \bar{B}^0 into a common final state F . In particular, if the state F is an eigenstate of CP, the time-dependent decay rate of an initial B^0 or \bar{B}^0 system is

$$\begin{aligned} \text{Rate}(B^0(t) \rightarrow F) &= e^{-\Gamma t} \left[1 - \text{Im} \left(\frac{p}{q} \frac{A_F^*}{A_F} \right) \sin \Delta M t \right] \\ \text{Rate}(\bar{B}^0(t) \rightarrow F) &= e^{-\Gamma t} \left[1 + \text{Im} \left(\frac{p}{q} \frac{A_F^*}{A_F} \right) \sin \Delta M t \right] \end{aligned} \quad (2.234)$$

giving rise to a time-integrated asymmetry

$$\text{Asym}(F) = \frac{\Gamma(B \rightarrow F) - \Gamma(\bar{B} \rightarrow F)}{\Gamma(B \rightarrow F) + \Gamma(\bar{B} \rightarrow F)} = \frac{x}{1+x^2} \text{Im} \left(\frac{p}{q} \frac{A_F}{A_F^*} \right) \quad (2.235)$$

As discussed in the previous section for decays induced by the quark transitions $b \rightarrow c + \bar{c} + d$ and $b \rightarrow u + \bar{u} + d$, the factor $\text{Im} \left(\frac{p}{q} \frac{A_F}{A_F^*} \right)$ has a simple interpretation:

$$\text{Im} \left(\frac{p}{q} \frac{A_F}{A_F^*} \right) = \begin{cases} \eta_F \sin 2\Phi_1 & \text{for } b \rightarrow c + \bar{c} + d \\ \eta_F \sin 2\Phi_2 & \text{for } b \rightarrow u + \bar{u} + d \end{cases} \quad (2.236)$$

where η_F is the CP eigenvalue of the state F and $\Phi_{1,2}$ are angles of the unitarity triangle. Further, the parameter x has the value $x_d = 0.7$ for B_d decays and an expected value $x_s \sim 10 - 20$ for B_s decays. Thus significant asymmetries are possible, especially for B_d .

In assessing the prospects for measuring an exclusive asymmetry, one needs to know the branching ratio of decay channels that can be reached via the above quark transitions, and that are eigenstates of CP. One must also take into account the efficiency for detecting the decay mode, since some of the particles in the final state may only be observable through decays that have limited branching ratios. One must also keep in mind that the identification of an exclusive decay requires detection of a vertex, which is only possible with limited efficiency.

In Tab. 2.25 we have listed some characteristic decay channels for B_d and B_s together with branching ratios taken from Ref. 6, and a crude estimate of efficiency. Channels with a $J/\psi, \phi$ or a K_s in the final state have obvious advantages from the point of view of experimental detectability. As can be seen from the Table, however, the event rates for $10^7 Z^0$'s, in exclusive decay modes, are exceedingly small, and do not engender optimism about the detectability of exclusive asymmetries in the B_d^0 and B_s^0 systems.

Charged B Decays

CP-violating asymmetries are also possible in the decays of charged B -mesons in exclusive modes. If a transition $B^+ \rightarrow f^+$ is mediated by an effective Hamiltonian consisting of two pieces,

$$H = g_1 H_1 + g_2 H_2 \quad (2.237)$$

where g_1 and g_2 are complex relative to one another (as for example in eq. (201), the decay amplitude will have the form

$$A(B^+ \rightarrow f^+) = g_1 A_1 e^{i\alpha_1} + g_2 A_2 e^{i\alpha_2} \quad (2.238)$$

where A_1, A_2 are real and the phase factors $e^{i\alpha_1}, e^{i\alpha_2}$ represent the effects of strong final state interaction. CPT invariance dictates that the amplitude for the conjugate process $B^- \rightarrow f^-$ is

$$A(B^- \rightarrow f^-) = g_1^* A_1 e^{i\alpha_1} + g_2^* A_2 e^{i\alpha_2} \quad (2.239)$$

so that one expects an asymmetry in the decay rates

$$A_{sym} = \frac{2A_1 A_2 \text{Im}(g_1^* g_2) \sin(\alpha_1 - \alpha_2)}{|g_1|^2 A_1^2 + |g_2|^2 A_2^2 + 2A_1 A_2 \text{Re}(g_1^* g_2) \cos(\alpha_1 - \alpha_2)} \quad (2.240)$$

The factor $\text{Im}(g_1^* g_2)$ is given by the parameters of the Hamiltonian (e.g. by the unitarity triangle) while the factor $\sin(\alpha_1 - \alpha_2)$ depends on strong interaction phase shifts. The latter are, in general, unknown but have no reason to be negligible. Thus a sizable

Tab. 2.25: Expected Rates and Asymmetries for Exclusive B Decays.

	Quark Transit.	Decay Channel	Branch. Ratio ^(a)	Efficiency ^(b)	#Events $10^7 Z^0_{(c)}$	Expected Asymmetry
B_d	$b \rightarrow c\bar{c}s$	$J/\psi \bar{K}^0$	$0.8 * 10^{-4}$	4%	0.2	$\sim 0.5 \sin 2\Phi_1$
		$J/\psi \bar{K}^{0*}$	$3.6 * 10^{-4}$	4%	0.9	
B_d	$b \rightarrow c\bar{c}d$	$J/\psi \rho$	$8 * 10^{-6}$	14%	0.07	$\sim 0.5 \sin 2\Phi_1$
		$D^+ D^-$	$3 * 10^{-4}$	0.6%	0.1	
B_d	$b \rightarrow c\bar{u}s$	$(D^0/\bar{D}^0)K_s \rightarrow K_s \pi^0 K_s$	$\sim 10^{-4}$	$\sim 1\%$	~ 0.06	$\sim 0.5 * \sin(\Phi_1 - \Phi_2)$
B_s	$b \rightarrow c\bar{c}s$	$J/\psi \phi$	$2.4 * 10^{-4}$	7%	1.0	$O(1\%)$
		$D_s \bar{D}_s$	$0.5 * 10^{-2}$	0.16%	0.2	
B_s	$b \rightarrow c\bar{u}s$	$(D^0/\bar{D}^0)\phi \rightarrow K_s \pi^0 \phi$	10^{-5} -10^{-4}	0.5%	0.001 -0.01	$\sim 0.1 \sin \Phi_3$
B^\pm	$b \rightarrow c\bar{c}s$	$J/\psi K^-$	$0.8 * 10^{-4}$	14%	3.3*	?
		$J/\psi K^{*-}$	$3.6 * 10^{-4}$	4%	4.3*	
B^\pm	$b \rightarrow c\bar{c}d$	$J/\psi \rho^-$	$1.6 * 10^{-5}$	14%	0.7*	?
		$J/\psi \pi^-$	$0.4 * 10^{-5}$	14%	0.2*	
B^\pm	$b \rightarrow c\bar{u}s$	$B^- \rightarrow D^0 K^-$	$5 * 10^{-4}$	1%	0.3	?

(a) From Ref.7

(b) Includes $BR(K^0 \rightarrow \pi^+ \pi^-) = 30\%$, $BR(J/\psi \rightarrow e^+ e^- + \mu^+ \mu^-) = 14\%$, $BR(D^- \rightarrow K^- \pi^+ \pi^-) = 8\%$, $BR(D^0 \rightarrow \bar{K}^0 \pi^0) = 3\%$, $BR(D_s \rightarrow \phi \pi^+) = 8\%$, $BR(\phi \rightarrow K^+ K^-) = 50\%$.

(c) Based on $f_u = f_d = 0.4$, $f_s = 0.15$ and lepton-tagging factor of 10%.

* Without requirement of lepton in opposite side jet.

asymmetry is possible in cases where the interfering amplitudes $g_1 A_1$ and $g_2 A_2$ are of comparable size.

Channels that are theoretically interesting are "charmless" decay modes such as $B^\pm \rightarrow K^\pm \phi$ or $B^\pm \rightarrow p\bar{p}\pi^\pm$ [8]. However with expected branching ratios of $\sim 10^{-4}$ and expected asymmetries at the 1% level, no useful signal can be expected at LEP. From the point of view of observability, the decays $B^\pm \rightarrow J/\psi K^\pm$ and $B^\pm \rightarrow J/\psi K^{*\pm}$ are attractive (see Tab. 2.25). It should be noted that charged B -mesons are self-tagging, in the sense that the total charge of the decay products identifies the meson as being B^+ or B^- . Further, the occurrence of a J/ψ with a clearly separated vertex is a unique signal of B -decay, and obviates the need for a leptonic tag in the opposite-side jet. Because of this, event numbers of the order of 1 – 10 are possible in channels containing a J/ψ .

Nevertheless, the prospects of a meaningful CP-violating measurement are poor, especially so when one considers that the asymmetries expected from eq. (240) are unlikely to exceed a few percent.

Conclusion

The decays of $10^7 Z^0$'s at LEP will deliver a sample of about $1.5 * 10^5$ events that can be associated with $Z^0 \rightarrow b\bar{b}$, with one of the jets containing a lepton. This sample is expected to contain about 7200 same-sign dilepton events, divided about equally between l^+l^+ and l^-l^- . A measurement of the asymmetry between l^+l^+ and l^-l^- is a measure of the parameter $\langle B_1|B_2 \rangle$ describing CP-violation in the mass matrix of the $B_d - \bar{B}_d$ and $B_s - \bar{B}_s$ systems, and could detect a non-zero value at the level of $\langle B_1|B_2 \rangle \approx 0.01$. Exclusive B -decays can also be searched for, but the level of statistics will be at best 1-10 events per channel. Based on these estimates, CP-violating exclusive asymmetries require an increase of the luminosity to at least $10^8 Z$ decays.

REFERENCES

- [1] L.Wolfenstein, *Ann.Rev.Nucl.Part.Sci.* **36** (1986) 137.
- [2] A.J. Buras and J.-M. Gérard, *Phys. Lett.* **203 B** (1988) 272.
- [3] I.Bigi, V.A.Khoze, N.G.Uraltsev and A.I.Sanda, in "CP Violation", Ed. C.Jarlskog (World Scientific, Singapore).
- [4] T.Altomari, L.Wolfenstein and J.D.Bjorken, *Phys. Rev. D* **37** (1988) 1860.
- [5] J.S.Hagelin, *Nucl. Phys. B* **153** (1981) 123.
- [6] M.Bauer, B.Stech and M.Wirbel, *Z. Phys. C* **34** (1987) 103.
- [7] M.Lusignoli, *Z. Phys. C* **41** (1989) 645.
- [8] S.Barshay, E.Eich and L.M.Sehgal, *Phys. Lett.* **202 B** (1988) 402;
G.Eilam, M.Gronau, J.L.Rosner, *Phys. Rev. D* **39** (1989) 819;
J.-M. Gerard and Wei-Shu-Hou, *Phys. Rev. Lett.* **62** (1989) 855.

3. Top and Toponium*

At the time of writing it is not excluded with absolute certainty that a top quark will be found in the energy range of LEP. The search for a heavy quark will therefore be an obvious task also during the early stages of LEP. Furthermore top might decay dominantly into a charged Higgs which would prevent detection at hadron colliders. A number of questions can exclusively be studied at an e^+e^- collider: the precise determination of the top meson mass, a measurement of the weak couplings through production rates and angular distributions of the decay products and the exploration of the interquark potential at short distances through toponium spectroscopy. Detailed studies concerned with theoretical [1, 2] and experimental [3, 4, 5] aspects of open top production in e^+e^- collisions at the Z resonance and beyond have been published earlier. In this chapter we will therefore focus on the basics of standard top production and decay, together with some more exotic possibilities which are at present the exclusive domain of e^+e^- colliders.

3.1. TOP IN THE CONTINUUM

3.1.1. PRODUCTION

The production cross section of a heavy quark is given by eq. (1) in Born approximation with the weak couplings chosen appropriately:

$$\begin{aligned}\sigma &= \beta \frac{3 - \beta^2}{2} \sigma^{VV} + \beta^3 \sigma^{AA} \\ &= \sigma_B^V + \sigma_B^A\end{aligned}\tag{3.1}$$

where

$$\begin{aligned}\sigma^{VV} &= \frac{4\pi\alpha^2(m_Z^2)e_e^2e_Q^2}{s} + \frac{G_\mu\alpha(m_Z^2)}{\sqrt{2}} e_e e_Q v_e v_Q \frac{m_Z^2(s - m_Z^2)}{(s - m_Z^2)^2 + (\frac{s}{m_Z}\Gamma_Z)^2} \\ &\quad + \frac{G_\mu^2}{32\pi}(v_e^2 + a_e^2)v_Q^2 \frac{m_Z^4 s}{(s - m_Z^2)^2 + (\frac{s}{m_Z}\Gamma_Z)^2} \\ \sigma^{AA} &= \frac{G_\mu^2}{32\pi}(v_e^2 + a_e^2)a_Q^2 \frac{m_Z^4 s}{(s - m_Z^2)^2 + (\frac{s}{m_Z}\Gamma_Z)^2}\end{aligned}\tag{3.2}$$

Γ includes the $t\bar{t}$ channel [see the first section].

QCD corrections are far more important than in the case of light quarks as a consequence of the $1/\beta$ Coulomb singularity which predicts a step function for the vector part of the rate close to threshold. The exact formulas are given in chapter 2, compact

*J.H. Kühn, P.M. Zerwas

approximations [6, 7] read

$$r_V = \beta \frac{(3 - \beta^2)}{2} \left[1 + \frac{4}{3} \alpha_s \left(\frac{\pi}{2\beta} - \frac{3 + \beta}{4} \left(\frac{\pi}{2} - \frac{3}{4\pi} \right) \right) \right]$$

$$r_A = \beta^3 \left[1 + \frac{4}{3} \alpha_s \left(\frac{\pi}{2\beta} - \left(\frac{19}{10} - \frac{22}{5} \beta + \frac{7}{2} \beta^2 \right) \left(\frac{\pi}{2} - \frac{3}{4\pi} \right) \right) \right] \quad (3.3)$$

The evaluation of these formulas close to threshold is subject to various uncertainties: For s far larger than $4m^2$ the difference between energy and momentum for the scale μ of $\alpha_s(\mu^2)$ is unimportant. When approaching the threshold region, the choice $\mu^2 = 4\vec{p}^2$ mimics the onset of the nonperturbative behaviour. Close to threshold only the vector piece remains, with the axial vector part suppressed $\propto \beta^2$. The yet uncalculated higher order corrections are expected to alter the $\mathcal{O}(\alpha_s)$ result significantly in the region where the first order correction exceeds the Born term, i.e. up to ~ 4 GeV above threshold. Summing up higher order corrections in analogy to QED [8] would suggest for the correction factor [9] $r_V \rightarrow z/(1 - e^{-z})$ with $z = \frac{4\pi}{3} \frac{\alpha_s}{\beta}$. However, a perturbative treatment based on a Coulombic potential seems disputable in a region where nonperturbative effects from the long range part of the potential cannot be ignored. Here a pragmatic approach [7] is advocated which is based on local duality: The averaged densely spaced high radial excitations below and above threshold are well reproduced by the QCD corrected cross section eqs. (1, 3) with $m_t = m_T - 400$ MeV and the running coupling constant $\alpha_s(\vec{p}^2)$. The interpolation is adequate down to the low-lying resonances — in regions where purely perturbative arguments are bound to fail. The resulting cross section is shown in Fig. 3.1 as a function of \sqrt{s} for $m_t = 55$ GeV. The figure demonstrates that the prescription of eq. (3) provides an adequate description of the $t\bar{t}$ threshold region.

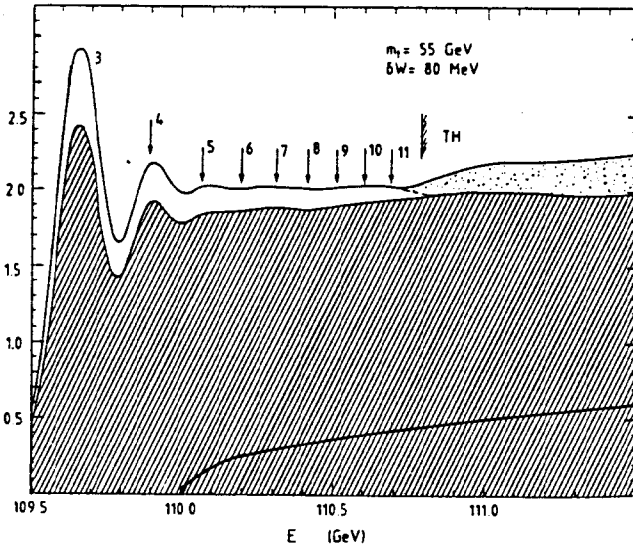


Fig. 3.1: Threshold for $m_t = 55$ GeV. Dashed area: fraction of SQD events. The contribution from the axial-vector current is indicated by the dotted area. The solid line within the shaded region corresponds to the parton term without QCD corrections. The difference between the upper and lower lines characterizes the change of the fermion/antifermion cross section alone.

Genuine electroweak corrections have to be evaluated separately for $e^+e^- \rightarrow t\bar{t}$ as a consequence of the large top mass. The resulting decay rates are expected to differ

less than $\mathcal{O}(1\%)$ from the lowest order prediction. These differences will presumably be masked by the uncertainties resulting from higher order perturbative and nonperturbative QCD corrections. QED corrections are given by eq. (3) with $\frac{4}{3}\alpha_s \rightarrow \alpha$ and can be ignored for all practical purposes, except for initial state radiation which has to be treated in the usual way.

The opening of a new channel broadens the Z width. As a result of unitarity,

$$\sigma_X = \frac{12\pi}{m_Z^2} \frac{\Gamma_{ee}\Gamma_X}{\Gamma_{tot}^2}$$

this leads to a slight decrease of the hadronic cross section on top of the Z peak

$$\frac{\delta\sigma(had)}{\sigma(had)} = (1 - 2B_h) \frac{\delta\Gamma_h}{\Gamma_h} \approx -0.4 \frac{\delta\Gamma_h}{\Gamma_h} \quad (3.4)$$

and to a sizeable effect on the μ -pair (or any other leptonic) rate

$$\frac{\delta\sigma(\mu^+\mu^-)}{\sigma(\mu^+\mu^-)} = -2 \frac{\delta\Gamma_h}{\Gamma} \quad (3.5)$$

In this way one can get first indications of a new heavy quark independent of its decay mode through a measurement of leptonic or hadronic cross sections or their ratio.

Eqs. 2.21-2.28 can be used also for top quarks to predict the *angular distribution* of the quark and the forward backward asymmetry in Born approximation. The QCD correction to the forward backward asymmetry can be found in Ref. 11. In passing we note that a full understanding of t quark production (including polarization) and decay mechanism (in particular the angular and energy distribution of the lepton) is required to deduce m_t [1] or A_{FB} [2] from the decay products.

Top quarks are produced with a high degree of *polarization*. The polarization vector lies in the t production plane. The longitudinal component is generally large for $2m_t$ not too close to m_Z . More details can be found in [1] including a discussion of the small normal component induced by $\gamma - Z$ interference effects and QCD radiative corrections.

3.1.2. TOP DECAY IN THE STANDARD MODEL

a) Decay rate

The decay of top mesons has been treated entirely on the basis of the spectator model. Neglecting lepton masses, the semileptonic decay rate in Born approximation reads [12]

$$\Gamma_{SQD} = \frac{G_F^2 m_t^5}{192\pi^3} f\left(\frac{m_t^2}{M_W^2}, \frac{m_b^2}{m_t^2}\right) \quad (3.6)$$

where

$$f(\rho, \mu) = 2 \int_0^{(1-\sqrt{\mu})^2} \frac{dz}{(1-z\rho)^2 + (\Gamma_W/M_W)^2} \cdot [(1-\mu)^2 + z(1+\mu) - 2z^2][1 + \mu^2 + z^2 - 2(\mu z + \mu + z)]^{1/2}$$

$$= \begin{cases} 2\rho^{-4} [6(\rho + (1-\rho)\log(1-\rho)) - 3\rho^2 - \rho^3] & \text{if } \mu = 0 \\ (1-\mu^2)(1-8\mu+\mu^2) - 12\mu^2\log\mu & \text{if } \rho = 0 \end{cases}$$

with the W propagator and the non-zero b mass explicitly taken into account. After bridging the threshold by numerical integration, the decay rate into a real W reads [10]

$$\Gamma_W = \frac{G_F}{8\pi\sqrt{2}} m_t^3 |V_{tb}|^2 \frac{2p_W}{m_t} \left\{ \left[1 - \left(\frac{m_b}{m_t} \right)^2 \right]^2 + \left[1 + \left(\frac{m_b}{m_t} \right)^2 \right] \left(\frac{m_W}{m_t} \right)^2 - 2 \left(\frac{m_W}{m_t} \right)^4 \right\}$$

$$\xrightarrow{m_t \gg m_W} 180 \text{ MeV} |V_{tb}|^2 \left(\frac{m_t}{m_W} \right)^3 \quad (3.7)$$

QCD corrections to the leptonic rate are conventionally cast into the form

$$\Gamma_{SL} = \Gamma_{SL}^{(0)} \left(1 - \frac{2}{3} \frac{\alpha}{\pi} f(\text{QCD}) \right)$$

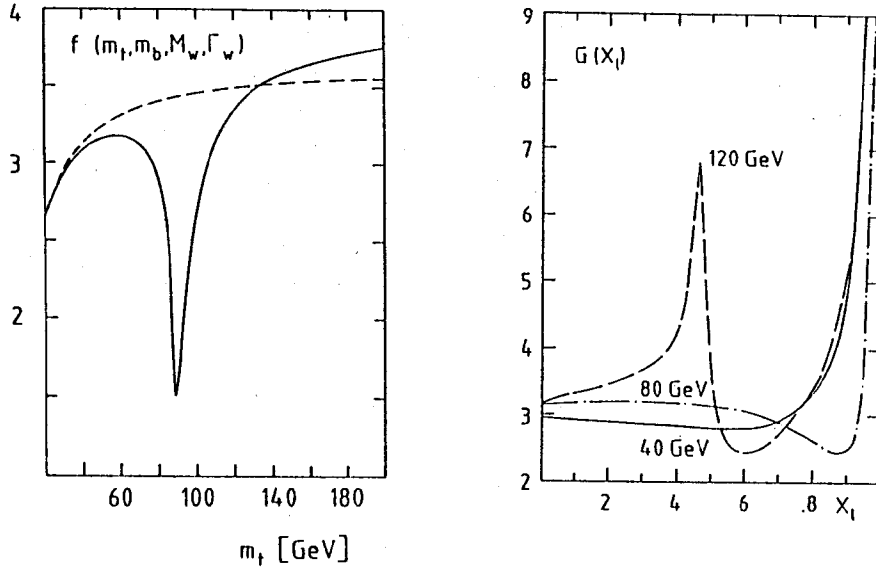


Fig. 3.2: a) QCD correction to the free quark decay rate without (dashed line) and with (solid line) W propagator [13].

b) Correction factor for the electron spectrum in top decay for different values of m_t . Solid / dash-dotted / dashed line: $m_t = 40/80/120$ GeV [14].

The function $f^{(QCD)}$ (which is affected by the W propagator and the non-zero b mass) is displayed in Fig. 3.2a. It is close to 3 in the mass region of interest for LEP.

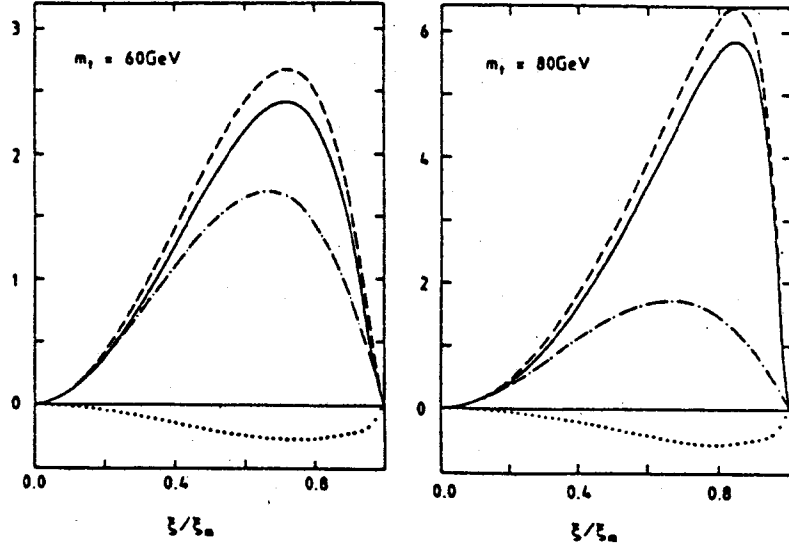


Fig. 3.3: Differential distribution $\frac{d\Gamma}{dx_L} / \frac{G_F^2 m_t^5}{192\pi^3}$ versus ξ/ξ_m for different top quark masses. Dash-dotted line: lowest order prediction without W propagator; dashed line: lowest order prediction with W propagator; dotted line: QCD correction; solid line: final result for quark decay. Ref. 14.

Analytic formulas can be found in Ref. [15]. The complete free quark decay rate follows from

$$\Gamma_{quark} = \frac{G_F^2 m_t^5}{192\pi^3} f\left(\frac{m_t^2}{M_W^2}, \frac{m_b^2}{m_t^2}\right) \left[1 - \frac{2\alpha_s}{3\pi} f^{(QCD)}\right] \left[3 + 6\left(1 + \frac{\alpha_s}{\pi}\right)\right] \quad (3.8)$$

b) Lepton Spectrum

Also the lepton spectrum from t decay is affected by the b -mass, the W propagator and QCD correction. In Born approximation the positron spectrum reads [14]

$$\frac{d\Gamma^{(0)}}{dx_\ell} = \frac{G_F^2 m_t^5}{16\pi^3} \frac{x_\ell(x_M - x_\ell)}{\gamma\rho} \text{Arctan} \left(\frac{\gamma\rho x_\ell(x_M - x_\ell)}{(1 + \gamma^2)(1 - x_\ell) - \rho x_\ell(x_M - x_\ell)} \right) \quad (3.9)$$

where

$$\text{Arctan}(x) = \begin{cases} \arctan(x) & \text{for } x \geq 0 \\ \pi + \arctan(x) & \text{for } x < 0 \end{cases}$$

$$x_\ell = 2E_\ell/m_t \quad x_M = 1 - m_b^2/m_t^2; \quad \rho = m_t^2/M_W^2; \quad \gamma = \Gamma_W/m_W;$$

In the narrow width approximation ($\gamma \rightarrow 0$) and for $m_t < M_W$ the spectrum simplifies to

$$\frac{d\Gamma^{(0)}}{dx_\ell} \xrightarrow{\gamma \rightarrow 0} \frac{G_F^2 m_t^5}{16\pi^3} \frac{x_\ell^2(1 - x_\ell)^2}{(1 - x_\ell) - \rho x_\ell(x_M - x_\ell)}; \quad (3.10)$$

QCD corrections to the spectrum are customarily expressed in the form

$$\frac{d\Gamma}{dx_\ell} = \frac{d\Gamma^{(0)}}{dx_\ell} \left(1 - \frac{2\alpha_s}{3\pi} G(X_\ell)\right) \quad (3.11)$$

The function G is shown in Fig. 3.2b, the complete spectrum in Fig. 3.3.

It should be noted that the spectrum in Born approximation from the decay of a polarized top quark factorizes into energy and angular dependent terms

$$\frac{d\Gamma(0)}{dx_\ell d\cos\theta} = \frac{d\Gamma(0)}{dx_\ell} \frac{1 + \cos\theta}{2} \quad (3.12)$$

In contrast to B meson decays, where only scalar mesons decay weakly, in top decays the angular distribution (12) is reflected in the observable lepton distribution. As a consequence of the tiny mass difference between spin singlet (T) and triplet (T^*) mesons the M1 transition rate $\Gamma(T^* \rightarrow T + \gamma)$ is small compared to the quark decay rate. T^* thus decays weakly (or semiweakly, if $t \rightarrow H^+ b$ is allowed) and the original quark polarization is reflected in the distribution of the decay products, diluted by a depolarization factor $f \approx 1/2$ [16]. A study of lepton distributions can thus determine the quark polarization, a study of the H^+ spectrum in the decay $t \rightarrow b + H^+$ could reveal the relative strength of the right- versus left-handed couplings.

In models with more than one Higgs doublet [17, 18, 19] one expects charged scalar particles that could be produced in semi-weak decays of top particles [20]. The coupling relevant in this context can be written as

$$A(t \rightarrow D + H^+) = \sqrt{\frac{G_\mu}{2}} m_t \bar{D} [v_{Dt}^L (1 - \gamma_5) + v_{Dt}^R (1 + \gamma_5)] t \quad (3.13)$$

where D denotes a down type quark. The semiweak decay rate [10]

$$\begin{aligned} \Gamma(t \rightarrow D + H^+) &= \\ &= \frac{G_\mu m_t^3}{8\pi\sqrt{2}} \frac{2P_H}{m_t} \left[|v_{Dt}^L|^2 + |v_{Dt}^R|^2 \left(1 + \frac{m_D^2}{m_t^2} - \frac{m_H^2}{m_t^2} \right) + 4 \operatorname{Re}(v_{Dt}^L v_{Dt}^{R*}) \frac{m_D}{m_t} \right] \\ &\approx 20 \text{ MeV} \left(\frac{m_t}{40 \text{ GeV}} \right)^3 \left(1 - \frac{m_H^2}{m_t^2} \right)^2 \end{aligned} \quad (3.14)$$

exceeds the normal weak decay rate by a large factor. The discovery of top quarks at hadron colliders, that relies heavily on the normal semileptonic decay mode, would then be impossible at the present time. For the angular distribution of the H^+ from the decay of a fully polarized t quark one finds the angular distribution

$$\frac{dN(H^+)}{d\cos\theta} = \frac{|v_{Dt}^R|^2 - |v_{Dt}^L|^2}{|v_{Dt}^R|^2 + |v_{Dt}^L|^2} \frac{1 + \cos\theta}{2} \quad (3.15)$$

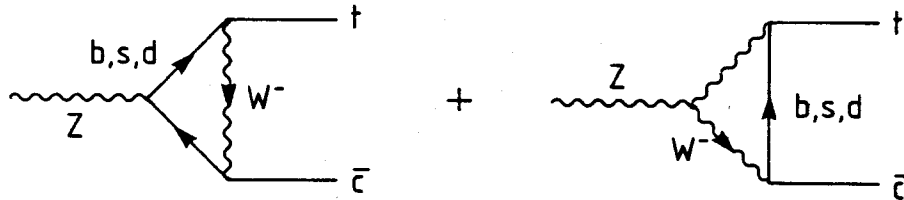
3.1.3. TOP PRODUCTION THROUGH FLAVOUR CHANGING NEUTRAL CURRENTS

The top mass accessible for LEP I is evidently limited by the kinematics of pair production to $\sqrt{s_{max}}/2 = 55$ GeV. The flavour-changing reactions

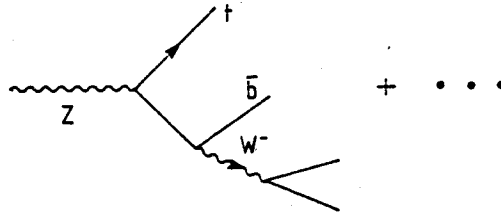
$$Z \rightarrow t\bar{c} \text{ or } \bar{t}c \quad (3.16)$$

would extend this range by nearly a factor two.

In the Standard Model this reaction proceeds through the GIM suppressed amplitudes



with a tiny result $\propto \frac{g_W^2}{4\pi^2} |V_{bc}|^2 (m_b^2/M_Z^2)$, leading to a branching ratio [21] below 10^{-8} . Another process which would allow top production together with three other *light* fermions for top masses above $m_Z/2$ proceeds through the diagrams shown below,



The branching ratios are tiny [22] extending from 10^{-8} downwards in the interesting top mass range.

Extensions of the Standard Model with natural flavour conservation, based on multi-Higgs models [23], which allow for a wide range of parameters consistent with present experiments, may enhance the branching ratio up to $10^{-6} - 10^{-4}$ — still below the reach for experiments.

Allowing for mass dependent deviations from “natural flavour conservation”, branching ratios of $10^{-5} - 10^{-4}$ [24] or even up to 10^{-3} [25] can be accommodated, in a way consistent with all present experimental bounds on FCNC which typically involve lighter quarks only.

3.2. TOPONIUM(Θ)

The search for heavy quark-antiquark bound states has been one of the prime targets of e^+e^- experiments. In the past months, however, it has become less likely — if not ruled out—that a toponium resonance will be found in the LEP I energy range with the properties predicted in the minimal Standard Model. The anticipated properties of quarkonia with masses in the LEP energy range have been studied in the theoretical [26] as well as the experimental [27, 3, 28] reference frame in great detail. We will collect in this section the basic points relevant for the *full* range of LEP, looking however also into those cases where the heavy quark could have escaped detection at hadron colliders.

3.2.1. SPECTROSCOPY

For quarks with high masses a huge number of S-wave narrow bound states $N \approx 2\sqrt{m_t/m_c}$ is predicted from potential models, with up to 9 to 18 radial excitations for m_t between 30 to 100 GeV. Including orbital and spin degrees of freedom several hundred narrow bound states are predicted below threshold. However, while the detection of the lowest spin triplet S-waves will be feasible throughout the full range of LEP, the observation of P-states will be difficult, if not impossible, if $m_\Theta \geq m_Z$ or if t quarks decay dominantly into charged Higgs particles.

QCD inspired potentials, with logarithmically softened Coulomb singularities at small distances and with a linear rise at large distances, have been successful in describing charmonium and $(b\bar{b})$ -spectroscopy. Characteristic examples are the Richardson potential [29]

$$V_R(r) = -\frac{4}{3} \frac{48\pi^2}{33 - 2n_f} \int \frac{d^3\vec{q}}{(2\pi)^3} \frac{e^{i\vec{q}\vec{r}}}{\vec{q}^2 \log(1 + \vec{q}^2/\Lambda_R^2)} \quad (3.17)$$

[$n_f = 3$; scale parameter $\Lambda_R = 398$ MeV] which behaves like

$$\begin{aligned} V_R(r) &\xrightarrow{r \rightarrow 0} -\frac{4}{3} \frac{6\pi}{33 - 2n_f} \frac{1}{r \log(1/\Lambda_R r)} \\ V_R(r) &\xrightarrow{r \rightarrow \infty} +\frac{4}{3} \frac{6\pi}{33 - 2n_f} \Lambda_R^2 r \end{aligned} \quad (3.18)$$

for large and small distances respectively; and a potential which incorporates two-loop corrections in the short distance behaviour [30], with the perturbative QCD scale parameter not identified with the string tension,

$$\begin{aligned} V_J(r) &= -\frac{16\pi}{25} \frac{1}{r f(r)} \left[1 - \frac{462 \ln f(r)}{625 f(r)} + \frac{2\gamma_E + \frac{53}{75}}{f(r)} \right] + dr e^{-gr} + ar \\ f(r) &= \ln[(1/\Lambda_{\overline{MS}} r)^2 + b] \end{aligned} \quad (3.19)$$

The following set of parameters has been derived from $(c\bar{c})$ and $(b\bar{b})$ spectroscopy:

$$\Lambda_{\overline{MS}} = 200 \text{ MeV} \quad a = 0.159 \text{ GeV}^2 \quad b = 20 \quad g = 0.344 \text{ GeV} \quad d = 0.255 \text{ GeV}^2$$

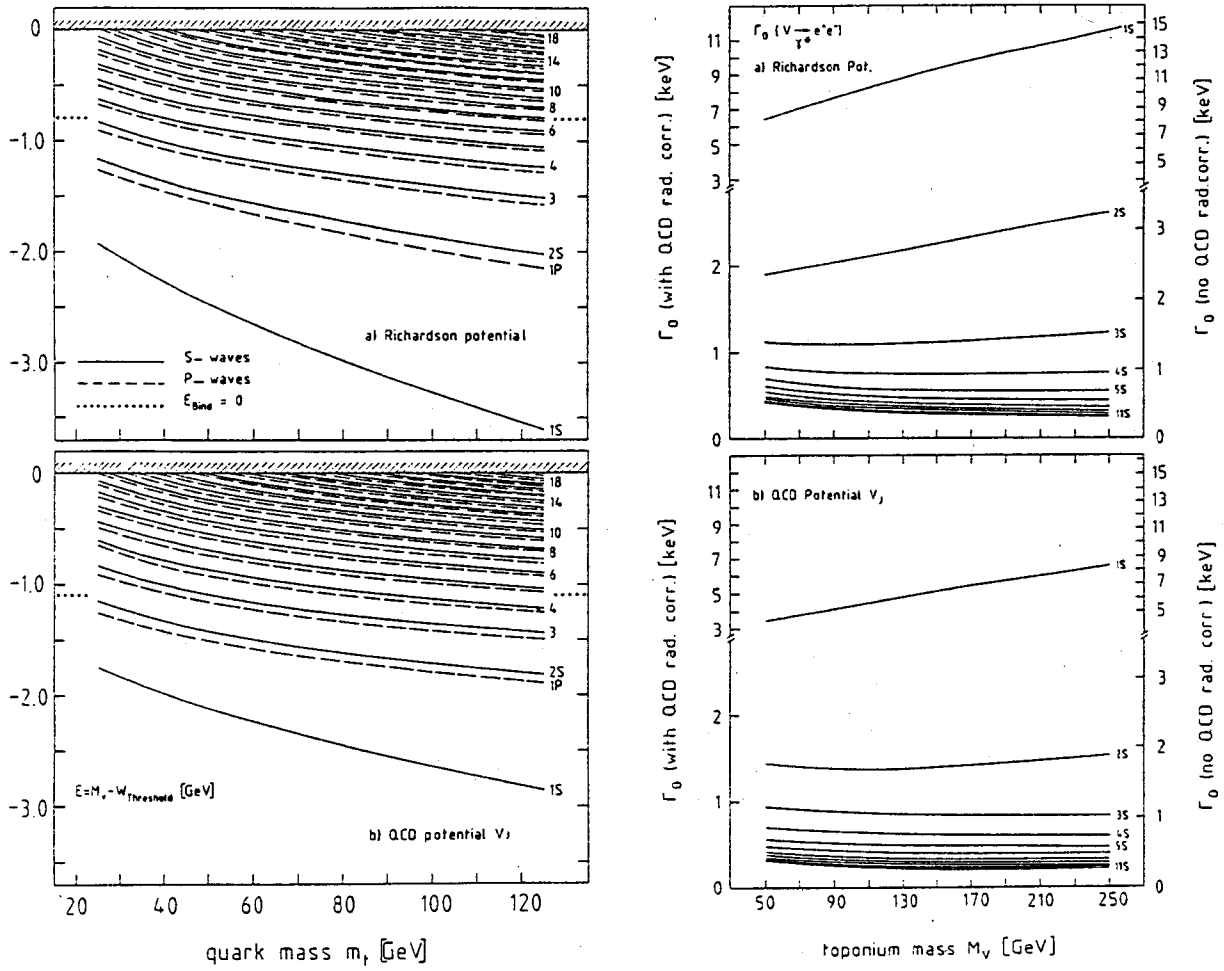


Fig. 3.4: Energy levels of S -wave and P -wave toponia and the fictitious electromagnetic decay rate Γ_0 [Eq. (1.9)], parametrizing the quark wave function for S waves at the origin, as a function of the top quark mass for (a) the Richardson potential and (b) the two-loop QCD potential V_J from [30] with $\Lambda_{\overline{MS}} = 200$ MeV. (From Ref. 26.)

Solving the Schrödinger equation for V_R and V_J , a convenient parametrization of the results is given by [$\delta \equiv 1 - m_t/45\text{GeV}$]

$$\begin{aligned} E_B &= \epsilon_0 + \epsilon_1\delta + \epsilon_2\delta^2, \\ \Gamma_0 &= \gamma_0 \left(\frac{m_t}{45\text{ GeV}} \right)^{\gamma_1} [1 + \gamma_2\delta + \gamma_3\delta^2] \end{aligned} \quad (3.20)$$

E_B is the binding energy so that the toponium mass is $M_\theta = E_B + 2m_t$. Γ_0 denotes the (artificial) decay rate to e^+e^- through the virtual photon

$$\Gamma_0 \equiv \Gamma(\theta \xrightarrow{\gamma} e^+e^-) = 4\alpha_s^2 e_t^2 \frac{|R(0)|^2}{M_\theta^2} \left(1 - \frac{16}{3} \frac{\alpha_s}{\pi} \right) \quad (3.21)$$

$$\alpha_s = \frac{12\pi}{23 \log(M_\theta/200\text{ MeV})^2}$$

which measures the wave function at the origin, and determines the production rate in e^+e^- collisions. The coefficients are displayed in Table 1 for the Richardson potential and for V_J . Energy levels as well as Γ_0 are shown in Fig. 3.4.

	Richardson potential				QCD potential V_J			
Energy levels [GeV]								
	ϵ_0	ϵ_1	ϵ_2		ϵ_0	ϵ_1	ϵ_2	
$1S$	-1.568	0.894	0.113		-0.937	0.586	0.068	
$1P$	-0.710	0.494	0.079		-0.351	0.366	0.065	
$2S$	-0.612	0.484	0.080		-0.259	0.389	0.072	
$\Gamma_0[\text{keV}]$								
	γ_0	γ_1	γ_2	γ_3	γ_0	γ_1	γ_2	γ_3
$1S$	7.718	0.156	-0.187	-0.015	4.150	-0.248	-0.602	-0.004
$2S$	2.031	-0.108	-0.269	-0.012	1.386	-0.137	-0.109	0.069

Tab. 3.1: Parameters of fits to the S-wave properties, as specified in (20). The corresponding fits for higher radial excitations and for dipole transition rates are presented in Ref. 31.

Evidently the measurement of the energy differences and in particular of $\Gamma_0(1S)$ would allow to distinguish between the various cases. The potential down to distances of $\mathcal{O}(10^{-2} \text{ fm})$ could be explored in this way. This point is further illustrated in Fig. 3.6, where the mass separation is given as a function of the quark mass for various interquark potentials and Λ values. The sensitivity to Λ is somewhat attenuated by the interplay of the non-perturbative remnants of the $q\bar{q}$ force. The statistical and systematic uncertainty in the measurement of the 1S-2S gap was estimated [3] to be $\pm 20 \text{ MeV}$ so that the measurement is sensitive to QCD terms of second order.

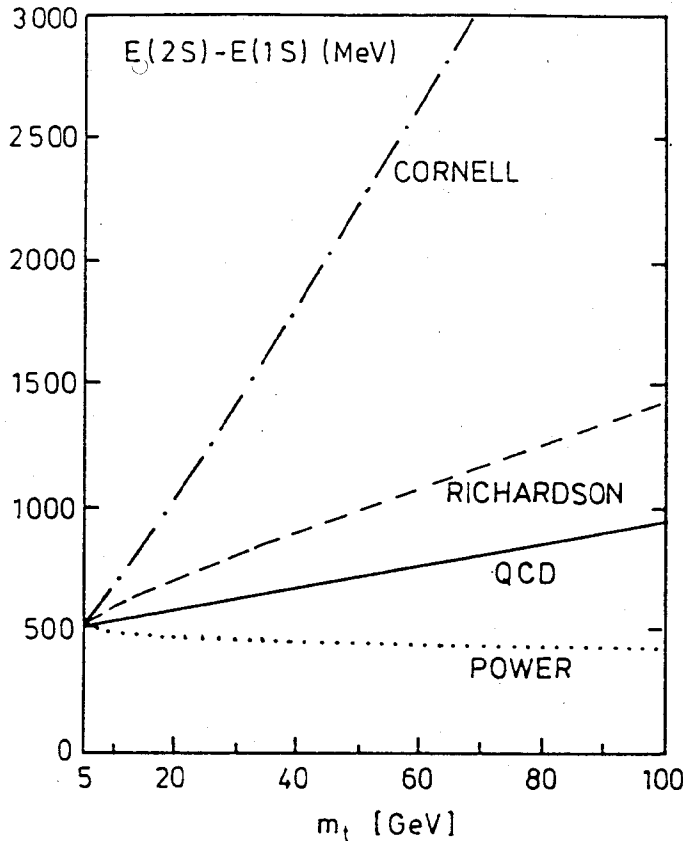


Fig. 3.5: Predictions for the 1S-2S mass difference as a function of the top quark mass for various potentials. (From Ref. 26.)

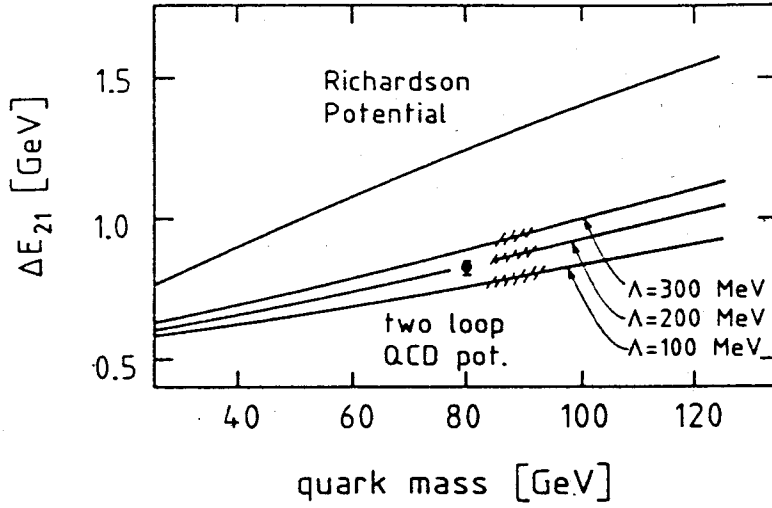


Fig. 3.6: Sensitivity of the $1S - 2S$ mass splitting to the details of the interquark potential. (a) Richardson's one-loop potential. (b) QCD two-loop potential V_J [30] for various values of $\Lambda_{\overline{MS}}$; the uncertainties due to the interpolation are indicated by the dashed bands; the error bar corresponds to the expected measurement error of ± 20 MeV at LEP. (From Ref. 3.)

3.2.2. MAIN DECAY MODES

The main decay modes of the 1^{--} spin triplet ground state $1^3S_1(t\bar{t})$ are (i) the electroweak annihilation of $t\bar{t}$ through γ, Z and W exchange [32, 33, 34, 12]; (ii) single t quark decays [32, 12, 35, 10]; and (iii) the strong decays into three or more gluons (and photons) [36, 37, 38, 39]. Higgs decays will be discussed separately later in this section, decays predicted in supersymmetric models are treated elsewhere [40, 26].

1.) DECAY INTO FERMIONS

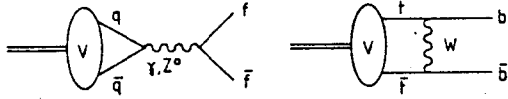
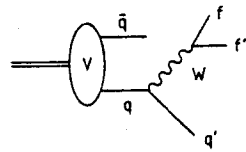
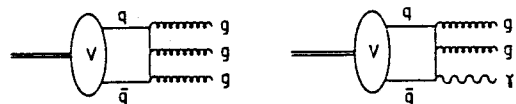


Fig. 3.7: The main decay modes of 1^{--} toponium resonances to lowest order.

2.) SINGLE QUARK DECAY



3.) GLUON AND PHOTON DECAY



Each of these decay modes has its own interesting physical implications. The strength of the electroweak annihilation channel measures the short-distance behavior of the interquark potential through the wave function at the origin, the electric charge and the vector coupling of t quarks to Z while the contribution from W exchange depends on the

charged current coupling between t and b quarks. The lifetime of the top quark itself can be determined through single t quark decays [41]. The partial widths for decays into gluons or gluons plus a photon measure the quark-gluon coupling constant. Jet distributions due to higher order multi-gluon decays reflect the presence of the 3-gluon coupling. The branching ratios of all these channels vary strongly with the toponium mass from the 50 GeV region through the Z domain to the energy range above 100 GeV. While for low mass values gluon decays play a dominant role, these modes are overwhelmed by Z mediated annihilation decays in the 80 to 100 GeV range. At still higher energies single t quark decays dominate over all the other modes. *Mutatis mutandis*, higher radial S -wave excitations follow the same pattern, with an increasing weight, however, of the single quark decays also in the low energy region.

a) Electroweak Annihilation

The electroweak annihilation of the 1^{--} spin triplet ($t\bar{t}$) ground state 1^3S_1 proceeds in general through a complicated mixture of photon, Z and W -exchange amplitudes [32, 33, 34, 12]. The Born diagrams for various fermionic final states, to be supplemented by QCD and electroweak radiative corrections, are displayed in Fig. 3.7. Expressed in terms of the purely electromagnetic width $\Gamma_0 = \Gamma(\theta \xrightarrow{\gamma} e^+e^-)$ introduced earlier, the decay widths can be written as [$y \equiv 2 \sin^2 \theta_W$]

$$\Gamma(1^3S_1 \rightarrow f\bar{f}) = c_f \frac{\Gamma_0}{e_f^2} \left[\left| e_f e_f + \frac{1}{y^2} \frac{v_t v_f M_V^2}{M_V^2 - M_Z^2 + i M_Z \Gamma_Z} - \delta_f \frac{\chi_W}{24 \sin^2 \theta_W} \right|^2 + \left| \frac{1}{y^2} \frac{v_t a_f M_V^2}{M_V^2 - M_Z^2 + i M_Z \Gamma_Z} - \delta_f \frac{\chi_W}{24 \sin^2 \theta_W} \right|^2 \right] \quad (3.22)$$

where the neutral current vector and axial vector couplings are given by

$$\begin{aligned} v_f &= 2[I_{3f}^L + I_{3f}^R] - 4e_f \sin^2 \theta_W \\ a_f &= 2[I_{3f}^L - I_{3f}^R] \end{aligned} \quad (3.23)$$

I_{3f}^L and I_{3f}^R are the weak isospins of the left and right-handed fermions. While $I_{3f}^R = 0$ in the standard model, the left-handed isospins are $+1/2$ for charge $+2/3$ quarks and neutrinos, $-1/2$ for charge $-1/3$ quarks and charged leptons. The Weinberg angle will be chosen as $\sin^2 \theta_W = 0.23$ and the weak boson masses $m_Z = 93$ GeV and $m_W = 82$ GeV. W exchange is switched on by setting $\delta_f = 1$ for bottom quarks [$\delta_f = 0$ otherwise] and

$$\chi_W = \frac{M_V^2}{M_W^2} \frac{M_W^2}{M_V^2 + M_W^2/8} \quad (3.24)$$

c_f accounts for the color degrees of freedom, being 1 for leptons and 3 for quarks. Radiative QCD corrections alter this factor to $3(1 + \alpha_s/\pi)$ for annihilation channels into light

quarks. The factor $(1 - \frac{16}{3} \frac{\alpha_s}{\pi})$ accounting for the QCD radiative corrections due to the exchange of transverse gluons at the top quark-current vertex [42] has been absorbed in the definition of Γ_0 in (21). [The exchange of Coulombic gluons is part of the confining potential.] Decays into bottom quarks require a special treatment due to the W -exchange diagram. The analytic result for the corresponding correction can be found in [43].

A rapid variation of $\Gamma(^3S_1 \rightarrow f\bar{f})$ is caused by the Z exchange $\sim 1/[(M_\theta^2 - M_Z^2)^2 + (M_Z\Gamma)^2]$ when the toponium mass comes close to the Z mass, overwhelming all other decay mechanisms. This is apparent from Fig. 3.8 where partial widths and branching ratios for $1^3S_1(t\bar{t})$ and $2^3S_1(t\bar{t})$ are displayed for toponium masses up to 175 GeV the threshold value for decays into real W 's. The total width varies from ~ 100 keV for low masses up to ~ 10 MeV in the Z range. For still higher masses the width grows rapidly due to single quark decays. The annihilation amplitudes are proportional to the toponium wave function at the origin. Fixing the potential by means of the level spacing, Γ_0 can be calculated and the neutral current vector coupling of the top quark can be determined by measuring Γ_{ee} .

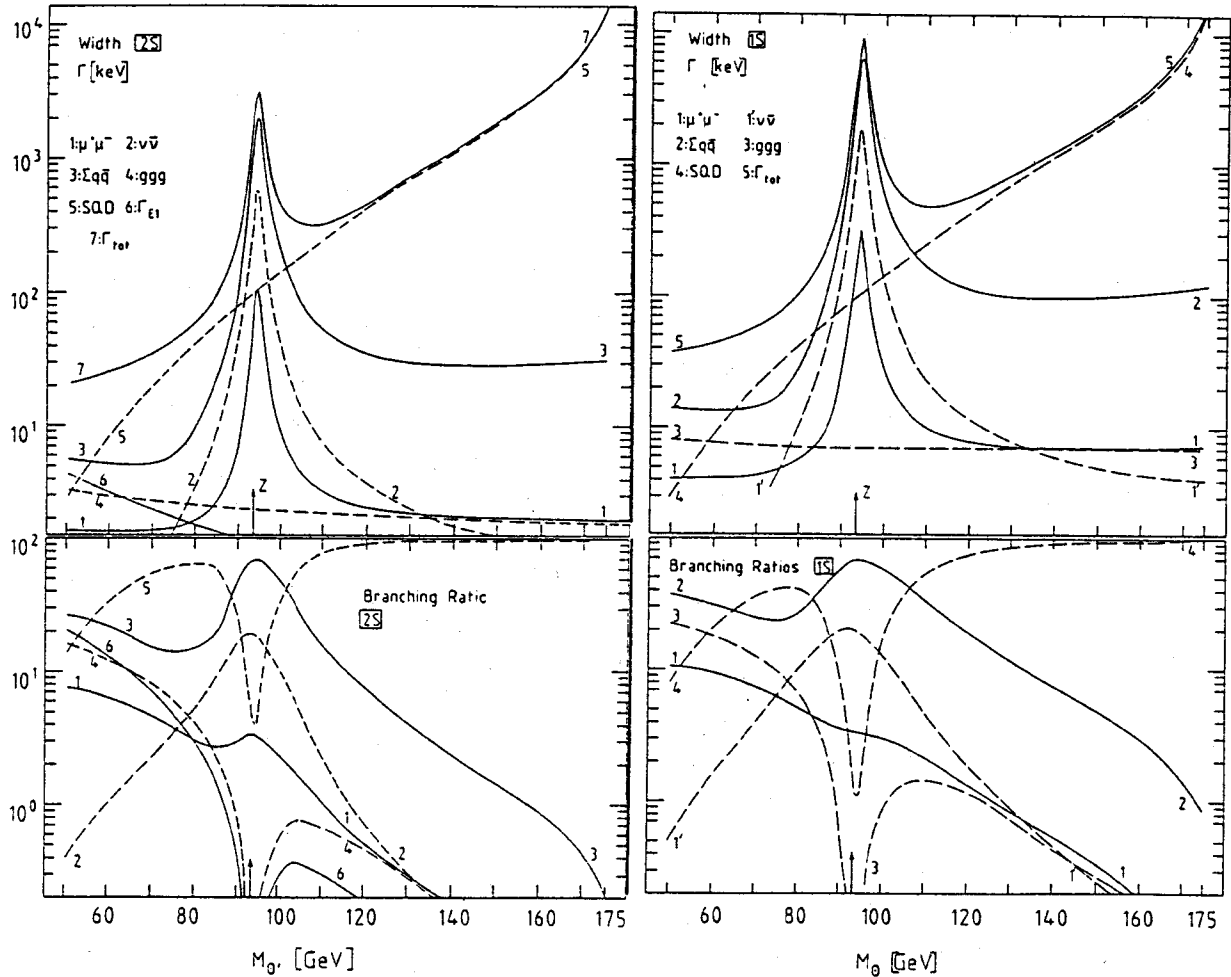


Fig. 3.8: Partial widths (a) and branching ratios in percent (b) for $1^3S_1(t\bar{t})$ and for $2^3S_1(t\bar{t})$ as a function of the toponium mass [potential V_J].

b) Single Quark Decays

With increasing mass the probability for a top quark to decay weakly $t \rightarrow b+W$ [W virtual or real] before annihilating with \bar{t} becomes more and more important [32, 12, 35, 10] (see Fig. 3.7). The final state consists of a b -quark jet plus two leptons or two light-quark jets, and a $\bar{T} = (\bar{t}q)$ open top meson [or baryon] at rest which will subsequently decay weakly. The width rises with the fifth power of the top quark mass, becoming the dominant contribution for $m_\theta > 110$ GeV,

$$\Gamma_{SQD} = 18 \frac{G_F^2 m_t^5}{192\pi^3} f\left(\frac{m_t^2}{M_W^2}, \frac{m_b^2}{m_t^2}\right) \quad (3.25)$$

where the phase space factor f takes the effect of W propagator and the non-zero b quark mass into account and is given in sect.3.1.1.

The partial width Γ_{SQD} is shown as a function of the toponium mass in Fig. 3.9. Above 100 GeV the majority of events consists of $SQDs$. Of course, once the threshold for top quark decays into real W bosons $t \rightarrow b + W$ is passed at $M_\theta \geq 176$ GeV, this mode would almost exclusively exhaust all other toponium decays,

$$\Gamma_W = 2 \frac{G_F}{8\pi\sqrt{2}} m_t^3 |V_{tb}|^2 \frac{2p_W}{m_t} \left\{ \left[1 - \left(\frac{m_b}{m_t} \right)^2 \right]^2 + \left[1 + \left(\frac{m_b}{m_t} \right)^2 \right] \left(\frac{m_W}{m_t} \right)^2 - 2 \left(\frac{m_W}{m_t} \right)^4 \right\}$$

$$\xrightarrow{m_t \gg m_W} 360 \text{ MeV} |V_{tb}|^2 \left(\frac{m_t}{m_W} \right)^3 \quad (3.26)$$

raising the toponium width quickly to the GeV range [Fig. 3.9].

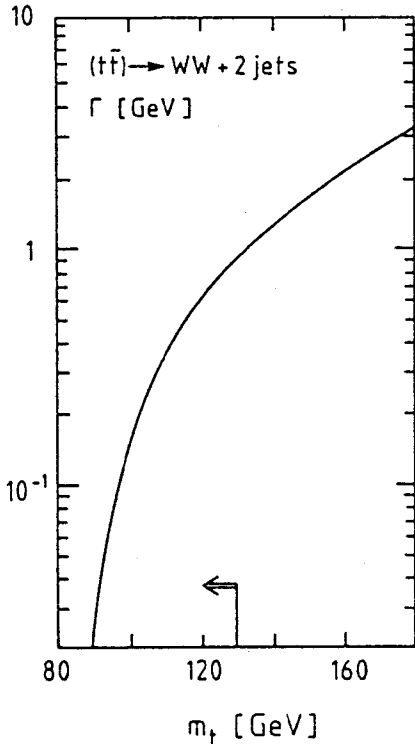


Fig. 3.9: Rate for toponium decays into real W 's. The arrow indicates the region where the width is smaller than the level spacing.

The lifetime of t quarks is then shorter than the characteristic revolution time and toponium bound states cannot form anymore beyond $m_t \approx 125$ GeV [16, 10]. Above this mass value the width becomes larger than the level spacing.

All these decay channels produce in general six well separated quanta in the final state, leptons and quarks turning into jets. Compared to the final states in electroweak annihilation and gluon decays, these events will have high sphericity [44, 41]. An additional signature of these events is provided by the rather large lepton and kaon yield evaluated in detail for the analogous case of Z decays to top quark pairs in [1]. It thus appears that the lifetime of top quarks can be determined indirectly by measuring $Br(SQD)$, $Br(\mu^+\mu^-)$ and Γ_{ee} through the cross section. Evidently this method breaks down for masses so large that the μ -pair branching ratio becomes too small compared to SQD .

Hard, isolated leptons will be produced directly in the top quark decay $(t\bar{t}) \rightarrow \bar{T} + B + \bar{l} + \nu + X$ and in the subsequent decay of the top hadron $\bar{T} \rightarrow \bar{B} + l + \bar{\nu} + X$, with a branching ratio of approximately 1/9 for each lepton species. For large quark masses comparable to M_W the W propagator has an important influence on the shape of the lepton spectrum [32, 13] whereas the influence of QCD corrections is relatively minor, as discussed in sect.3.2.2.

The spectrum of leptons and the decay rate due to single top decays inside toponium are also affected by bound-state corrections through the slight virtuality of the decaying t quark and the smearing of the momentum distribution [13]. The resulting [normalized] spectrum is compared in Fig. 3.10 with the spectrum from top quark decay. Also the lepton spectrum for the decays of the spectator T meson will be smeared, and the two distributions are in fact different. In practice only their sum will be observed. Compared to the spectrum without bound-state corrections its maximum is shifted to a lower ξ value by about 0.1 and a small excess of leptons with ξ beyond 1 could be observed. The slight virtuality of the weakly decaying top quark leads furthermore to an important reduction of the decay rate [13].

c) Strong Decays

At low energies quarkonia are gluon factories, [Fig. 3.7], [36, 37, 38, 39]. This role is lost unfortunately when the mass increases and electroweak decay modes become dominant. Partial widths and branching ratios for $\theta \rightarrow ggg$ and $\theta \rightarrow \gamma gg$,

$$\Gamma(\theta \rightarrow ggg) = \frac{10}{81} \frac{\pi^2 - 9}{\pi} \alpha_s^3 \frac{\Gamma_0}{\alpha^2 e_t^2} \quad (3.27)$$

$$\frac{\Gamma(\theta \rightarrow \gamma + gg)}{\Gamma(\theta \rightarrow ggg)} = \frac{36}{5} \frac{\alpha e_t^2}{\alpha_s} \quad (3.28)$$

are displayed in Fig. 3.8. For M_θ above 80 GeV the branching ratio B_{3g} drops below 10%.

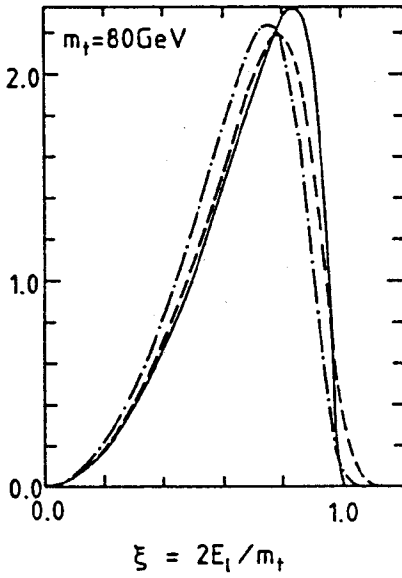


Fig. 3.10: Normalized distributions of lepton energies versus ξ . Solid curve: no bound-state corrections; dash-dotted curve: leptons from t quark decay; dashed curve: leptons from the spectator (T -meson) decay.

Higher-order corrections to the hadronic and photonic decay widths require herculean efforts that have been undertaken in [39]. Expressed in terms of (the QCD corrected) Γ_0 to eliminate the non-perturbative binding effects, the hadronic decay width is given by

$$\frac{\Gamma_{hadrons}}{\Gamma_0} = \frac{10(\pi^2 - 9)}{81\pi e_t^2} \frac{\alpha_{\overline{MS}}(\mu^2)^3}{\alpha^2} \left\{ 1 + \frac{\alpha_{\overline{MS}}(\mu^2)}{\pi} \left[-14.0 + \frac{3}{2}b_0(1.16 + \log \frac{2\mu}{M_\theta}) \right] \right\} \quad (3.29)$$

$$\frac{\alpha_{\overline{MS}}(\mu^2)}{4\pi} = \frac{1}{b_0 \log(\mu^2/\Lambda_{\overline{MS}}^2)} \left[1 - \frac{b_1}{b_0^2} \frac{\log \log(\mu^2/\Lambda_{\overline{MS}}^2)}{\log(\mu^2/\Lambda_{\overline{MS}}^2)} \right]$$

$b_0 = 11 - \frac{2}{3}n_f$ and $b_1 = 102 - \frac{38}{3}n_f$ where $n_f = 5$ is the number of light quark flavours; $\Lambda_{\overline{MS}}$ is correspondingly the value of the QCD scale parameter associated with 5 flavours. μ can be chosen such that the $\mathcal{O}(\alpha_s)$ corrections vanish: $\mu = 0.53M_\theta$. The scale of the \overline{MS} quark-gluon coupling constant in the Born term ratio is then fixed and the QCD parameter $\Lambda_{\overline{MS}}^{(5)}$ can be extracted for five quark flavour degrees of freedom.*

Spin Triplet Radial Excitations

Simple rules can be followed to derive the partial widths for $n^3S_1(t\bar{t})$ states from $1^3S_1(t\bar{t})$. The SQD width is universal for all $(t\bar{t})$ states, depending only on the mass of the top quark. All annihilation channels are proportional to $\Gamma_0(n)$, and they become quickly less important with rising n than $SQDs$ [except in a narrow interval around Z]. This is exemplified for the $2S$ state in Fig. 3.8.

Radially excited S waves can decay electromagnetically into P waves. The rate for the dominant electric dipole transitions follows from

$$\Gamma_{E1}(n^3S_1 \rightarrow \gamma + m^3P_J) = \frac{4(2J+1)}{3} \frac{\alpha e_t^2 E_\gamma^3}{9} |D_{mn}|^2 \quad (3.30)$$

*The corresponding analysis of charmonium and bottomium decays has led to a Λ value of $\Lambda_{\overline{MS}}^{(4)} = 199 \pm 22$ MeV, [45].

$$D_{mn} = \langle mP|r|nS \rangle$$

Parametrizations for the sum of all $E1$ transitions from a given state n are collected in Ref. 26 for the Richardson as well as the two-loop potential V_J . These partial widths are small, $\mathcal{O}(1 \text{ keV})$, compared with the other channels. Hadronic transitions $n(tt) \rightarrow n'(tt) + \text{hadrons}$ are similarly marginal [46].

3.2.3. HIGGS DECAYS

Decays of a heavy quarkonium can lead to important clues on the Higgs sector within the standard model and, more generally, on any scalar or pseudoscalar particle with appreciable coupling to heavy quarks.

Radiative Toponium Decay into Higgs Particles

An inevitable consequence of the standard model is the existence of at least one neutral Higgs particle. If this particle is lighter than toponium, the decay $\theta \rightarrow H\gamma$ [Fig. 3.11] could proceed with an appreciable rate [Fig. 3.12] as suggested by Wilczek [47].

$$\frac{\Gamma(\theta \rightarrow H\gamma)}{\Gamma_0} = \frac{G_F}{\sqrt{2}} \frac{M_\theta^2}{4\pi\alpha} \left[1 - \frac{M_H^2}{M_\theta^2} \right] \quad (3.31)$$

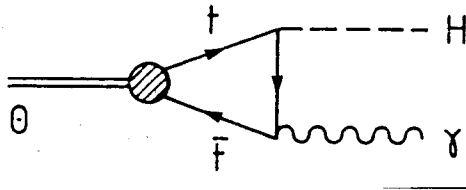


Fig. 3.11: Toponium decay into a Higgs meson plus a photon.

In models with more than one Higgs doublet, as motivated by CP violation through the Higgs sector [17] or supersymmetric extensions of the standard model (see e.g. Ref. 18), the Yukawa coupling of the neutral scalar to top quarks is no longer predictable and also pseudoscalars could appear with *a priori* unknown couplings. To deduce these fundamental quantities it is mandatory to have full control of QCD and bound-state corrections to the decay rate.

To investigate corrections to the lowest order result two—partially overlapping—regions have to be distinguished, the *perturbative region*, where $k \gg E_B$, and the *nonrelativistic region*, where $k \ll m$.

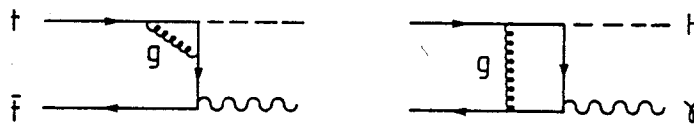


Fig. 3.13: $\mathcal{O}(\alpha_s)$ corrections to the decay $\theta \rightarrow H\gamma$.

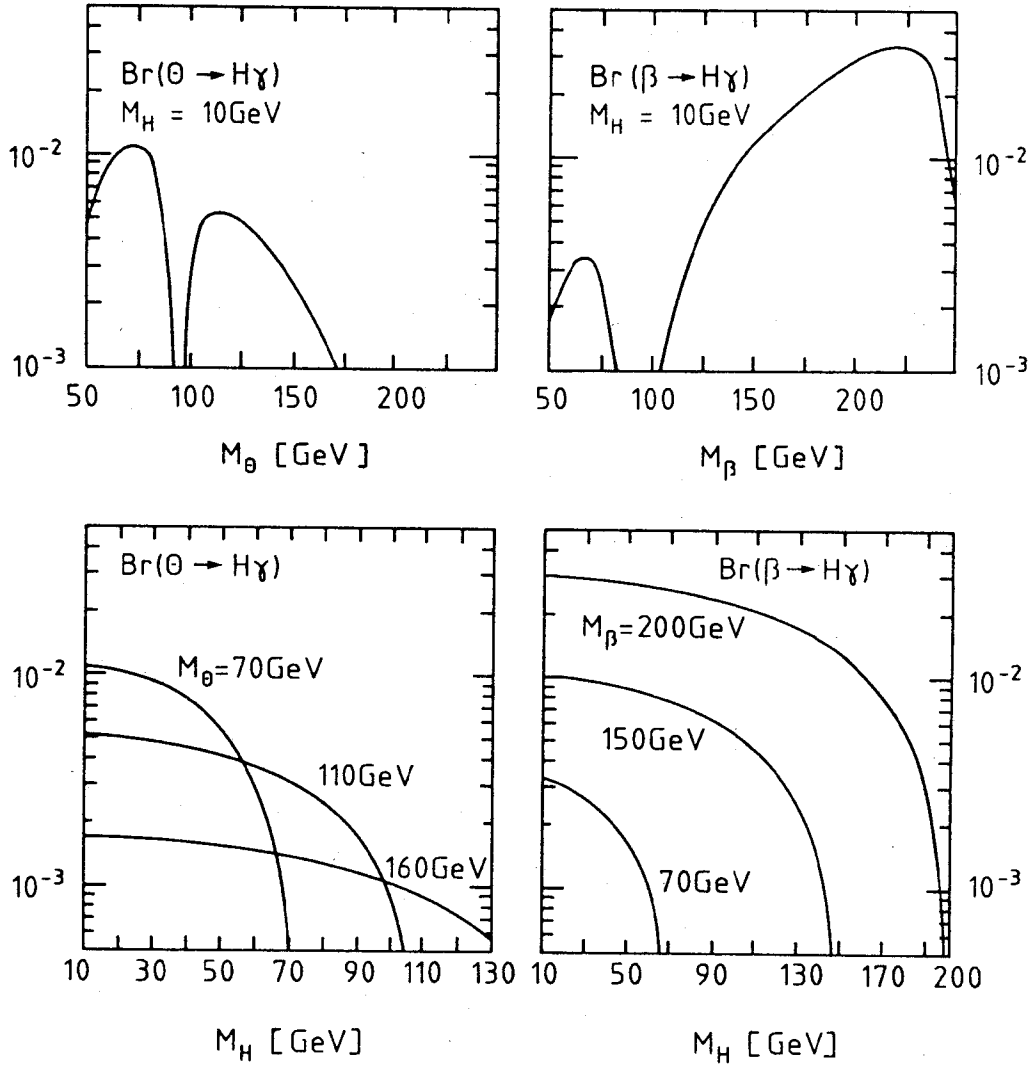


Fig. 3.12: Branching ratios for the θ [and $\beta = (b'\bar{b}')$] decays into Higgs plus photon [including QCD corrections].

Perturbative region ($k \gg E_B$): After emission of a hard photon of momentum $k \gg E_B$ the weakly bound quark is highly virtual. It propagates over a sufficiently short period of time so that a perturbative treatment, based on the Feynman diagrams shown in Fig. 3.13, is adequate. For the decay into a scalar the corrections have been calculated in Ref. 48. Subtraction of the Coulomb singularity from the gluon exchange diagram [Fig. 3.13] renders the amplitude infrared finite and one finds as reduction factor to the rate*

$$\Gamma_{QCD}(\theta \rightarrow S + \gamma) = \Gamma_{\text{Born}} \left[1 - \frac{4}{3} \frac{\alpha_s}{\pi} a_s(z) \right] \quad (3.32)$$

$$a_s(z) = \frac{4z^2 + z - 4}{2z^2} \left[\mathcal{L}(1-2z) - \mathcal{L}(1) \right] + \frac{4(z^2 - 1)}{z^2} \left[\frac{\pi^2}{4} - \arctan^2 \sqrt{\frac{1-z}{z}} \right] \\ - \frac{4(z^2 - 2)}{z(1-z)} \sqrt{\frac{1-z}{z}} \arctan \sqrt{\frac{1-z}{z}} + \frac{8z^3 + 7z^2 - 13z + 4}{z(2z-1)^2} \log 2z + \frac{7z-4}{2z-1}$$

*We choose a form for a_s that has been derived in Ref. 49.

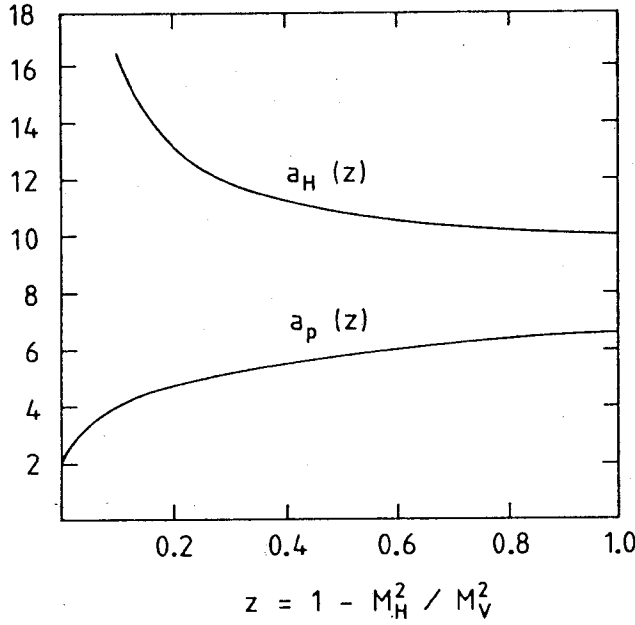


Fig. 3.14: The functions $a_s(z)$ and $a_{ps}(z)$ (from Refs. 48, 49).

where \mathcal{L} denotes the dilogarithm $\mathcal{L}(x) \equiv -\int_0^x dt t^{-1} \ln |1-t|$ and $z \equiv 1 - M_H^2/M_\theta^2$. $a_s(z)$ exhibits the limiting behaviour

$$\begin{aligned} a_s(z) &\xrightarrow{z \rightarrow 1} 7 + 6 \ln 2 - \frac{\pi^2}{8} = 9.93 \\ a_s(z) &\xrightarrow{z \rightarrow 0} \frac{4\pi}{3} z^{-1/2} + 1 \end{aligned} \quad (3.33)$$

and is displayed in Fig. 3.14. In principle the choice of the mass scale in α_s is not fixed. For a small Higgs mass the dominant contributions to the correction originate from hard gluons, for increasing Higgs mass, however, softer gluons become more important, which suggests a Higgs and toponium mass dependent scale proportional to $(M_\theta^2 - M_H^2)$ [48]. Adopting for definiteness $\Lambda = 200$ MeV and a toponium mass of 80 GeV the resulting reduction factor is huge, varying between 0.46 and 0.35 for M_H between 0 and 60 GeV, and decreases to 0.2 for $M_H = 70$ GeV. [Note that the reduction is less drastic if one normalizes the rate relative to the e^+e^- decay rate, which in itself is reduced by a factor $(1 - \frac{16}{3} \frac{\alpha_s}{\pi})$.] Above this mass range the applicability of perturbative QCD becomes even more doubtful since the correction diverges $\sim z^{-1/2}$. In this region it is more appropriate to take the full bound state dynamics into account, even if one has to sacrifice the relativistic treatment. For completeness we also give the result for the decay into a pseudoscalar Higgs particle, derived in [49]. In the same notation as above the correction factor reads

$$\begin{aligned} \Gamma_{QCD}(\theta \rightarrow PS + \gamma) &= \Gamma_{\text{Born}} \left[1 - \frac{4}{3} \frac{\alpha_s}{\pi} a_{ps}(z) \right] \quad (3.34) \\ a_{ps}(z) &= \frac{4z-1}{2z} \left[\mathcal{L}(1-2z) - \mathcal{L}(1) \right] + \frac{2(2z-1)}{z} \left[\frac{\pi^2}{4} - \arctan^2 \sqrt{\frac{1-z}{z}} \right] \\ &\quad + 4 \sqrt{\frac{1-z}{z}} \arctan \sqrt{\frac{1-z}{z}} + \frac{8z^2 - 7z + 1}{(2z-1)^2} \log 2z + \frac{7z-3}{2z-1} \end{aligned}$$

QCD corrections in the *nonrelativistic region* ($k \ll m$) are treated in more detail in Refs. 50, 51, 52.

Charged Scalars

In models with more than one Higgs doublet [17, 18, 19] one expects charged scalar particles that could be produced in semi-weak decays of top particles and in the corresponding SQD of toponium** [53, 54, 27, 10, 3]. The coupling relevant in this context can be written as

$$A(t \rightarrow DH) = \sqrt{\frac{G_F}{2}} m_t \bar{D} \left[v_{Dt}^L (1 - \gamma_5) + v_{Dt}^R (1 + \gamma_5) \right] t \quad (3.35)$$

D denotes a down type quark and $v_{Dt}^{R,L}$ involves a combination of quark and Higgs field mixing angles and of quark masses. This leads to the following semiweak decay rate

$$\Gamma(t \rightarrow D + H^+) = \frac{G_F m_t^3}{8\pi\sqrt{2}} \frac{2p_H}{m_t} \left[(|v_{Dt}^L|^2 + |v_{Dt}^R|^2) \left(1 + \frac{m_D^2}{m_t^2} - \frac{m_H^2}{m_t^2} \right) + 4 \operatorname{Re}(v_{Dt}^L v_{Dt}^{R*}) \frac{m_D}{m_t} \right] \quad (3.36)$$

If kinematically allowed and not suppressed or enhanced by extremely small or large couplings [$v = \mathcal{O}(1)$] the toponium decay rate

$$\begin{aligned} \Gamma_{H^\pm} &= \Gamma(t \rightarrow D + H^+) + \Gamma(\bar{t} \rightarrow \bar{D} + H^-) \\ &\approx 40 \text{ MeV} \left(\frac{m_t}{40 \text{ GeV}} \right)^3 \left(1 - \frac{m_H^2}{m_t^2} \right)^2 (|v_{Dt}^L|^2 + |v_{Dt}^R|^2) \end{aligned} \quad (3.37)$$

exceeds the normal weak decay rate by the large factor $10^3 (40 \text{ GeV}/m_t)^2$.

Although then exceeding all other modes by a correspondingly large factor, it would still be small compared to the $1S - 2S$ mass difference, and the low lying resonances would exist as well defined individual entities, as long as m_t is below $\sim 100 \text{ GeV}$. On the other hand, a width of 40 MeV is comparable to the energy resolution envisaged for LEP, and a direct experimental measurement of the width seems to be feasible in such a case.

Apart from the lower limit on charged scalars from PETRA ($m_{H^\pm} \geq 19 \text{ GeV}$) little is known about masses and mixing angles of charged Higgs particles. One can thus expect rather stringent bounds from toponium decays and prove or disprove a variety of models. As a specific example let us consider a two-Higgs doublet model suggested for example from the minimal supersymmetric extension of the standard model. In this case the couplings to the physical charged Higgs bosons are written as

$$v_{bt}^L = \tan \beta; \quad v_{bt}^R = \frac{m_b}{m_t} \cot \beta. \quad (3.38)$$

**If this decay mode is kinematically forbidden, charged scalars could nevertheless affect rates and angular distributions of $b\bar{b}$ -final states [53].

$\tan \beta$ is given by the ratio of the vacuum expectation values v_2/v_1 . Quark mixing angles have been ignored. The L-coupling $\tan \beta$ could in principle be very small and the rate strongly suppressed. However, it is readily seen that even the minimal charged Higgs decay rate, which is obtained for $\tan^2 \beta = m_t/m_b$ and for Higgs masses nearly up to the kinematic limit, would dominate open top and also toponium decay rates.

3.2.4. TOPONIUM IN e^+e^- COLLISIONS

The only place where one might hope to study toponium states in the near future is resonant e^+e^- production. Some aspects are specific to this case, and they will therefore be discussed in detail.

- (1) The production amplitude for fermion-antifermion final states will receive not only contributions from toponium, but also from the continuum due to virtual Z and γ exchange [34]. Although many of the resulting wild interference patterns will be washed out by the experimental beam energy spread, some remain detectable and may even dominate the behaviour of the cross section.
- (2) Production rates on and off resonance depend sensitively on the beam polarization [55] and the specific final state [34]. (Even for unpolarized beams the resonance will be polarized; this effect can be observed in $SQDs$.)
- (3) The forward-backward asymmetries [33, 34] can be remarkably large and quite different on and off resonance. Transversely polarized e^+e^- beams will induce azimuthal asymmetries. The size of asymmetries will be affected by higher-order electroweak corrections [56].
- (4) The cross sections for high radial excitations and for open top production will merge in practice such that a clear distinction between these two regions might become difficult [7]. Just like the total cross section, also the asymmetries are in general affected by the interference between resonance and continuum amplitudes. The consequences of smearing effects due to the beam energy resolution must be carefully taken into account [31].

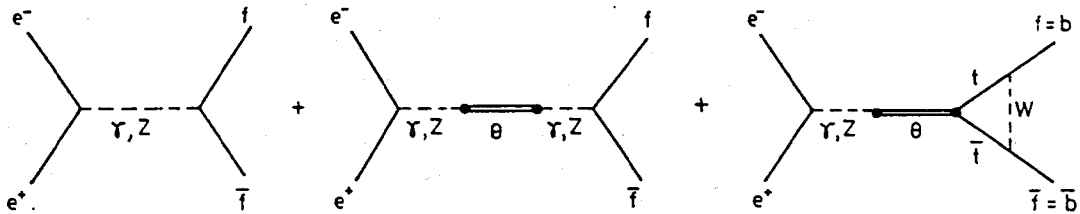


Fig. 3.15: Fermion-antifermion production in e^+e^- collisions close to the toponium resonance.

The full amplitude of the reaction $e^+e^- \rightarrow f\bar{f}$ is a superposition of γ , Z and toponium exchange. For specified helicities $\frac{1}{2}h_e, \frac{1}{2}h_f = \pm\frac{1}{2}$ of the initial and final fermions, the

amplitude [Fig. 3.15] may be written as [34]

$$\mathcal{M} = \mathcal{F} \cdot \mathcal{J} \quad (3.39)$$

where

$$\begin{aligned} \mathcal{F} &= \frac{e^2 e_e e_f}{s} + \left(\frac{e}{y}\right)^2 \frac{(v_f - h_f a_f)(v_e - h_e a_e)}{s - M_Z^2 + iM_Z \Gamma_Z} + (M_V^2 f_V)^2 \frac{(\lambda_f - h_f \lambda'_f)(\lambda_e - h_e \lambda'_e)}{s - M_V^2 + iM_V \Gamma_V} \\ &= \frac{1}{s} \mathcal{F}_B + (M_V^2 f_V)^2 \frac{1}{s - M_V^2 + iM_V \Gamma_V} \mathcal{F}_R \end{aligned} \quad (3.40)$$

and

$$\begin{aligned} \lambda_f &= \frac{e^2}{M_V^2} \left[e_f e_V + \frac{1}{y^2} \frac{v_f v_V M_V^2}{s - M_Z^2 + iM_Z \Gamma_Z} - \delta_f \frac{\chi_W}{24 \sin^2 \theta_W} \right] \\ \lambda'_f &= \frac{e^2}{M_V^2} \left[+ \frac{1}{y^2} \frac{a_f v_V M_V^2}{s - M_Z^2 + iM_Z \Gamma_Z} - \delta_f \frac{\chi_W}{24 \sin^2 \theta_W} \right] \end{aligned} \quad (3.41)$$

[λ_e, λ'_e correspondingly. The notation is the same as in Sect.3.2.2.] The fermionic currents which carry all dependence on polar and azimuthal scattering angles ϑ and φ , have been split off,

$$\mathcal{J} = -2\sqrt{s} h_f h_e (1 + h_f h_e \cos \vartheta) e^{i h_e \varphi} \quad (3.42)$$

The final states of “direct” toponium decays like ggg and $SQDs$ do not have a counterpart in the continuum. They add incoherently to the total cross section.

If the mass of a spin 1 quarkonium state is close to the Z -boson mass (a possibility which has recently become unlikely), mixing effects will occur which transform the bare states into new, generally not orthogonal physical states [57, 58, 31, 59–62]. The strength of the mixing is given by the ratio of the quarkonium- Z interaction energy relative to the [complex] energy gap between the unmixed states. This ratio remains very small for all toponium states,

$$\left| \frac{g_W M_V^2 f_V}{(M_V^2 - M_Z^2) - i(M_Z \Gamma_Z - M_V \Gamma_V)} \right| \ll 1 \quad (3.43)$$

because, however small the mass gap, the Z width is always 3 to 4 orders of magnitude larger than the toponium width, so that the imaginary part of the denominator never vanishes. In fact, for the parameters discussed before, the mixing angle is just a few percent. Expanding all quantities in the mixing angle consistently, one just reproduces lowest order electroweak perturbation theory - up to corrections which amount to less than 1%, as shown e.g. in Ref. 31.

a) *The Total Cross Section*

The fermion production cross section for unpolarized beams,

$$\sigma(s) = \frac{s}{48\pi} \sum_{h_f, h_e} |\mathcal{F}|^2 \quad (3.44)$$

exhibits a rapid variation in the resonance region. As long as either the photon or the Z dominates, σ varies between the unitarity limit

$$\sigma_{max}(f\bar{f}) = \frac{12\pi}{M_V^2} B(e^+e^-) B(f\bar{f}) \quad (3.45)$$

and (a near) zero. For the photon this phenomenon is well-known from J/ψ production (see e.g. [63]) and near the Z the same phenomenon occurs.

In contrast to the $f\bar{f}$ production cross section, those final states which originate from "direct decays" [gluon decays and SQD's] will exhibit the usual Breit-Wigner resonance enhancement,

$$\sigma(direct) = \frac{12\pi\Gamma(e^+e^-)\Gamma(direct)}{(s - M_V^2)^2 + (M_V\Gamma_V)^2} \quad (3.46)$$

For a wide range of masses the interference effects will be rendered unobservable once the inherent energy spread of the beams is taken into account, which increases with energy in fact. This tendency is already apparent when one moves from J/ψ to Υ . Remnants of the interference effects are still visible in the μ -pair cross section around J/ψ . In the Υ region an incoherent sum of the continuum and the properly smeared resonance is fully adequate. For toponium the same approximation is no longer valid, however, once the toponium mass is close to M_Z and as long as production *and* decay are dominated by the Z . In this case the standard resonance bump may even turn into a dip [58, 31, 59, 61], a consequence of the non-real character of the continuum Z amplitude. Whereas the γ continuum amplitude and the resonance amplitude are relatively imaginary to each other $\sim \frac{1}{M_V^2} + \frac{1}{M_V^2} \frac{g_\gamma^2}{iM_V\Gamma_V}$ so that they add incoherently if smeared, the Z continuum and the toponium interfere destructively at $M_V \approx M_Z$, $\sim \frac{1}{iM_Z\Gamma_Z} + \frac{1}{iM_Z\Gamma_Z} \frac{g_Z^2}{iM_V\Gamma_V} \frac{1}{iM_Z\Gamma_Z}$. On top of the resonance the cross section (normalized to the pointlike cross section) can be expressed in the form

$$\langle R(M_V) \rangle = \frac{(M_V^2 - M_Z^2)^2 - (M_Z\Gamma_Z)^2}{(M_V^2 - M_Z^2)^2 + (M_Z\Gamma_Z)^2} R_V(f) + R_{cont} \quad (3.47)$$

$R_V(f)$ is the well-known resonance enhancement if interference effects [and radiative corrections*] are ignored and a Gaussian cms energy spread δW is assumed,

$$R_V(f) = \frac{9\pi}{2\alpha^2} \frac{\Gamma(e^+e^-)B(f\bar{f})}{\sqrt{2\pi} \delta W} \quad (3.48)$$

*Here and in all subsequent discussions the effects of initial state radiation are left out. Before unfolding these corrections, the resonance cross sections are smaller by a factor of about 60% [27].

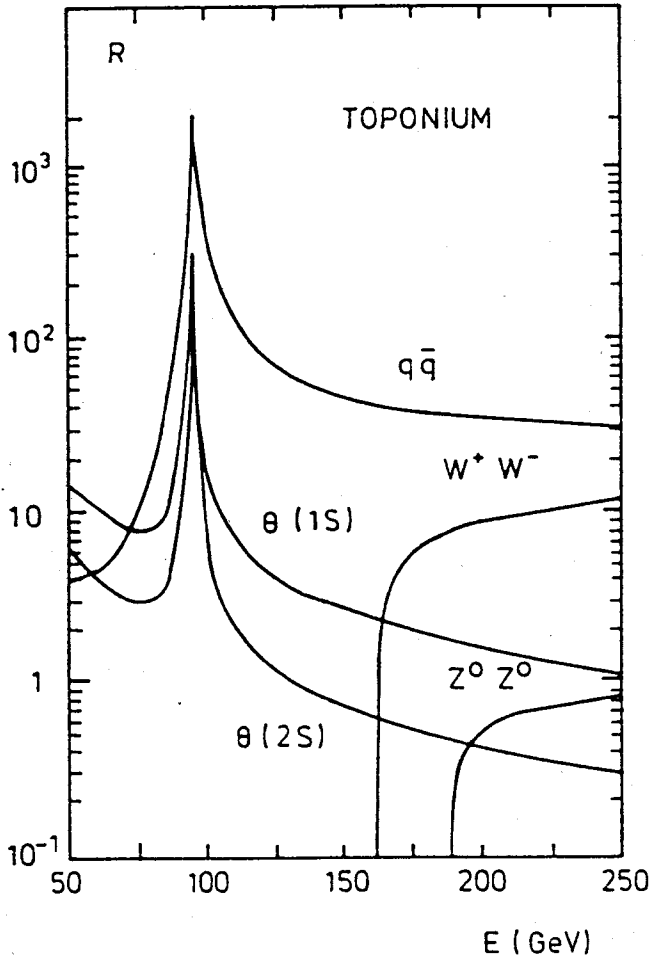


Fig. 3.16: Total cross section in units of the γ point cross section for the toponium $1S$ and $2S$ states [LEP beam spread], compared with the continuum cross sections for $q\bar{q}$ and W^+W^- [3].

The resonance enhancement R_V for all hadronic final states is compared in Fig. 3.16 with the main continuum contributions. The cross section is illustrated for the expected LEP energy spread [3] $\delta W[MeV] = 5 - 0.21\sqrt{s} + 0.007s$. Also in the more general case $W \neq M_V$ the folding of the cross section with the resolution function

$$\langle \sigma(W) \rangle = \int dW' r([W' - W]/\delta W) \sigma(W') \quad (3.49)$$

can be worked out analytically for toponium resonances whose widths Γ_V are much smaller than the beam spread δW [26]. Away from the Z this shape is given to a good approximation by a Gaussian—modulo effects of initial state radiation.

b) Asymmetries

Various asymmetries can be defined on a quarkonium resonance. The polarization asymmetry is defined as

$$\alpha(RL) = \frac{\sigma_R - \sigma_L}{\sigma_R + \sigma_L} \quad (3.50)$$

where σ_R, σ_L denote the cross sections for right-handed, left-handed electrons. Neglecting background channels for the moment, we find that on top of the resonance

$$\alpha(RL)^{on} = -\frac{2\text{Re}(\lambda_e^* \lambda_e')}{|\lambda_e|^2 + |\lambda_e'|^2} \quad (3.51)$$

is independent of the final state. The asymmetry is displayed as a function of the toponium mass in Fig. 3.17 and compared with the asymmetry in $\mu^+\mu^-$ production of the continuum. Weak corrections to this result are studied in [56]. Forward-backward asymmetries and azimuthal asymmetries can only be studied in a mass region where annihilation into $f\bar{f}$ states plays an important role, i. e. for masses ≤ 110 GeV. (Details and further references can be found in Ref. 26.)

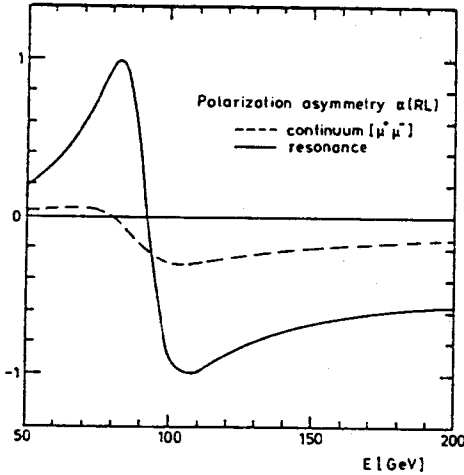


Fig. 3.17: The polarization asymmetry $\alpha(RL)$ on top of an S -wave toponium resonance as a function of the toponium mass, compared with the corresponding value of the $\mu^+\mu^-$ continuum.

c) High Radial Excitations

The mass levels and the electronic widths of higher radial excitations will be most useful to measure the force between heavy quarks at different distances. The flavour independence of the confining force can be investigated by comparing the result from toponia with the potential for charm and bottom quarkonia. To establish the location of the threshold requires a good understanding of the transition between resonance region and open top production. Due to the small level spacing that is comparable to the energy spread of e^+e^- machines, and due to the dominance of SQD's for high radial excitations, the open top threshold and the upper part of the resonance region look rather similar for nearly all top masses as far as the magnitude of the smeared cross section and topologies of the final state are concerned.

d) Open-Top Threshold

The open top meson threshold can be estimated [64] from charm and bottom production. If the bottom sector is taken as a guide the toponium threshold energy W_T^{thr} is related to the top mass through

$$W_T^{thr} = 2m_t + (m_{\Upsilon''} - 2m_b) + 225 \text{ MeV} \quad (3.52)$$

This holds true for any potential model in as much as it agrees approximately with a logarithmically varying potential in the long range $\mathcal{O}(1 \text{ fm})$. From the binding energy

$E_B(\Upsilon'') = 572$ MeV of the Richardson potential one finds

$$W_T^{thr} = 2m_t + 792 \text{ MeV} \quad (3.53)$$

The suitably averaged t resonance cross sections are approximately dual to the cross section for t quark production once the α_s correction is taken into account. The correction factors to the massless parton model results for vector and axial vector currents are given in sects. 2.2 and 3.1.1.

The cross section comes already quite close to the massless parton result, and the threshold suppression factor is largely offset by QCD corrections (see sect.3.1.1.) The hadronic widths of resonances above threshold has been estimated to rise significantly, to $\mathcal{O}(100 \text{ MeV})$ or even much more with increasing quark mass [65]. Since these widths are comparable to the level spacings, no well separable resonances may exist above threshold. The quark model is thus expected to approximate the cross section for top production sufficiently well above threshold and to join even smoothly to the resonance region. A characteristic example for this situation was shown in the previous section.

REFERENCES

- [1] J.H. Kühn, A. Reiter and P.M. Zerwas, *Nucl. Phys. B* **272** (1986) 560.
- [2] S. Jadach and J.H. Kühn, *Phys. Lett.* **191 B** (1987) 313.
- [3] LEP200 Study Group on "New Leptons and Quarks", P. Igo-Kemenes et al., Proceedings, LEP200 Workshop, Aachen, 1986.
- [4] A. Ali, in Proceedings, LEP200 Workshop, Aachen, 1986.
- [5] F. Porter, Proceedings, 2nd Mark II Workshop on SLC Physics, SLAC-306, 1986.
- [6] J. Schwinger, "Particles, Sources and Fields", Vol.II (Addison-Wesley, New York, 1973).
- [7] S. Güsken, J.H. Kühn and P.M. Zerwas, *Phys. Lett.* **155 B** (1985) 185.
- [8] A. Sommerfeld, "Atombau und Spektrallinien", Bd.2 (Vieweg, Braunschweig, 1939).
- [9] T. Appelquist and H.D. Politzer, *Phys. Rev. Lett.* **34** (1975) 43; *Phys. Rev. D* **12** (1975) 1404.
- [10] I. Bigi, Y. Dokshitzer, V. Khoze, J. Kühn and P. Zerwas, *Phys. Lett.* **181 B** (1986) 157.
- [11] J. Jersak, E. Laermann and P.M. Zerwas, *Phys. Lett.* **98 B** (1981) 363 and *Phys. Rev. D* **25** (1982) 1218.
- [12] J.H. Kühn, *Acta Phys. Pol. B* **12** (1981) 374.
- [13] M. Jezabek and J.H. Kühn, *Phys. Rev. Lett.* **207** (1988) 91.
- [14] M. Jezabek and J.H. Kühn, *Nucl. Phys. B* **320** (1989) 20.
- [15] M. Jezabek and J.H. Kühn, *Nucl. Phys. B* **314** (1989) 1.
- [16] J.H. Kühn, *Acta Phys. Austr., Suppl.* **24** (1982) 203.
- [17] S. Weinberg, *Phys. Rev. Lett.* **37** (1976) 657.
- [18] R.A. Flores and M. Sher, *Ann. Phys. (N.Y.)* **148** (1983) 95.
- [19] See e.g. H.P. Nilles, Proceedings, 6th Int. Conference on $p\bar{p}$ Physics, Aachen, 1986.
- [20] see J.H. Kühn and P.M. Zerwas, *Phys. Rep.* **167** (1988) 321, sect. 4.2 and references therein.

- [21] A. Axelrod, *Nucl. Phys. B* **209** (1982) 349;
M. Clemens et al., *Phys. Rev. D* **27** (1983) 570;
V. Ganapathi et al., *Phys. Rev. D* **27** (1983) 579;
G. Mann and T. Riemann, *Annalen d. Phys.* **4C** (1983) 334.
- [22] A. Axelrod, *Phys. Rev. D* **29** (1983) 2027.
- [23] G. W.-S. Hou and R.G. Stuart, MPI-PAE/PTh 54/88;
J.L. Hewett, S. Nandi and T.G. Rizzo, OSU Researchnote 201,IS-J-2983; M.J. Savage, preprint CALT-68-1496(1988);
C. Busch, preprint ITP-UH 9/88.
- [24] W. Buchmüller and M. Gronau, ITP-UH 11/88, DESY-88-171.
- [25] R. Barbieri and L.J. Hall, LBL-26126, UCB-PTH-88/25.
- [26] J.H. Kühn and P.M. Zerwas, *Phys. Rep.* **167C** (1988) 321.
- [27] LEP Study Group on Toponium Physics, W. Buchmüller et al., MPI-PAE/PTh 85/85 and Physics at LEP CERN 86-02.
- [28] J.D. Jackson, S. Olsen and S.-H.H. Tye, Proceedings, 1982 Summer Study on Elementary Particles and Fields, Snowmass, 1983.
- [29] J.L. Richardson, *Phys. Lett.* **82 B** (1979) 272.
- [30] K. Igi and S. Ono, *Phys. Rev. D* **33** (1986) 3349.
- [31] S. Güsken, J.H. Kühn and P.M. Zerwas, *Nucl. Phys. B* **262** (1985) 393.
- [32] K. Fujikawa, *Prog. Theor. Phys.* **61** (1979) 1186.
- [33] J. Bernabéu and P. Pascual, *Nucl. Phys. B* **172** (1980) 93.
- [34] L.M. Sehgal and P.M. Zerwas, *Nucl. Phys. B* **183** (1981) 417.
- [35] T.G. Rizzo, *Phys. Rev. D* **23** (1981) 1987.
- [36] H. Fritzsch and K.H. Streng, *Phys. Lett.* **74 B** (1978) 90.
- [37] S.J. Brodsky, T.A. DeGrand, R.R. Horgan and D.G. Coyne, *Phys. Lett.* **73 B** (1978) 203.
- [38] H. Koller, K.H. Streng, T.F. Walsh and P.M. Zerwas, *Nucl. Phys. B* **193** (1981) 61; *Nucl. Phys. B* **206** (1982) 273.
- [39] P.B. Mackenzie and G. Peter Lepage, *Phys. Rev. Lett.* **47** (1981) 1244.
- [40] J.H. Kühn, *Acta Phys. Pol.* **B 16** (1981) 969.
- [41] J.H. Kühn and K.H. Streng, *Nucl. Phys. B* **198** (1982) 71.
- [42] R. Barbieri, R. Gatto, R. Kögerler and Z. Kunszt, *Phys. Lett.* **57 B** (1975) 455.
- [43] G. Köpp, I. Schmitt and P.M. Zerwas, *Phys. Lett.* **201 B** (1988) 538.
- [44] G. Goggi and G. Penso, *Nucl. Phys. B* **165** (1980) 429.
- [45] W. Kwong, P.B. Mackenzie, R. Rosenfeld and J.L. Rosner, Preprint Chicago EFI 87-31.
- [46] Y.P. Kuang and T.-M. Yan, *Phys. Rev. D* **24** (1981) 2874.
- [47] F. Wilczek, *Phys. Rev. Lett.* **39** (1977) 1304.
- [48] M.I. Vysotsky, *Phys. Lett.* **97 B** (1980) 159.
- [49] P. Nason, *Phys. Lett.* **175 B** (1986) 223.
- [50] J. Pantaleone, M.E. Peskin, S.-H.H. Tye, *Phys. Lett.* **149 B** (1984) 225.
- [51] J. Polchinski, S. Sharpe, T. Barnes, *Phys. Lett.* **148 B** (1984) 493.
- [52] W. Bernreuther and W. Wetzel, *Z. Phys. C* **30** (1986) 421.
- [53] R.W. Robinett, *Phys. Rev. D* **33** (1986) 736;
E. Golowich and R.W. Robinett, *Phys. Rev. D* **34** (1986) 888.
- [54] J. Leveille, Proceedings, Cornell Z^0 Theory Workshop, 1981.
- [55] I.I.Y. Bigi, J.H. Kühn and H. Schneider, Preprint MPI-PAE 28/78 (1978).
- [56] B. Grzadkowski, P. Krawczyk, J.H. Kühn and R.G. Stuart, *Phys. Lett.* **176 B** (1986) 456; *Nucl. Phys. B* **281** (1987) 18.
- [57] F.M. Renard, *Z. Phys. C* **1** (1979) 225.

- [58] J.H. Kühn and P.M. Zerwas, *Phys. Lett.* **154 B** (1985) 446.
- [59] P.J. Franzini and F.J. Gilman, *Phys. Rev. D* **32** (1985) 237.
- [60] A. Martin, *Phys. Lett.* **156 B** (1985) 411.
- [61] L.J. Hall, S.F. King and S.A. Sharpe, *Nucl. Phys. B* **260** (1985) 510.
- [62] M. Chaichian and M. Hayashi, *Phys. Rev. D* **32** (1985) 144.
- [63] J.D. Jackson and D.L. Scharre, *Nucl. Instr. and Methods* **128** (1975) 13.
- [64] C. Quigg and J.L. Rosner, *Phys. Rep.* **56C** (1979) 167.
- [65] S. Ono, *Z. Phys. C* **8** (1981) 7.

4. Extending the Standard Model

4.1. THE FOURTH GENERATION*

It has often been conjectured that additional heavier quarks might exist — either just embedded in a fourth generation or in extensions of the generation multiplets themselves. The formulas given in the previous chapters apply equally well to these cases after the proper choices of charge and weak isospin quantum numbers are made for the rates of fermionic decays etc. The phenomenology of such states, however, will in general be drastically different. In such a lucky situation open b' production could easily be detected and eventually also the corresponding onium states $\beta \equiv (b'\bar{b}')$ could be studied.

a) b' quarks

The production cross section for b' quarks can be derived from the corresponding formulae for top production after a suitable adjustment of coupling constants. The part of the cross section which is induced through the neutral vector current is nearly a factor four larger than the corresponding one for t . Therefore a relatively large branching ratio $Z \rightarrow b'\bar{b}'$ of about 5% would be expected once b' is kinematically accessible. In the LEP200 region, on the other hand, b' production through the photon plays the dominant role and, as a result, the production rate is about a factor two below the one for t quarks of the same mass. Standard cuts on the event topology allow to discover b' in the full range of LEP [1].

Various possibilities are conceivable for b' decays depending on presently unknown mixing angles and mass assignments. If $m_{b'} > m_t$, the charged current decay $b' \rightarrow t + W^*$ is expected to dominate. The decay rate (including QCD corrections) can directly be read off from the corresponding formulas for top decay after substituting $t \rightarrow b', b \rightarrow t$. The electron spectrum from the semileptonic mode would correspond to the neutrino spectrum in top decay. It reads in Born approximation [2]

$$\begin{aligned} \frac{d\Gamma^0}{dx_\ell} = & \frac{G_F^2 m_t^5}{16\pi^3} |V_{tb'}|^2 \frac{1}{\xi^2} \left\{ \left[\xi^2 x_\nu (x_M - x_\nu) - \xi (x_M - 2x_\nu) - 1 + \gamma^2 \right] \right. \\ & \times \frac{1}{\xi\gamma} \operatorname{Arctan} \left(\frac{\xi\gamma y_m}{1 + \gamma^2 - \xi y_m} \right) \\ & \left. + \frac{1}{2\xi} [\xi (x_M - 2x_\nu) + 2] \ln \left(\frac{1 + \gamma^2}{(1 - \xi y_m)^2 + \gamma^2} \right) - y_m \right\} \end{aligned} \quad (4.1)$$

where

$$\gamma = \frac{\Gamma_W}{m_W} \quad x = \frac{2E_\ell}{m_{b'}} \quad x_M = 1 - \left(\frac{m_t}{m_{b'}} \right)^2 \quad y_m = \frac{x_\ell (x_m - x_\ell)}{(1 - x_\ell)} \quad \xi = \frac{m_{b'}^2}{m_W^2}$$

*J.H. KÜHN

$$\text{Arctan}(x) = \begin{cases} \arctan(x) & \text{for } x \geq 0 \\ \pi + \arctan(x) & \text{for } x < 0 \end{cases} \quad (4.2)$$

In the four fermion limit $\xi = \gamma = 0$ one obtains

$$\frac{d\Gamma^{(0)}}{dx_{ell}} \rightarrow \frac{G_F^2 m_t^5}{16\pi^3} |V_{qb'}|^2 x_\ell^2 (1 - x_\ell) \quad (4.3)$$

QCD corrections to these formulae can be found in Ref. 2.

The decay pattern could become more involved if $m_{b'} < m_t$. The leading charged current decay $b' \rightarrow c + W^*$ is then suppressed by the small mixing angle $V_{cb'}$. The same formulae for rate and spectrum apply as before leading, however, to a significant reduction of the decay rate.

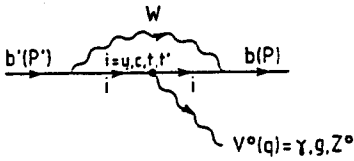


Fig. 4.1: A typical graph leading to induced FCNC couplings

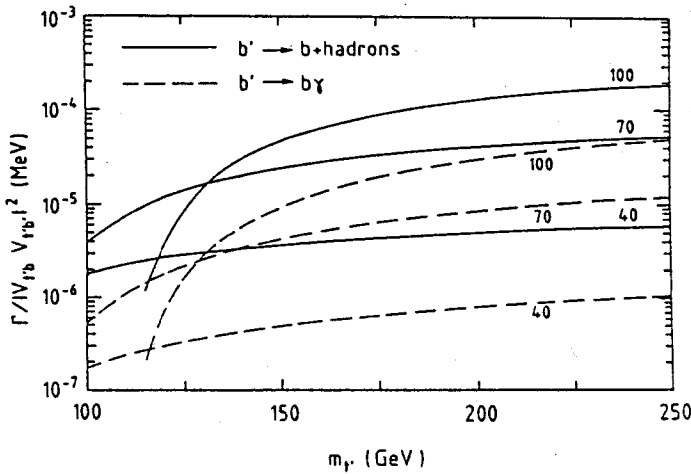


Fig. 4.2: Rates for $b' \rightarrow b + \text{hadrons}$ and $b' \rightarrow b\gamma$ (with common mixing coefficients factored out) vs. m_t , for $m_{b'} = 40, 70$ and 100 GeV. $m_t = m_{b'} + 10$ GeV has been assumed. (From Ref. [3]).

Depending on the mass assignment for t - and t' -quarks and the choice of mixing angles, induced flavour changing neutral current decays (Fig. 4.1) could compete or might even dominate the lowest order result. For $m_{b'}$ below $m_Z/2$ this requires $|V_{cb'}|/(V_{t'b}V_{t'b'}) \lesssim 10^{-2}$ and a large mass difference between t and t' to inhibit GIM cancellations. Under these assumptions $b' \rightarrow b + \text{hadrons}$ could become dominant, leaving even room for the decay $b' \rightarrow b + \gamma$ with a branching ratio in the 10% range [3](Fig. 4.2).

It has been argued in Ref. 4 that, if $m_H < m_{b'}$, the Higgs decay $b' \rightarrow b + H$ is almost certain to dominate over $b' \rightarrow c + W^*$, and that it certainly dominates the FCNC decays. Standard search strategies at hadron colliders, looking for hard isolated leptons, would of course not be sensitive to such possibilities — leaving interesting options for e^+e^- experiments.

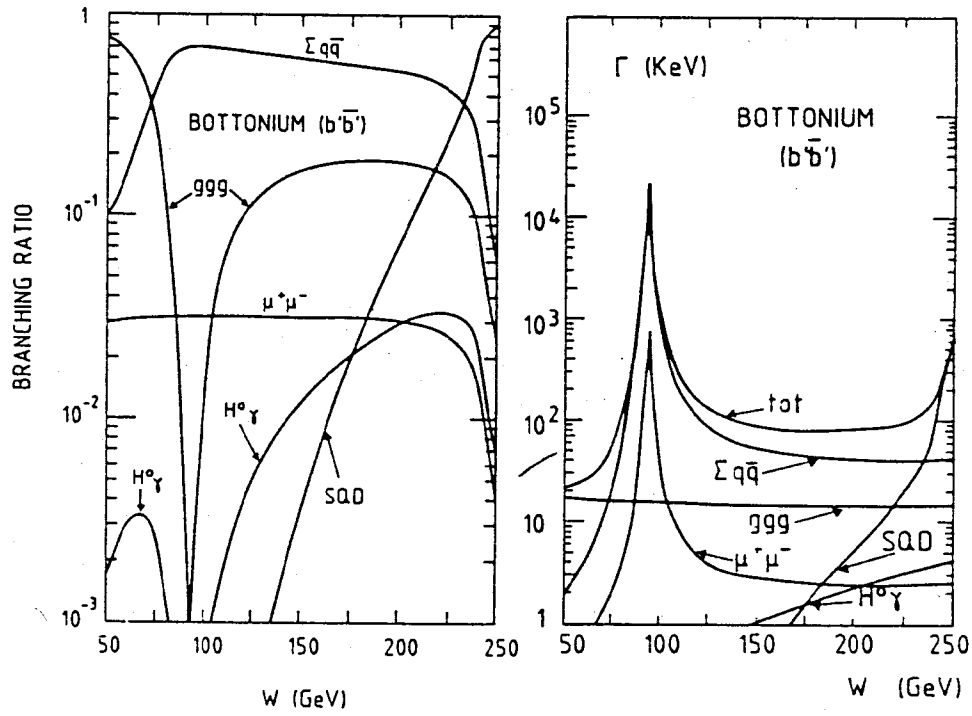


Fig. 4.3: Decay rates and branching ratios for the most prominent decay modes of β as a function of the mass [1].

b) Bound states

It is thus conceivable that b' will appear in the mass range up to 100 GeV that is spanned by LEP. $\beta = (b'\bar{b}')$ bound states could then be formed. β decays differ from toponium decays because of their strong SQD suppression by small mixing angles. The most important similarities and differences between the phenomenology of β and θ are as follows:

- (i) Predictions for the *level spacings* and the *wave functions* as discussed in for toponium are unaffected.
- (ii) For the *electroweak couplings* to the virtual photon and Z that govern the production in e^+e^- annihilation and the decays into $f\bar{f}$, the appropriate charge $e_{b'} = -1/3$ and the vector coupling constant $v_{b'} = -1 + \frac{4}{3}\sin^2\theta_W$ have to be inserted.
- (iii) If its mass is close to M_Z , its decay rates, the effects on the Z *mass shift* and the changes in the cross sections would be enhanced by a factor $[v_{b'}/v_t]^2 = 2.8$ so that its width would be comparable to the energy spread of LEP. Also the effects on the Z mass would become noticeable.
- (iv) If the mass is sufficiently far above the Z , its width will be far smaller than that of a toponium state of the same mass since *SQD's* are strongly suppressed. Whether they would still constitute an important decay mode depends sensitively on the mass and mixing angles of b' . Their presence or absence could thus provide significant information on the mixing angles [5]. Taking, for illustration, a state with a mass of 150 GeV and a rate for annihilation decays of 50 keV, and assuming that SQD's could

be detected down to a branching ratio of 10%, a Cabibbo suppression factor down to a level of 2×10^{-3} would be accessible experimentally. Decay rates and branching ratios of the most prominent standard decay modes of β as a function of its mass are shown in Fig. 4.3, assuming for illustrative purpose $V_{tb} = 0.05$. Annihilation into $f\bar{f}$ final states is by far dominant, so that the detection of such resonances above the $f\bar{f}$ continuum is extremely difficult for masses beyond the Z where the resonance-to-continuum ratio falls below 0.02. In this high energy region such a state could only be discovered in a dedicated search with a considerably reduced e^+e^- beam energy spread. This would open a window to *large Higgs masses*, since $B(\beta \rightarrow H\gamma)$ is at the level of several percent up to the highest masses.

4.2. LEPTONIC DECAYS OF NEUTRAL D- AND B-MESONS*

Experimental bounds on decay rates of K-, D- and B- mesons to lepton pairs e^+e^- , $\mu^+\mu^-$, $\tau^+\tau^-$, $e^\pm\mu^\mp$, $e^\pm\tau^\mp$ and $\mu^\pm\tau^\mp$ (cf. Fig. 4.4) provide important information on the strength of flavour changing neutral current interactions. The observed branching ratio for $K_L \rightarrow \mu^+\mu^-$ and the present limit on $K_L \rightarrow \mu^\pm e^\mp$ are of order 10^{-8} whereas the present bounds for $D^0(\bar{D}^0)$ and $B^0(\bar{B}^0)$ decays to lepton pairs is of order 10^{-4} [6]. At LEP these limits will be significantly improved. From 10^7 Z^0 bosons one will obtain about 10^6 D^0 or \bar{D}^0 , 10^6 B^0 or \bar{B}^0 and $5 \cdot 10^5$ B_s or \bar{B}_s mesons. Here we have assumed branching ratios $BR(Z^0 \rightarrow c\bar{c}) \approx 0.12$, $BR(Z^0 \rightarrow b\bar{b}) \approx 0.15$ and a production of $u\bar{u}$, $d\bar{d}$ and $s\bar{s}$ pairs from the vacuum with relative probabilities $u : d : s \approx 2 : 2 : 1$. Since D- and B-meson decays into e^+e^- , $\mu^+\mu^-$ and $e^\pm\mu^\mp$ pairs can be detected with high efficiency it will be possible to obtain bounds on the corresponding branching ratios of order 10^{-6} . Even more important will be the totally new information on $B_s(\bar{B}_s)$ mesons which so far have not been observed. For the first time these mesons will allow to test flavour changing neutral couplings of quarks belonging to the second and third generation which, in many models, are expected to be much larger than flavour changing couplings among the first two generations.

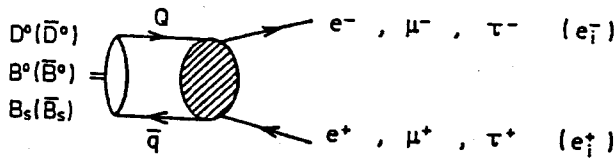


Fig. 4.4: Decays of K-, D-, and B-mesons to lepton pairs.

Operator Analysis

Leptonic decay rates of mesons measure the strengths of four fermion operators involving

*W. BUCHMÜLLER, F. HOOGVEEN

two quarks and two leptons which may, or may not, flip quark and lepton helicities (cf. Fig. 4.5). The most general effective interaction is given by

$$L_{eff}^S = \frac{1}{(\Lambda_{LL}^u)^2} \bar{u}_L u_R \bar{e}_L e_R + \frac{1}{(\Lambda_{LR}^u)^2} \bar{u}_L u_R \bar{e}_R e_L + h.c. \\ + (u \rightarrow d) \quad (4.4)$$

$$L_{eff}^V = \frac{1}{(\Lambda_{LL}^u)^2} \bar{u}_L \gamma^\mu u_L \bar{e}_L \gamma_\mu e_L + \frac{1}{(\Lambda_{LR}^u)^2} \bar{u}_L \gamma^\mu u_L \bar{e}_R \gamma_\mu e_R \\ + \frac{1}{(\Lambda_{RL}^u)^2} \bar{u}_R \gamma^\mu u_R \bar{e}_L \gamma_\mu e_L + \frac{1}{(\Lambda_{RR}^u)^2} \bar{u}_R \gamma^\mu u_R \bar{e}_R \gamma_\mu e_R \\ + (u \rightarrow d) \quad (4.5)$$

L_{eff}^S describes helicity changing interactions, L_{eff}^V helicity conserving interactions where the coefficients are matrices in flavour space. The decay widths obtained from vector operators are suppressed by $(m_l/m_M)^2$ compared to those obtained from scalar operators, where m_l and m_M denote lepton and meson mass respectively. Tensor operators, which in general also occur, do not contribute to the decay of pseudoscalar mesons. We note that the scale parameters defined in eqs. (4,5) are smaller by a factor $\sqrt{4\pi}$ compared to those defined by the convention for contact interactions used in [6].

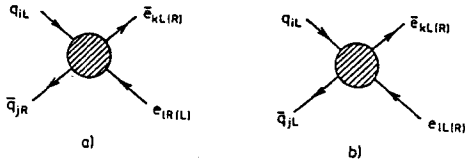


Fig. 4.5: Helicity changing (a) and helicity conserving (b) contact interactions of quarks and leptons.

The effective interactions of eqs. (4,5) can be generated through the exchange of spin 0 or spin 1 particles which couple either to quark-lepton pairs (leptoquarks) or to quark and lepton pairs (Higgs and neutral vector bosons). Flavour changing contact interactions have been discussed by a number of authors [7-11] and the most general leptoquark lagrangian has been given in [12]. Here we will consider only some couplings which illustrate the various possibilities and the implications of a combined analysis of D- and B- decays. Let \vec{W} be an isovector boson with zero hypercharge, D and G scalar leptoquarks, and U and X vector leptoquarks with $SU(3)_C \times SU(2)_W \times U(1)_Y$ quantum numbers:

$$D \sim [3, 1; -\frac{1}{3}] \quad U \sim [3, 1; +\frac{2}{3}] \\ G \sim [3, 2; +\frac{7}{6}] \quad X \sim [3, 3; +\frac{2}{3}]$$

Assuming the absence of quark-quark couplings in order to guarantee baryon number conservation, the most general renormalizable interactions are given by

$$L_I = (g_D^q \bar{q}_L i \tau_2 l_L^c + g_D^u \bar{u}_R e_R^c) D + (g_G^q \bar{q}_L e_R + g_G^u \bar{u}_R l_L i \tau_2) G$$

$$\begin{aligned}
& + (g_U^e \bar{e}_R \gamma_\mu d_R^c + g_U^q \bar{q}_L \gamma_\mu l_L) U^\mu + g_X \bar{q}_L \gamma_\mu \bar{\tau} l_L \vec{X}^\mu \\
& + (g_W^l \bar{l}_L \gamma_\mu \bar{\tau} l_L + g_W^q \bar{q}_L \gamma_\mu \bar{\tau} q_L) \vec{W}^\mu
\end{aligned} \tag{4.6}$$

The exchange of these scalar and vector bosons gives rise to effective interactions containing those of eq. (4, 5). After some Fierz transformations one obtains for the corresponding non-vanishing coefficients:

$$\begin{aligned}
\frac{1}{(\Lambda_{LL}^u)^2} &= -\frac{g_D^q g_D^{u*}}{2m_D^2} - \frac{g_G^q g_G^{u*}}{2m_G^2} \\
\frac{1}{(\Lambda_{LR}^d)^2} &= -2 \frac{g_U^q g_U^{e*}}{m_U^2} \\
\frac{1}{(\bar{\Lambda}_{LL}^u)^2} &= +\frac{g_D^q g_D^{q*}}{2m_D^2} - 2 \frac{g_X g_X^*}{m_X^2} + \frac{g_W^q g_W^l}{m_W^2} \\
\frac{1}{(\bar{\Lambda}_{LR}^u)^2} &= -\frac{g_G^q g_G^{q*}}{2m_G^2} \\
\frac{1}{(\bar{\Lambda}_{RL}^u)^2} &= -\frac{g_G^u g_G^{u*}}{2m_G^2} \\
\frac{1}{(\bar{\Lambda}_{RR}^u)^2} &= +\frac{g_D^u g_D^{u*}}{2m_D^2} \\
\frac{1}{(\bar{\Lambda}_{LL}^d)^2} &= -\frac{g_U^q g_U^{q*}}{m_U^2} - \frac{g_X^* g_X}{m_X^2} - \frac{g_W^q g_W^l}{m_W^2} \\
\frac{1}{(\bar{\Lambda}_{LR}^d)^2} &= -\frac{g_G^q g_G^{q*}}{2m_G^2} - 2 \frac{g_U^q g_U^{e*}}{m_U^2} \\
\frac{1}{(\bar{\Lambda}_{RR}^d)^2} &= -\frac{g_U^e g_U^{e*}}{m_U^2}
\end{aligned} \tag{4.7}$$

The result shows that the induced effective interactions are qualitatively different for different exchanged particles. One has:

D – exchange: $D^0(\bar{D}^0)$ decays only

U – exchange: $B^0(\bar{B}^0)$, $B_s(\bar{B}_s)$ decays only

G – exchange: $D^0(\bar{D}^0)$ and $B^0(\bar{B}^0)$, $B_s(\bar{B}_s)$ decays, but B decays helicity suppressed

X – exchange: $D^0(\bar{D}^0)$ and $B^0(\bar{B}^0)$, $B_s(\bar{B}_s)$ decays, with fixed ratio of decay widths:

$$\Gamma(D \rightarrow e_i^+ e_j^-) / \Gamma(B \rightarrow e_i^+ e_j^-) = 4m_D / m_B$$

These different possibilities illustrate the importance of a combined analysis of D- and B-decays.

Branching Ratios

Since we are only interested in order of magnitude estimates it is sufficient to approximate

the total width by the contribution from the spectator diagram:

$$\begin{aligned}\Gamma(D^0) &\approx \frac{5}{192\pi^3} G_F m_c^5 \\ \Gamma(B^0) &\approx \Gamma(B_s) \approx \frac{9}{192\pi^3} G_F^2 m_b^5 |V_{cb}|^2\end{aligned}\quad (4.8)$$

where G_F , m_c , m_b and V_{cb} denote the Fermi constant, c- and b- quark masses and the KM matrix element respectively. It is now straightforward to compute the branching ratio for a decay induced by a helicity changing operator with scale Λ or a helicity conserving operator with scale $\bar{\Lambda}$. The result depends on the ratio of the Higgs vacuum expectation value $v = (2\sqrt{2}G_F)^{-1/2} = 174$ GeV to the scale $\Lambda(\bar{\Lambda})$. Using $m_c \approx 1.5$ GeV, $m_b \approx 4.8$ GeV, $f_D \approx f_B \approx 100$ MeV, $|V_{cb}| \approx (0.2)^2$ one obtains:

helicity changing decays:

$$\Gamma(D \rightarrow e_i^+ e_j^-) \approx \frac{24\pi^2}{5} \left(\frac{f_D}{m_c}\right)^2 \left(\frac{v}{\Lambda}\right)^4 \approx 0.2 \left(\frac{v}{\Lambda}\right)^4 \quad (4.9)$$

$$\Gamma(B \rightarrow e_i^+ e_j^-) \approx \frac{24\pi^2}{9} \left(\frac{f_B}{m_b}\right)^2 \frac{1}{|V_{cb}|^2} \left(\frac{v}{\Lambda}\right)^4 \approx 7.1 \left(\frac{v}{\Lambda}\right)^4 \quad (4.10)$$

helicity conserving decays:

$$\Gamma(D \rightarrow e_i^+ e_j^-) \approx \frac{24\pi^2}{5} \frac{m_i^2 + m_j^2}{m_c^2} \left(\frac{f_D}{m_c}\right)^2 \left(\frac{v}{\Lambda}\right)^4 \approx 2 \cdot 10^{-3} \frac{m_i^2 + m_j^2}{2m_\mu^2} \left(\frac{v}{\Lambda}\right)^4 \quad (4.11)$$

$$\Gamma(B \rightarrow e_i^+ e_j^-) \approx \frac{24\pi^2}{9} \left(\frac{f_B}{m_b}\right)^2 \frac{1}{|V_{cb}|^2} \left(\frac{v}{\Lambda}\right)^4 \frac{m_i^2 + m_j^2}{m_b^2} \approx 5 \cdot 10^{-3} \frac{m_i^2 + m_j^2}{2m_\mu^2} \left(\frac{v}{\Lambda}\right)^4 \quad (4.12)$$

The eqs. (9–12) can be used to obtain from the present experimental bounds on D^0 and D^0 decays the corresponding mass scales Λ and $\bar{\Lambda}$. In table I these mass scales are compared with the corresponding limits attainable at LEP. Since $\Lambda(\bar{\Lambda})$ increases as $(BR(M \rightarrow e_i^+ e_j^-))^{-1/4}$ the improvement of two order of magnitude in the branching ratio from 10^{-4} to 10^{-6} does not appear very impressive in terms of $\Lambda(\bar{\Lambda})$, which is the relevant physical quantity. The most important progress will be the completely new information on $B_s(\bar{B}_s)$ mesons for which many theoretical models predict much larger flavour changing interactions than for K- and D- mesons.

Theoretical Models

i) Standard Model

Here operators of the form given in eqs. (4, 5) are generated through radiative corrections. The one-loop contributions are shown in Fig. 4.6. From the complete expression [13] only the V–A current–current interaction, which arises from Fig. 4.6a and the Z–boson terms

in Fig. 4.6b,c, contribute to the decay of pseudoscalar mesons. The result is ([13,14] cf. eq. (5)):

$$\begin{aligned} \frac{1}{(\bar{\Lambda}_{LL}^{(u)})^2}_{ij} &= \frac{g^2}{128\pi^2 m_W^2} \sum_k V_{u_i d_k}^* V_{u_j d_k} f_L^{(u)}(x_k) \quad , \quad x_k = \frac{m_{d_k}^2}{m_W^2} \\ \frac{1}{(\bar{\Lambda}_{LL}^{(d)})^2}_{ij} &= \frac{g^2}{128\pi^2 m_W^2} \sum_k V_{u_k d_i}^* V_{u_k d_j} f_L^{(d)}(y_k) \quad , \quad y_k = \frac{m_{u_k}^2}{m_W^2} \end{aligned} \quad (4.13)$$

where the functions $f_L^{(u)}$ and $f_L^{(d)}$ are given in [13,14]. The dominant contribution comes from the s -quark, respectively the t -quark, in the loop and one finally obtains ($m_t \approx m_W$, $V_{ts} \approx (0.2)^2$, $V_{td} \approx (0.2)^3$):

$$\begin{aligned} (\bar{\Lambda}_{LL}^{(u)})_{uc} &\approx v \left(\frac{3g^2}{32\pi^2} \frac{m_s^2}{m_W^2} \log \frac{m_W^2}{m_s^2} |V_{cs} V_{us}| \right)^{-1/2} \approx 1000 \text{ TeV} \\ (\bar{\Lambda}_{LL}^{(d)})_{db} &\approx v \left(\frac{g^2}{16\pi^2} \frac{5}{8} |V_{tb} V_{td}| \right)^{-1/2} \approx 50 \text{ TeV} \\ (\bar{\Lambda}_{LL}^{(d)})_{sb} &\approx v \left(\frac{g^2}{16\pi^2} \frac{5}{8} |V_{tb} V_{ts}| \right)^{-1/2} \approx 20 \text{ TeV} \end{aligned} \quad (4.14)$$

All values of $\bar{\Lambda}$ are much too large to be probed at LEP. The corresponding branching ratios to $\mu^+ \mu^-$ pairs are $BR(D^0 \rightarrow \mu^+ \mu^-) \approx 10^{-18}$, $BR(B^0 \rightarrow \mu^+ \mu^-) \approx 10^{-12}$, $BR(B_s \rightarrow \mu^+ \mu^-) \approx 10^{-11}$, clearly far below the sensitivity attainable anywhere in the foreseeable future.

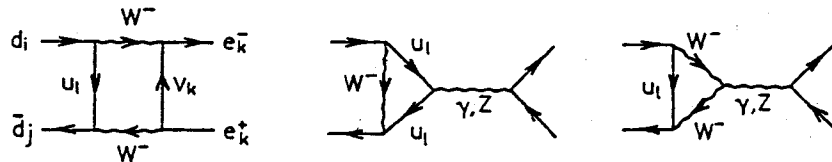
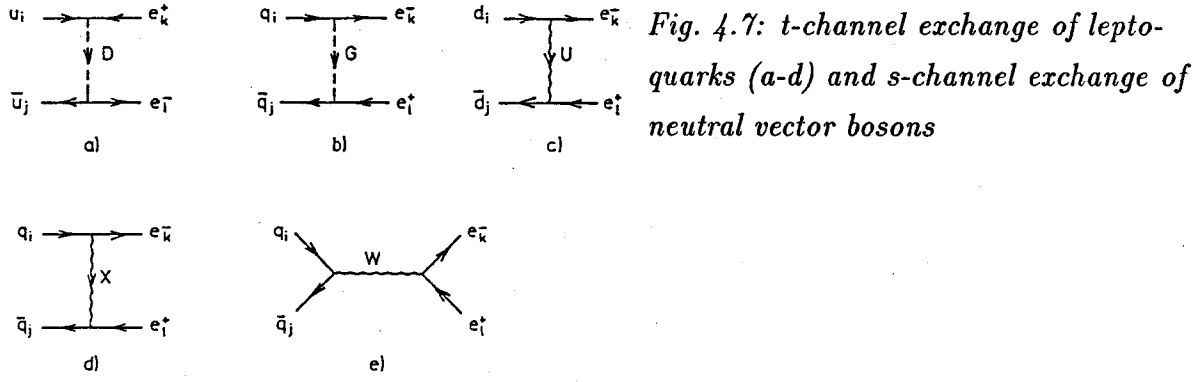


Fig. 4.6: One-loop contributions in the Standard Model to quark-lepton contact interactions.

ii) s-Channel exchanges

Various extensions of the Standard Model, such as Extended Technicolor Models (ETC) [15] or multi-Higgs models, which are also motivated by superstring-inspired supergravity theories [16,17] predict the existence of scalar or vector bosons whose s -channel exchange (cf. Fig. 4.7) leads to operators listed in eq. (4,5).

For instance the ETC model described by Eichten et al. [18] contains a neutral pseudo-Goldstone boson P^0 which couples to quark pairs with strength $(m_1 + m_2)V_{12}/(2F_\pi)$ and to leptons with strength $(m_1 + m_2)/(2F_\pi)$, where $F_\pi = (8G_F/\sqrt{2})^{-1/2} \approx 124 \text{ GeV}$.



With $m_{p0} \approx 40$ GeV one obtains for the strength of the corresponding, helicity changing $(\bar{b}s)(\bar{\mu}\mu)$ interaction:

$$\Lambda \approx \frac{2F_\pi}{(m_b m_\mu)^{1/2}} \frac{1}{|V_{cb}|^{1/2}} m_{p0} \approx 70 \text{ TeV} \quad (4.15)$$

Masiero et al. [19] have proposed an interesting ETC scenario in which only semileptonic FCNC occur which violate separate lepton numbers and conserve "generation number". For a techniquark condensate $\langle \bar{T}T \rangle \approx v^3 \approx (174 \text{ GeV})^3$ one estimates:

$$\begin{aligned} D^0 \longrightarrow \mu^- e^+ : \quad \bar{\Lambda} &\sim \left(\frac{\langle \bar{T}T \rangle}{m_u} \right)^{1/2} \approx 30 \text{ TeV} \\ B_s \longrightarrow \mu^- \tau^+ : \quad \bar{\Lambda} &\sim \left(\frac{\langle \bar{T}T \rangle}{m_s} \right)^{1/2} \approx 6 \text{ TeV} \end{aligned} \quad (4.16)$$

One may also to have *s*-channel exchange of vector bosons with flavour changing quark couplings (cf. Fig. 4.7e). For instance, if the Z^0 -boson would couple to all quark pairs, as it was recently suggested for up-quarks [20], i.e. ,

$$\lambda_{ij} \simeq \frac{m_{u_i} m_{u_j}}{m_W^2} \quad (4.17)$$

one would have (assuming $m_t = O(m_W)$) $\lambda_{bs} \simeq 10^{-2}$ (cf. also [21]) and therefore:

$$B_s \longrightarrow e_i^- e_i^+ : \quad \bar{\Lambda} \sim \left(\frac{\lambda_{bs} g}{m_W^2} \right)^{1/2} \sim 2 \text{ TeV} \quad (4.18)$$

A value of 10^{-2} for λ_{bs} is not excluded by current experiments (cf. [17], [22]). We conclude that theoretical expectations for *s*-channel exchanges lead to mass scales $\Lambda, \bar{\Lambda}$ most of which are beyond the sensitivity at LEP. However, our current knowledge does not exclude larger effects, such as the mass scales discussed above which would lead to observable rates (Tab. 4.1)

iii) t-Channel exchanges

The classic process which generates effective quark-lepton interaction of the type given

Process	Present bounds			Bounds at LEP	
	BR(Ref. 6)	$\bar{\Lambda}$ [TeV]	Λ [TeV]	$\bar{\Lambda}$ [TeV]	Λ [TeV]
$D^0 \rightarrow \mu^+ \mu^-$	$1.1 \cdot 10^{-5}$	0.6	2	1	4
$e^+ e^-$	$1.3 \cdot 10^{-4}$	0.02	1	0.1	4
$\mu^+ e^-$	$1.2 \cdot 10^{-4}$	0.3	1	1	4
$B^0 \rightarrow \mu^+ \mu^-$	$5 \cdot 10^{-5}$	0.6	3	1.5	9
$e^+ e^-$	$8 \cdot 10^{-5}$	0.04	3	0.1	9
$\mu^+ e^-$	$5 \cdot 10^{-5}$	0.5	3	1	9
$B_s \rightarrow \mu^+ \mu^-$				1	8
$e^+ e^-$		—		0.1	8
$\mu^+ e^-$				1	8

Tab. 4.1: Bounds on branching ratios and mass scales of vector ($\bar{\Lambda}$) and scalar (Λ) contact interactions. The bounds obtainable at LEP correspond to the assumed branching ratios $\text{BR}(D^0 \rightarrow e_i^+ e_j^-) < 10^{-6}$, $\text{BR}(B^0 \rightarrow e_i^+ e_j^-) < 10^{-6}$, $\text{BR}(B_s \rightarrow e_i^+ e_j^-) < 2 \cdot 10^{-6}$.

in eqs. (4,5) is the exchange of leptoquarks (cf. Figs. 4.7a-d). Most popular are vector leptoquarks of Pati-Salam type [23,8] with the quantum numbers of right-handed up-quarks (U^μ in eq. (6) and scalar leptoquarks of SU(5)-type [17,24] which carry the quantum numbers of right-handed down-quarks (D in eq. (6)) and which form a complete 5-representation of SU(5) together with the ordinary Higgs doublet. The most general Lagrangian for leptoquarks with renormalizable couplings has been given in [12].

The Pati-Salam type leptoquarks couple only to down-quarks. From $K_L \rightarrow \mu^+ \mu^-$ and $K_L \rightarrow \mu^\pm e^\mp$ one obtains the lower bound $(\bar{\Lambda}^d)_{ds} > 60 \text{ TeV}$ [8]. The expectations for B-decays depend on the dependence of $\bar{\Lambda}$ on the quark masses. For mass independent couplings, which are expected for gauge bosons, one has $(\bar{\Lambda}^d)_{sb} = (\bar{\Lambda}^d)_{ds}$ which is far beyond the range accessible at LEP. Also conceivable is a mass dependence corresponding to eq. (17) which yields

$$(\bar{\Lambda}^d)_{sb} \approx \left(\frac{m_d}{m_b}\right)^{1/2} (\bar{\Lambda}^d)_{ds} \approx 3 \text{ TeV} \quad (4.19)$$

which can be tested at LEP.

SU(5)-type leptoquarks couple up-quarks to charged leptons and down-quarks to neutrinos. Constraints from quark-lepton universality of the weak interactions yield the bound [24]

$$(\bar{\Lambda}^u)_{uc} > 2 \text{ TeV}$$

which is already too large to be tested at LEP. However, no corresponding bound exists so far for the scalar mass parameter $(\Lambda^u)_{uc}$.

Summary

It appears feasible to improve at LEP the current experimental bounds on branching ratios of D^0 - and B^0 - mesons to lepton pairs by two orders of magnitude down to 10^{-6} . For scalar contact interactions this corresponds to a sensitivity in the mass parameter up to $\Lambda \simeq 9$ TeV, for which some theoretical models predict flavour changing neutral currents. Particularly interesting is the combined analysis of D - and B - meson decays which allows to identify the source of flavour violation.

Most important will be the new information on B_s - mesons which, for the first time, will test flavour changing couplings between quarks of the second and third generations. Although the experimental signature for τ leptons is not as clean as those for electrons and muons, efforts should be made to obtain stringent limits on the decay modes $D^0 \rightarrow \mu^- e^+$, $B^0 \rightarrow \tau^+ e^-$ and $B_s \rightarrow \tau^+ \mu^-$ whose observation would provide a clue to the puzzle of replication of quark-lepton families (Fig. 4.8).

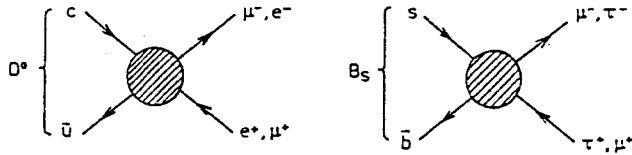


Fig. 4.8: D - and B -decays which conserve "generation number".

4.3. NON-STANDARD FERMIONS*

In many extensions of the Standard Model there exist non-standard fermions which may show up at LEP, either through effects of mixing with the standard fermions, or directly produced. Below, the physics of two possible kinds of non-standard fermions will be summarized. These are mirror fermions [25] and exceptional fermions [1, 26].

Mirror fermions arise naturally when the fermion families are unified within one spinor representation of a large orthogonal group [27–34] or within high-dimension representations of large unitary groups [35–40] or exceptional groups [41]. Mirror fermions necessarily appear in the particle spectrum when an extended supersymmetry ($N \geq 2$) [42] is imposed on a gauge theory, as well as in the Kaluza-Klein theories [43]. They appear also in some composite models [44]. The members of an ordinary $V - A$ family are classified in the following set of left- and right-handed isospin doublets and singlets of $SU(2)_I \times U(1)_Y$

$$\begin{aligned} \begin{bmatrix} \nu_e \\ e^- \end{bmatrix}_L & \quad \begin{matrix} \nu_{eR} \\ e^-_R \end{matrix} \\ \begin{bmatrix} u_i \\ d_i \end{bmatrix}_L & \quad \begin{matrix} u_{iR} \\ d_{iR} \end{matrix} \end{aligned} \quad (4.20)$$

*M. ROOS, P.M. ZERWAS

The corresponding components of a $V + A$ mirror family are classified according to

$$\begin{array}{cc} N_L & \left[\begin{array}{c} N \\ E^- \end{array} \right]_R \\ E_L^- & \\ U_{iL} & \left[\begin{array}{c} U_i \\ D_i \end{array} \right]_R \\ D_{iL} & \end{array} \quad (4.21)$$

The index $i = 1, 2, 3$ denotes the quark colors. The electric charges of the members of a mirror family are identical with those of the corresponding components in the ordinary family. As is clear from (20) and (21), the only difference between ordinary and mirror fermions is that they enter the weak interactions in the opposite chirality states, the former in the left-handed states and the latter in the right-handed states.

Exceptional fermions are non-standard states belonging to the 27-dimensional representation of the exceptional group E_6 [45] which predicts a rich spectrum of new vectorial neutral and charged leptons and isoscalar charge $-\frac{1}{3}$ quarks [46, 47],

$$\begin{array}{cccccc} \left[\begin{array}{c} \nu_e \\ e^- \end{array} \right]_L & \nu_{eR} & \left[\begin{array}{c} \nu_E \\ E^- \end{array} \right]_L & \left[\begin{array}{c} \nu_E \\ E^- \end{array} \right]_R & n_L & \\ & e_R^- & & & & \\ \left[\begin{array}{c} u_i \\ d_i \end{array} \right]_L & u_{iR} & D_{iL}^{1/2} & D_{iR}^{1/2} & & \end{array} \quad (4.22)$$

Similarly for the other generations. They could either affect the ordinary chiral fermions through mixing [48–50] or they can be produced directly in e^+e^- annihilation [48, 49, 51, 52]. We will focus on E_6 in two versions.

(i) The new exceptional fermions are treated in analogy to the ordinary quarks and leptons, with the usual assignments of lepton and baryon quantum numbers, so that they can mix with the chiral fermions [48–50]. These new fermions could easily be detected since they decay partly into neutral-current channels, producing clear signatures such as $E^- \rightarrow e^-e^+e^-$ and $D_{1/2} \rightarrow de^+e^-$.

(ii) E_6 with supersymmetric extension had been suggested as a possible 4-dimensional field-theoretic limit of the heterotic superstring [47, 46]. Depending on the assignment of lepton and baryon quantum numbers and the choice of the Yukawa potential, the properties of the new colored particles are of special interest. The scalar particles, leptoquarks and diquarks, either decay into jet+lepton or jet+jet final states that are both easy to detect [52, 53]. The new fermions could reveal themselves through decays into jet+lepton+ χ , where χ , the lightest massive supersymmetric particle, escapes detection.

4.3.1. CONSTRAINTS: NON-STANDARD EFFECTS ON STANDARD FERMIONS

If the masses of non-standard (NS) fermions are generated during the spontaneous breaking of $SU(2) \times U(1)$ gauge symmetry, they cannot be heavier than about 250 GeV. One may even produce them copiously at LEP. On the other hand, these fermions may manifest themselves already at the energies available today. It is quite possible that NS neutrinos are much lighter than charged NS fermions, which in turn must be heavier than about 40 GeV [54] [this UA1 limit assumes that such neutrinos are very light], or heavier than about 26 GeV [55]. Light NS neutrinos could be produced *e.g.* in μ , π and K decays. Charged NS fermions, if they mix with their ordinary partners, would manifest themselves as deviations from the purely $V - A$ structure of the weak interactions of the known fermions [56, 28, 29]. Such deviations can also be signatures of a right-handed gauge boson W_R in a left-right symmetric gauge model, but LR models, mirror models and exceptional models lead in general to different parametrizations of the currents and can in principle be distinguished from each other.

Besides the modifications in the Lorentz structure of the currents, another consequence of NS mixing is the existence of non-diagonal neutral currents ($\bar{L}\ell, \bar{N}\nu, \bar{Q}q$) which are forbidden in the standard model as a result of the GIM mechanism [57]. In mirror mixing the GIM mechanism does not work, because the mixed objects have opposite axial vector couplings, leaving a net non-diagonal *axial* vector current. All the neutral *vector* couplings including the electromagnetic couplings are in contrast untouched by the mixing. The situation is somewhat analogous in the case of E_6 , where one can have non-diagonal lepton currents and down-quark ($\bar{D}_{1/2}d$) currents. The frustration of the GIM mechanism is a novel feature of NS mixing and can be used to distinguish NS leptons and quarks from the heavy fermions of ordinary type. To give an example, the decay channel $L^- \rightarrow \ell^- \ell^+ \ell^-$ is possible (though suppressed by a mixing factor) for an NS lepton, but not for a sequential lepton.

The NS *mixing of quarks* is severely constrained by the non-observation of flavour changing neutral currents (FCNC) [56, 58]. Since the GIM mechanism is not valid for NS mixing, an $\bar{s}dZ$ coupling may be induced by NS mixing if the s and d quarks contain an NS impurity. As a result a $K_L - K_S$ mass difference is generated by a Z exchange diagram.

Even if the FCNC currents were absent at tree level, they would be induced by radiative corrections. In the standard model the $K_L - K_S$ mass difference is generated by weak interactions of second order in G_F due to the famous box-diagrams [59] with up-type quarks u, c and t as internal states. In the presence of NS mixing, the internal states may be replaced by heavier mirror quarks U, C and T with appropriate mixing factors in the vertices. The exceptional $D_{1/2}$ -quark does not appear in these box diagrams, but its

mixing with the ordinary down-type quark would affect the relevant Cabibbo-Kobayashi-Maskawa matrix elements. A comparison of the ensuing mass difference to the measured value leads to the mixing angle [56, 58] $\theta_q \lesssim 10^{-4}$ for mirror quark masses $O(100 \text{ GeV})$. If one takes this bound as a generic one for all the quark-NS quark mixing angles, there is no chance to see deviations from the $V - A$ structure of quark currents at LEP. We will therefore concentrate on the leptonic currents.

Consider for example the *mirror mixing of the electron*. The mass Lagrangian is given by

$$\mathcal{L}_m = (\bar{e}'_R \ \bar{E}'_R) \begin{pmatrix} m_{ee} & m_{eE} \\ m_{eE} & m_{EE} \end{pmatrix} \begin{pmatrix} e'_L \\ E'_L \end{pmatrix} + h.c. \quad (4.23)$$

where we use primes to indicate weak eigenstates. We will assume that the mass matrix is hermitian. Then the diagonalization is characterized by one rotation angle and one finds

$$\begin{aligned} e &= \cos \theta_e e' + \sin \theta_e E', \\ E &= -\sin \theta_e e' + \cos \theta_e E', \end{aligned} \quad (4.24)$$

where e and E are the mass eigenstates and the mixing angle θ_e is given by

$$|\tan 2\theta_e| = \left| \frac{2m_{eE}}{m_{EE} - m_{ee}} \right| \simeq 2 \left| \frac{m_{eE}}{m_{EE}} \right|. \quad (4.25)$$

The eigenvalues of the mass are

$$m_{E,e} = \frac{1}{2}(m_{EE} + m_{ee}) \pm \frac{1}{2}\sqrt{(m_{EE} - m_{ee})^2 + 4m_{eE}^2} \simeq \begin{cases} m_{EE} + \frac{m_{eE}^2}{m_{EE}} \\ m_{ee} - \frac{m_{eE}^2}{m_{EE}} \end{cases} \quad (4.26)$$

Similarly one can define NS mixing for the other fermions.

The analysis of the V, A structure of the weak currents shows [25] that in all cases the results are consistent with no mirror mixing within simultaneous 90% confidence limits. The upper limits for the different mirror mixing angles range from 14.3° to 25.5° when the mirror neutrinos N_e and N_μ are very heavy, $m_N \gtrsim 18 \text{ GeV}$, or very light, $m_N \lesssim 1 \text{ eV}$. In the range between, $1 \text{ eV} \lesssim m_N \lesssim 18 \text{ GeV}$, these bounds are surpassed by the results of searching for production and subsequent decay of new neutral leptons and by the astrophysical and cosmological constraints.

The existence of NS mixing also affects the W and Z masses and the cross-sections for ordinary lepton-antilepton and quark-antiquark pair production, however only through sines of small mixing angles. The effects on charm $D^0 \bar{D}^0$ mixing of the E_6 $D_{1/2}$ -quark is negligible unless the $D_{1/2}$ -quark has a mass of several 100 GeV.

Since *NS neutrinos* may be very light, there is evidently a much larger variety of experimental constraints for them than for the charged NS fermions. There exist many studies on constraints for a new "heavy" neutrino [60]. Usually the new neutrino is taken

to be a *sequential neutrino* (ν_{4L}) transforming as a member of a new left-handed $SU(2)_L$ doublet or an $SU(2)_L$ *singlet neutrino* ν_R or n_L as in E_6 . The essential differences between such neutrinos and a mirror neutrino N are the following:

- i) In the sequential neutrino case the GIM mechanism is operative, forbidding non-diagonal Z couplings $Z\nu_4\nu_i$, $i = 1, 2, 3$. In the mirror neutrino case non-diagonal couplings $Z\nu N$ may appear.
- ii) For a singlet neutrino ν_R the Z -coupling $Z\nu_R\nu_R$ is suppressed by a factor $\sin^2\theta$, where θ is the mixing angle between ν_R and a doublet neutrino ν_L . For the mirror neutrinos the coupling ZNN is of full weak interaction strength, as are the exceptional neutrino couplings $Z\nu_E\nu_E$.

Important bounds on the mass *vs.* mixing angle follow from the effects on the cosmic photon flux of the radiative decay of a heavy neutrino $N \rightarrow \nu + \gamma$. This decay will occur in the standard model if neutrino flavours mix [61], and in the NS models if leptons and NS leptons mix [56, 28, 29, 62].

4.3.2. PRODUCTION AND DECAY SIGNATURES OF NON-STANDARD FERMIONS

a) Z decay widths and FB asymmetries

The main reactions for NS lepton production at LEP would be Z decays

$$\begin{aligned} Z &\rightarrow L^- L^+ \\ &\rightarrow N \bar{N}, \end{aligned} \tag{4.27}$$

which proceed with full weak interaction strength. Here L and N stand for any one family of charged and neutral doublet leptons. The decay rate as a function of the NS lepton masses m_L and m_N is given by

$$\begin{aligned} \Gamma(Z \rightarrow L^- L^+) &= \frac{Gm_Z^3}{24\sqrt{2}\pi} \left(1 - \frac{4m_L^2}{m_Z^2}\right)^{\frac{1}{2}} \\ &\times \left[(|v_\ell|^2 + |a_\ell|^2) \left(1 - \frac{m_L^2}{m_Z^2}\right) + (|v_\ell|^2 - |a_\ell|^2) 3 \frac{m_L^2}{m_Z^2} \right] \end{aligned} \tag{4.28}$$

where v_ℓ and a_ℓ are neutral current couplings

$$\left. \begin{aligned} v &= 2(I_L^3 + I_R^3) - 4Q \sin^2 \theta_W \\ a &= 2(I_L^3 - I_R^3) \end{aligned} \right\} \text{ mod. mixing} \tag{4.29}$$

If L is a mirror lepton, one has

$$\begin{aligned} v_\ell &= -1 + 4 \sin^2 \theta_W \\ a_\ell &= \cos 2\theta_\ell \end{aligned} \tag{4.30}$$

and if it is an exceptional lepton [49]

$$\begin{aligned} v_\ell &= -2 + 4 \sin^2 \theta_W \\ a_\ell &= 0 \end{aligned} \quad (4.31)$$

In (31) we have neglected a possible but small mixing between Z and the new gauge boson Z' corresponding to the extra $U(1)$ symmetry in the E_6 model. [Note that G in (30) is not exactly the Fermi constant measured in μ -decay since the μ -decay is also affected by the mixings [25].]

If the mirror neutrino N is a Dirac particle, the decay rate for $Z \rightarrow N\bar{N}$ is obtained from (28) by replacing m_L by m_N and v_ℓ by unity. If N instead is a Majorana particle, the rate is given by

$$\Gamma(Z \rightarrow NN)_{Maj.} = \frac{Gm_Z^3}{6\sqrt{2}\pi} \left(1 - \frac{4m_N^2}{m_Z^2}\right)^{\frac{3}{2}} |a_\ell|^2 \quad (4.32)$$

The corresponding result for the E_6 Dirac neutrino is obtained by putting $v_\ell = +2$ in eq. (28). Isosinglet neutrinos couple to the Z boson only through mixing so that the Z decay widths into these channels will be very small.

If the decays (27) are kinematically forbidden or highly suppressed, the mixed channels

$$\begin{aligned} Z &\rightarrow \nu_\ell \bar{N} + \bar{\nu}_\ell N \\ &\rightarrow L^- \ell^+ + \ell^- L^+ \end{aligned} \quad (4.33)$$

would dominate. These channels are slowed down, however, by a mixing angle. For example,

$$\Gamma(Z^- \rightarrow L^- \ell^+) = \frac{Gm_Z^3}{24\sqrt{2}\pi} (|\tilde{v}_\ell|^2 + |\tilde{a}_\ell|^2) \left(1 - \frac{m_L^2}{m_Z^2}\right) \left(1 - \frac{m_L^2}{2m_Z^2} - \frac{m_L^4}{2m_Z^4}\right) \quad (4.34)$$

where we have assumed $m_\ell \ll m_L$. In the mirror lepton case one has $\tilde{v}_\ell = 0$, $\tilde{a}_\ell = \sin^2 2\theta_\ell$, and in the exceptional lepton case $\tilde{v}_\ell = \tilde{a}_\ell = \eta$, where η is a mixing parameter.

The production of mirror quarks and $D_{1/2}\bar{D}_{1/2}$ pairs at LEP is completely analogous to the production of ordinary $q\bar{q}$ pairs. The partial Z decay width derives from (28) by adding the color factor $N_c = 3$ and substituting the appropriate neutral current couplings; mod. mixing,

$$\begin{aligned} \text{mirror quarks:} \quad v_Q &= \pm 1 - 4Q \sin^2 \theta_W \quad \text{up/down} \\ a_Q &= \mp 1 \\ E_6 D_{1/2} \text{ quarks:} \quad v_D &= \frac{4}{3} \sin^2 \theta_W \\ a_D &= 0 \end{aligned}$$

The mixed ordinary-mirror channel $Z \rightarrow Q\bar{q}$ and $Z \rightarrow D_{1/2}\bar{d}$ can be treated in analogy to (34) apart from the additional color factor $N_c = 3$.

In principle the most straightforward method to distinguish a mirror fermion from an ordinary fermion would be to search for a right-handed interaction in the angular distributions of the decay products. One clear signal of this kind would be the *forward-backward asymmetry* A_{FB} in e^+e^- collisions. In mirror fermion production $e^+e^- \rightarrow F\bar{F}$, A_{FB} has the same absolute value as the asymmetry in the production $e^+e^- \rightarrow f\bar{f}$ of ordinary fermions of the same mass, however with the *opposite sign* [63]

$$A_{FB}(e^+e^- \rightarrow F\bar{F}) = -A_{FB}(e^+e^- \rightarrow f\bar{f}) \quad (4.35)$$

These asymmetries have been elaborated at length in the first section, including non-zero mass effects, and this discussion will therefore not be repeated here.

By contrast, *no forward-backward asymmetry* is expected in the production of E_6 vector leptons and quarks.

A complementary analysis for the production of non-standard fermions away from the Z peak can be found in the literature. Most of the apparatus described in the first section of this Report carries over in a straightforward way by substituting the appropriate vector and axial-vector couplings eq. (29) for the mirror particles [25] and the E_6 type vector leptons and quarks.

b) *Decay patterns and signatures*

In the following we shall describe the main signatures of non-standard leptons and quarks based on their characteristic decay patterns. NS particles exhibit a pattern of allowed decays and suppressed or forbidden decays which is different from that of sequential $V-A$ leptons.

Let us first consider the case of NS doublet leptons E and N which are sufficiently light so that they could appear in the final states of weak gauge boson decays. The dominant decay channels for a charged lepton of the e -family (assuming $m_E > m_N$) are

$$\begin{aligned} E^- &\rightarrow N e^- \bar{\nu}_e \\ &\rightarrow N q \bar{q} \end{aligned} \quad (4.36)$$

and for an NS neutrino (assuming $m_N > m_E$)

$$\begin{aligned} N &\rightarrow E^- e^+ \nu_e \\ &\rightarrow E^- q \bar{q} \end{aligned} \quad (4.37)$$

where q stands for ordinary quarks. In case these processes are kinematically suppressed,

the dominant channels would be

$$\begin{aligned}
E^- &\rightarrow e^- \ell^+ \ell^- \\
&\rightarrow e^- \bar{\nu}_\ell \nu_\ell \\
&\rightarrow e^- q \bar{q} \\
&\rightarrow \nu_e \ell^- \bar{\nu}_\ell \\
&\rightarrow \nu_e q \bar{q}
\end{aligned} \tag{4.38}$$

where $\ell = e, \mu, \tau$, and

$$\begin{aligned}
N &\rightarrow e^- \ell^+ \nu_\ell \\
&\rightarrow \nu_e \ell^- \ell^+ \\
&\rightarrow \nu_e \nu_\ell \bar{\nu}_\ell \\
&\rightarrow \nu_e q \bar{q}
\end{aligned} \tag{4.39}$$

These channels have larger phase space than the processes (36) and (37), but the decays are slowed down by a mixing angle.

The decay signature of a charged NS lepton would thus be marvelous 3-charged lepton final states or an isolated light lepton plus missing energy, or two quark jets plus an isolated lepton or missing energy. The signature of an NS neutrino would be a charged lepton or quark pair plus missing energy.

An exciting signal for the production of a non-standard charged lepton in Z decays would be the observation of multi-lepton final states [49]

$$\frac{\Gamma(Z \rightarrow E^+ E^- \rightarrow e^+ \ell^+ \ell^- + e^- \ell^+ \ell^-)}{\Gamma(Z \rightarrow e^+ e^-)} \sim \text{a few } 10^{-3} \tag{4.40}$$

with lepton triades clustering at m_E . They cannot be faked by sequential heavy leptons.

Similar purely leptonic final states in NS neutrino production which are relatively free of background, have been estimated to occur at a rate [64]

$$\frac{\Gamma(Z \rightarrow N \bar{N} \rightarrow \ell^+ \ell^- \ell^+ \ell^- \nu_\ell \bar{\nu}_\ell)}{\Gamma(Z \rightarrow \nu_\ell \bar{\nu}_\ell)} \lesssim (5.5 - 2.8) \times 10^{-3} \tag{4.41}$$

The same process is possible also for a sequential neutrino, the relative width [64] being one order of magnitude larger than (41). Another purely leptonic channel is

$$Z \rightarrow N \bar{N} \rightarrow \ell^+ \ell^- + \text{neutrinos} \tag{4.42}$$

with a signature of two isolated charged leptons plus missing transverse energy. The same final state would arise also from a pair of charged mirror (or sequential) leptons, but the angular distribution of the final state charged leptons would differ in the two cases.

A striking signature of NS neutrino production in Z -decay would be a monojet plus missing energy due to the process $Z \rightarrow \nu \bar{N}$, $\bar{N} \rightarrow \bar{\nu} qq$ where the two quark jets are not separated. This process is not possible for a sequential heavy neutrino since it requires non-diagonal Z -couplings. The monojet cross section due to the presence of a mirror neutrino was estimated [64] to be

$$\frac{\Gamma(Z \rightarrow \text{monojet} + \text{missing energy})}{\Gamma(Z \rightarrow \nu_e \bar{\nu}_e)} \lesssim 0.22 - 0.12 \quad (4.43)$$

for $m_N = 20 - 40$ GeV, and with $\phi_\ell, \theta_\ell \lesssim 10^{-2}$ for the mirror mixing angles (ϕ_ℓ is the $\nu_\ell N$ mixing angle and θ_ℓ is the ℓL mixing angle).

If the NS lepton is lighter than the weak gauge bosons, its dominant decay channels are as in (36) (assuming $m_L > m_N$). The main contribution to the decay amplitude comes from W -exchange, since the Z -exchange process involves non-diagonal couplings suppressed by mixing. The decay width in the limit of vanishing masses of the final state fermions f_i is given by [65]

$$\Gamma(L \rightarrow N f_1 \bar{f}_2) = \frac{G m_L^5}{192 \pi^3} \left[\frac{|V|^2 + |A|^2}{2} f\left(\frac{m_N}{m_L}\right) + \frac{|V|^2 - |A|^2}{2} 2 \frac{m_N}{m_L} g\left(\frac{m_N}{m_L}\right) \right] \quad (4.44)$$

where

$$\begin{aligned} f(x) &= 1 - 8x^2 + 8x^6 - x^8 - 12x^4 \ln x^2, \\ g(x) &= -1 - 9x^2 + 9x^4 + x^6 - 6x^2(1 + x^2) \ln x^2 \end{aligned} \quad (4.45)$$

and V and A are the vector and axial vector couplings of the LN current. For mirror leptons one has $V = \cos(\phi_\ell - \theta_\ell) \simeq 1$, $A = -\cos(\phi_\ell + \theta_\ell) \simeq -1$. Thus the second term in (44) is negligible. An order-of-magnitude estimate of the lifetime is then

$$\tau_L \simeq 10^{-18} \text{ sec} \cdot \left[f\left(\frac{m_N}{m_L}\right) \right]^{-1} \left(\frac{20 \text{ GeV}}{m_L} \right)^5. \quad (4.46)$$

In the case $m_L < m_N$ the dominant decay channels of L would be as in (38) which are suppressed by mixing. The lifetime for the charged current decays (the two last channels listed) would then be

$$\tau_L \simeq 10^{-18} \text{ sec} \cdot \left[(\sin \phi_\ell \cos \theta_\ell)^2 + (\cos \phi_\ell \sin \theta_\ell)^2 \right]^{-1} \left(\frac{20 \text{ GeV}}{m_L} \right)^5. \quad (4.47)$$

For mixing angles $\phi_\ell, \theta_\ell \sim 10^{-3}$ and $m_L \sim 40$ GeV the flight path would be long enough to be reconstructed in vertex detectors. Similar estimates [48] apply to the exceptional charged and neutral leptons E and ν_E .

Mirror quarks either decay unsuppressed into each other, e.g. for $m_D > m_U$

$$D \rightarrow U + W_{virt}^- \rightarrow (e^- \bar{\nu}_e \text{ etc.})$$

followed by subsequent U quark decay through mixing with the light chiral quarks in CC and NC channels

$$\begin{aligned} U &\rightarrow d + W_{virt}^+ (\rightarrow e^+ \nu_e \text{ etc.}) \\ U &\rightarrow u + Z_{virt} (\rightarrow e^+ e^- \text{ etc.}) \end{aligned} \quad (4.48)$$

If $m_U > m_D$ the sequence is reversed correspondingly.

On the other hand, E_6 type $D_{1/2}$ quarks decay only through mixing with d, s, b quarks if they carry the usual lepton and baryon quantum numbers,

$$\begin{aligned} D_{1/2} &\rightarrow u + e^- \bar{\nu}_e \text{ etc.} \\ D_{1/2} &\rightarrow d + e^- e^+ \text{ etc.} \end{aligned}$$

with an estimated ratio of $NC/CC \sim 1/8$. [The SUSY case will be discussed in the next subsection.] The CC decay width is effectively governed by a 4th column of CKM elements V_{uD}, V_{cD} and V_{tD} . Because of unitarity, V_{uD} must be very small, whereas V_{cD} and V_{tD} could still be several tens of percents. One cannot even exclude the "anti-diagonal" possibility that V_{tb} is very small and V_{tD} near 100%, although it is disfavoured [5]. One consequence of this is that t -hadrons have slightly longer lifetimes than in the standard model, and some of B -physics undoubtedly gets modified. If the $D_{1/2}$ -quark were lighter than the t -quark, the lifetime of $D_{1/2}$ -hadrons could be similar to the b -quarks. One may estimate [2] the $D_{1/2}$ -lifetime to be

$$\tau_{D_{1/2}} \simeq 10^{-18} \text{ sec} \cdot (\sin \theta_D \cos \theta_D)^{-2} \left(\frac{20 \text{ GeV}}{m_{D_{1/2}}} \right)^5, \quad (4.49)$$

where θ_D is an effective down quark mixing angle.

4.3.3. LEPTOQUARKS AND DIQUARKS

The fundamental 27-dimensional representation contains a host of new fermions (22). In particular the quark sector is extended by an isosinglet charge $-\frac{1}{3}$ particle in each family $[D_L^{1/2}, D_R^{1/2}]$ and its color-triplet spin 0 supersymmetry partners D_0 and \bar{D}_0^c in superstring inspired models. The Yukawa interactions involving D 's are then described by the following superpotential

$$\begin{aligned} L_y &= \lambda_Q D Q Q + \lambda'_Q D^c u^c d^c & (a) \\ &+ \lambda_L D^c L Q + \lambda'_L D u^c e^c & (b) \\ &+ \lambda_\nu D d^c \nu^c & (c) \end{aligned} \quad (4.50)$$

[Q, L denote the ordinary left-handed quark and lepton doublets, respectively; ν^c is the singlet neutrino.] To avoid rapid proton decay and to make Dirac neutrino masses vanish naturally, only one of the sets (a-c) can be realized in nature. If the D 's carry

baryon number $B = +1/3$ and lepton number $L = +1$ they will be called leptoquarks, if $B = -2/3$ and $L = 0$, diquarks. We shall concentrate on the alternatives (a) and (b) in the following, and focus mainly on the decay signatures and the production of scalar particles at the Z peak. Fermions follow the patterns outlined before, and off-resonance production is described in all details in Ref. [52]*. [The formation of one real plus one virtual D_0 in the mass range $m_Z/2 < 2m_D < m_Z$ has been considered in [66].]

The partial width for

$$Z \rightarrow D_0 \bar{D}_0 \quad \text{or} \quad D_0^c \bar{D}_0^c$$

is given by

$$\Gamma_D = \frac{Gm_Z^3}{16\sqrt{2}\pi} \beta^2 Z_D^2 \quad (4.51)$$

where

$$Z_D = -e_D \sin^2 \theta_W = \frac{1}{3} \sin^2 \theta_W \quad (4.52)$$

denotes the Z charge of the D_0/\bar{D}_0^c particles [for the sake of simplicity mixing effects are disregarded]. Thus the ratio $\Gamma(Z \rightarrow D_0 \bar{D}_0 + D_0^c \bar{D}_0^c)/\Gamma(Z \rightarrow \mu^+ \mu^-)$ amounts to a few percent, (see Fig. 4.9).

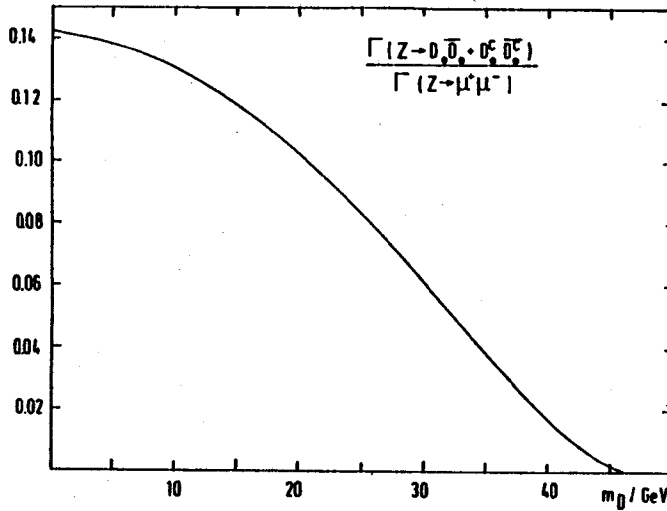


Fig. 4.9: The ratio $\Gamma(Z \rightarrow D_0 \bar{D}_0 + D_0^c \bar{D}_0^c)/\Gamma(Z \rightarrow \mu^+ \mu^-)$ as a function of the D mass.

Assuming the scalar D_0 's to be lighter than their spin $\frac{1}{2}$ partners $D_{1/2}$ the following decay channels are open, depending on whether the D 's are leptoquarks or diquarks:

$$\begin{aligned} \text{leptoquarks: } D_0 &\rightarrow n_R + e_R^- \\ \bar{D}_0^c &\rightarrow u_L + e_L^- \end{aligned}$$

*The entries for the Yukawa couplings in Table 2 of [52] should be multiplied by (-4) and the gauge coupling should read g_V^2 .

$$\begin{aligned}
& \rightarrow d_L + \nu_{eL} \\
\text{diquarks: } D_0 & \rightarrow \bar{u}_R + \bar{d}_R \\
\bar{D}_0^c & \rightarrow \bar{u}_L + \bar{d}_L
\end{aligned}$$

Barring large Yukawa couplings the decay widths

$$\begin{aligned}
\Gamma(D_0 \rightarrow ue^-) &= \frac{\lambda_L'^2 m_D}{16\pi} & \Gamma(D_0 \rightarrow \bar{u}\bar{d}) &= \frac{4\lambda_Q^2 m_D}{4\pi} \\
\Gamma(\bar{D}_0^c \rightarrow ql) &= \frac{\lambda_L^2 m_D}{16\pi} & \Gamma(\bar{D}_0^c \rightarrow \bar{u}\bar{d}) &= \frac{\lambda_Q'^2 m_D}{16\pi}
\end{aligned} \tag{4.53}$$

are small in the LEP mass range. The spin $\frac{1}{2}$ $D_{1/2}$ particles decay either into $D_0\bar{\chi}$ or $q\bar{\ell}/\bar{q}\ell$ and $\bar{q}\bar{q}$ as elaborated in [53].

Scalar leptoquarks can easily be recognized through $(\ell^\pm \text{ jet})$ bumps in the final states without missing energy. Scalar diquarks can be reconstructed from bumps in jet-jet invariant mass distributions. $D_{1/2}\bar{D}_{1/2}$ fermion decays produce 4-jet final states plus missing energy which could be confused with the hadronic decay of a new sequential lepton with a massless neutrino partner, but the kinematical distributions would be sufficiently distinctive [1].

REFERENCES

- [1] LEP200 Study Group on "New Leptons and Quarks", P. Igo-Kemenes et al., Proceedings, LEP200 Workshop, Aachen, 1986, Eds. A. Böhm and W. Hoogland.
- [2] M. Jezabek and J.H. Kühn, *Nucl. Phys. B* **314** (1989) 1, *Nucl. Phys. B* **320** (1989) 20.
- [3] W.S. Hou and R.G. Stuart, *Phys. Rev. Lett.* **62** (1989) 617.
- [4] B. Haeri, A. Soni, G. Eilam, *Phys. Rev. Lett.* **62** (1989) 719.
- [5] S. Güsken, J.H. Kühn and P.M. Zerwas, *Nucl. Phys. B* **262** (1985) 393.
- [6] Particle Data Group, *Phys. Lett.* **204 B** (1988) 1.
- [7] R.N. Cahn and H. Harari, *Nucl. Phys. B* **176** (1980) 135.
- [8] O. Shanker, *Nucl. Phys. B* **206** (1982) 253.
- [9] W. Buchmüller and D. Wyler, *Nucl. Phys. B* **268** (1986) 621.
- [10] I.I. Bigi, G. Köpp and P.M. Zerwas, *Phys. Lett.* **166 B** (1986) 238.
- [11] D. Wyler, Zuo Lectures 1988.
- [12] W. Buchmüller, R. Rückl and D. Wyler, *Phys. Lett.* **191 B** (1987) 442.
- [13] T. Inami and C.S. Lim, *Prog. Theor. Phys.* **65** (1981) 297; *ibid.* 1772(E).
- [14] W. Buchmüller and F. Hoogeveen, in preparation.
- [15] For a review, see E. Farhi and L. Susskind, *Phys. Rep. C* **74** (1981) 277.
- [16] J.P. Derendinger, L.E. Ibanez and H.P. Nilles, *Nucl. Phys. B* **267** (1986) 365.
- [17] B.A. Campbell et al., *Int. J. Mod. Phys. 2* (1987) 831.
- [18] E. Eichten et al., *Phys. Rev. D* **34** (1986) 1547.
- [19] A. Masiero, E. Papantonopoulos and T. Yanagida, *Phys. Lett.* **115 B** (1982) 229.
- [20] W. Buchmüller and M. Gronau, *Phys. Lett.* **220 B** (1989) 641.
- [21] G. Eilam and T.G. Rizzo, *Phys. Lett.* **188 B** (1987) 91.
- [22] P. Langacker and D. London, *Phys. Rev. D* **38** (1988) 886.

- [23] J.C. Pati and A. Salam, *Phys. Rev. D* **10** (1974) 275.
- [24] W. Buchmüller and D. Wyler, *Phys. Lett.* **177 B** (1986) 377.
- [25] J. Maalampi and M. Roos, Helsinki Report HU-TFT-88-17, *Phys. Rep. C* (1989) to be published; Univ. of Helsinki Report HU-TFT-89-11 and *Z. Phys. C* (1989) to be published.
- [26] J.L. Hewett and T. Rizzo, MAD/PH/446, Nov. 1988.
- [27] H. Fritzsch and P. Minkowski, *Ann. Phys. (N.Y.)* **93** (1975) 193.
- [28] J. Maalampi and K. Enqvist, *Phys. Lett.* **97 B** (1980) 217.
- [29] F. Wilczek and A. Zee, *Phys. Rev. D* **25** (1982) 553,
see also *Spinors and Families*, Princeton preprint (1979) (unpublished).
- [30] M. Gell-Mann, P. Ramond and R. Slansky, in *Supergravity*, Eds. P. van Nieuwenhuizen and D.Z. Freedman (North-Holland, Amsterdam, 1979).
- [31] K. Enqvist and J. Maalampi, *Nucl. Phys. B* **191** (1981) 189.
- [32] H. Sato, *Phys. Rev. Lett.* **45** (1980) 1997.
- [33] J. Maalampi, *Nucl. Phys. B* **198** (1982) 519.
- [34] Other references are included in: R. Mohapatra and B. Sakita, *Phys. Rev. D* **21** (1980) 1062;
A. Davidson et al., *Phys. Rev. Lett.* **45** (1980) 1135;
M. Ida, Y. Kayama and T. Kitazoe, *Prog. Theor. Phys.* **64** (1980) 1745;
Z. Ma, T.S. Tu, P.Y. Xue and X.J. Zhou, Beijing University preprint BIHEP-TH-3 (1980) (unpublished);
Y. Fujimoto, *Phys. Rev. D* **26** (1982) 3183.
- [35] H. Georgi, *Nucl. Phys. B* **156** (1979) 126.
- [36] P.H. Frampton, *Phys. Lett.* **88 B** (1979) 299.
- [37] I. Umemura and K. Yamamoto, *Phys. Lett.* **100 B** (1981) 34.
- [38] C.W. Kim and C. Roiesnel, *Phys. Lett.* **93 B** (1980) 343.
- [39] M. Chaichian, Yu. N. Kolmakov, N.F. Nelipa, *Nucl. Phys. B* **186** (1981) 275,
Phys. Rev. D **25** (1982) 1377 and *Nucl. Phys. B* **202** (1982) 126.
- [40] N.S. Baaklini, *Phys. Rev. D* **21** (1980) 1932, *D* **23** (1981) 2719.
- [41] I. Bars and M. Günaydin, *Phys. Rev. Lett.* **45** (1980) 859;
S.E. Konshtein and E.S. Fradkin, *Pisma ZETF* **32** (1980) 575;
M. Koca, *Phys. Lett.* **107 B** (1981) 73;
S.M. Barr, *Phys. Rev. D* **37** (1988) 204.
- [42] For a review see: P. Fayet and S. Ferrara, *Phys. Rep. C* **32** (1977) 249x;
P. van Nieuwenhuizen, *ibid.* **C 68** (1981) 189.
- [43] For a general review, see: M.J. Duff, B.E.W. Nilsson and C.N. Pope, *Phys. Rep.* **130** (1986) 1;
T. Appelquist, A. Chodos and P. Freund, *Modern Kaluza-Klein Theories*, (Addison-Wesley, Reading, Mass., 1987).
- [44] R. Gatto and J. Casalbuoni, *Phys. Lett.* **93 B** (1980) 47;
P. Senjanović, *Fizika* **15** (1979) 126.
- [45] F. Gürsey, P. Ramond and P. Sikivie, *Phys. Lett.* **60 B** (1976) 177;
Y. Achiman and B. Stech, *Phys. Lett.* **77 B** (1978) 389;
Q. Shafi, *Phys. Lett.* **79 B** (1978) 301;
H. Ruegg and T. Schmücker, *Nucl. Phys. B* **161** (1979) 388;
R. Barbieri and D.V. Nanopoulos, *Phys. Lett.* **91 B** (1980) 369.
- [46] J.L. Rosner, Chicago preprints EFI 85-34 and 86-19.
- [47] E. Cohen, J. Ellis, K. Enqvist and D.V. Nanopoulos, *Phys. Lett.* **165 B** (1985) 76.
- [48] V. Barger, N.G. Deshpande, R.J.N. Phillips and K. Whisnant, *Phys. Rev. D* **33** (1986) 1912.
- [49] F. Del Aguila, E. Laermann and P. Zerwas, *Nucl. Phys. B* **297** (1988) 1.
- [50] K. Enqvist, J. Maalampi and M. Roos, *Phys. Lett.* **176 B** (1986) 396;
J. Maalampi and M. Roos, *Phys. Lett.* **195 B** (1987) 489.
- [51] T.G. Rizzo, *Phys. Rev. D* **34** (1986) 2699;
J.L. Hewett and T.G. Rizzo, *Z. Phys. C* **34** (1987) 49.

- [52] D. Schaile and P.M. Zerwas, Proceedings of the La Thuile/CERN Workshop on Future Accelerators, La Thuile/CERN 1987, ed. J. Mulvey, Report CERN 87-07.
- [53] V.D. Angelopoulos, J. Ellis, H. Kowalski, D.V. Nanopoulos, N.D. Tracas and F. Zwirner, *Nucl. Phys. B* **292** (1987) 59.
- [54] C. Albajar et al. (UA1 Coll.), *Phys. Lett.* **185 B** (1987) 233.
- [55] H. Sagawa et. al. (AMY Collab.), *Phys. Rev. Lett.* **60** (1988) 93;
I. Adachi et al. (TOPAZ Collab.), *Phys. Rev. Lett.* **60** (1988) 97;
- [56] K. Enqvist, K. Mursula and M. Roos, *Nucl. Phys. B* **226** (1983) 121.
- [57] S.L. Glashow, J. Iliopoulos and L. Maiani, *Phys. Rev. D* **2** (1970) 1285.
- [58] I. Umemura and K. Yamamoto, *Phys. Lett.* **108 B** (1982) 37.
- [59] M.K. Gaillard and B.W. Lee, *Phys. Rev. D* **10** (1974) 897.
- [60] See, e.g., F. Boehm and P. Vogel, *Ann. Rev. Nucl. Part. Sci.* **34** (1984) 125;
F. Gilman, *Comments Nucl. Part. Phys.* **16** (1986) 231;
N. Terazawa, M. Kawasaki, and K. Sato, *Nucl. Phys. B* **302** (1988) 697.
- [61] W. Marciano and A. Sanda, *Phys. Lett.* **67 B** (1977) 303;
S. Petcov, *Yad. Fiz.* **25** (1977) 641, **25** (1977) 1336 (E).
- [62] J. Maalampi, K. Mursula and M. Roos, *Phys. Rev. Lett.* **56** (1986) 1031.
- [63] S. Gottlieb and T. Weiler, *Phys. Rev. D* **32** (1985) 1119.
- [64] H. Haber and M.H. Reno, FERMILAB-PUB-86/41-T (1986).
- [65] I. Liede, J. Maalampi and M. Roos, *Nucl. Phys. B* **134** (1978) 339.
- [66] N.D. Tracas and S. Vlassopoulos, Nat. Tech. Univ. Report, Athens, NTUA-17/88.